THE EFFECT OF CÒMPLEXES ON COMBUSTION

LINH ANTHONY NGUYEN

Doctor of Philosophy

THE UNIVERSITY OF ASTON IN BIRMINGHAM

JULY 1993

THE UNIVERSITY OF ASTON IN BIRMINGHAM

THE EFFECT OF COMPLEXES ON COMBUSTION

LINH ANTHONY NGUYEN

Submitted for the Degree
of Doctor of Philosophy.

July 1993.

SUMMARY

The twin goals of low and efficient fuel use and minimum emissions are increasingly being addressed by research in both the motor and the catalyst industries of the world. This study was designed to attempt to investigate these goals. For diesel engine vehicles, this can be achieved by improving the efficiency of the fuel combustion in the combustion chamber. By having a suitable oxidation catalyst in the fuel one would expect the efficiency of the fuel combustion to be increased and that fewer partial oxidation products to be formed. Also by placing a catalyst converter in the exhaust system partial oxidation products may be converted to more desirable final products. Finally, in this research the net catalytic effect of using an additive treated fuel and a blank ceramic monolith to trap the metal in the exhaust gases for potential use as catalytic converter was investigated.

Suitable metal additives must yield a stable solution in the fuel tank. That is, they should not react with the air, water and rust that are always present. The research was targeted on the synthesis of hydrocarbon-soluble complexes that might exhibit unusually slow rates of ligand substitution. For materials containing metal ions, these properties are best met by using multi-dentate ligands that form neutral complexes. Metal complexes have been synthesised using acetylacetone derivatives, schiff base ligands and macrocyclic polyamine ligands, as potential pro-oxidant additives. Their thermal stabilities were also investigated using a differential thermal analysis instrument.

The complexes were then investigated as potential additives for use in diesel fuel. The tests were conducted under controlled conditions using a diesel combustion bomb simulating the combustion process in the D.I. diesel engine, a test bed engine, and a vehicle engine. Also, a blank exhaust box (γ-alumina coated ceramic monolith) was used to trap the emitted metal oxide after the combustion processes so that the catalytic converter potential for exhaust gas treatment could be investigated.

It was found that there exists a relationship between additive activity and the rate of additive decomposition. Greater catalytic effect occured with additives having faster rates of decomposition than those with a lower rate. The $Ce(DPM)_3$ additive showed the greatest catalytic activity of those tested, as it had the fastest rate of decomposition compared to the others. Thermal analysis shows that $Ce(DPM)_3$ decomposed completely at $300^\circ C$, while the rest still decomposed at $550^\circ C$. This suggests that the rate of additive effect is temperature dependence as demonstrated in the combustion bomb test, where most the catalytic effect occured at $500^\circ C$ and not at $600^\circ C$.

Keywords: Cerium Complexes, Additive, Diesel, Combustion, Exhaust Emissions.

To my parents, and

my grandad, sadly lost, but not forgotten.

ACKNOWLEDGEMENTS

List of Contents

LIST OF FIGURES

LIST OF ABBREVIATIONS

ac	Acetic Acid
acacH	Acetylacetone
A/F	Air/Fuel Ratio
AH	Anti-Oxidant
AVG	Average
BDC	Bottom Dead Centre
$CDCl_3$	Deuterated Chloroform
CO	Carbon Monoxide
COD	1,5-Cyclooctadiene
CYCLAM	1,4,8,11-Tetracyclotetradecane
CYCLEN	1,4,7,10-Tetraazacyclododecane
DI	Direct Injection
DMF	Dimethylformamide
DMSO	Deuterated Dimethyl Sulfoxide
D_2O	Deuterium Oxide
DOTA	1,4,8,11-Tetracyclotetradecane Tetraacetic Acid
DPM-H	Dipivaloylmethane
DTA	Differential Thermal Analysis
ECE	Economic Commission for Europe
EGDME	Ethylene Glycol Dimethyl Ether
EGR	Exhaust Gas Recirculation
F	Force on the Dynamometer Scale
FTIR	Fourier Transform Infra-Red
FTNMR	Fourier Transform Nuclear Magnetic Resonance
HC	Hydrocarbons
H_3-naphtren	N,N',N''-tris-(salicylaldehyde)-tris-2-aminoethylimine

H$_3$-saltren	N,N',N"-tris-(2-hydroxy-1-naphthaldehyde)-tris-2-aminoethylimine
H$_3$-^{t}Bu-saltren	N,N',N"-tris-(5-tertiarybutylsalicylaldehyde)-tris-2-aminoethylimine
IDI	Indirect Injection
NOTA	1,4,7-Triaazacyclononane
NOx	Nitrogen Oxides
ODTA	1-Oxa-4,7,10-triazacyclododecane Triacetic Acid
P	Pressure
ROOH	Hydroperoxide
SEM	Scanning Electron Microscope
SI	Spark-Ignition
SOx	Sulphur Oxides
STG	Standard Deviation
t	Time
T	Torque
TACN	1,4,7-Triazacyclononane
TDC	Top Dead Centre
TETA	1,4,8,11-Tetracyclotetradecane Tetraacetic Acid
TG	Thermogravimetry
THF	Tetrahydrofuran
TLC	Thin Layer Chromatography
TMS	Tetramethylsilane
Ts	p-Toluenesulfonyl
VIA	Versatile Interface Adapter

Chapter 1

Automotive Pollutant Formation and Control

1.1 INTRODUCTION

The pollution of the atmosphere by the motor vehicle, primarily the gasoline engine, causes world-wide concern over the environment. Atmospheric pollution was first observed in the early 1940s by the residents of Los Angeles in the form of photochemical smog. Studies[1,2] of this phenomenon showed that the smog formation was caused by the inter-action of nitrogen oxides and hydrocarbons in sunlight, producing harmful lachrymatory compounds that caused impairment to health and damage to vegetation.

The first recorded observation of smog formation was in a letter Tyndall had written to the Royal Society of London[3], which reads as follows: " The vapour of nitrite of amyl was permitted to enter an experimental tube while the beam from the electric lamp was passing through it. For a moment the tube was optically empty, nothing whatever being seen within it. But, before a second has elapsed a shower of particles was precipitated on the beam. The cloud, thus generated, became denser as the light continue to act, showing at some phases, iridescence." Tyndall goes on to say: "It is probably the synchronism of the vibration of one portion of the molecule with the incident waves that enable the amplitude of those vibrations to augment until the chain which binds the parts of the molecule together is snaped asunder." Therefore, Tyndall was the first man to simulate a Los Angeles smog, and his explanation of the reaction mechanism still holds to this day, although other chemists may have more difficult ways of expressing the same thought.

Smogs were later experienced in Tokyo. The dispersion of photochemical smog and its precursors can be retarded by climatic conditions and has become a particular problem in Los Angeles, Mexico City, and Tokyo. This situation is by no means confined to the U.S.A. and Japan, however, as photochemical smog and related phenomena have been observed in some European cities, notably in Madrid[4] and Athens[5].

The internal combustion engine has been shown to be a major source of pollution which produces principally carbon monoxide (CO), hydrocarbon (HC), nitrogen oxides (NOx),with small amounts of sulphur oxides (SOx), lead (Pb) and particulates[6]. Exhaust gases from motor vehicles account for as much as 90, 60 and 40 per cent of man-made carbon monoxide, hydrocarbon and nitrogen oxide emissions, respectively[7].

Growing concern with the contribution by the car to the pollution of the environment has resulted in increasingly severe world-wide automobile emission legislation with the strictest controls being imposed in the United States and Japan.

Legislation has been enacted (initially in California but extending to the rest of the United States) to limit noxious emissions from automobiles. This culminated in the USA with the signing of the 1970 Clean Air Amendments Act[8] which called for a 90 per cent reduction of carbon monoxide and hydrocarbon emissions from 1970 model year levels by 1975, and 90 per cent reduction of nitrogen oxides emissions from 1971 model year levels by 1978. Prior to 1975 ignition and carburation modifications were used in conjunction with secondary air injection and thermal reactors, all of these techniques having a generally detrimental effect on fuel economy. However, since 1975, catalyst technology has been successfully introduced, giving rise to two major side effects. First, most vehicle manufacturers were able to re-tune engines for better economy while relying on the catalyst to control emissions. Better engine control is also a requirement of the use of catalysts. Secondly, it ensured that the trend to lead-free petrol was maintained as conventional automobile catalysts are poisoned by lead.

The emission levels in Europe permitted by legislation over the years have been progressively lowered, but when compared with those of the United

States they are presently far higher. The existing European regulations for controlling noxious emissions from motor cars were introduced in 1971 for hydrocarbon and carbon monoxide reduction[9]. When compared with the U.S. Federal regulations in per cent reduction in emissions (in 1971), Europe stands at a 40% reduction while the U.S. Federal regulations are at a 60% reduction for hydrocarbon and carbon monoxide. In 1979 came the introduction of European regulation for nitrogen oxides reduction, which compares to the introduction in the U.S. in 1973. By 1990, however, the European regulation had improved vastly in terms of hydrocarbon and carbon monoxide reductions with up to 90% of the reduction required by the U.S. Federal regulation. Nitrogen oxides reduction, however, needs more improvement to compare with the standard set in the U.S.

So, the twin goals of low and efficient fuel use and minimum emissions are increasingly being addressed by research in both the motor and catalyst industries of the world. It is one of our aims in this study to attempt to investigate the above goals. Focussing primarily on diesel engined vehicles, this can be achieved by improving the efficiency of the fuel combustion in the combustion chamber. By having a suitable oxidation catalyst in the fuel, one would expect the efficiency of the fuel combustion to be increased and also fewer partial oxidation products to be formed.

Current research in this field has concentrated mainly on developing additives which comprise of organic compounds rather than coordination compounds, with very few papers published concerning organometallic additives. Recently, Sexton and co-workers[10] have reported a fuel-oil additive comprising a C_{13-25} alkyl nitrate, optionally together with an ashless dispersant, especially macrocyclic polyamines and a foam inhibitor (e.g. siloxane-polyoxyalkylene copolymer), that enhances combustion and reduces particle emissions. Gonzalez[11] has shown in his work that combustion can be

improved with the use of combustion promoters which comprise 1-15 vol.% aromatic amines, 1-45 vol.% aromatic hydrocarbon solvents, 1-15 vol.% aliphatic ketone solvents, and 1-85 vol.% aliphatic ether and paraffinic/naphthenic solvents. Reduced emissions of NO_x, CO, unburned hydrocarbons, smoke and particulates were also observed. Hart and co-workers[12] show diesel fuel combustion can also be improved with the addition of polymeric additives. These are fuel-soluble polymers (no. av. mol. wt. 200-50000) having a backbone carrying a plurality of the same or different functional groups, e.g. a nitrated and hydrolysed ethylene/vinyl acetate copolymer. Tachibana and co-workers[13] have studied the effect of ozone on combustion in compression ignition engines and their work shows that the addition of O_3 to the intake air during combustion improves the combustion characteristics. In terms of exhaust emissions, a small decrease in CO, hydrocarbons, and particulates, and a small increase in NO_x were observed with O_3 addition under fixed operating conditions. Khinkova[14] reports that additive mixtures, all containing oxygen compounds, such as dicyclohexyl peroxide, isooctanol, p-xylene, cumyl hydroperoxide, and di-tert-Bu peroxide, can act as a diesel fuel combustion improver, for the reduction of smoke and soot emissions. Buxton[15] shows that combustion in a diesel engine can be improved by the addition of peresters of the formula R_1COOOR_2, where R_1 is a C_{5-20} secondary or tertiary alkyl group, and R_2 is a C_{4-10} tertiary alkyl group, e.g., tert-Bu-per-2,2,4-trimethylhexanoate or tert-Bu-per-2-ehtylhexanoate.

However, this research was focused on organometallic and coordination compounds as the potential additives for improving diesel fuel combustion rather than on organic compounds. Recent research[16-24] in this area has shown that organometallic compounds of Fe, Mn, Ti, Zr and Pt-group metals can improve combustion and reduce exhaust emissions in diesel fuel combustion. Robert and co-workers[16-17] demonstrated two methods for

reducing pollution emissions from a diesel engine with the use of organometallic platinum-group coordination compound additives. One method reduces the emissions of NO_x from a diesel engine without significant loss of fuel efficiency and without significant increases in CO and hydrocarbon emissions. The injection timing of a diesel engine is set at a point sufficient to obtain reductions in the NO_x emissions from the engine, and an additive which comprises a fuel-soluble organometallic Pt-group metal coordination compound is admixed with the fuel. In the other method the same additive as in the first method is used to regenerate a diesel engine particulate trap. More details of these Pt-group compounds are given later in the chapter. Zeller and Westphal[18] studied the effect of iron-based fuel additives for diesel soot control, and of those additives tested, they found that a ferrocene-based compound reduced diesel particulate matter by 4-45%, depending on the engine operating conditions. The reductions in particulate matter were caused by the catalytic oxidation properties of an Fe_2O_3 coating that developed inside the engine's combustion chamber. The Fe_2O_3 coating also led to a decrease in gas-phase hydrocarbons and oxygen, but a increase in CO_2 and NO_x. The increase in NO_x, approximately 12%, is considered to be the only adverse effect of the ferrocene-based fuel additive. Wallace[19] reports on a manganese carbonyl compound that acts as a combustion improver in diesel fuel. The additive was tested with a diesel engine running at 1569 rpm under 75% load using diesel fuel containing the soluble manganese compound [methylcyclopenta-dienylmanganese tricarbonyl (I)]. Hydrocarbon emissions were reduced by 41%. In the last few years, Robert and co-workers[21,22] have also reported a method for improving the perfomance of internal combustion engines. It involves mixing the fuel with an additive containing several Pt-group metal compounds at a dose level equivalent to a supply of 0.01-1 ppm of Pt-group metal in the fuel. Suitable Pt-group metal compounds include (a) Pd acetylene complexes, (b) Rh or Ir allyl complexes, e.g., $Rh(C_3H_5)_3$ and $Ir(C_3H_5)_3$, (c) Pt(IV) compounds having the general

formula R_1PtR_2, where R_1= aryl, alkyl, or their mixtures; and R_2= hydroxyl, acetylacetonate, cyclopentadienyl or pentamethyl cyclopentadienyl, and (d) a compound of the general formula L_1MR_3, where L_1 is substituted butadiene or cyclohexadiene, M=Rh or Ir, and R_3= cyclopentadienyl or pentamethyl cyclopentadienyl. However, before describing the present research in more detail a fuller understanding of exhaust emissions is needed. It is also worth mentioning that noxious exhaust emissions can be further reduced by placing a catalyst converter in the exhaust system to convert partially oxidised material to more desirable final products.

1.2 EXHAUST EMISSIONS FROM GASOLINE AND DIESEL COMBUSTION

Table 1.1 Typical Emission Concentrations in Exhaust Gases from Petrol and Diesel Engines in 1970					
	Carbon Monoxide %	Hydro-carbon ppm	Nitrogen Oxides ppm	Sulphur Dioxide ppm	Particulates g/m^3
Diesel Engine	0.1	300	4000	200	0.5
Petrol Engine	10	1000	4000	60	0.01

The internal combustion engine pollutes the atmosphere, mainly through its exhaust products. The major pollutants from spark ignition (S.I.) engines are carbon monoxide, oxides of nitrogen and hydrocarbons. The diesel engine, generally a lower pollutant generator, also emits a small amount of sulphur dioxide from the sulphur content of the fuel but, more importantly from a regulatory stand point, it emits particulate matter and smoke. A further

pollutant, although non-toxic, is carbon dioxide, the main product of combustion, which contributes to the postulated 'greenhouse' effect.

The concentration of pollutants varies from engine to engine and also depends upon the operating mode of the engine. For comparison purposes, figures typical of the two engine systems are given in Table 1.1[23]

The origin of the various emissions in exhaust gases stems from the combustion processes ocurring in the engine.

1.2.1 Carbon Monoxide

This is formed during the combustion process when there is insufficient oxygen available for complete combustion. Carbon monoxide emissions from S.I. engines are primarily dependent on the air:fuel ratio which governs the availability of the oxygen to complete the combustion of hydrocarbons. When this reaction fails to go to completion carbon monoxide is emitted; it follows that as one goes fuel-rich compared to the stoichiometric ratio of 14.7:1 air:fuel, the CO values increases rapidly. At the stoichiometric ratio, although in principle there is sufficient oxygen, due to imperfect mixing some carbon monoxide is still formed. Diesel engines, unlike S.I. engines, operate with excess air under all conditions, so there is less carbon monoxide in their exhaust gases. Even so, with insufficient mixing of the air fuel mixture and particularly at high load conditions, a significant concentration of carbon monoxide is produced.

All efforts in controlling emissions of CO are, therefore, concentrated on the completion of oxidation of CO rather than attempting to inhibit its formation. If sufficient oxygen and residence time is available at flame temperatures, CO concentrations fall to very low levels after reaction. The problem can be minimised by good engine design and by limiting the power output of the

engine. Fuel composition and fuel additives have little effect upon carbon monoxide concentrations.

1.2.2 Hydrocarbons

Fuel that escapes combustion arises from several causes. The most obvious is that which is retained at low temperature in crevices into which it is forced by compression, namely the sparkling plug and in the gap between piston and cylinder above the piston ring. During the expansion stroke this flows out but as temperatures have dropped it is only partially burned[24]. This inability to complete the combustion of the fuel affects the combustion efficiency. The most important reason for the incomplete burning of fuel, as with carbon monoxide production, is insufficient mixing between the fuel, air and combustion products. If the air and fuel are completely mixed on the macro-scale and sufficient time is given for a reaction to take place after mixing on the micro-scale, complete burning could take place at stoichiometric fuel-air mixture ratios. The temperature must be sufficiently high for the reaction to be completed during the period of contact between the fuel and air. The combustion products can be used as the heat source for raising the air-fuel mixtures above the ignition temperature. When insufficient mixing takes place, excess air above the stoichiometric ratio is required in order to complete combustion. Excess air reduces the combustion efficiency by lowering the temperature and increasing convectional heat losses via the increased mass flow rate of exhaust gases. The general aim of minimising pollutants and maximising combustion efficiency is achieved in practice by increasing the efficiency of mixing between fuel, air and combustion products, increasing the residence time, and minimising the amount of excess air used.

The relative concentrations of hydrocarbon emissions are greatly influenced by the composition of the fuel. For fuel containing large concentrations of olefins and aromatics, the exhaust gases contain relatively high

concentrations of reactive hydrocarbon and polynuclear organic compounds. The highly reactive hydrocarbons are the participants in the production of smog, whereas other organic compounds may be virtually unreactive in this respect.

1.2.3 Nitrogen Oxides

Oxides of nitrogen are formed during the combustion process, mainly as a result of chemical reactions between atmospheric oxygen and nitrogen. The oxides of nitrogen are referred to as NOx. The two major oxides of nitrogen emitted from combustion systems are nitric oxide, NO, and nitrogen dioxide, NO_2. Concentrations of nitrogen dioxide are generally considerably lower than those of NO. Pollution arising from NO leads to physical discomfort, smarting eyes and feelings of suffocation in locations with high smog concentration as mentioned earlier. NO_2 is one of the most toxic of commonly encountered gases and can be a serious health hazard.

Nitric oxide is formed from the nitrogen and oxygen in the combustion air at the very high temperatures present in the combustion chambers of both diesel and S.I. engines. The reactions are usually termed the extended Zeldovich reactions[25], after the person who first called attention to the effect of atomic nitrogen and oxygen under high temperature conditions. He proposed the following reactions:

$$O + N_2 \rightleftharpoons NO + N \qquad (1)$$

$$N + O_2 \rightleftharpoons NO + O \qquad (2)$$
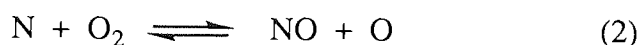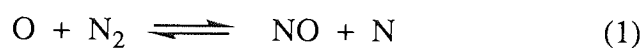
The rates of the reactions rise exponentially with temperature. This is the underlying problem facing all attempts to reduce the formation of NOx in an internal combustion engine because thermal efficiency increases with increasing temperature. In practice, as often, a compromise has to be made between efficiency and pollution. The consequences of this are that

calculation and experimentation have to be conducted as accurately as possible.

The early classic work in this area was performed by Newhall[26] and Starkman[27] who used the Zeldovich chain reactions and spectroscopic measurements of NO through windows in the combustion chamber of an experimental engine as a basis for their calculations.

The Zeldovich reactions have been shown to be an over-simplification of the complex interactions that take place in a combustion chamber where both pressure and temperature are high. A third reaction must be included to account for the formation of nitric oxide. The three equations are usually termed the Extended Zeldovich reactions:

$$O + N_2 \rightleftharpoons NO + N \qquad (1)$$

$$N + O_2 \rightleftharpoons NO + O \qquad (2)$$

$$N + OH \rightleftharpoons NO + H \qquad (3)$$
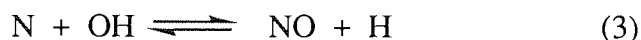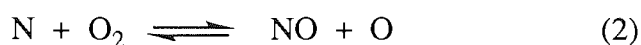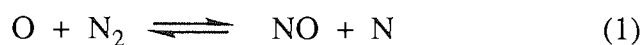
Reaction (3) becomes important only in near-stoichiometric and in rich flames that are held at high temperature long enough to produce significant amounts of nitric oxide.

1.2.4 Particulates

Particulates are a characteristic associated more with the diesel engine than the S.I. engine. Different types of particulates are emitted from diesel engines under different modes and operating conditions. The particulate matter emitted from combustion chambers has three possible sources: (i) matter which was not combustible; (ii) material which was capable of being burned but was not burned; and (iii) material formed during the process of combustion. Temperature conditions in most combustion chambers are sufficiently high for the complete vapourisation of liquids so that, except for

conditions of very rich low-temperature burning, all emitted particulate matter will be in the solid phase. Particulate matter can be deposited on surfaces within the combustion chamber or may be emitted with the exhaust gases. Most pollution problems arise from particulates which are so small that they are held in suspension as they are transported by the exhaust gases. The particulate matter may be clearly visible as smoke or water vapour, but small concentrations of particles can be significant sources of pollution without being visible.

The common black smoke emission consists of irregularly shaped, agglomerated, fine carbon particles. Solid carbon particles formed in flames are known as *soot*. Soot can be formed from purely gaseous fuels but is more commonly formed when liquid fuels are used.

The formation of carbon particles in flames is due to the thermal decomposition of hydrocarbons. Whilst at high temperatures these decompose largely into carbon and methane in a very short time, some pyrolysis processes even occur in the preheating zones of flames. Small hydrocarbon or organic molecules act as nuclei for the formation of soot which, after growth, become relatively large particles containing many thousands of atoms with a high carbon:hydrogen ratio.

Dehydrogenation to C_1 or C_2 radicals, followed by condensation to solid carbon, has been found, as has polymerisation to very large hydrocarbon molecules which then lose hydrogen and form graphite. Both polymerisation and oxidation proceed by chain reactions, usually involving free radicals. Soot is formed from products of some of these chain reactions.

1.2.5 Sulphur Oxides

Sulphur dioxide, SO_2, and sulphur trioxide, SO_3, are formed from the sulphur-containing compounds in the fuel upon reaction with oxygen. The deposition of sulphur oxides, sulphates and sulphuric acid on metallic surfaces causes severe corrosion problems, both inside and outside the combustion equipment. Corrosion is usually associated with the conversion of SO_2 to SO_3, which then hydrates and condenses as sulphuric acid on cooled surfaces. This problem can be solved if sulphur is extracted from the fuel prior to its introduction into the combustion chamber, or special provision is made for sulphur removal before emission from the combustion chamber.

1.3 CONTROL OF EXHAUST EMISSIONS

A number of emission techniques have been devised in an attempt to reduce emissions of all pollutants, but mostly for HC, CO and NOx, over all engine operating modes. They arose from a large number of studies[28-50] over the years.

1.3.1 Catalytic Converters and Thermal Reactors

Our discussion has so far focused on engine emissions. Further reductions in emission can be obtained using reactors in the exhaust system. These reactors include catalytic converters and thermal reactors. Catalytic converters can be responsible for the oxidation of HC and CO and also the reduction of NOx. A more detailed description of a catalytic converter is discussed in Chapter 7.

Chandler and co-workers[51] developed the concept of non-flame exhaust gas reactors. Their investigations cover basic studies of the relationship of temperature, oxygen, and residence time to oxidation rates with external, supplementary, and exhaust gas heating. Oxidation after passage through the exhaust port can be enhanced with a thermal reactor, which is an enlarged

exhaust manifold that bolts directly onto the cylinder head. Its function is to promote rapid mixing of the hot exhaust gases (with secondary air which is required with fuel-rich engine operation to produce a net oxidising atmosphere), as well as to keep the gases at a high enough temperature for a sufficient time to oxidise most of the HC and CO which leave the cylinder.

1.3.2 Lean-burn Engine

Lean-burn engines have been under development since the 1970s. The diesel is a successful example of a true lean-burn engine. It was in recognition of the advantages of diesel engines in terms of fuel economy and lower levels of nitrogen oxide pollution that emissions engineers in the motor industry sought to produce petrol engines that would operate with air:fuel ratios as lean as those possible in diesel engines. However, successful and widespread usage of such engines has been restricted by increasingly strict control on the level of pollutants emitted under the full range of engine operating conditions[52]. Recent developments have included the evolution of lean operating two-stroke engines[53].

The lean-burn operation involves the burning of fuel with an excess of air. At air:fuel ratios greater than 20:1 the production of nitric oxides and carbon monoxide is considerably reduced and better fuel economy is obtained. However, emissions of hydrocarbons increase. There is, however, sufficient excess oxygen in the exhaust gas to enable those hydrocarbons to be removed simply by fitting an oxidation catalyst into the exhaust system. The lean-burn condition is achieved by encouraging turbulence in the engine's cylinders and by the propagation of a large flame area at the early stages of the combustion process. Heat losses from the engine are minimised by designing a combustion chamber with a minimum surface area:volume ratio.

1.3.3 Exhaust Gas Recirculation

Exhaust Gas Recirculation (EGR) as a method of nitrogen oxide control has been reported already[41,54-57]. EGR is a simple method of reducing oxides of nitrogen. Addition of exhaust gas, of which carbon dioxide and water vapour are major constituents, to the combustible mixture will lower the combustion temperature during the combustion process in the engine cylinder. Since the amount of nitric oxide produced in the engine cylinder from atmospheric nitrogen and oxygen increase exponentially with the combustion temperature, even a moderate decrease in temperature will result in a significant decrease in nitric oxide production.

1.3.4 Diesel Particulate Control

The diesel engine, because of its characteristically lean operation, has intrinsically low hydrocarbon and carbon monoxide emissions and has little trouble meeting the regulation standards. The major problem to be overcome in diesel exhaust emission control is that of particulates. Recent advances in engine technology have resulted in substantial reductions in particulate emissions. Further advances in engine control technologies will undoubtedly be made, but are unlikely to achieve the required reductions without the use of exhaust after-treatment systems of some sort.

These systems usually involve the use of an exhaust particulate filter and provide some means of filter regeneration by promoting the continous or periodic combustion of the collected particulate matter. Filtration or trapping is typically achieved by utilising either a ceramic wall flow filter or a wire mesh trap. Cleaning or regeneration of the particulate trap is required to maintain acceptable exhaust back pressure. This is typically achieved either by use of a burner to periodically raise the exhaust temperature above the ignition point of the trapped particulate ($\sim$600 $^{\circ}$C) and/ or by use of a catalyst to promote particulate combustion at lower and more easily achieved

temperatures. The published literature shows extensive reports of work on diesel particulate emissions[47,58-64].

Catalytic trap oxidisers have the disadvantage of requiring an active regeneration mechanism to remove particulate build-up. Recent advances in diesel engine technology have greatly reduced the formation of particulates, with the result that air quality standards might now be met by the use of flow-through catalyst monoliths[46,48,65,66]. These catalysts have the advantage of being passive systems which do not require regeneration.

1.3.5 Antismoke Additive

A very considerable amount of effort has gone into investigations of antismoke additives for diesel engines and their mode of operation[67-72]. When the additives were first introduced, it was thought that there were two possible mechanisms for their effectiveness. Either the additive could act as a dispersant, breaking down the soot particles into a finer form so that they were less visible, with no reduction in the total weight of soot emitted, or alternatively it could have an effect on the combustion process, actually reducing the total emission of soot as well as giving a reduction in visible smoke. Subsequent work has shown that this latter explanation is correct. Attention has been focused mainly on fuel additives containing barium as an active ingredient. These additives have demonstrated a dramatic effectiveness in reducing smoke from diesel engines.

1.4 ADDITIVES IN GASOLINE AND DIESEL FUEL COMBUSTION

A wide range of additives has been used by the petroleum manufacturers for both gasoline and diesel fuels and are more important today than they have ever been. This is due to a very significant change in the composition of both fuels over the past decade resulting from the phasing out of lead alkyls from gasoline and the depression of the fuel oil market. With the recent trend for

an increasing conversion of heavier material to lighter products, both gasoline and diesel now contain more cracked components than in the past. This means that the olefin content of these fuels has increased. Olefins are less stable with respect to oxidation than are the paraffinic and aromatic components and hence they are more likely to form deposits in a vehicle system. They also have a poorer cetane number.

The cetane number is the most universally accepted measure of the ignition quality of diesel fuels. The better the fuel quality, the higher the cetane number. The cetane number of a diesel fuel is determined by comparing its ignition quality with two reference fuel blends of known cetane numbers, n-cetane (n-hexanedecane), with a cetane number of 100, and heptamethyl nonane, whose cetane number is 15, under standard operating conditions. This is done by varying the compression ratio for the sample and each reference fuel to obtain a fixed delay period between the start of injection and ignition.

Most fuels therefore need additives in order to overcome their deficiencies. To compensate for the loss of lead alkyls, oxygenated components are also now widely used in gasoline, but this can cause a number of difficulties which must be overcome by use of the appropriate additives.

Owen[73] shows the many applications of gasoline and diesel fuel additives. In the gasoline engines, we can see some of the examples of the importance of additives in enhancing the oxidation stability and protecting the vehicle fuel systems. There are a large number of additives that can confer benefits before the fuel reaches the combustion chamber of an engine. These may be added to ensure that the gasoline does not deteriorate on storage, that it is free from problems during distribution and that deposit formation and corrosion do not occur in the fuel system of an engine.

Owen also discusses some of the additives which influence diesel fuel combustion. These additives consist of the cetane improvers, diesel detergents and smoke suppressants, which were mentioned earlier in the chapter. Combustion in the diesel engine is achieved by compression ignition. Rapid compression of air within the cylinders generates the heat required to ignite the fuel as it is injected. Cetane improvers are compounds which readily decompose to give free radicals and thus enhance the rate of chain initiation in diesel combustion, and hence improve the ignition characteristics. Chemical compounds such as alkyl nitrates, ether nitrates and dinitrates of polyethylene glycols are known as cetane improvers.

When molecular oxygen reacts with high molecular weight organic materials, such as hydrocarbons, radical chain reactions occur, leading to degradation. These reactions are usually unwelcome, and so they have been intensively investigated. Their general mechanistic features are now well known and can be illustrated as follows:

1   Chain initiation

$$R - H \longrightarrow R^{\bullet}$$

2   Chain propagation

$$R^{\bullet} + O_2 \longrightarrow R - O - O^{\bullet}$$

$$R - O - O^{\bullet} + R'H \longrightarrow R - O - OH + R''^{\bullet}$$

3   Chain termination

$$R^{\bullet} + R^{\bullet} \longrightarrow R - R$$

$$R - O - O^{\bullet} + R^{\bullet} \longrightarrow R - O - O - R$$

$$R - O - O^{\bullet} + AH \longrightarrow R - O - O - H + A^{\bullet}$$

In the initiation stage, free radicals are generated by the homolytic cleavage of a hydrocarbon bond. This can occur either thermally or due to the presence of oxygen. Once a hydrocarbon free radical ($R^{\bullet}$) is formed it can consume a molecule of oxygen to form a peroxide radical ($R-O-O^{\bullet}$), which in turn can

react with a further hydrocarbon molecule thereby generating another hydrocarbon free radical. The oxidation process is therefore self-perpetuating and is only terminated, in the absence of an anti-oxidant (AH), by reactions which lead to the removal of free radicals.

Ageing is the most commonly encountered oxidative degradation of organic materials under ambient conditions. To counter it small quantities of anti-oxidants are added to slow the rates of oxidation. Often they are complexes of transition metals which can cycle between different oxidation states and so intervene in electron transfer reactions, or which can coordinate to peroxides and cause peroxide decomposition. In a different context, at higher temperatures fire resistance and flame retardation of polymers are important. These metal-ion-based additives are often used, but their action can alter according to the conditions. Some additives can become pro-oxidants by catalysing the production of free radicals during peroxide decomposition. It is this feature which is of interest to the author and around which this research is based.

The aim of this research is to produce pro-oxidant additives and investigate their role in reducing the formation of partial oxidation products. The two goals of low emissions of exhaust pollutants coupled with improved fuel economy have resulted in world-wide research and development. Previous investigations involving the use of platinum group metals in internal combustion engines have led to the development of the catalytic converter for emissions reduction (see Chapter 7). Platinum-based catalyst systems have been used on motor vehicles solely to reduce exhaust emissions, by promoting oxidation/reduction processes in the exhaust gases after they have left the engine. Here, the author intend to describe investigations into the use of some high molecular weight materials containing metal ions as potential pro-oxidant additives.

The patent literature contains claims[74,75] that some organometallic additives produce an increase in the efficiency of diesel engines. The best improvements to date are claimed for complexes of platinum group metals. One patent[76] contains the claim that a fuel additive containing a platinum metal compound of the illustrated formula has increased the operating efficiency of internal combustion engines in terms of increased power output per unit of fuel burned, and reduced the emissions of particulates and noxious gases such as carbon monoxide and oxides of nitrogen.

M= platinum group metal

R= benzyl, phenyl or nitrobenzyl
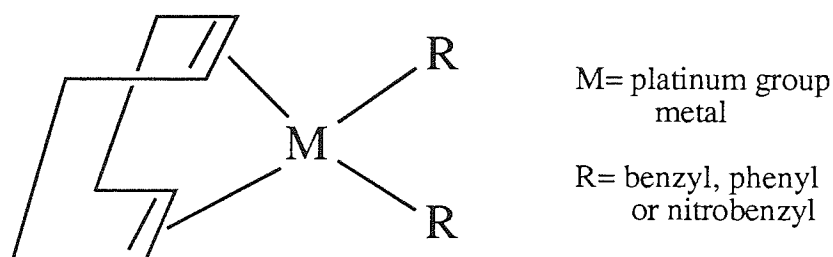
The trouble with platinum group metals is that in 1991, 34% of the Western world's demand for platinum and 83% for rhodium was already due to the use of "three-way" autocatalysts and was still rising. It seems impractical to develop another vehicular use from which the precious metals can not even be recovered. Also, if the additive is primarily intended to serve as pro-oxidant, platinum group metals are not the most obvious choice. Neither are the reported organic materials used as the carriers for the metals fully suitable. Therefore we seek a different range of additives.

From the chain reactions mentioned above, it can be seen that the primary product of alkane oxidation is hydroperoxide, ROOH, which can be a source of radicals by O-O fission. These reactions are extremely slow unless a free radical initiator is present. If we can produce a compound which will increase the production of free radicals during peroxide decomposition, this will enhance the oxidation process in the combustion chamber and eventually lead to an improved fuel efficiency.

Parshall[77] has reported that soluble metal complexes enhance the yields and selectivities of such oxidations, even though the catalytic complex often does not interact directly with either the oxygen or hydrocarbon. The major function of the metal complex in many oxidation processes is the catalytic decomposition of hydroperoxide. In this way the metal enhances the formation of desirable products and stimulates the production of free radical species that initiate the radical chain reaction between the hydrocarbon and oxygen. These two effects can provide substantial control over the yield and the rate of the overall oxidation process.

Parshall showed that the metal ions which have the greatest catalytic effect can exist in two different oxidation states and operate by the transfer of one electron. The two important reactions which accelerate alkyl hydroperoxide decom-position are shown by cobalt ions[78]. One involves the oxidation of cobalt(II) via the formation of a complex in which the hydroperoxide becomes a ligand on the cobalt ion:

$$Co^{II} + ROOH \longrightarrow [Co(HOOR)] \longrightarrow Co^{III} + RO^{\cdot} + OH^{-}$$

Electron transfer from cobalt to oxygen occurs after complexation. Weakening of the O-O bond facilitates breakdown of the complex and formation of the energetic alkoxy radical. In the second reaction cobalt(III) is reduced with formation of the more stable alkylperoxy radical.

$$Co^{III} + ROOH \longrightarrow Co^{II} + ROO^{\cdot} + H^{+}$$

The processes occur simultaneously in solution so that the net reaction is:

$$2ROOH \longrightarrow ROO^{\cdot} + RO^{\cdot} + H_2O$$

This results in an increase in oxidation efficiency which, if transferred to combustion, should lead to greater fuel efficiency and fewer pollutants formed by incompleted combustion.

Two likely modes of action for a successful additive are to provide pro-oxidants, and to continuously form small quantities of a heterogeneous

catalyst during combustion. The known effectiveness of platinum complexes is probably due to the second of these alternatives. Here we will concentrate on the lanthanides, especially cerium, as the metal ions in our systems. They could operate by either mechanism, and have existing uses related to the present problem. CeO_2 is used commercially in domestic "self-cleaning" ovens where it prevents the formation of tarry deposits, and was used in gas mantles as the best available catalyst for coal-gas combustion. The +3 oxidation state of cerium is characteristic of all the lanthanides, both in solid compounds and in solutions in water and other solvents, but important here is that cerium also has a +4 oxidation state, which it can easily attain. The high cost of the metal which would be a major drawback to the extensive use of the precious metals would not relate to cerium. Cerium is often called a "rare earth" element, but in reality cerium is not rare compared to a number of the elements that we usually consider to be common. It is the most abundant of the lanthanides. Industrially, mixed lanthanide oxides are used as catalysts in petroleum cracking and are known to catalyse the oxidation of CO even by nitrogen oxides[79]. Therefore the lanthanides are an obvious group of elements to try in this context.

Having established which metals to study, it is then necessary to select suitable ligands for complexation. A fuel additive must yield a stable solution in the fuel tank. That is, it should not react with the air, water and rust that are always present. The research target should focus on the synthesis of hydrocarbon-soluble complexes that might exhibit unusually slow rates of ligand substitution. For materials containing metal ions, these properties are best met by using multi-dentate ligands that form neutral complexes and by the use of highly sterically hindered ligands.

Multi-dentate ligands, those that form more than one bond to a metal, almost always have greater stability constants than do unidentates, and often dissociate from metal more slowly. That is because dissociation occurs one

bond at a time, and so after partial dissociation a chelate ligand is still held to the metal and has a much greater chance of recombination. Slower rates of dissociation are not always found, e.g. if the ligand is flexible the presence of H^+ in solution can enhance dissociation by protonating the free donor atom and allowing it to rotate away from the proximity of the metal. This phenomenon is seen, for example, with the ligand 2,2'-bipyridyl. Increases in the steric crowding around the central metal have the effect of slowing the substitution reactions. This type of ligand should be ideal in providing the large stability constants for reaction of the metal ions and the lipophilic-like solubility that are obviously needed for fuel additives. However, since we should not aim to increase the NOx or SOx exhaust emissions of vehicles, additives containing significant amounts of N and S should be avoided. Some suitable ligands are already known, containing for example carboxylic acid and beta-diketone units. The following ligands were chosen as they fitted some or all the above requirements necessary to make suitable metal additives. The author approached this research by attempting to synthesise the cerium and other metal complexes using the following ligands (i) acetylacetone and it derivatives; (ii) Schiff-base ligands and (iii) macrocyclic polyamines ligands.

In the next chapter, the author describe all the methods that were used to synthesise the ligands and their complexes, and also to characterise any unknown compounds by using Infra-red and Nuclear Magnetic Resonance techniques. At this point, it is also important to stress that the metal complexes must have some thermal stability, as diesel fuel is often pre-heated immediately prior to its combustion. Therefore the effect of heat on additives must be important. The investigation of this is described in Chapter 3 with the use of a differential thermal analysis instrument.

The remaining chapters deal with engine testing, to assess the actual pro-oxidant role of the metal additives produced. In Chapter 4, the additives were

tested on a small scale in the laboratory using a diesel combustion bomb, simulating the combustion process in the direct injection diesel engine. In Chapters 5 and 6, descriptions are given of the testing of the additives on diesel and gasoline engines respectively. There was not sufficient time in this project to undertake a full investigation of the combustion process, as was originally hoped.

However, enough data were collected for the purpose of this thesis. Chapter 6 also gives a brief account of the role of the lanthanide metals, especially cerium, as oxidation catalysts for the after treatment of the exhaust gases, and at the same time as pro-oxidant additives in the fuel.

Chapter 2

"Synthesis and Characterisation of the Ligands and Their Metal Complexes"

2.1 INTRODUCTION

This chapter describes all the methods that were used by the author to synthesise the ligands and their metal complexes. All the synthetic methods used are either from past workers (which are mentioned later on) or from the authors own work. Spectroscopic evidence such as Infra-red (IR) and Nuclear Magnetic Resonance (NMR) have been used in the analysis of the products where possible. So, this chapter deals only with the initial part of the investigation, i.e. all the chemical aspects of the synthesised metal complexes.

Infra-red Spectroscopy

The study of IR spectra gives information on the various functional groups and bonds in molecules. The energy of most molecular vibrations correspond to that in the infra-red region of the electromagnetic spectrum. The usual range of an IR spectrum is between 4000 cm^{-1} at the high frequency and 600 cm^{-1} at the low frequency end, but in this research it was possible to go down as far as 220 cm^{-1} due to the equipment available to us at Aston.

Functional groups can be identified by their characteristic vibrational frequencies, which makes the IR spectrum the simplest, most rapid and often most reliable means of assigning a compound to its class. Vibrations of functional group are either stretching, bending, rocking, twisting or wagging in character.

Reports involving the IR spectroscopic studies of cerium chelate compounds are very few. Bunzli and Wessner[80], have reported on the IR spectra of cerium nitrates with 15-Crown-5 and 18-Crown-6 ethers. Adam and co-workers[81] made a detailed investigation of cerium ion and some salicylidene aromatic Schiff bases. They have assigned the absorption band of -OH stretching at 3400 cm^{-1} and the stretching of C=N and C-O at 1620 cm^{-1} and

1320-1270 cm^{-1} respectively. The absorption bands of M-L varied between 570-455 cm^{-1}. Randecka-Paryzek[82], has reported on a Hexa-aza 18-membered macrocyclic complex of Cerium (III).

Nuclear Magnetic Resonance Spectroscopy

NMR studies have provided us with information concerning the structure, bonding, and chemical exchange of the compounds. This technique involves the absorption of electromagnetic radiation in the radio-frequency region of the spectrum which results in changes in the orientation of spinning nuclei in a magnetic field.

The physical foundation of NMR spectroscopy lies in the magnetic properties of atomic nuclei. The transitions involved in NMR spectroscopy are between the spin states of nuclei with non-zero nuclear magnetic moments. When nuclei which possess magnetic moments (i.e. have spin greater than zero) are placed in an external field, the nuclear moments are oriented with respect to the field, leading to a nuclear energy level diagram i.e. stationary states and excited states. In the case of a hydrogen nucleus, two orientations of the rotating magnetic vector are possible, one oriented with the external field and the other against it. Through a high-frequency transmitter, transitions between states within the energy level diagram can be stimulated. The absorption of energy can be detected, amplified and recorded as a spectral line, the so-called resonance signal.

The amount of structural information given by an NMR spectrum is greatly enhanced by two factors. Firstly, the exact position of resonance is determined by the chemical environment of the nucleus. The proton magnetic resonance spectrum of an organic compound may therefore show several absorption bands, each corresponding to a particular proton or group of protons.

Secondly, a given band may be split into several peaks as a result of interactions between neighbouring nuclei. The two effects give rise to what are termed the chemical shift and spin-spin coupling or splitting. A third useful feature of the spectrum is the integrated area of an absorption peak which is directly proportional to the number of nuclei responsible for the signal. This facilitates structural correlations and provides a means of quantitative analysis.

All NMR spectra display lines with a certain width, i.e. absorption bands are seen rather than discrete lines. The NMR technique has a characteristic minimum line width which is governed by the nature of the de-excitation processes involved. This occurs because the energies of the excited states are not precisely defined, but cover a range which depends on the time-scale of the de-excitation process. The time-scales are usually expressed as half-lives, $t_{1/2}$, i.e. the time during which a 50% reduction in population occurs. Similarly, the energy range and the line width are measured as a half-width, ΔE, which is the difference between the upper and lower energies corresponding to 50% of the maximum intensity. Thus, the longer the half-life, the more sharply defined is the energy and the narrower the absorption line. Since the energies involved in NMR are quite modest, other de-excitation mechanisms become possible. The two most common involve imparting the energy to the surrounding molecules, spin-lattice relaxation, or sharing it with other nearby spin systems, spin-spin relaxation. The presence of paramagnetic centres induces shifts and nuclear spin relaxation, with consequent broadening of the lines.

Cerium and iron metals are paramagnetic; therefore paramagnetic broadening and shifting are present in these metal complexes and while assignments are not seriously in doubt, some can not be proved. It was decided against using NMR for studying the metal complex compounds prepared, but it was used on the free organic ligands of the compounds.

2.2 MATERIALS AND INSTRUMENTS

2.2.1 Chemicals

All chemicals were obtained from the usual commercial sources, i.e. Aldrich Chemical Company, Lancaster Synthesis, and Johnson Matthey PLC. The chemicals supplied were used without further purification.

2.2.2 Solvents

All solvents were obtained from the same commercial sources as above and were used directly without any further purification with the exception of tetrahydrofuran (THF). THF solvent was distilled over Na/benzophenone prior to use.

2.2.3 Infra-red Spectroscopy

IR absorption spectra were recorded on a Perkin-Elmer 1710 Infra-red Fourier Transform (FTIR) spectrometer which covers the range 4000-220 cm^{-1}. The spectra were recorded from samples prepared as potassium bromide (KBr) discs. A rough indication of the absorption intensity in the IR table is given by the symbol (s)- strong; (m)- medium; (w)- weak and (br)- broad.

2.2.4 Nuclear Magnetic Resonance Spectroscopy

All ^{1}H and ^{13}C NMR spectra displayed in this chapter were taken on a Bruker AC300 MHz FTNMR spectrometer. ^{13}C NMR spectra were recorded with the aid of software known as the J-modulated spin-echo sequence. This allows identification of the different types of carbon atoms more clearly, and can be seen on the ^{13}C NMR spectra where peak inversion of methylene and quaternary carbons occurs, i.e. CH_3 & CH peaks point up (+); CH_2 & C peaks point down (-). All ^{13}C NMR spectra are proton decoupled so that each absorption appears as a sharp singlet. The spectra of samples were recorded in $CDCl_3$, D_2O, or DMSO solution with tetramethylsilane (TMS) as internal standard.

2.2.5 Melting Points

The melting points of solid compounds were determined using a Gallenkamp Melting point apparatus which is heated electrically and the temperature recorded using a mercury thermometer.

2.2.6 pH Measurements

All pH measurements were obtained using a Corning 220 pH meter equipped with a Corning plastic-body combination electrode. It has a temperature range of 0-100 °C and measures pH from 0-14.

2.2.7 Thin Layer Chromatography (TLC)

TLC on silica was used to determine the number of species present in certain solutions and the chromatograms were developed with iodine. Silica plates were prepared by cutting out the required size (12x5 cm) from a ready to use thin-layers and the origin lines were applied on these plates (2 cm from the bottom of the plate). The developing solvent (1:1 of ether:hexane) was poured into the chromatographic tank to a depth of about 0.5 cm and the lid

was replaced. A prepared plate was applied with various sample 'spots' on to the origin line using a micropipette. The dry plate was placed into the tank, replaced the lid and allowed the chromatogram to run for about 30 mins. The tank was lined with sheet of filter paper which dip into the solvent in the base of the tank, this ensures that the chamber is saturated with solvent vapour. The plate was then removed and placed in another tank containing iodine tablets to locate the positions of the separated solutes.

2.2.8 Elemental Micro-Analysis

Elemental Micro-Analysis for carbon, hydrogen, and nitrogen were performed by Medac Ltd, Middlesex.

SECTION (A) : SYNTHESIS OF ACETYLACETONE DERIVATIVE METAL COMPLEXES AND THE PATENTED PLATINUM COMPLEX

2.3 SYNTHESIS AND CHARACTERISATION OF TRIS-(ACETYLACETON-ATE)-CERIUM(III), [Ce(acac)₃]

2.3.1 Introduction

A common approach in this kind of research is to begin by studying simpler systems and one of the simplest and most widely available ligands is acetylacetone or 2,4-pentanedione (acacH). It is important because if its complexes are successful as additives, then one must think of the cost of manufacture and of the availability of the reagents. Acetylacetone is a good chelating ligand and also able to provide a neutral complex. The fact that it is relatively non-polar, enhances its ability to dissolve in hydrocarbons. Acetylacetone exists in solution as equilibrium mixtures of two isomeric forms, the keto and the enol forms (scheme 2.1).

Scheme 2.1
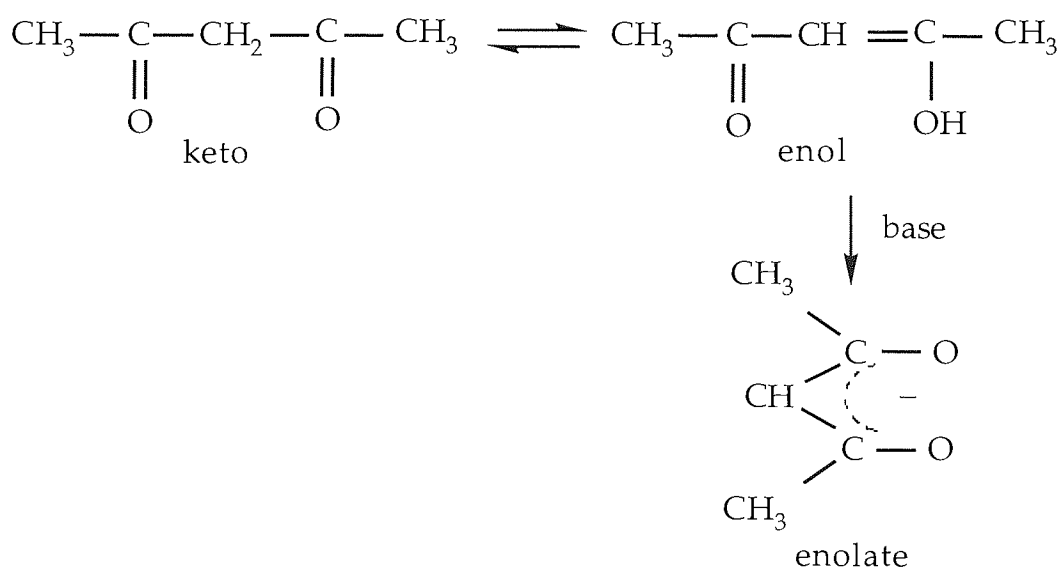
Reaction occurs by way of the less stable enolate form and enolisation is subjected to base catalysis. In aqueous solutions base attacks the molecule, removing a proton α to the carbonyl group, to give enolate ion. It is this anion of acetylacetone which reacts with metal ion to give the metal complex.

$$\left[\left(\begin{array}{c} CH_3 \\ \diagdown \\ CH \diagup ^{C-O} _{\diagdown _{C-O}} \diagup \\ CH_3 \end{array} M^{n+} \right)_x \right]^{n-x}$$
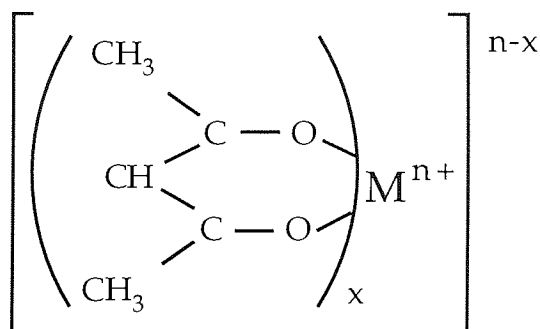
Morgan and Drew[83] were among the first people to study the coordination of the metal with acetylacetone. Many compounds of metal ions with acetylacetone are now known. The structures, types, properties, uses, nomenclature, and general methods of preparation of metal derivatives of acetylacetone are discussed in Inorganic Syntheses[84,85]. Uitert and Fernelius[86] were the first to study complex formation between the acetylacetone and cerium ions, but for this study a simpler method shown in Inorganic Syntheses[87] was followed.

With the exception of cerium, all other metal acetylacetonate complexes used for additive testing in Chapter 4 were bought directly from commercial sources, because of their availability and low cost.

2.3.2 Preparation of Tris-(acetylacetonate)-Cerium(III), [Ce(acac)$_3$]

The general reaction of synthesis as described in reference 87 is,

$$Ce(NO_3)_3.6H_2O + 3C_5H_8O_2 + 3NH_3 \longrightarrow Ce(C_5H_8O_2) + 3NH_4NO_3$$
$$+ 6H_2O$$
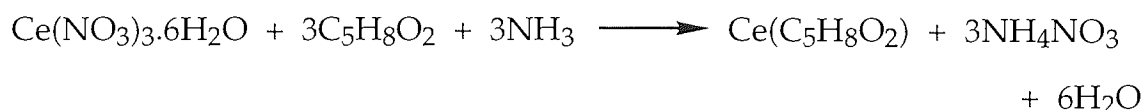
A solution containing cerium (III) nitrate hexahydrate (5.4 g, 0.013 mol) in 15 ml of 2.8M nitric acid was added, and stirred, to a second solution containing 6 ml of acetylacetone in 18 ml of 2M ammonia. The pH of the mixture was then brought up to 6.0 by dropwise addition of 2M ammonia. The mixture was stirred overnight.

The yellow precipitate of hydrated $Ce(acac)_3$ was filtered using suction on a Buchner funnel, and washed with three 25 ml portions of water before being dried in air at room temperature. Yield 5.33 g, 84%; m.p. 130-133 °C, lit m.p. 131-134 °C.

Anal: Calcd. for $CeC_{15}H_{21}O_6$. $4H_2O$: C,35.36; H,5.74%

Found: C,35.13; H,5.60%

2.3.3 Results and Discussion

The IR spectrum of this hydrated $Ce(acac)_3$ shows all the bands required for the chemical structure of the compound, and it also corresponds with literature data. All the peak assignments are shown in Table 2.1.

The product contains water molecules. This contributes to the light yellow colour of the crystals but when the water molecules are removed it changes to orange. Dehydration was not completed because it was left to dry in air. In the structure, water is bonded very strongly to $Ce(acac)_3$. Elemental analytical results show strong evidence that water is present in the cerium compound. Calculation shows there to be four water molecules per complex.

The melting point was slightly lower (130-133 °C) than the quoted value (131-134 °C) , but it is very difficult to follow the exact melting point because of the colour changes. The orange crystals decompose above 150 °C to a black colour crystal but do not melt until above 220 °C.

Table 2.1 IR Spectral Data for Ce(acac)$_3$

Wavenumber/ cm^{-1}	Assignment
3600-3100 (br)	-OH stretch of water
3010 (w)	-CH stretch
2970-2930 (w)	-CH stretch of methyl group
1600-1530 (s)	combination of C-C & C-O
1385-1360 (s)	CH$_3$ symmetrical deformation
1265 (m)	C-CH$_3$ & C-C
1020 (m)	CH$_3$ stretch
925 (m)	C-C & C-O
785-765 (m)	-CH stretch
660 (w)	C-CH$_3$, ring def. & M-O
535 (w)	ring def. & M-O
420-395 (w)	ring deformation

2.4 SYNTHESIS AND CHARACTERISATION OF TRIS-(DIPIVALOYLMETH-ANATO)-CERIUM(III), [Ce(DPM)$_3$]

2.4.1 Introduction

Having successfully prepared Ce(acac)$_3$, it was found that the compound is insoluble in some organic solvents and also in commercial fuels. To solve this problem, hydrocarbon chains must be added to the organic ligand. Adams and Hauser[88] described a method of preparing sterically hindered β-diketones of 2,2,6,6-tetramethyl-3,5-heptanedione or dipivaloylmethane (DPM), with a structure shown on the next page,

R'=R= $(CH_3)_3C$
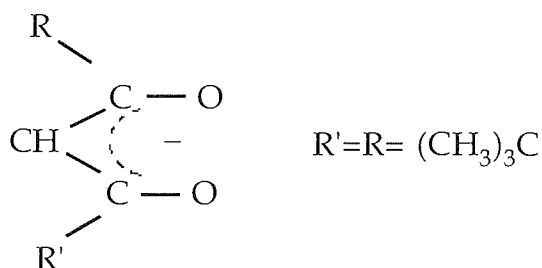
Dipivaloylmethane behaves in the same way as acetylacetone when reacting with metal ions. Dipivaloylmethanato chelates are remarkably soluble in a wide range of organic solvents including benzene and petroleum ether. Such properties would be expected as an extension of those of acetylacetonates. The hydrocarbon-like properties of metal chelates with this ligand are greatly increased, probably because the polar, metal-oxygen bonds are buried within a thicker hydrocarbon envelope.

On the assumption of these properties, it was then decided to synthesis the cerium complex of this ligand. It might be suitable in the hydrocarbon environment of the fuels. The metal complex was prepared using an adopted method described by Hammon[89].

2.4.2 Preparation of Dipivaloylmethane, [DPM-H]

Methyl pivalate (15 g, 0.13 mol) and sodium hydride (12 g) dispersed in mineral oil were added to dimethoxyethane (200 ml) in a 500 ml flask. The mixture was stirred with a magnetic stirrer and brought to the reflux temperature. A solution of pinacolone (13 g) in dimethoxyethane (20 ml) was added from a dropping funnel over a 2 hour period. Gas was evolved during the addition. Then concentrated hydrochloric acid (30 ml) was added as rapidly as possible to the mixture. The suspension became clear and a fine white precipitate was formed toward the end of the addition. The mixture was then cooled and poured into water (500 ml). Pentane (500 ml) was added, the mixture shaken and allowed to settle before the organic layer was

separated and then washed with five 100 ml portions of water. Finally it was concentrated by distillation.

Vacuum distillation was used to extract the concentrate through a 10-inch Vigreux column at 6 mmHg and was collected at 73-75 °C. Yield 12.36 g, 52%.

2.4.2.1 Preparation of Tris-(dipivaloylmethanato)-Cerium, [Ce(DPM)$_3$]

Ce(DPM)$_3$ was prepared by adding a solution of cerium (III) perchlorate (0.54g; 0.001mol) dissolved in distilled water (5 ml) to a second solution of dipivaloylmethane (1.25; 0.006mol) in excess and sodium hydroxide (0.24 g) dissolved in ethanol (25 ml). The mixture was stirred to give a yellow solution. Then the pH of the mixture was adjusted to 8 using a solution of 0.1M NaOH. A brown precipitate was formed immediately at this pH. The product was filtered, washed with 50% ethanol (25 ml) solution followed by water (25 ml), and dried over P_2O_5 in a desiccator for 24 hours. Yield 0.63 g, 91%; m.p.: 265-267 °C.

<div align="center">

Anal: Calcd. for $CeC_{33}H_{57}O_6$: C,57.45; H,8.33%

Found: C,57.52; H,8.41%

</div>

2.4.3 Results and Discussion

Dipivaloylmethane, [DPM -H]

An IR spectrum of DPM was obtained and all the peaks were assigned as shown in Table 2.2. The IR table for acac⁻ and DPM-H shows similaries between DPM-H and acacH with only one exception, this is the band of tertiary butyl group. The $C(CH_3)_3$ band of DPM was assigned at 1360 cm⁻¹, which matched up with literature value. The rest of the bands are roughly the same as acetylacetone bands. Therefore, the band assignments supports the proposed structure of the ligand DPM-H.

Table 2.2 IR Spectral Data for DPM-H

Wavenumber/ cm^{-1}	Assignment
2960 (s)	-CH stretch of methyl group
2925-2860 (m)	-CH stretch
1600 (br)	combination of C-C & C-O
1475-1455 (s)	CH$_3$ deformation
1360 (s)	C-CH$_3$ sym. defs.
1285-1120 (m)	C-O stretch
870 (m)	C-C & C-O stretch
790-730 (m)	-CH stretch

Figure 2.1 shows a ^{1}H NMR spectrum of DPM-H in CDCl$_3$ with TMS as reference standard. A sharp strong three-proton signal at 1.03 ppm is due to the protons of the six methyl groups. A sharp proton signal at 5.60 ppm is due to the proton of the methine (-CH-) group. The chemical shift of this group has been shifted down field. The reason for this is probably due to the existance of both the keto and the enol forms of this compound;
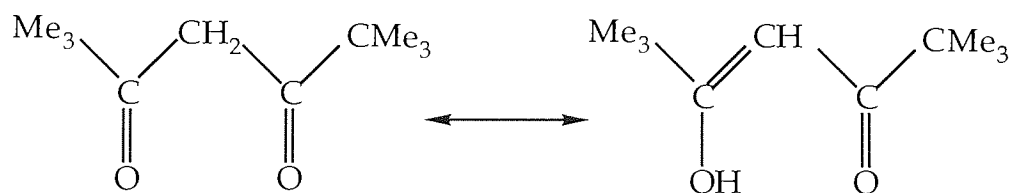
This is because proton chemical shifts are directly influenced by the electronegativity of adjacent groups. In the resonance structure, the oxygen electronegative substituents withdraw electron-density from the proton. This reduces the local magnetic field at the proton. Thus shielding of the proton is decreased and the signal is shifted down field. This would explain the
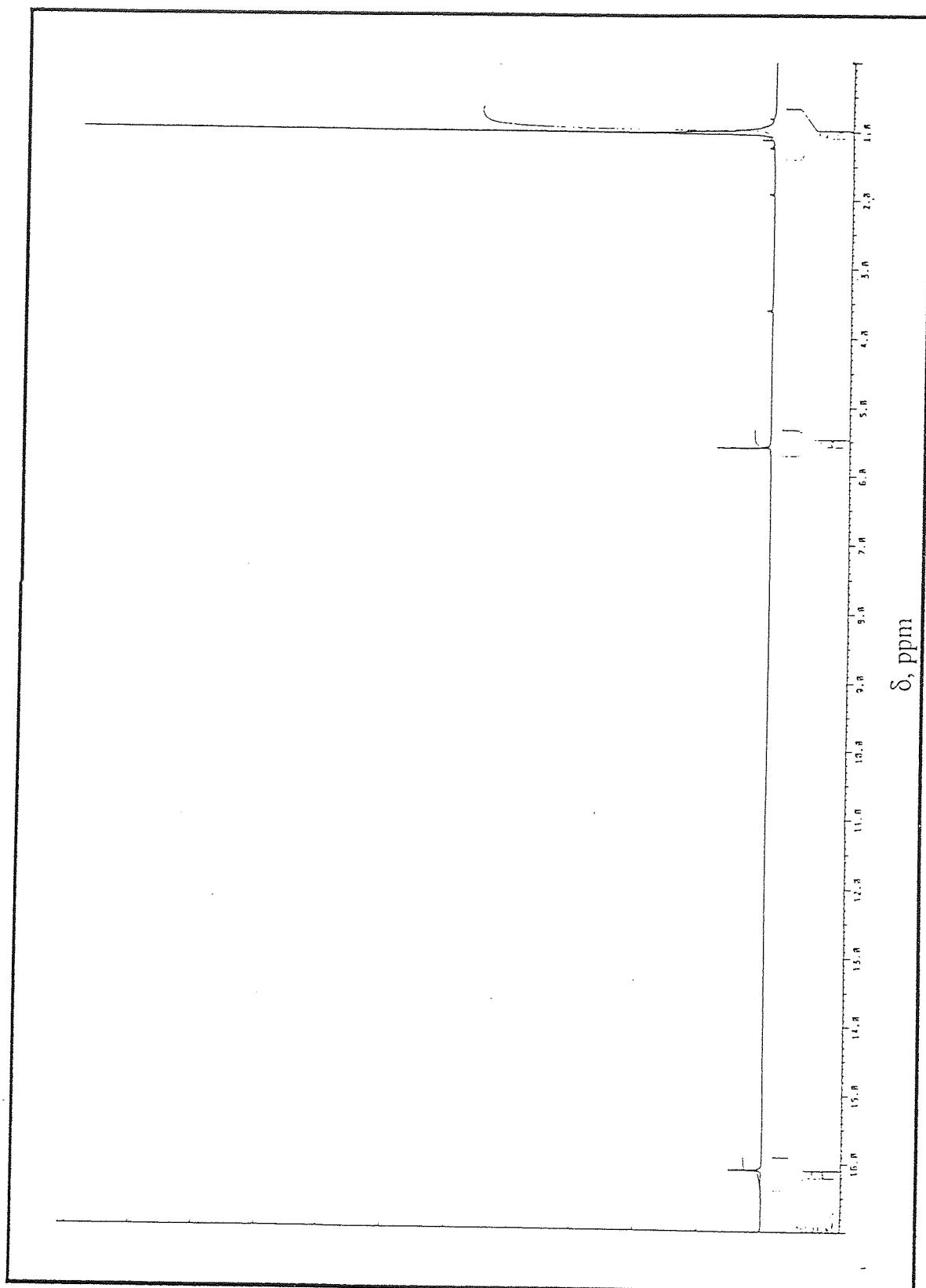
Figure 2.1 1H NMR Spectrum of Dipivaloylmethane

δ, ppm
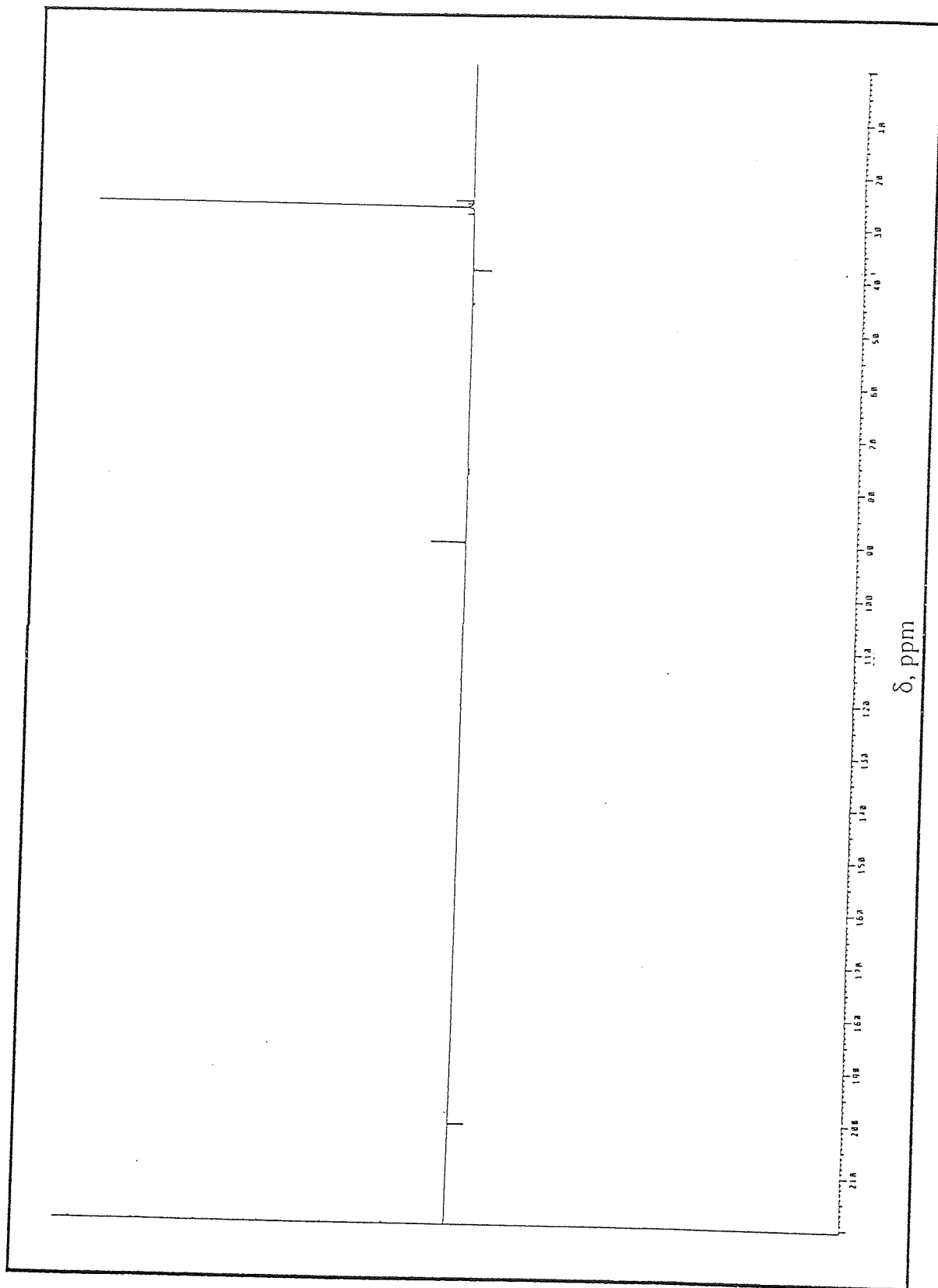
Figure 2.2 ^{13}C NMR Spectrum of Dipivaloylmethane

chemical shift of the -CH- group at 5.60 ppm. A sharp signal at 16.10 ppm is due to the proton of the OH group. The low field shift of the acidic proton is caused by hydrogen bonding. The ^{1}H NMR clearly indicates the enol form as the favourable structure, since the peaks for the keto form are virtually non-existance.

However, in the ^{13}C NMR spectrum (Figure 2.2) a small signal at 44.57 ppm can be clearly seen, which supports the ^{1}H NMR evidence for a small proportion of the compound structure exists as the keto as compared to the enol form. All the signals in this spectrum fully support the assignment of the above proton groups. From both spectra, it appears that all the data confirmed the ligand structures to be correct. Dipivaloylmethane exists as a resonance structure between the keto and the enol form, but mainly as enol.

Tris-(dipivaloylmethanato)-cerium (III), [Ce(DPM)3]

Table 2.3 IR Spectral Data of Ce(DPM)3

Wavenumber/ cm^{-1}	Assignment
2960 (s)	-CH stretch of methyl group
2925-2860 (m)	-CH stretch
1590-1500 (s)	combination of C-C & C-O
1400-1355 (s)	C-CH$_3$ sym. defs.
1250-1140 (s)	C-O stretch
870-800 (m)	C-C & C-O stretch
770-740 (m)	-CH stretch
600 (m)	M-O & ring def.
485-410 (m)	M-O & ring def
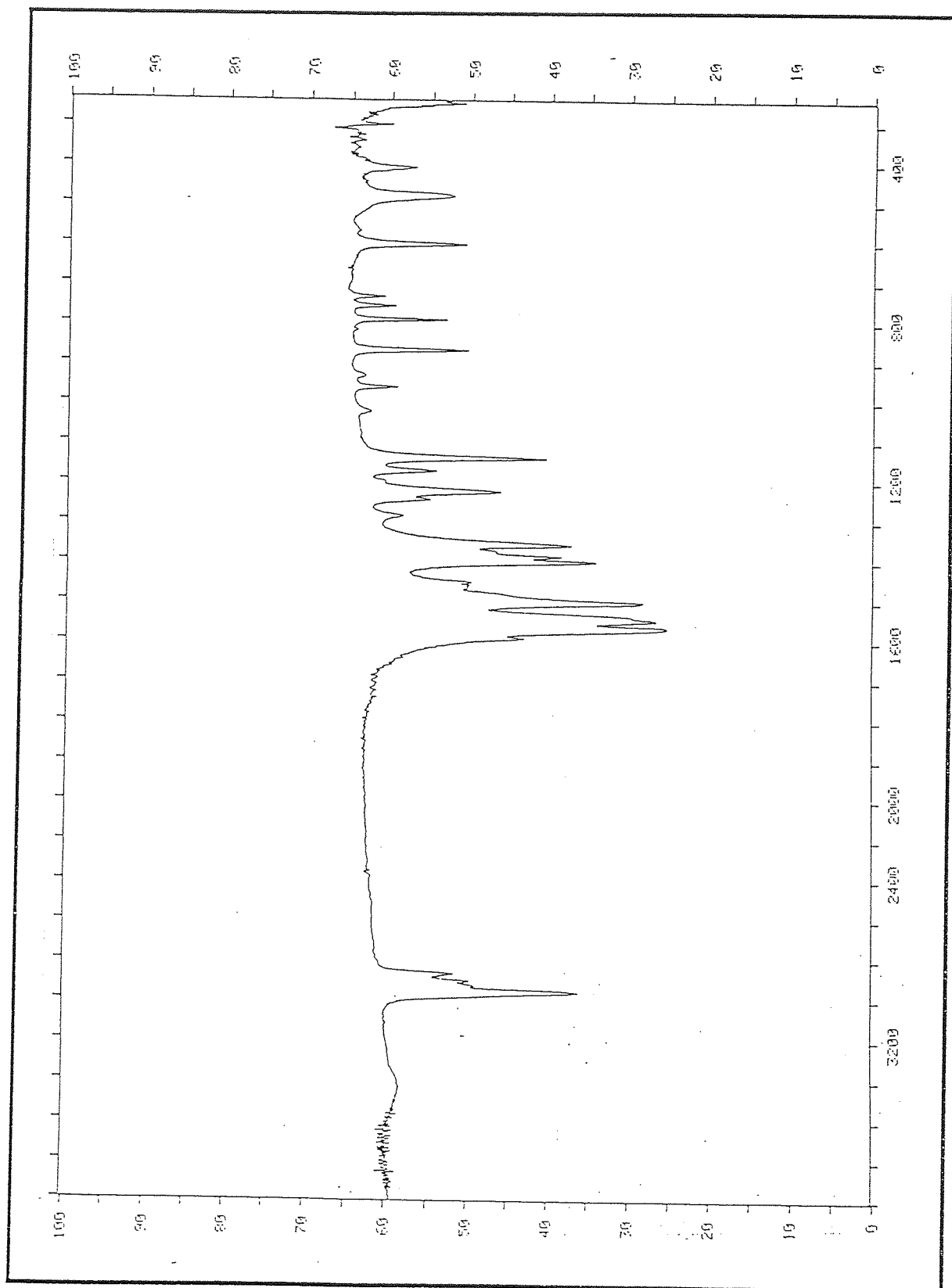
Figure 2.3 IR Spectrum of Tris-(dipivaloylmethanato)-Cerium (III)

The IR spectrum (Figure 2.3) of Ce(DPM)$_3$ is similar to the spectrum of the free ligand, but with the exception of the OH band in cerium compound. The coordination of the cerium ion to the ligand appears to shift the C-O and C-C stretching bands to lower frequencies (Table 2.3). Absorption bands below 600 cm^{-1} indicate that the metal ion is bonded to the ligand, thus being responsible for the ring deformation bands, which derive from the formation of a six membered ring.

Elemental analytical results for carbon and hydrogen gave good support to the identification of the product as Ce(DPM)$_3$. The data are almost identical to the expected data.

The Ce(DPM)$_3$ complex is remarkably soluble in a wide range of organic solvents and also soluble in commercial fuels, which is a significant factor. These results indicate the first successful attempt at synthesising a cerium complex suitable for testing as a fuel additive. The high melting point indicates this cerium complex to be stable to oxidation, which is required of any component to be added to the contents of a fuel tank.

The same method was used to synthesise other lanthanide metal complexes of the same ligand, specifically of lanthanum and europium.

2.5 SYNTHESIS OF BISMETHYL-(1,5-CYCLOOCTADIENE)-PLATINUM(II) [Pt(CH$_3$)$_2$(COD)]
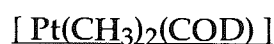
2.5.1 Introduction

The last chapter deals with a compound of the above formula which is reported to improve fuel efficiency and reduce the level of pollutants in exhaust emission gases. On the basis of this claim it would therefore provide a good reference point when trying out the diesel combustion bomb (see

Chapter 4). It was decided to synthesise this platinum complex on the information given by the patent holders.

Kistner and co-workers[90] were the first to report the preparation of such an organo-platinum compound in 1963, but here an improved synthetic route by Clark and Manzer[91] was used. It describes the preparation of the above compound in a three stage synthesis from K_2PtCl_4 with 98%, 98%, and 82% yields.

2.5.2 Preparation of Pt(CH$_3$)$_2$(COD)

(i) PtI$_2$(COD)

n-propanol (22 ml) was added to a solution of K_2PtCl_4 (2 g) in distilled water (30 ml). Also to this mixture, 1,5-cyclooctadiene (4 ml) and $SnCl_2$ (0.03 g), were added. The mixture was magnetically stirred for two days after which time a white solid was formed. The mixture was filtered, washed with distilled water (20 ml) and ethanol (10 ml), then air-dried. This gave a yield of 1.8 g (100%) for $PtCl_2$(COD). The dichloride was readily converted to the diiodide in 93% yield by the addition of a slight excess of NaI (1.5 g) to a suspension of $PtCl_2$(COD) in acetone. The solution immediately turned yellow and the acetone was removed by rotary evaporation. The residue was collected on a sinter and washed three times with 15 ml portions of distilled water and air-dried. This gave a yield of 2.5 g.

(ii) Pt(CH$_3$)$_2$(COD)

A slight excess of methyllithium (14 ml of a 1M solution in diethyl ether) was added to an ice-cold solution of PtI_2(COD) (2.5 g) in diethyl ether (25 ml), under nitrogen. The solution was stirred for 2 hrs and hydrolysed at 0°C with an ice-cold saturated aqueous solution of ammonium chloride. The ether

layer was separated and the aqueous layer extracted with three 20 ml portions of diethyl ether. The ether fractions were dried over anhydrous magnesium sulphate containing a small amount of activated charcoal. The mixture was filtered and the ether removed by rotary evaporation to give crystals of $Pt(CH_3)_2(COD)$. Yield 0.67 g, 45%; m.p. 93-95 ^{o}C, lit. m.p. 94-95 ^{o}C.

Anal: Cald for $Pt(CH_3)_2(COD)$: C,36.03; H,5.44%

Found: C,36.32; H,5.28%

2.5.3 Results and Discussion

Elemental analytical results and melting point evidence suggested the final product to be $Pt(CH_3)_2(COD)$. The chemistry of this compound has already been discussed in detail in reference 78, and is not described here. The final yield was of 45% rather than the literature claim of 87%. Even though the experiments were performed carefully, the author could not produce the desired final yield of the product as claimed by Clark and Manzer. A reason could be that the scale of their reaction was much larger, thus more chances of recovery during extractions and filtration. Due to cost restrictions their scale was not possible here.

SECTION (B): SYNTHESIS OF SCHIFF BASE LIGANDS AND THEIR METAL COMPLEXES

2.6 SYNTHESIS AND CHARACTERISATION OF N,N',N"-TRIS(SALICYL-ALDEHYDE)-TRIS-2-AMINOETHYLIMINE METAL COMPLEXES

2.6.1 Introduction

The preparation of cerium chelate compounds of Schiff bases was the next stage of the synthetic programme for metal complex fuel additives. Having worked with acetylacetone and its derivative, Schiff base ligands seemed to be

the next logical stage in the sequence of these ligands; for example Schiff bases derived from acetylacetone,

$$CH_3-C=N-(CH_2)_2-N=C-CH_3$$
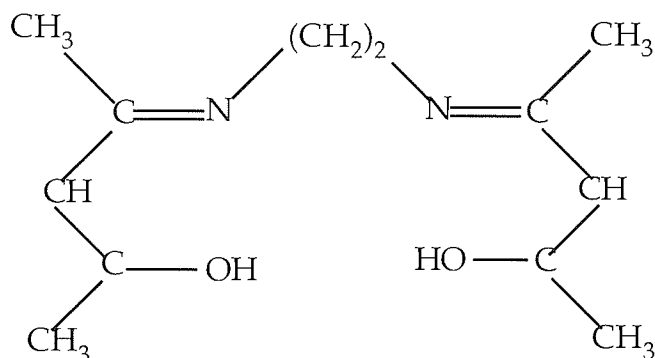
Schiff base is the general name used to describe N-substituted imines, which are produced by the condensation reaction of an aldehyde or a ketone with a primary amine.

Cerium(III) has already been established as the first choice core metal ion, so the Schiff bases used here must be able to accommodate the +3 charge, and to produce a neutral complex. One of these ligands can derive from the reaction between salicylaldehyde and tris-2-aminoethylamine. The product of this reaction is N,N',N"-tris-(salicylaldehyde)-tris-2-aminoethylimine or H$_3$saltren. This is an acidic (three OH groups), hexa- or hepta- dentate (4N3O) ligand. In reactions, the OH groups can deprotonate to form bonds with metal ions, therefore permitting the formation of neutral complexes. At the time of the synthesis of the cerium complex of this ligand there was no report of any such metal complex in the literature. However, a report has been published recently on the synthesis of lanthanide complexes of H$_3$saltren ligand[92].

2.6.2 Preparation of N,N',N"-tris-(salicylaldehyde)-tris-2-aminoethylimine

Tris(2-aminoethyl)amine (1.5 ml, 0.01mol) was added to a solution of salicylaldehyde (5.3 ml, 0.05 mol) dissolved in ethanol (30 ml). The mixture was stirred vigorously with a magnetic stirrer and yellow crystals formed

immediately. The yellow crystalline product was filtered, washed with ethanol (25 ml), and dried over silica gel in a desiccator for 24 hours. The product was recrystallised from methanol, but could be used without recrystallisation since the product is pure enough. Yield 4.1 g, 90%; m.p. 92-93 $^{\circ}$C.

$$\text{Anal: Cald for } C_{27}H_{30}N_4O_3: \text{ C,70.72; H,6.59; N,12.22\%}$$

$$\text{Found: C,71.26; H,6.59; N,12.13\%}$$

2.6.2.1 Preparation of N,N',N"-tris(salicylaldehyde)-tris-2-aminoethylimine Cerium (III), [Ce-saltren]

A solution of cerium perchlorate hexahydrate (0.55 g, 0.001 mol) in water (10 ml) was added to a solution containing saltren (0.46 g, 0.001 mol) dissolved in methanol (30 ml). The mixture was stirred and the pH was increased to 8 using a solution of 0.1M NaOH when a brown precipitate was formed. The mixture was then filtered, washed with methanol and finally dried in an oven at 60 $^{\circ}$C. Yield 0.56 g, 93%.

$$\text{Anal: Cald for } CeC_{27}H_{27}N_4O_3.2H_2O: \text{ C,51.67; H, 4.98; N,8.93\%}$$

$$\text{Found: C,51.42; H,4.65; N,8.88\%}$$

2.6.2.2 Preparation of N,N',N"-tris(salicylaldehyde)-tris-2-aminoethylimine Iron (III), [Fe-saltren]

A solution of FeCl$_3$ (0.16 g, 0.001 mol) dissolved in water (10 ml) was added to a second solution containing saltren (0.46 g, 0.001 mol) which was dissolved in methanol (30 ml). The mixture was stirred while the pH was adjusted to 6 by dropwise addition of 0.1M NaOH solution; deep purple micro-crystals were gradually formed. The purple crystalline mixture was filtered, washed with methanol, and dried in an oven at 60 $^{\circ}$C. Yield 0.47 g, 92%.

Anal: Cald for $FeC_{27}H_{27}N_4O_3$: C,63.42; H,5.32; N,10.96%

Found: C,63.13; H,5.33; N10.95%

2.6.3 Results and Discussion

Scheme 2.2
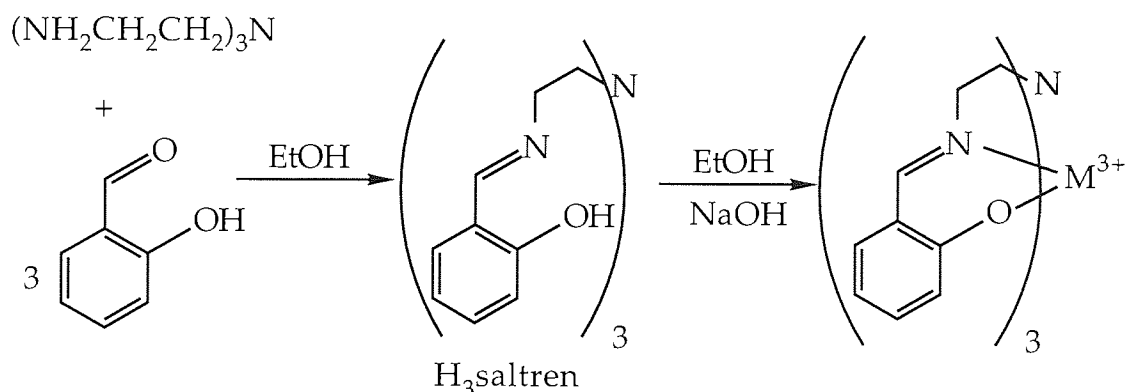
$H_3saltren$

H$_3$saltren

As with any newly synthesised organic compounds, the above ligand product was investigated using the conventional methods of IR and NMR spectroscopy to determine the structure. An IR spectrum of saltren was recorded (Fig. 2.4) and its bands were assigned (Table 2.4).

The fact that no absorptions occurred in the region 1715-1695 cm^{-1} indicates that the aldehyde group no longer exists in the compound; therefore reaction has taken place between the aldehyde and the triamine reagents. The absorption band at 1635 cm^{-1} indicates C=N (imine) group in the compound, thus proving that a condensation reaction has taken place in the reaction mixture. Characterisation of the product was further supported by the ^{1}H NMR spectrum. The ^{1}H NMR spectrum (Fig. 2.5) shows the absence of an amine group,therefore all the amine groups had reacted. All peaks from the spectrum were assigned and shown in Table 2.5.

Table 2.4 IR Spectral Data for H₃saltren

Wavenumber/ cm⁻¹	Assignment
3055-3004 (w)	Aryl C-H stretching
2940-2893 (m)	saturated -CH stretching
2817 (s)	-CH stretching of $N-CH_2$
1635 (vs)	C=N stretching
1611-1500 (m)	Aromatic rings
1460-1431 (m)	C-H deformation
1338 (m)	OH bending
1279-1026 (m)	C-OH stretching
775-756 (s)	1,2-disubstituted aromatic C-H, out of plane deformation

Table 2.5 ¹H NMR Spectral Data for H₃saltren

Chemical Shift (ppm)	Signal Assignment
2.79 (t, 6H)	$N-CH_2$
3.49 (t, 6H)	$=N-CH_2-$
6.05 (d, 3H)	C-H of Aryl
6.57 (t, 3H)	C-H of Aryl
6.90 (d, 3H)	C-H of Aryl
7.24 (t, 3H)	C-H of Aryl
7.78 (t, 3H)	CH=N
13.76 (s, 3H)	C-OH
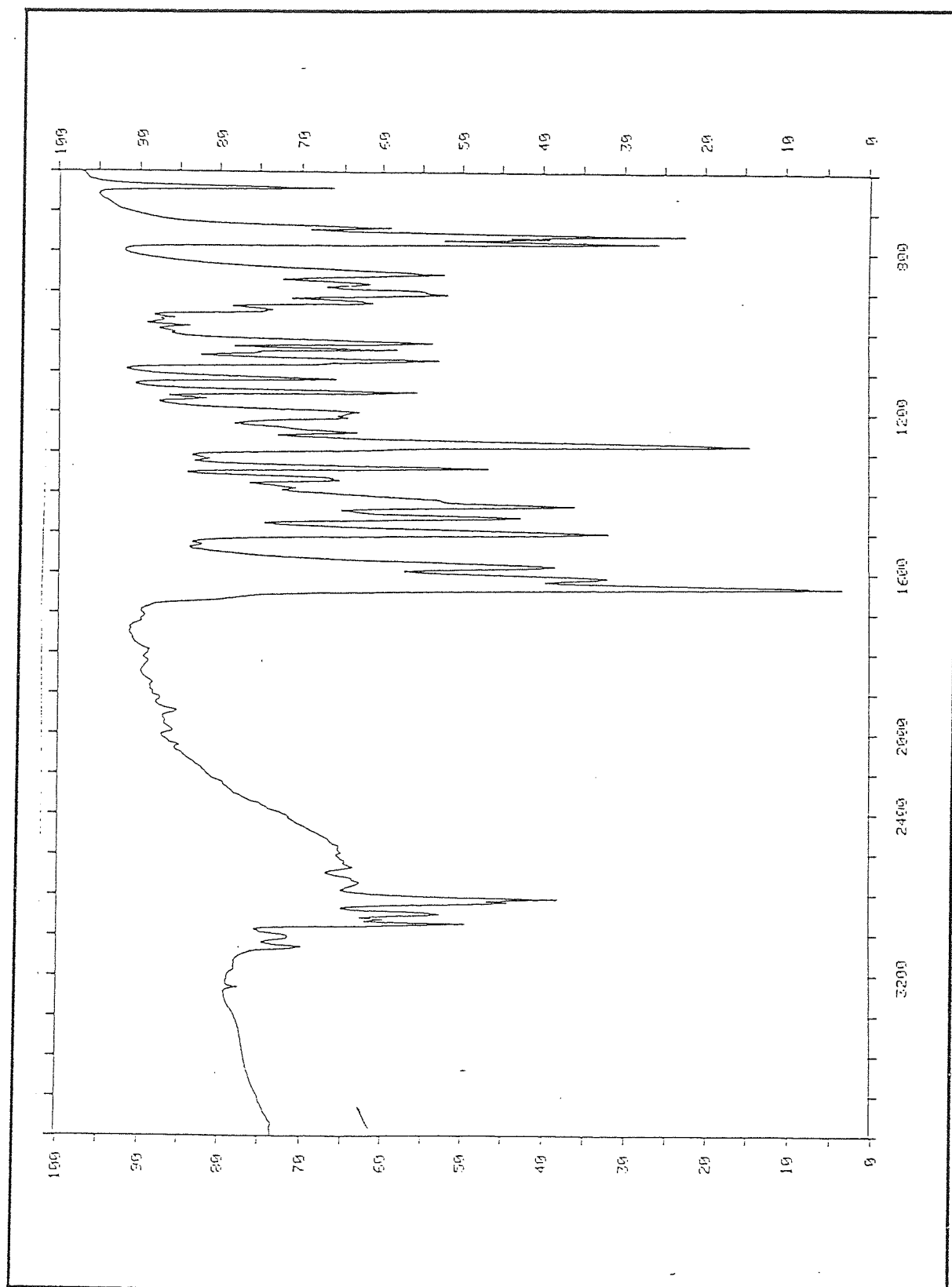
Figure 2.4 IR Spectrum of N,N',N'-Tris-(salicylaldehyde)-tris-2-aminoethylimine
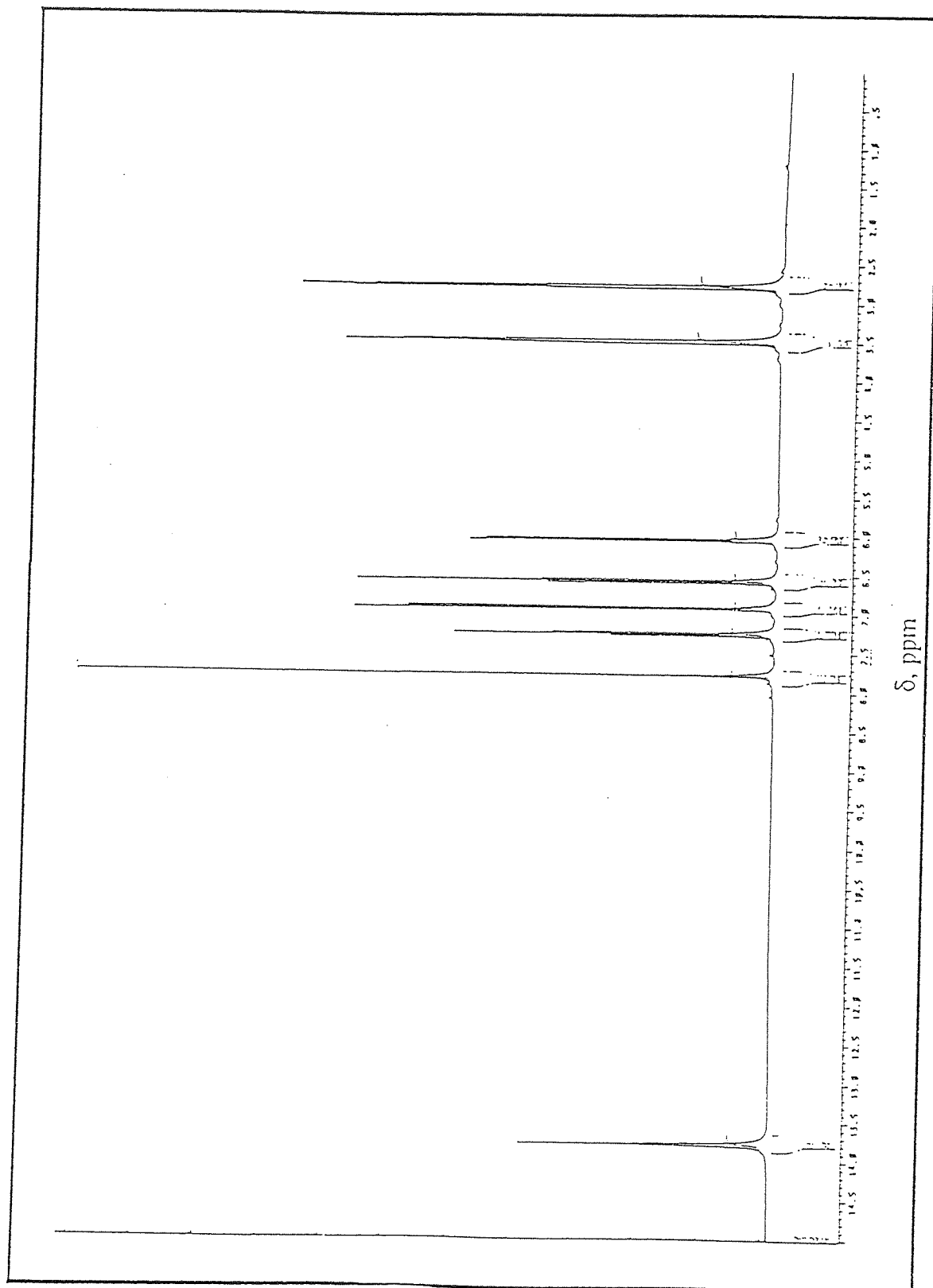
Figure 2.5 ^{1}H NMR Spectrum of N,N',N'-Tris-(salicylaldehyde)-tris-2-aminoethylimine

δ, ppm

The results from both techniques indicate that saltren has been successfully synthesised and the final proof comes from the results of elemental analysis. Therefore the structure is
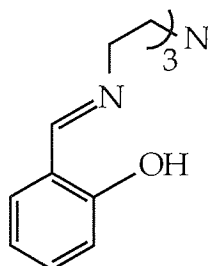
The saltren Schiff base ligand was easily prepared from the reaction of tris(2-aminoethyl)amine with three equivalent of salicylaldehyde. The reaction was catalysed by a mild acid. The first stage was a nucleophilic addition to the carbonyl group (see Scheme 2.3). Rapid proton transfer gave the product of the net addition of RNH_2 to C=O, a carbinolamine (such a substance is generally so reactive that it can not normally be isolated). A second acid-catalysed reaction occurred in which water was eliminated from the carbinolamine. The resulting product is the imine.

Scheme 2.3

carbinolamine

imine
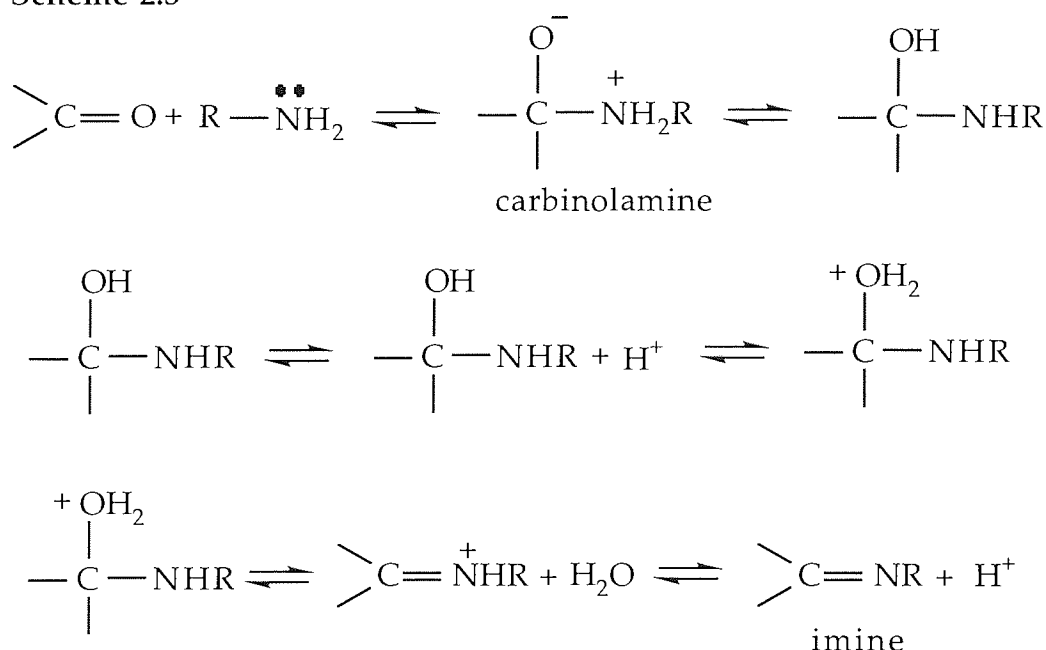
Ce-saltren

Having successfully prepared the free ligand, it was then necessary to investigate its coordination to the cerium (III) ion. Figure 2.6 shows the IR spectrum of the cerium complex of this ligand. The bands were assigned as shown in Table 2.6.

By comparing the IR spectrum of the cerium chelate product with the free ligand, the similarity of the bands between the two spectra can be observed, with the exception of those for water and metal chelate. The frequencies of the cerium complex spectrum has shifted slightly to lower frequencies compared to those of the free ligand. This indicates that cerium metal ions are coordinated to the free ligands, giving small changes of frequencies due to the influence of M-L bond. The absorption band of C=N has shifted from 1635 cm^{-1} to 1625 cm^{-1} in complex suggests cerium ion is not only coordinated to the negative charged oxygen but also chelates with the nitrogen atoms of the ligand. Absorption bands in the region below 600 cm^{-1} suggest ring formation between metal ion, oxygen, and nitrogen atoms, as a six membered ring. Elemental analytical results show that the cerium complex compound is associated with 2 water molecules, which explains the broad water absorption band in the region of 3440 cm^{-1}. The absorption bands of the spectrum cover all the functional groups required for the structure as do the analytical data.

It was noticed that the reaction to form a neutral metal complex only occurs under very basic conditions i.e. above pH 8. Earlier attempts to synthesis the complex showed that under neutral or acidic condition, cerium ions undergo reactions which retain the original anions in the product. Therefore producing an ionic metal complex which will be insoluble in hydrocarbon fuels has no value in this investigation. Subsequently, it was discovered that the neutral cerium metal complex is also insoluble in all

Figure 2.6 IR Spectrum of N,N',N'-Tris-(salicylaldehyde)-tris-2-aminoethylimine-Cerium (III)

common organic solvents, and only slightly soluble in tetrahydrofuran and acetone.

Inspection of the structure of Ce-saltren from molecular modelling reveals that the hexadentate capability of the ligand has been realised by removing the three "acidic" phenolic protons, with the formation of trigonal prismatic geometry. It appears that coordination to the central cerium ion is via all three phenolic oxygens and all three imine nitrogens. This strange stereochemistry arises from the steric constraints of saltren.
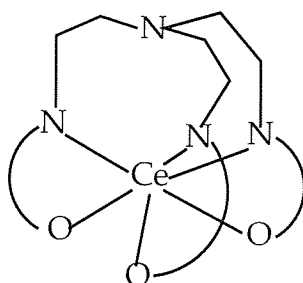
Table 2.6 IR Spectral Data for Ce-saltren

Wavenumber/ cm^{-1}	Assignment
3436 (br)	OH of water
3056-3018 (w)	Aryl C-H stretching
2887-2856 (m)	saturated -CH stretching
1625 (s)	C=N stretching
1595-1542 (m)	Aromatic rings
1471-1446 (s)	C-H deformation
1306-1032 (m)	C-OH stretching
758 (s)	1,2-disubstituted aromatic C-H, out of plane deformation
595 (m)	M-O
281 (m)	M-O

Fe-saltren

Again the similarity of absorption bands between the iron complex and the free ligand on the IR spectra can be observed clearly, as is the case with Ce-saltren (Table 2.7). The only real difference is in the Fe-O bands due to the different strength of metal-ligand bonding between iron and cerium ions. IR spectra of the metal complexes and the free ligand all contain a strong vibration band in the region of 1640-620 cm^{-1}, which is characteristic of the imine (C=N) stretching vibration of the Schiff base. In Fe-saltren spectrum, this band is at a lower wavenumber than the free ligand, indicative of coordination to the three imine groups, thus showing a hexa-dentate ligand. Elemental analysis provides support for the IR results.

Table 2.7 IR Spectral Data for Fe-saltren

Wavenumber/ cm^{-1}	Assignment
3052-3021 (w)	Aryl C-H stretching
2957-2865 (m)	saturated -CH stretching
1621 (s)	C=N stretching
1537 (m)	Aromatic rings
1479 (s)	C-H deformation
1318-1046 (m)	C-OH stretching
749 (s)	1,2-disubstituted aromatic C-H, out of plane deformation
531 (m)	M-O
442 (m)	M-O

In conclusion, lanthanide metal complexes of saltren ligand were easily prepared using the above method with methanol and under basic conditions. Reaction of saltren ligand with lanthanide metal and iron ions yields trigonal prismatic complexes. All metal complexes are virtually insoluble in all common solvents, polar and non-polar. Only slight solubility is found with acetone and THF solvents for these metal complexes.

The structure of such metal-saltren complexes has not been fully resolved which is partly due to the inability to use NMR analysis because of the paramagnetic nature of such complexes. It would thus be useful to try and produce a diamagnetic complex so that NMR analysis can be carried out. This would allow a detailed examination of the coordinated Schiff base making it possible to determine whether any carbon or proton resonances undergo shifting as a result of coordination.

2.7 SYNTHESIS AND CHARACTERISATION OF N,N',N''-TRIS(2-HYDR--OXY-1-NAPHTHALDEHYDE)-TRIS-2-AMINOETHYLIMINE METAL COMPLEXES

2.7.1 Introduction

Since metal complexes of saltren are insoluble in most solvents and fuels, further steps must be taken to increase their solubility. A likely way to increase the solubility in hydrocarbon solvents is to increase the hydrocarbon weight of the ligand. One such existing hydroxy-aldehyde which has a higher molecular weight than salicylaldehyde is 2-hydroxy-1-naphthaldehyde. This chemical compound is available commercially.

The reaction between the aldehyde and the trisamine in Scheme 2.4 would be

expected to follow the usual Schiff base formation reaction, i.e the condensation reaction, to give a Schiff base and a water molecule.

Scheme 2.4
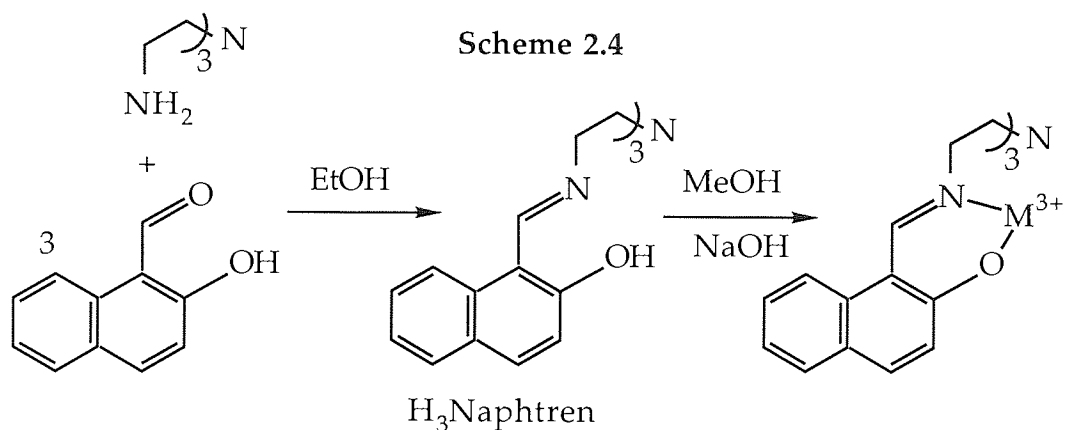
H₃Naphtren

2.7.2 Preparation of N,N',N''-tris(2-hydroxy-1-naphthaldehyde)-tris-2-amino ethylimine, [H₃naphtren]

An excess of 2-hydroxy-1-naphthaldehyde (6.0 g, 0.035 mol) was dissolved in hot ethanol (50 ml) and to this solution was added tris(2-aminoethyl)amine (1.46 g, 0.01 mol) A yellow precipitate formed immediately after the addition of amine to the solution. The mixture was stirred for 1 hr at around 60-70 °C, during which time more ethanol was added to compensate for any losses through evaporation, and then the mixture was stirred for another hour at room temperature. The yellow product was filtered off, washed with ethanol, and dried in an oven at 60 °C. Yield 5.2 g, 85%; m.p. 194-196 °C.

Anal: Cald. for $C_{39}H_{36}N_4O_3$: C,76.95; H,5.96; N,9.20%

Found: C,76.84; H,5.99; N,8.99%

2.7.2.1 Preparation of N,N',N''-tris(2-hydroxy-1-naphthaldehyde)-tris-2-aminoethylimine Cerium (III), Ce-naphtren

A mixture containing H₃naphtren (0.61 g, 0.001 mol) and cerium(III) nitrate hexahydrate (0.43 g, 0.001 mol) in methanol (50 ml) was refluxed for 12 hrs during which time the pH of the solution was maintained at 8 by the

dropwise addition of 0.1M NaOH solution. When cooled, the brown crystals were filtered off, washed with methanol, and dried in an oven at 60 °C. Yield 0.65 g, 87%.

Anal: Cald. for $CeC_{39}H_{33}N_4O_3.2H_2O$: C,59.91; H,4.77; N,7.16%

Found: C,58.21; H,4.31; N,7.16%

2.7.2.2 Preparation of N,N',N"-tris(2-hydroxy-1-naphthaldehyde)-tris-2-aminoethylimine Iron (III), Fe-naphtren

The above procedure was repeated for the synthesis of Fe-naphtren but with a maintained pH of 7. The reaction gave a purple solid as the product, as was found in the Fe-saltren reaction. Yield 0.43 g, 65%.

Anal: Cald for $FeC_{39}H_{33}N_4O_3.H_2O$: C,68.93; H5.19; N,8.24%

Found: C,68.79; H,4.86; N,7.61%

2.7.3 Results and Discussion

H3naphtren

Figure 2.7 shows the ^1H NMR spectrum of H3naphtren and the assignment of the peaks is listed in Table 2.8. Clearly the spectrum shows the absence of the NH_2 and the aldehydic proton signals which would be in the region of 9-10 ppm, thus indicating that a condensation reaction has taken place. The phenolic resonance signal at 13.47 ppm in $CDCl_3$ and DMSO was lost when D_2O was added to the solvent. In this ligand, the phenolic resonance signal is much further downfield than expected when compared with that of phenol (7.45 ppm). The shift downfield is explained by the hydrogen bonding of the phenolic OH with an unsaturated azomethine nitrogen, causing a decrease in the shielding at the hydroxy hydrogen, and also from the nearby aromatic rings. The phenolic OH is therefore susceptible to deshielding effects from the induced aromatic ring current.

The ^{13}C NMR spectrum (Fig. 2.8), in conjunction with ^{1}H NMR evidence confirms the structure of the H₃naphtren ligand, showing all the expected types of carbon atom. The strong infra-red band observed at 1635 cm^{-1} (characteristic of C=N band), also indicates that H₃naphtren has been successfully produced.

Table 2.8 ^{1}H NMR Spectral Data for H₃naphtren
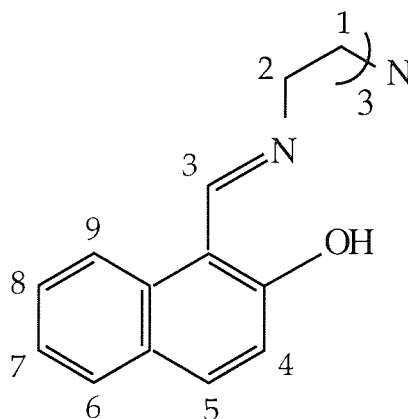
Chemical Shift (ppm)		Signal Assignment	
2.37	(t, 6H)	N-CH$_2$	(H1)
2.99	(t, 6H)	=N-CH$_2$-	(H2)
5.94	(d, 3H)	C-H of Aryl	(H5)
6.34	(t, 3H)	C-H of Aryl	(H7)
6.51	(t, 3H)	C-H of Aryl	(H8)
6.72	(m, 3H)	C-H of Aryl	(H6)
6.78	(m, 3H)	C-H of Aryl	(H9)
7.14	(d, 3H)	C-H of Aryl	(H4)
8.18	(s, 3H)	CH=N	(H 3)
13.47	(s, 3H)	O-H	

Figure 2.7 ^{1}H NMR Spectrum of N,N',N'-Tris-(2-hydroxy-1-naphthaldehyde)-tris-2-aminoethylimine
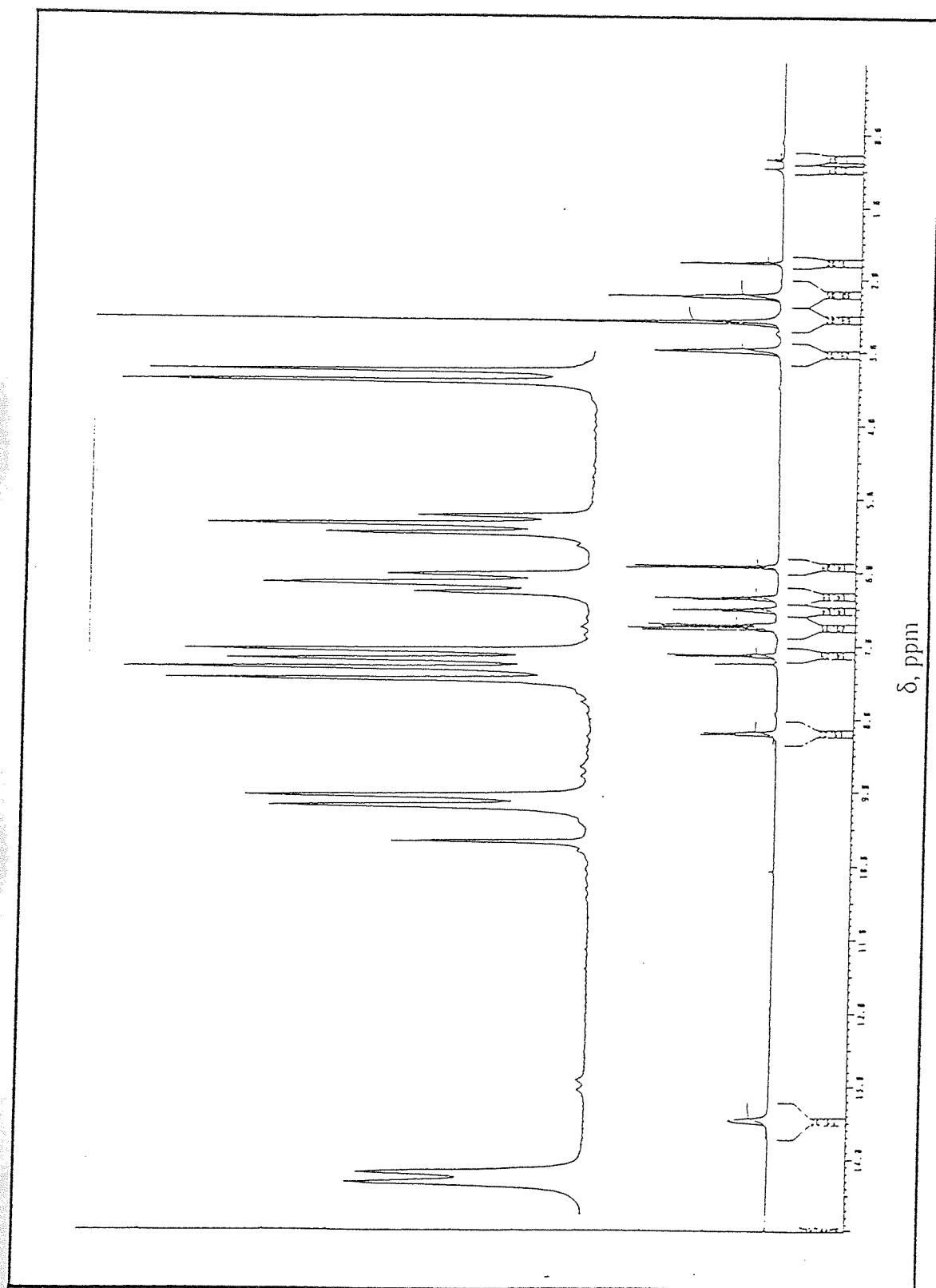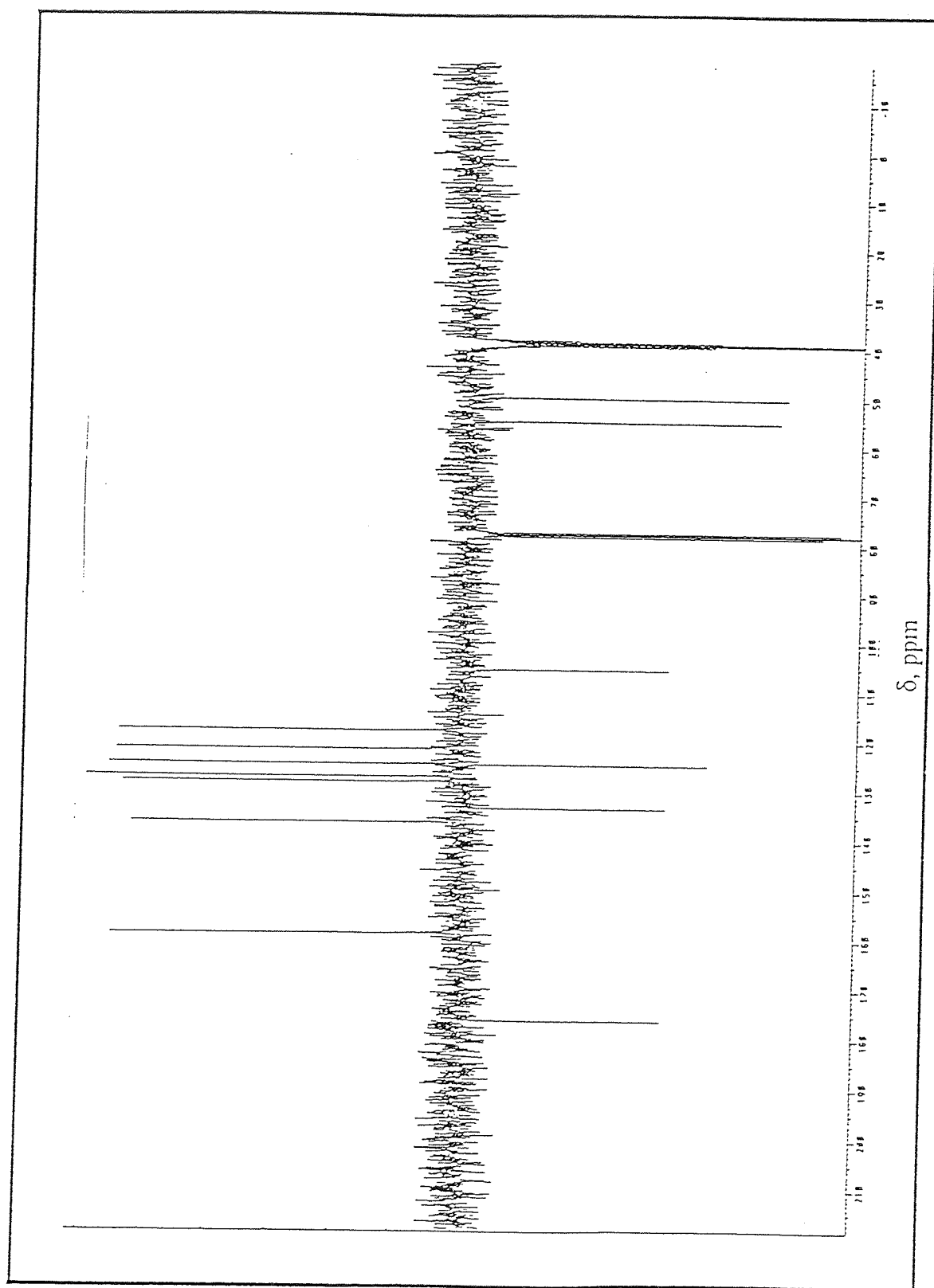
Figure 2.8 13C NMR Spectrum of N,N',N'-Tris-(2-hydroxy-1-naphthaldehyde)-tris-2-aminoethylimine
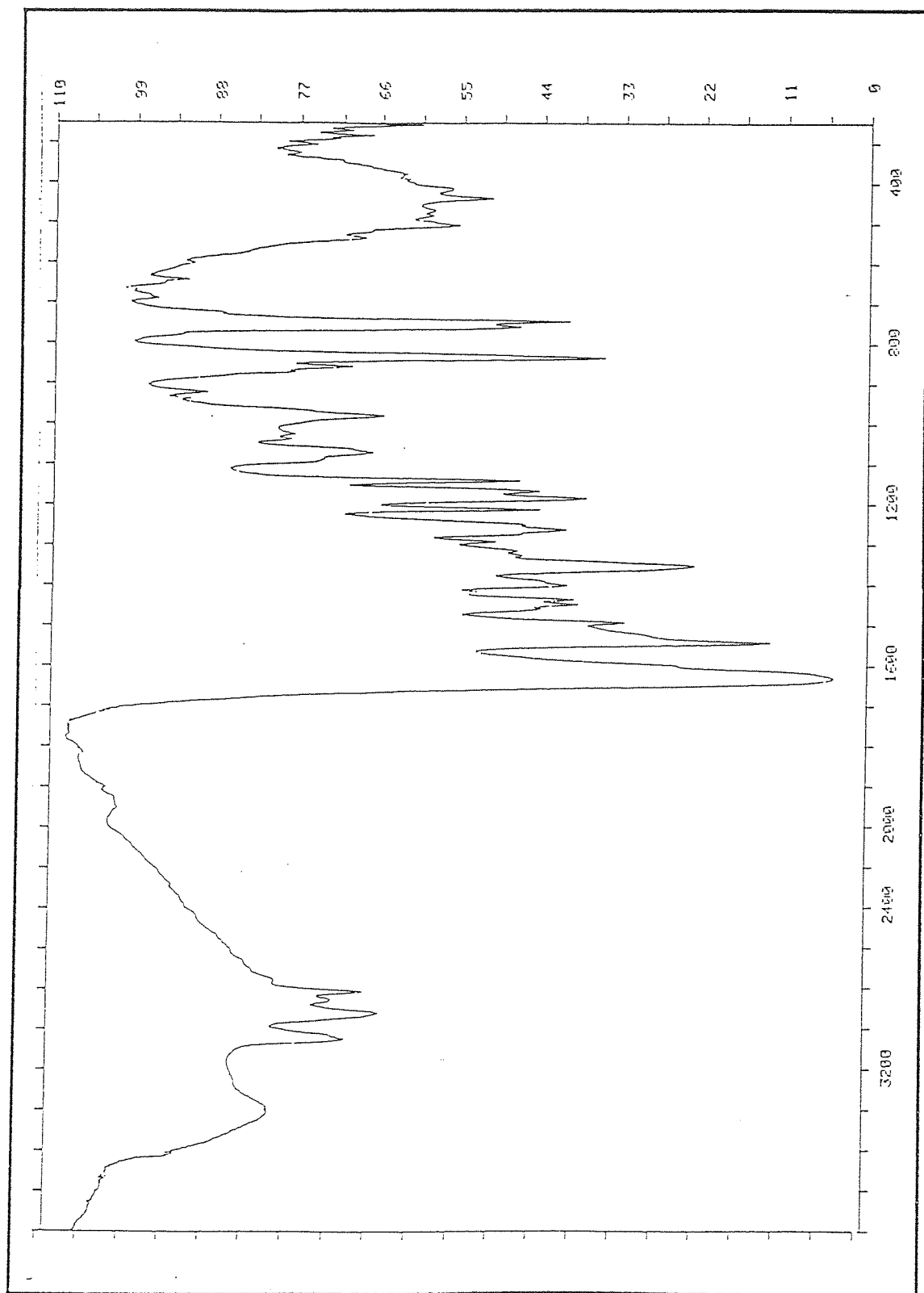
Figure 2.9 IR Spectrum of Ce-naphtren
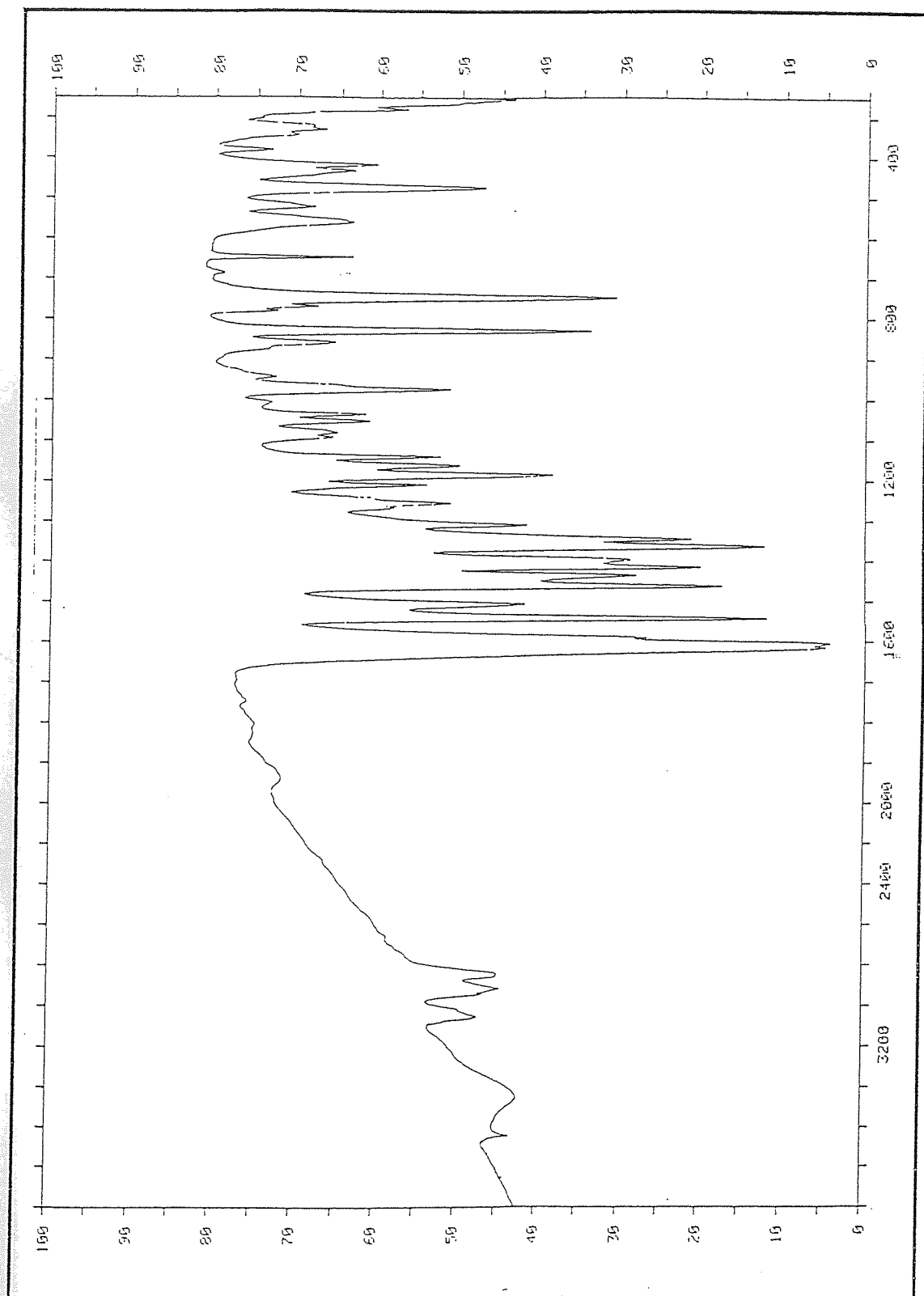
Figure 2.10 IR Spectrum of Fe-naphtren

Ce-naphtren

The IR spectrum of this compound (Fig. 2.9) contains a strong band at 1631 cm^{-1} which may be assigned to the C=N stretching vibration. Complexation was accompanied by a shift to a slightly lower frequency of this band. The C-O (phenolic) stretching vibration bands were observed in the region 1350-1260 cm^{-1}. In addition to these bands, there is also a series of bands in the region 1250-1140 cm^{-1} which may be assigned to H_2C-N stretching vibrations. The position of these bands remains largely unchanged upon coordination of the ligand to cerium.

Bands characteristic of C-H deformation for the two-substituted naphthalene rings are observed in the range 835-740 cm^{-1} for the Ce-naphtren complex. The C-C stretching bands are observed in the regions 1600-1500 cm^{-1} and 1490 cm^{-1}, while C-H stretches (aliphatic) are observed in the range 2940-2865 cm^{-1}. In addition the complex spectrum exhibits strong bands at 504 cm^{-1}, 437 cm^{-1}, and 413 cm^{-1} due to Ce-O stretching vibrations. Lastly, there is a broad band at 3442 cm^{-1} due to water in the spectrum of the cerium complex. Elemental analytical data obtained, also show that water molecules are present in the cerium compound at a 2:1 ratio.

Fe-naphtren

Figure 2.10 shows the IR spectrum of Fe-naphtren, and again the similarities between the spectra of the iron and cerium complexes can be clearly seen. A weak band at 3053 cm^{-1} can be assigned for the C-H stretching vibration of the aryl groups of the ligand, while C-H stretches (aliphatic) are observed in the range 2920-2850 cm^{-1}. The imine structure of the ligand is clearly indicated by the intense and well resolved (C=N) bands in the range 1615-1604 cm^{-1}. Again complexation has shifted this band to a lower frequency. The rest of the bands are assigned as for the cerium complex, except for the Fe-O

stretching vibration bands which are in the regions of 551 cm^{-1}, 475 cm^{-1}, and 255 cm^{-1}. The broad band at 3456 cm^{-1} can be assigned to the O-H band of the water molecule. Again elemental analysis suggests that the iron complex contains water with an Fe:H$_2$O ratio of 1:1.

Having successfully synthesised these two metal complexes, their solubility property in organic solvents must be examined if they are going to be used as additive in fuels. The metal complexes dissolve to some degree in most polar organic solvents such as ethanol, THF, but are only slightly soluble in commercial fuels. Therefore some success was achieved in the goal of producing cerium hydrocarbon soluble complex. Unfortunately, the cerium complex is less soluble than the iron complex in all tested solvents. Overall this indicates that increasing of ligand molecular weight by adding more hydrocarbons on the ligand structure does increase the solubility of the metal complex in organic solvents. In order to achieve even better solubility, a bigger side chain than the naphthalene ring is needed.

2.8   SYNTHESIS AND CHARACTERISATION OF N,N',N"-TRIS(5-t-BUTYL-SALICYLALDEHYDE)-TRIS-2-AMINOETHYLIMINE METAL COMPLEXES

2.8.1   Introduction

The synthesis of naphtren metal complexes has established that by increasing the lipophilic character of the H$_3$saltren ligand also increases the solubility of the metal complexes in organic solvents. It is our target to achieve the goal of high solubility in these solvents and still make use of the H$_3$saltren as the core structure of a new ligand. Next it was decided to use the tertiary butyl group as the side chain for substitution on to the salicylaldehyde aromatic ring, since it is already known that this group provides good solubility for the complex of the dipivaloylmethane ligand. There are two potential routes

which can be used to produce the desired substituted salicylaldehyde compound. Scheme 2.5 illustrates the reactions of these routes.

Scheme 2.5

= t-Butyl   Ts= Tosyl
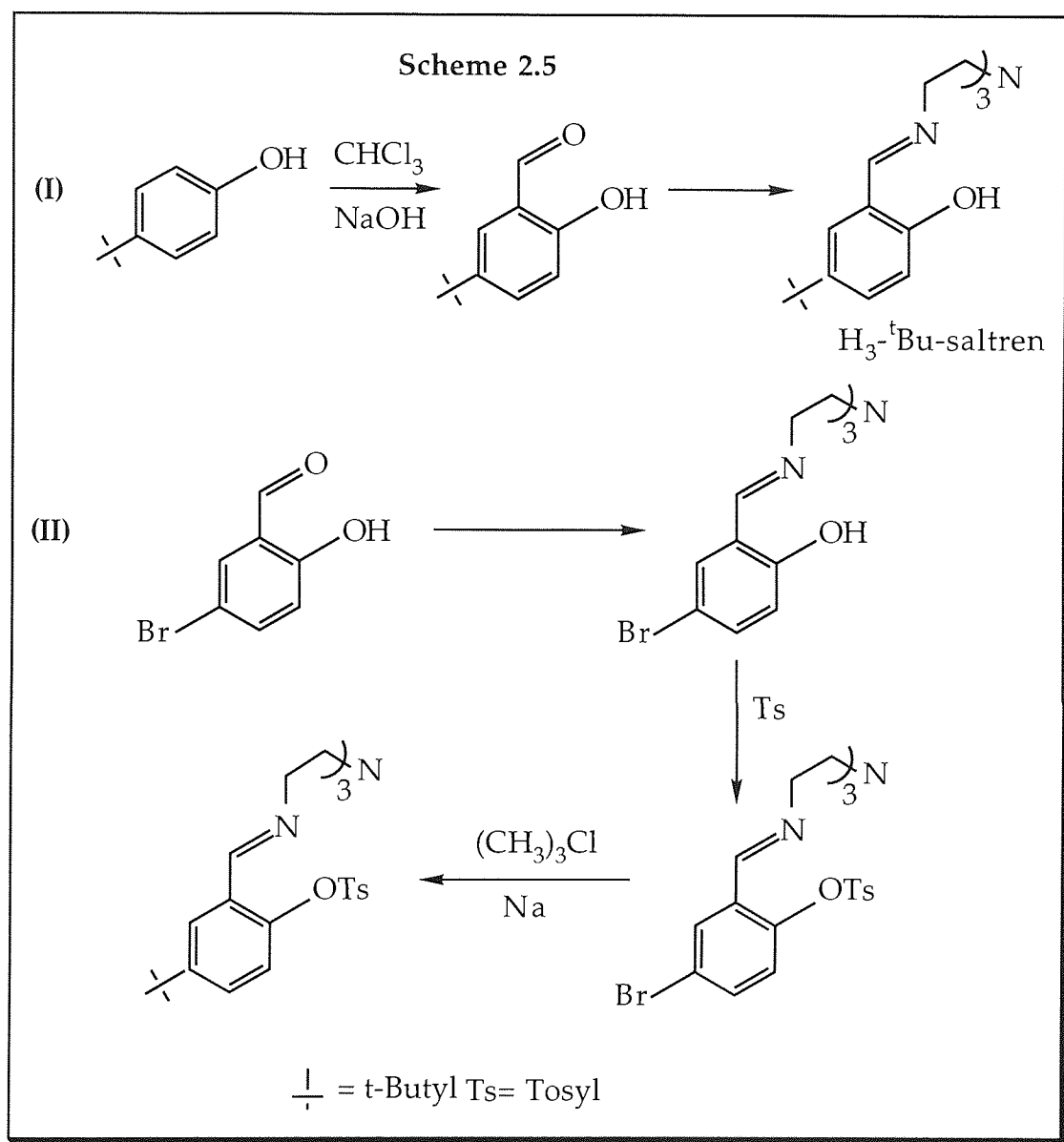
2.8.2   Preparation of N,N',N"-tris(5-t-butylsalicylaldehyde)-tris-2-aminoethyl-imine, [H3-tBu-saltren]

A 1-litre three-necked flask was equipped with a thermometer, a separating funnel, a condenser and a stirring bar. To this was placed 4-tert-butylphenol (52 g, 0.35 mol) and absolute ethanol (150 ml). The stirrer was started and a solution of sodium hydroxide (100 g) in water (200 ml) was rapidly added.

The resulting solution was heated to 70-80 °C on a stirrer/isomantle and 40 ml of chloroform (60 g, 0.50 ml) was placed in the separating funnel. The chloroform was introduced dropwise and the temperature of the reaction adjusted so that the mixture refluxed gently. Upon adding the chloroform, a colour change to orange was immediately observed, which eventually led to a dark solution. Precipitation of a bright orange solid occurred towards the end of the addition of chloroform. This was probably due to the sodium salt of the phenolic aldehyde. The mixture was stirred for a further 2 hr after the addition of the chloroform was complete.

Concentrated hydrochloric acid was then added dropwise to the stirred mixture until the contents of the flask reached pH 3; a dark oil, accompanied by a considerable amount of sodium chloride, separated. Sufficient water was added to dissolve the salt, the oil was then extracted with ether. The ethereal solution was washed with water, dried with anhydrous magnesium sulphate, and finally the solvent was removed. The residue was distilled under reduced pressure at 121-123 °C/ 10 mmHg to yield the slightly coloured aldehyde product. Upon cooling the distillate solidified. The yield of 5-tert-butylsalicylaldehyde was 35 g , 58%.

IR and NMR spectra of this product were obtained the NMR spectra contained evidence of tert-butyl phenol as an impurity in the aldehydic product. I was unable to remove this starting reagent by distillation, but purification was achieved by column chromatography using a solvent mixture of 1:1 of ether:hexane to give a final yield (liquid) of 28 g, 45%. This product is 5-tert-butylsalicylaldehyde.

Tris(2-aminoethyl)amine (1.46 g, 0.01 mol) was added to 5-tert-butylsalicylaldehyde (5.5 g, 0.03 mol) dissolved in ethanol (25 ml). The mixture was stirred and immediately a yellow sticky solid formed. This was

quickly washed with cold ethanol (15 ml), drained, redissolved in a further 30 ml of ethanol and then the solvent was removed to leave a non-sticky yellow solid. Yield 4.15 g, 66%.

2.8.2.1 Preparation of N,N',N"-tris(5-t-butylsalicylaldehyde)-tris-2- amino-ethylimine Cerium (III), [Ce-^{t}Bu-saltren]

H_3-^{t}Bu-saltren (0.63 g, 0.001 mol) was dissolved in methanol (25 ml), and a solution of cerium(III) nitrate hexahydrate (0.43 g, 0.001 mol) dissolved in distilled water (5 ml) was then added. This produced a dark mixture, but no precipitation occurred. The pH of the mixture was then raised to 8 by dropwise addition of 0.1M NaOH solution. At this pH a dark coloured precipitate formed. The solid was filtered off, washed with water, and dried in an oven at 100 ^{o}C. Yield 0.58 g, 76%.

Anal: Cald for CeC$_{39}$H$_{51}$N$_4$O$_3$: C,61.31; H,6.73; N, 7.33%

Found: C,60.53; H,6.70; N,7.35%

2.8.2.2 Preparation of N,N',N"-tris(5-t-butylsalicylaldehyde)-tris-2- amino-ethylimine Iron (III), [Fe-^{t}Bu-saltren]

The same procedure was used to synthesise the iron complex, but the pH of the mixture was raised to 7 rather than 8. Yield 0.51 g, 75%.

Anal: Cald for FeC$_{39}$H$_{51}$N$_4$O$_3$: C,68.92; H,7.56; N, 8.24%

Found: C,69.62; H,7.70; N,8.12%

2.8.3 Results and Discussion

5-tert-butylsalicylaldehyde

The IR spectrum of ^{t}Bu-H$_3$saltren ligand (Fig 2,11) shows strong bands in the region 1658-1622 cm^{-1}, assigned to the C=O stretching vibrations. The bands for this aldehyde stretching vibrations are lower than usual due to

intramolecular hydrogen bonding with the ortho hydroxy group. A weak band at 3072 cm^{-1} due to aryl C-H stretching is also seen. Bands in the region 1600-1500 cm^{-1} are assigned to the benzene ring, while those in the region 1395-1365 cm^{-1} are due to the tertiary butyl group vibrations. The IR spectrum clearly identifies the presence of the aldehyde group added to the starting benzene ring.

Table 2.9 ^{1}H NMR and ^{13}C NMR Spectral Data for 5-tert-butylsalicylaldehyde
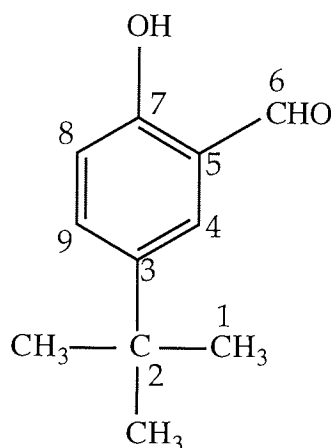
^{1}H NMR			^{1}H NMR		
δ (ppm)	assignment		δ (ppm)	assignment	
1.27	(s, 12H)	(CH$_3$)$_3$	31	(CH$_3$)$_3$	C1
6.85	(d, 1H)	Ar-H	34	C(CH$_3$)$_3$	C2
7.48	(d, 1H)	Ar-H	117	Ar-C	C9
7.54	(t, 1H)	Ar-H	120	Ar-C	C3
9.82	(s, 1H)	CHO	130	Ar-C	C4
10.86	(s, 1H)	OH	134	Ar-C	C8
			143	Ar-C	C5
			160	Ar-OH	C5
			197	CHO	C6
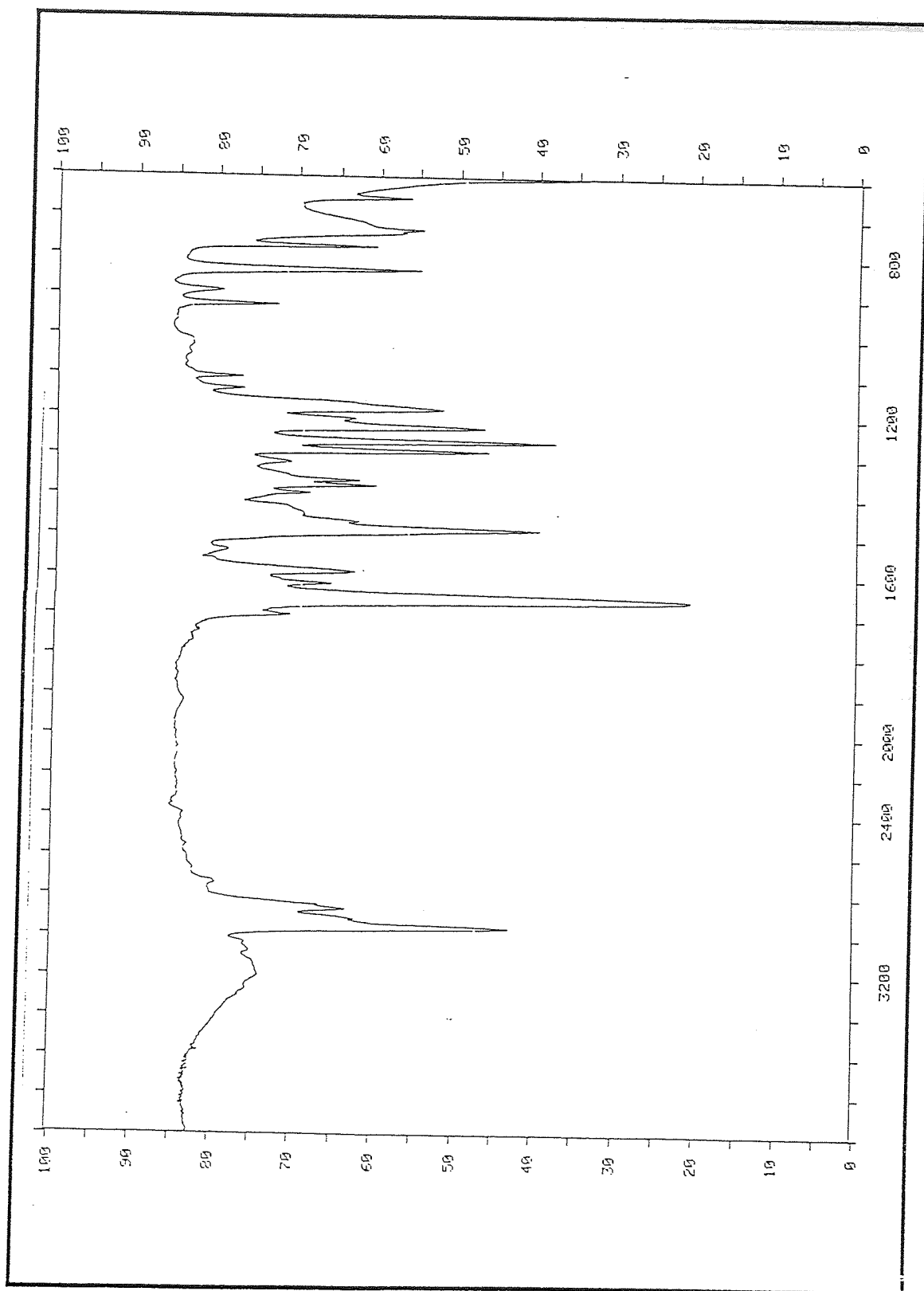
Figure 2.11 IR Spectrum of 5-tert-butylsalicylaldehyde
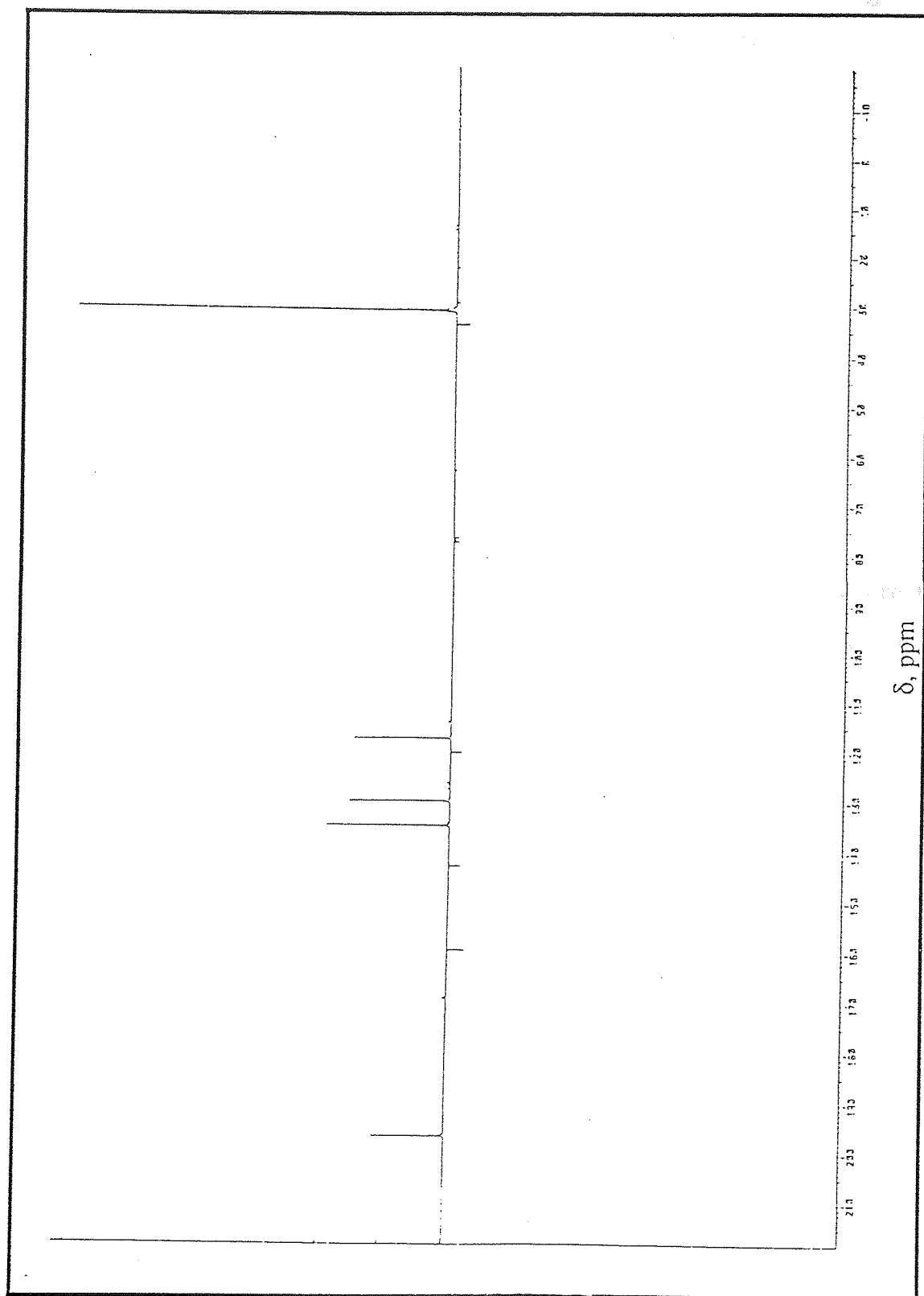
Figure 2.12 ^{13}C NMR Spectrum of 5-tert-butylsalicylaldehyde

There is further evidence of this in the ^{1}H NMR spectrum. There is a peak of 9.82 ppm, assigned to the aldehyde proton, and the phenolic proton is further downfield than usual because of the intramolecular hydrogen bonding. This therefore points to a nearby aldehyde group. The ^{13}C NMR spectrum (Fig. 2.12) also shows a peak in the low field region of 197 ppm which may be assigned to the aldehydic carbon.

Even when great care was expended to assure that the distillations were slow to achieve maximum separation, pure 5-tert-butylsalicylaldehyde could not be separated by vacuum distillation. The final distillates contained traces of tert-butylphenol impurity, which are easily detected in the NMR spectra. The impurity was later separated using silica gel on column chromatography with ether and haxane as the solvent solution.

This reaction is an example of the Reimer-Tiemann reaction[93] where the treatment of phenols with chloroform in basic solution gives aldehyde, e.g.

OH

$+$ CHCl$_3$ $\xrightarrow[\text{- 3HCl}]{\text{OH}^- - H_2O}$ OH CHO $+$ p-hydroxybenzaldehyde

salicylaldehyde
40%
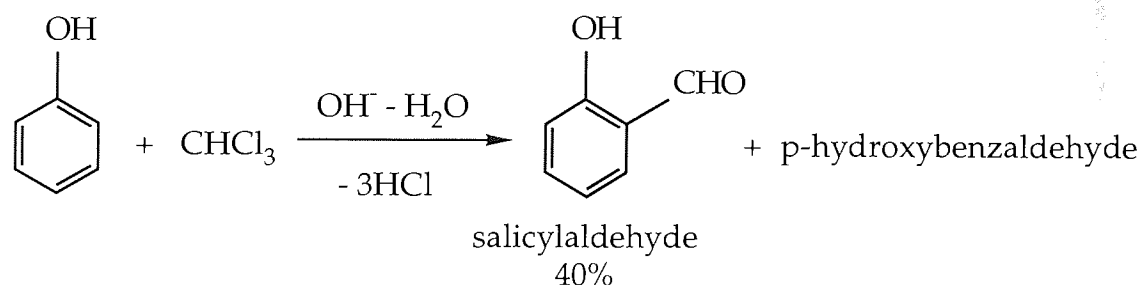
The overall formylation reaction of the aldehyde compound (scheme 2.7) is of interest in that it involves the generation from chloroform and alkali of the reactive intermediate, dichlorocarbene (I). This effects electrophilic substitution in the reactive phenolate ions giving the p-tert-butylbenzylidene dichloride (II) which is then hydrolysed in the alkaline medium to the corresponding hydroxy aldehyde. The phenolic aldehyde is isolated from the reaction media after acidification and the product of this reaction is solely the

o-hydroxy-tert-butylbenzaldehyde, since the para position is already occupied by the tertiary butyl group.

Scheme 2.7

(I)

(II)
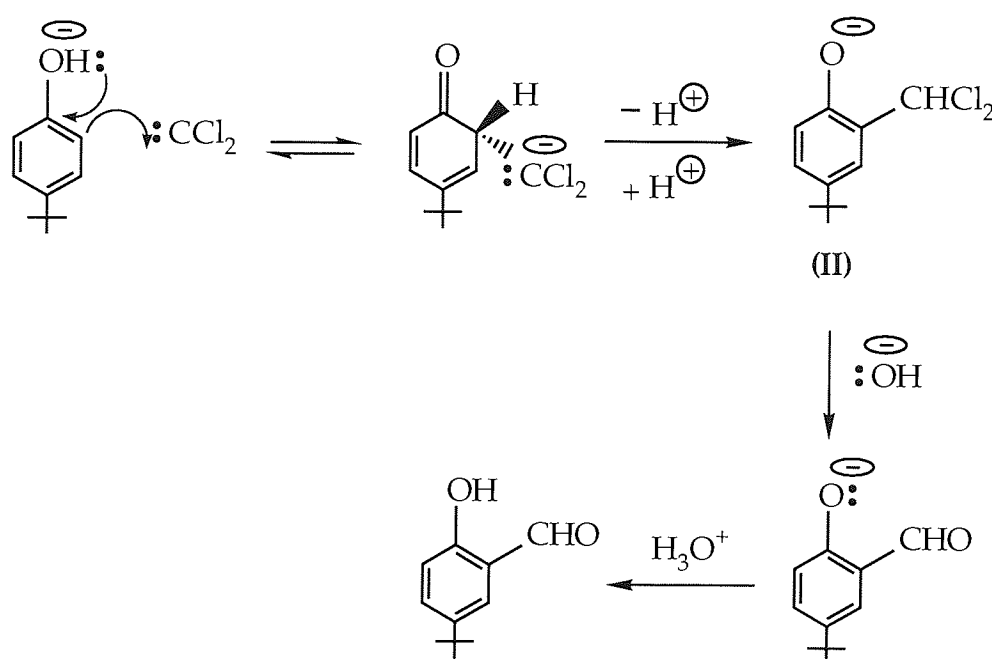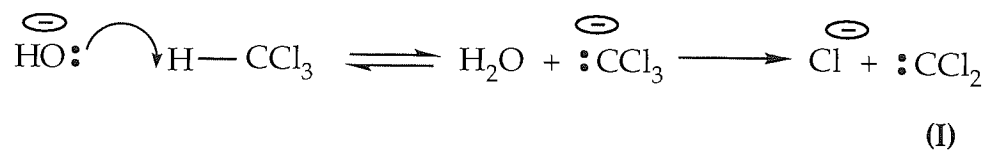
H_3 ^tBu-saltren

Scheme 2.6

H_3-^{t}Bu-saltren

-92-
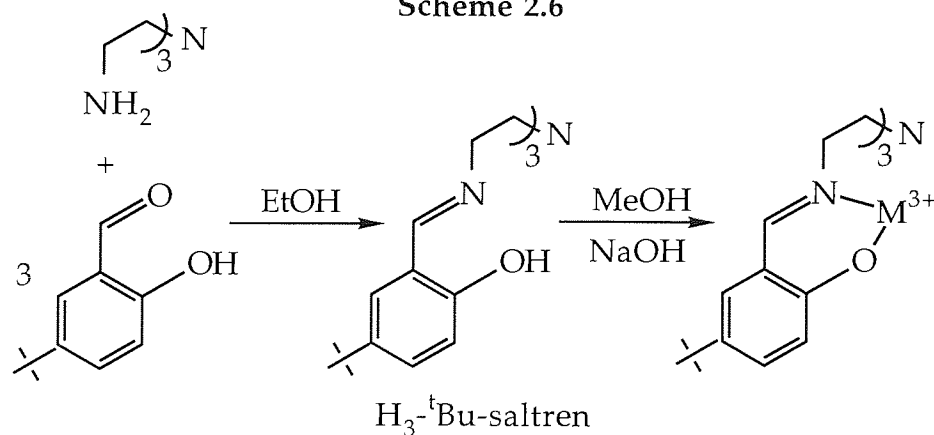
The IR spectrum of H_3-^{t}Bu-saltren shows a strong absorption band at 1637 cm^{-1} which may be assigned to C=N stretching vibration. This is the only band of real interest to us since the reaction involves the formation of this bond. Nevertheless all the vibration bands for the aromatic rings, tertiary butyl groups, C-H stretching and deformation of aliphatic hydrocarbon, and also C-O stretching were assigned.

The ^{1}H NMR spectrum shows all the signals required for the structure of the H_3-^{t}Bu-saltren ligand. A strong sharp signal at 1.28 ppm belongs to the protons of the six methyl groups. Signals at 2.88 ppm and 3.68 ppm are due to the protons of the methylene groups adjacent to the two nitrogen atoms of the tripod ligand. The proton signal at 8.27 ppm can be assigned to the methine group of the imine bond. This methine signal, when compared to that of the initial aldehyde (9.82 ppm) reagent signal, shows a shift to a higher field in the Schiff base. This indicates that the oxygen atom was removed during the course of the condensation reaction between the two starting reagents and accounts for the difference in chemical shift for the methine group due to the substituted nitrogen atom for the oxygen atom. A broad signal in the region 13.30 ppm is due to the hydroxy proton.

The ^{13}C NMR spectrum (Fig. 2.13) shows all eleven different carbon environments expected for the ligand structure; see Table 2.10. The extra bands at 56 ppm and 58 ppm, not listed in Table 2.9, are due to the methylene groups of the amine, CH_2N and CH_2-N= respectively. The signal at 166 ppm is of the methine group attached to the imine bond with a shift of @ 30 ppm to a higher field compared to that of the aldehyde, due to the different electronegativity of the adjacent atom.

Table 2.10 ^{1}H NMR and ^{13}C NMR Spectral Data for H$_3$-^{t}Bu-saltren
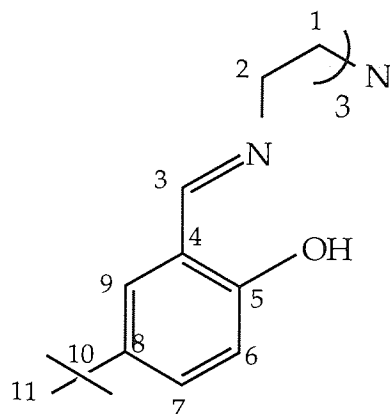
^{1}H NMR				^{1}H NMR	
δ (ppm)		assignment		δ (ppm)	assignment
1.28	(s, 27H)	(CH$_3$)$_3$		31	C11
2.88	(t, 6H)	C-CH$_2$		34	C10
3.68	(t, 6H)	CH$_2$-N=		56	C1
6.84	(d, 3H)	Ar-H		58	C2
7.18	(d, 3H)	Ar-H		116	C9
7.34	(t, 3H)	Ar-H		118	C8
8.27	(s, 3H)	CH=N		128	C7
13.30	(s, 3H)	OH		129	C6
				141	C4
				159	C5
				166	C3

The H$_3$-^{t}Bu-saltren Schiff base ligand was prepared under the same alcoholic condition as were used for the other two schiff bases. Scheme 2.5 illustrates two routes of preparing this ligand. The method described in this section follows route (I). Route (II) was attempted, but with little success. With the
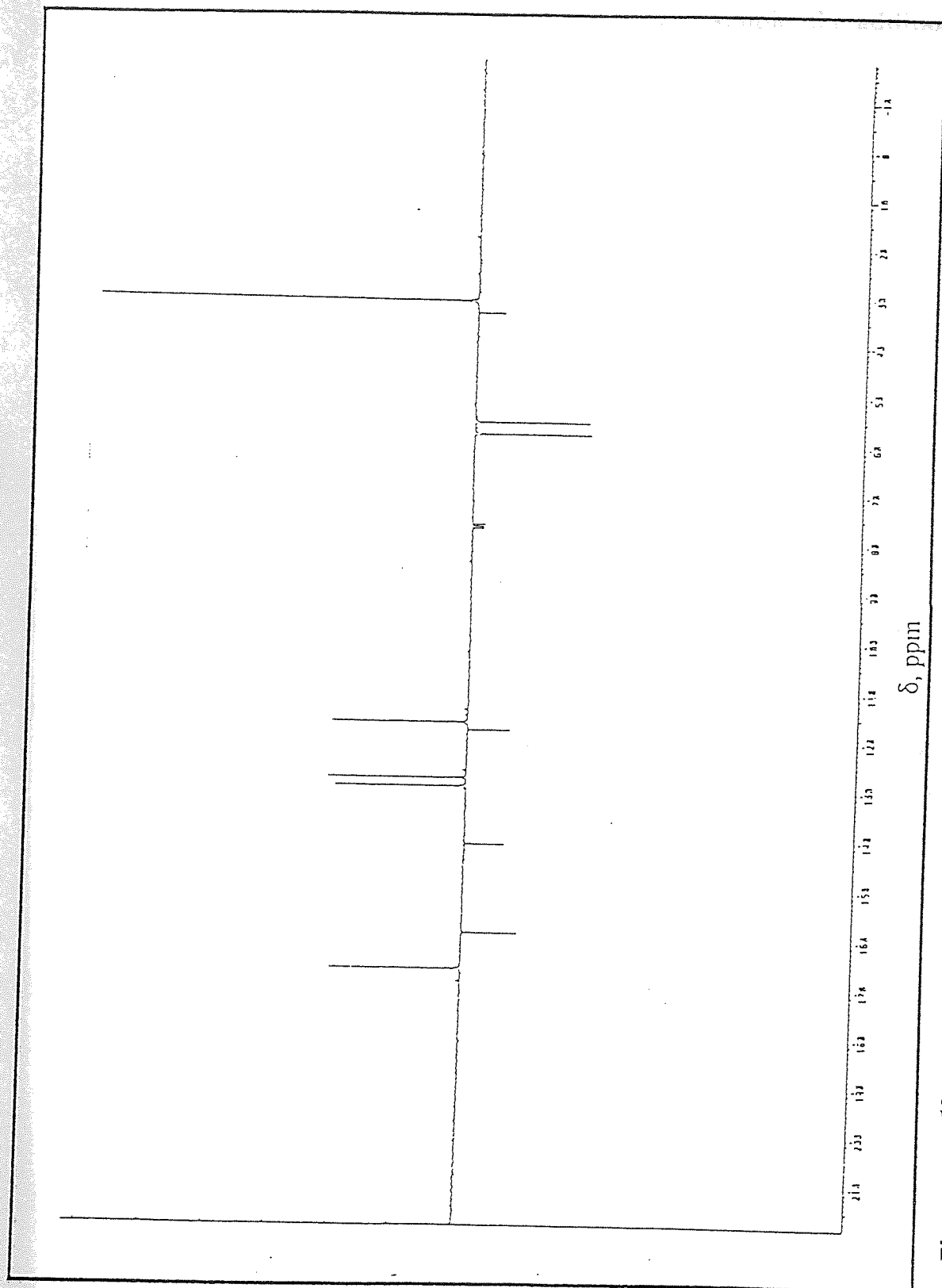
Figure 2.13 13C NMR Spectrum of N,N',N'-Tris-(5-tert-buytlsalicylaldehyde)-tris-2-aminoethylimine

success of route (I), the time spent on route (II) was cut short. Only the first step was completed, but from the illustration this route would clearly involve many tedious organic reactions. The first stage was simple: the addition of the trisamine to the bromo substituted salicylaldehyde gave the bromo substituted Schiff base compound. In the next stage the hydroxy group has to be protected before proceeding with the reaction with sodium metal and alkyl halide. A tosylate group can be used to protect the phenolic group. As this is only the first part of the planned research work, further investigations of this route were curtailed.

Ce-^{t}Bu-saltren

Figure 2.14 shows the IR spectrum of the above cerium complex. A broad band in the region 3415 cm^{-1} may be asigned to OH stretching of the water molecule. Weak bands at 3021 cm^{-1} and 1500 cm^{-1} are due to C-H stretching vibrations of the aryl groups. The strong band at 835 cm^{-1} is produced by the out of plane C-H bending vibrations of the aromatic rings. The other strong band, at 1626 cm^{-1}, is the C=N stretching vibration of the complex ligand; slightly lower than that of the free ligand (1637 cm^{-1}). This indicates cerium coordination to the nitrogen atoms.

The C-H bands of the tertiary butyl groups are at 1385 cm^{-1} and 1362 cm^{-1}, while bands in the region 1300-1100 cm^{-1} are due to the C-0 stretching vibrations, bands due to coordination between cerium metal and oxygen atoms are assigned at 527 cm^{-1}, 422 cm^{-1}, and 374 cm^{-1}.

Elemental analytical data provides more evidence for the successful synthesis of the Ce-^{t}Bu-saltren complex. The actual yield of the cerium complex was further increased by the addition of water to the mixture when complexation
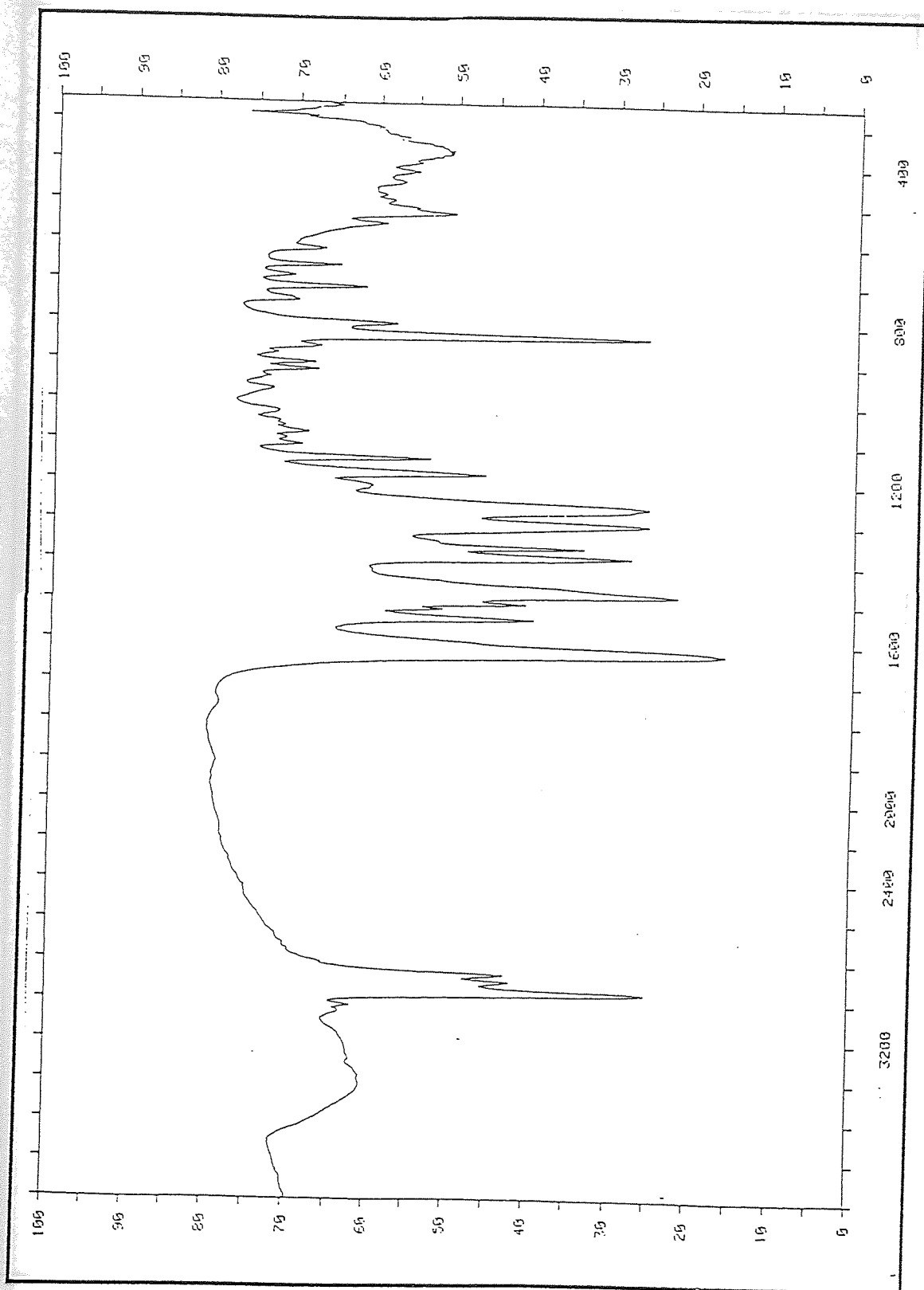
Figure 2.14 IR Spectrum of Ce-tBu-saltren
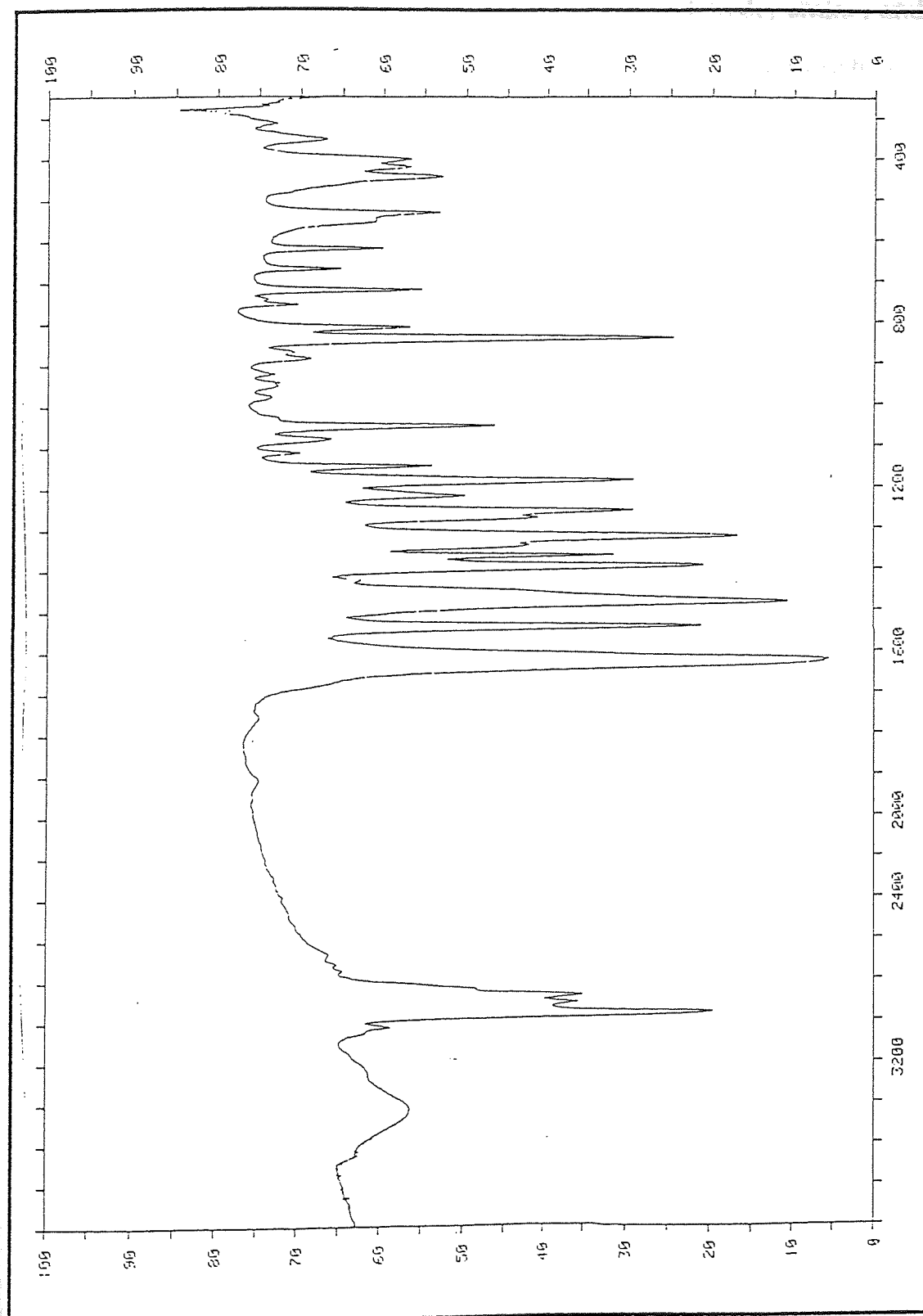
Figure 2.15 IR Spectrum of Fe-tBu-saltren

was completed. This occurs because the cerium complex is soluble in methanol, but not in water. This cerium complex can be synthesised directly from a methanolic solution of a mixture of the aldehyde, amine, and metal salt. The yields for these two methods are the same. The existence of this latter easy process would enhance the chances of the complex's becoming a successful commercial fuel additive. The shortening of the route would reduce the cost of production.

Fe-^{t}Bu-saltren

Again, the IR spectrum (Fig. 2.15) of the iron complex of the same ligand produced similar bands to those observed for the cerium complex. The C=N stretching vibration band is shifted (1620 cm^{-1}) because of the metal ion. This band is at a lower energy for Fe than for Ce, which suggests that the strength of bonding between iron and the nitrogen atom is weaker. Fe-O vibrational bands are assigned at 530 cm^{-1} and 443 cm^{-1}.

Elemental analytical results show agreement between the calculated and found values. The combination of all these data proves that the iron complex was synthesised.

The metal complexes of H$_3$-^{t}Bu-saltren ligand are much more soluble in polar organic solvents than the previous Schiff base metal complexes and to some degree also in commercial fuels. The complexes also demonstrate that an aliphatic side chain has a greater effect on solubility than an aromatic side chain. Having achieved the goal of producing a hydrocarbon soluble cerium complex, the next target was to investigate their pro-oxidant additive potential in commercial fuels (mainly diesel).

SECTION (C) : SYNTHESIS OF THE MACROCYCLIC LIGANDS

2.9 INTRODUCTION

The field of coordination chemistry of macrocyclic compounds has undergone spectacular growth during the past 30 years. This growth has largely been due to the synthesis of a greater number and variety of synthetic macrocycles which behave as coordinating ligands for metal ions. The growth of interest in complexes of macrocyclic compounds is partly responsible for the development of the field of bio-inorganic chemistry, since it has been recognised that many complexes containing synthetic macrocyclic ligands may serve as models for biologically important species which contain metal ions in the ligand environments.

PORPHIN   CHLORIN   CORIN
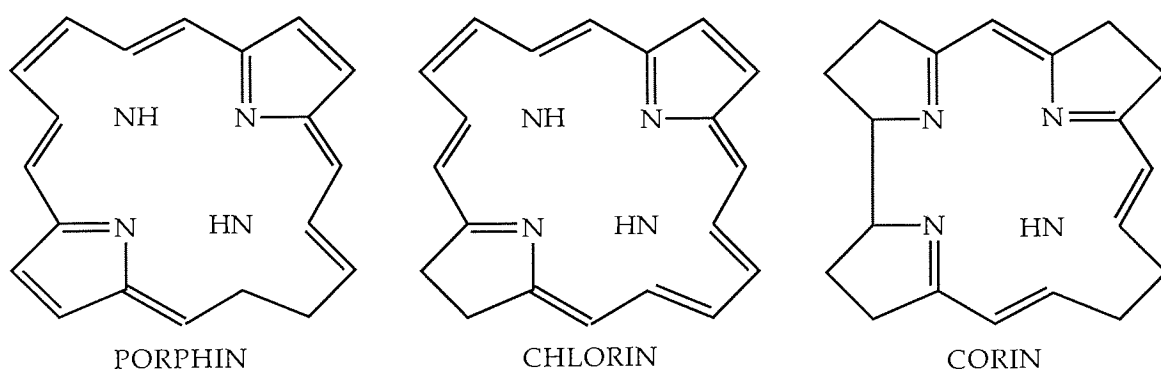
Complexes of porphyrins, chlorophylls and corrins have been investigated because of their relation to important naturally occurring species containing macrocycles such as heme and chlorophyll. In the biological systems, these ligands are generally bound to iron, magnesium and cobalt metal.

An example of biological compounds that contain a metal ion in a naturally occurring macrocyclic ligand is Vitamin B_{12} where Co(III) ion is coordinated with a corrin which has substituents incorporated into the ring structure. Much interest in this field of chemistry indicates the importance of coordination between the metal ions and the macrocyclic ligands. Having

previously illustrated our interest in cerium as the central cation of the complex compound, thoughts on suitable ligands for complexation needed to be considered.

The discovery of cyclic polyethers or the crown ether family by Pederson[94] in 1967 shows the selectivities between macrocyclic ligands and metal ions. Pederson reported syntheses of over 50 crown ethers in which the size of the macrocyclic rings, the number of ether oxygen atoms, and the number and type of substituent groups on the ring varied widely. Structures of some typical crown ethers and their trivial names are given below.
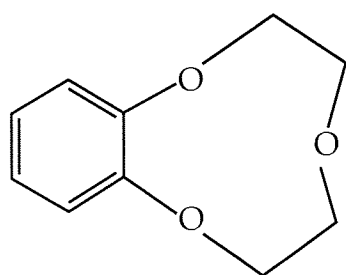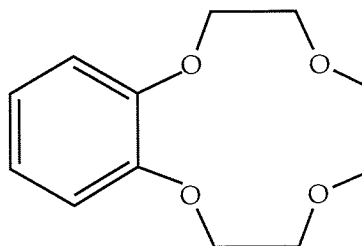
Benzo-9-crown-3   Benzo-12-crown-4   18-crown-6
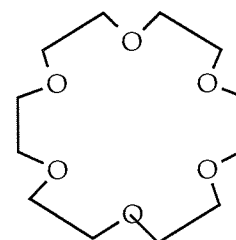
Pederson showed that these compounds have an unusual ability to form relatively strong complexes with alkaline and alkaline earth ions. In fact, some of the alkaline salts of 18-crown-6 substituted ligands can be solubilised in non-polar organic solvents. The solubilities of these compounds in aprotic solvents are increased by the presence of tertiary butyl groups. Saturated cyclic polyethers as a group are much more soluble in all solvents than the corresponding benzo compounds. The same paper also reported cerium(III) complexes of the crown ether family.

The main objective in macrocycle design is to synthesise macrocycles which are able to discriminate the different cations. Many factors influencing the selectivities of macrocycles for cations have been determined. These factors may be roughly divided into macrocycle cavity dimensions, substituent effects, donor atom type, number, and arrangement[95-97].

Investigations of crown ethers demontrate that these ligands complex most strongly to those metal ions whose diameter best matches the diameter of the cavity formed by the ring upon complexation[98]. In this condition, it is reasoned that the bond energies between ligand and cation will be greatest as all the donor groups can participate fully. If the macrocylic ring is too large, the metal ion will "fall through" the cavity or if the ring is too small the metal can only sit on top and not fit inside.

Incorporating substituents such as phenyl and cyclohexyl groups into the macrocyclic rings leads to a stiffening of their skeletons and may alter both ligand binding strength and selectivity. Selectivities may also be modified by variation of the side arms. Cyclic polyamine compounds containing two carboxylate groups as side arms showing unique selectivity toward lanthanide cations as a group was reported by Chang and Rowland[99]. Cyclic polyamine is another family of the macrocyclic ligands, this family of compounds are the same as the crown ether family in every respect, except that the nitrogen atom replaces the oxygen atom.

The number and kind of donor atoms also play important roles in macrocycle selectivities. Substitution of nitrogen for an ether oxygen in a crown ether ring reduces the affinity of the ligand for the alkali, alkaline earth, and lanthanide cations but favours the transition metal cations; while sulphur-donor atoms interact preferentially with silver and mercury cations.

Having already established that the cerium(III) cation has an affinity towards carboxylate groups, three carboxylate groups are required to achieve a neutral complex. This is essential for the metal complex solubility in nonpolar organic solvents. To date there has been no report of macrocyclic compounds containing carboxylate groups incorporated directly onto the hydrocarbon skeleton of the macrocyclic ring and not at the donor atoms. However, there

are a number of papers describing compounds in which the carboxylate groups act as side arms on the nitrogen donor atoms of cyclic polyamines[100-110]. These polyaza polycarboxylic macrocycles containing only 3 or 4 nitrogen donor atoms are of interest here, e.g. 1,4,7-triazacyclononane triacetic acid (NOTA) (see Figure 2.17).

All polyaza macrocyclic ligands containing three or four nitrogen atoms in the ring in these reports show ring sizes of no more than 15 atoms. From the information obtained from crown ethers, it can be said that these rings are not large enough to accommodate the trivalent cations in the internal cavity of the ring. However, by attaching the carboxylate side arm groups onto the nitrogen donor atoms these ligands are then able to coordinate with the trivalent cation by encapsulation. That is, by letting the cation sit on top of the N atoms, while the carboxylate side arms are used to wrap around the cation. This can be seen more clearly from the diagram on the next page with an extra oxygen atom being coordinated directly above the ligand structure. Desreux and co-workers[111] have studied in detail this type of coordination of lanthanide cations with the aid of X-ray crystallography, and have produced the structure of the EuDOTA complex (Fig. 2.16).

Desreux and co-worker[106] recently reported the formation of highly stable lanthanide complexes of DOTA. They display a host of unusual properties associated with these complexes. Properties which are not exhibited by the complexes of similar but non-cyclic ligand such as EDTA. The lanthanide chelates of DOTA ligand are remarkably rigid, highly symmetric, and adopt the same geometry in solution and in the solid state[103]. The lack of lability is most unusual in lanthanide chemistry[112] and has been assigned to the steric requirements of the 12- and 14-membered cycles. The authors even go as far as to say that complexes of DOTA compounds are by far the most stable

lanthanide complexes known to date. Their high stability could turn out to be especially important for the separation of the lanthanides as a class.
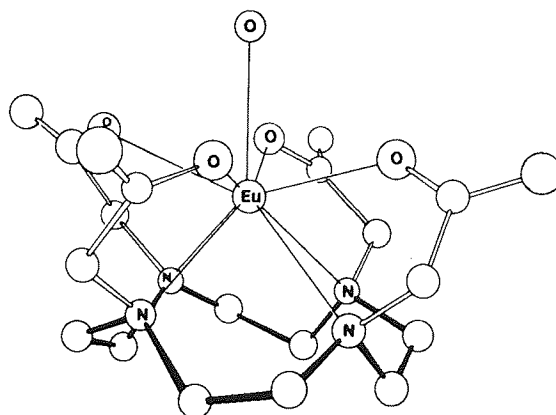
Figure 2.16 Structure of the Eu(III) complex of DOTA

A stability study of lanthanide complexes of NOTA was reported by Sherry and co-workers[107]. NOTA is a hexadentate chelate like EDTA, but with three donor nitrogen and three donor oxygen atoms. La(NOTA) complexes show progressive increases in stability with decreases in cation size, showing a similar trend to that of the Ln(EDTA) complexes but with lower stability constants. The trend in stability of the Ln(NOTA) complexes is a result of the restricted size of the triazacyclononane ring of NOTA, which is therefore unable to accommodate the larger cations. These cations are too large for the combined steric requirements of the triaza ring and the acetate groups. Near the middle of the lanthanide series, the chelate may then accommodate the cations into a position well above the plane defined by the three nitrogen atoms, with the acetate in equatorial positions relative to the cation. Once this critical size requirement is met, the stability constants increase with increasing charge density. Wieghardt[105] and his team also observed very stable complexes of NOTA with many first-row transition metals in the oxidation states of +2 and +3.

Clearly, from all this information, one can visualise the possibility of these groups of macrocycle ligands providing stable complex formations with

cerium and other trivalent cations, thus offering another group of potential cerium pro-oxidant additives. Unfortunately there are no reports of these type of macrocyclic complexes being soluble in organic solvents, so problems such as those with the complexes of Schiff base ligands had to be overcome. The same approach can be used again. Hydrocarbons therefore have to be incorporated into the polyamine ligand ring in order to increase the metal complex solubility in organic solvents.

The first step of the syntheses is of macrocycle ligands which contain 3N, 4N or O$_3$N donor atoms, before introducing hydrocarbon groups into their ring structures. This proved to be far more difficult than might appear on paper. The rather time-consuming experimental preparations were multi-step, with the final product yield often being low. Some of these steps were performed under high dilution and because of this, a sizeable scale-up procedure was not possible. Attempts at these preparations only produced unmanageable 'gums' as products rather than the crystalline materials reported. Obviously this team of workers gained considerable experience over a number of years in handling these compounds, and much of the necessary expertise has not been translated into print. This section of the chapter reports the synthesis of the three groups of macrocycle ligands which later described (see Fig. 2.17), and the attempts to introduce hydrocarbon groups onto the macrocyclic ligand ring. The success of the work discussed in this section was limited due to a shortage of time. However enough foundations were laid down for future work to build on.

All recent papers concerning the nitrogen analogues of crown ether compounds refer to the synthetic procedure described by Richman and Atkins[113] in 1974, as the standard preparation for cyclic polyamine compounds; even though Koyama and Yoshino[114] had reported the same compounds earlier. The method described by Searle and Geue[115] was used

instead of the above two methods. This is basically an improved Richman-Atkins procedure. Macrocyclic polyamines and amine-ethers are said to be readily prepared without high-dilution techniques by this improved general procedure. Cyclic polyamines are synthesised by cyclisation involving one reagent with two terminal NH_2 groups converted into p-toluenesulfonamide sodium salts, $-(Ts)N^-Na^+$, and a second reagent with two alcohol groups converted into p-toluene sulfonate ester groups, -OTs. Alternatively an alkyl dihalide such as Br-R-Br can be used as the second reagent. The sodium salts have enhanced nucleophilicity compared to the tosylates amines, -NHTs, and the sulfonate esters[116] are more effective leaving groups than the halides used in previous procedure[114].

The entire procedure illustrated in Figure 2.18 involves preparation of the tosylated starting compounds, conversion into amine disodium salts, cyclisation in dry dimethylformamide (DMF), and removal of tosyl groups. Syntheses of cyclic polyamines thus remain tedious, and at certain times it is difficult to obtain the pure polyamine product.
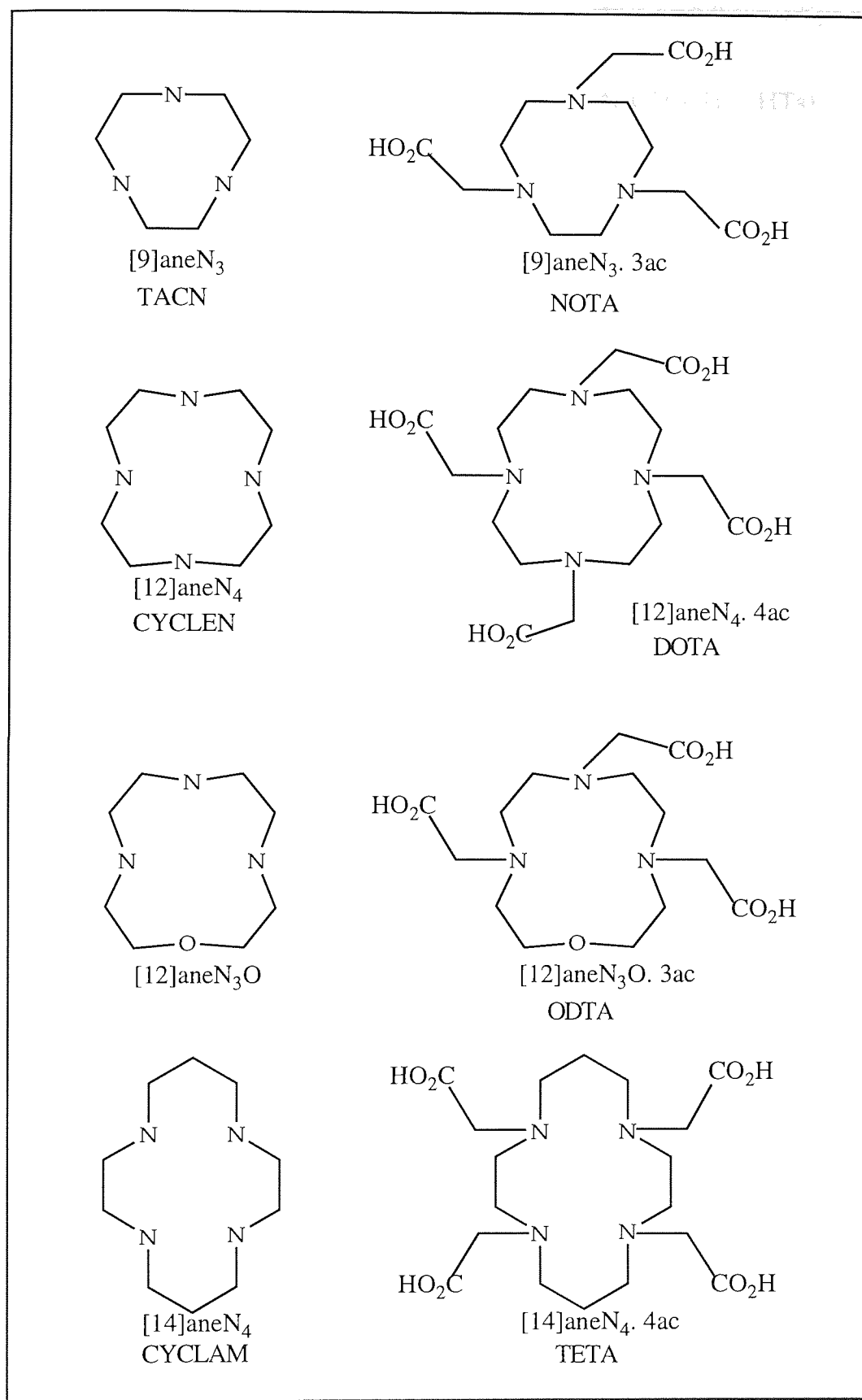
Figure 2.17 Structures of Some Ligands Discussed in Section C

A. $HN(CH_2CH_2NH_2)_2$ $\xrightarrow[NaOH]{CH_3C_6H_4SO_2Cl}$ $TsN(CH_2CH_2NHTs)_2$

1

B.   **1** $\xrightarrow[\substack{C_2H_5OH \\ reflux}]{C_2H_5ONa}$ $TsN(CH_2CH_2\overset{-}{N}\overset{+}{Na}Ts)_2$

2

C. $HOCH_2CH_2OH$ $\xrightarrow[pyridine,\ 0\,^{\circ}C]{Ts}$ $TsOCH_2CH_2OTs$

3

D.   **2 + 3** $\xrightarrow[110\,O\,^{\circ}C]{DMF}$

4

E.   **4** $\xrightarrow[\substack{30\%\ HBr \\ reflux}]{CH_3CO_2H}$

 . 3 HBr

5

$Ts = p\text{-}CH_3C_6H_4SO_2{}^{-}$
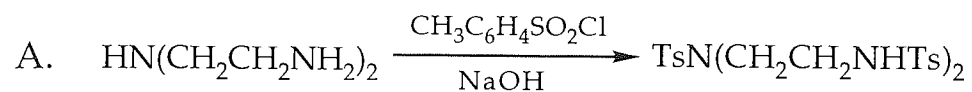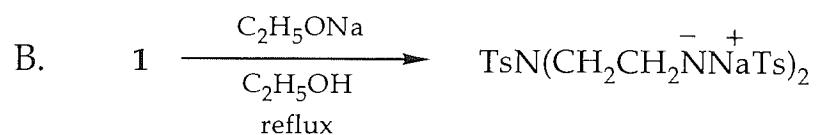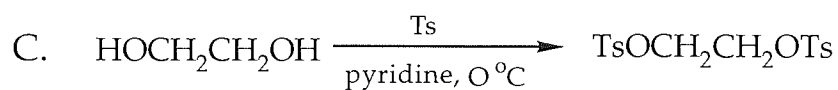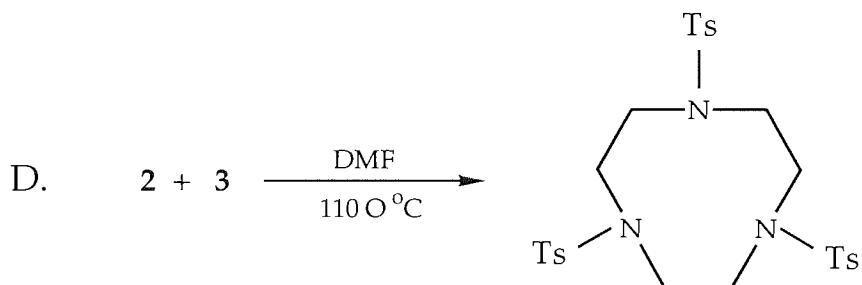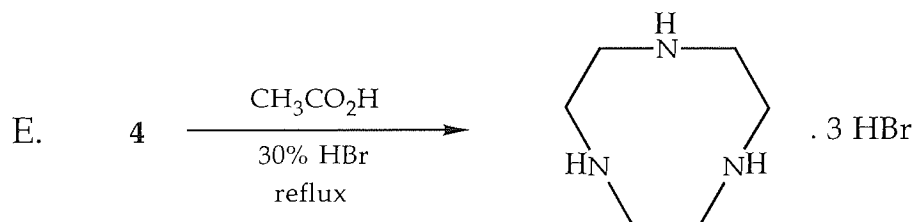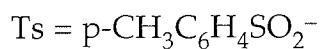
Figure 2.18 Routes of 1,4,7-Triazacyclononane Synthesis

2.10 EXPERIMENTAL PROCEDURES

2.10.1 Preparation of 1,4,7-Triazacyclononane trihydrobromide[102] (5)

A. Tris(p-toluenesulfonyl)diethylenetriamine (1)

A solution of p-toluenesulfonyl chloride (240 g, 1.25 mol) in ether (1litre) was added dropwise to a mechanically stirred solution of diethylenetriamine (41.3g, 0.4 mol) and sodium hydroxide (48 g, 1.2 mol) in water (400ml). The mixture was stirred for 2 hr at room temperature and a white precipitate coagulated. The product was filtered off, washed with water and methanol. It was recrystallised from a large volume of methanol (10 L) and gave fine fluffy needles. Yield 125 g, 55%; m.p. 173-174 °C, lit. 173-175 °C.

Anal: Cald for $C_{25}H_{31}N_3O_6S_3$: C,53.08; H,5.52; N,7.43%

Found: C,52.94; H,5.52; N,7.39%

^{13}C NMR in $CDCl_3$: δ 2.10, 3C, CH_3; 41.6, 2C, CH_2NH; 48.4, 2C, CH_2NCH_2; 126.5, 126.8, 129.7, 129.9, 4C+2C+4C+2C, Ar; 135.3, 137.4, 142.8, 143.4, total 6C, quaternary Ar.

B. N,N',N''-tris(p-toluenesulfonyl)diethylenetriamine-N,N'-disodium salt (2)

Two equivalents of sodium ethoxide (6.8 g, 0.10 mol) in ethanol (100 ml) were added to triamine **1** (28.3 g, 0.05 mol) in boiling ethanol (200 ml). The mixture was refluxed for 20 minutes and then solvent was extracted under vacuum to yield the disodium salt of triamine **2**.

C. 1,2-di(p-toluenesulfonyloxy)ethane (3)

Solid p-toluenesulfonyl chloride (160 g) was added in portions to a stirred solution of ethane-1,2-diol (24.9 g, 0.4 mol) in pyridine (250 ml) at 0 °C. After

leaving at room temperature for 1 day, ice was added and the mixture was refrigerated. The white product was filtered off, washed with water, ethanol, and water and air-dried. It was recrystallised from hot acetone (250 ml) with the addition of ether. Yield 105 g, 71%; m.p. 123-125 °C, lit. 123-125 °C.

^{13}C NMR in CDCl$_3$: δ 21.6, 2C, CH$_3$; 66.7, 2C, CH$_2$; 127.9 and 130, 4C+4C, Ar; 132.2 and 145.3, 2C+2C, quaternary. Ar.

D. 1,4,7-tris(p-toluenesulfonyl)-1,4,7-triazacyclononane (4)

The sodium salt 2 (30.5 g, 0.05 mol) was dissolved in DMF (500 ml) and transferred to a 2L, three-necked flask equipped with an addition funnel and a thermometer. The mixture was heated to 110 °C, and an equivalent of 3 (18.5 g, 0.05 mol) in DMF (250 ml) was added dropwise over a period of 2 hours while the solution was vigorously stirred   The now yellow solution was stirred at 110 °C for a further 10 hr. The volume of DMF was reduced to one-fourth of the initial volume, and then the gradual addition of water gave a tacky off-white precipitate. This was filtered off, washed with water and ethanol. The product was recrystallised from hot benzene. A white product was precipitated by reducing the volume of the benzene to crystallisation and ethanol was added to the solution. Yield 24.5 g, 83%; m.p. 221-222 °C, lit. 222-223 °C.

Anal: Cald for C$_{27}$H$_{33}$N$_3$O$_6$S$_3$: C,54.80; H,5.62; N,7.10%

Found: C,54.69; H,5.57; N,7.09%

^{13}C NMR in CDCl$_3$: δ 21.5, 3C, CH$_3$; 51.8, 6C, CH$_2$; 127.5 and 129.8, 6C+6C, Ar; 134.6 and 143.9, 3C+3C, quat. Ar.

^{1}H NMR in CDCl$_3$: δ 2.41, s, 9H, CH$_3$; 3.40, s, 12H, CH$_2$; 7.31 & 7.67, d+d, 12H, Ar

E. *1,4,7-triazacyclononane trihydrobromide* **(5)**

The tosylated **4** (17.8 g, 0.03 mol) was hydrolysed by heating in 30% hydrobromic-acetic acid (900 ml; 50 ml/ g), which was prepared by adding 9 volumes of glacial acetic acid to 16 volumes of 47% hydrobromic acid. The mixture was refluxed for 2 days, after which time the solution was reduced to one-tenth of its initial volume. When cooled, diethyl ether-ethanol (1:1) was added to the mixture until crystallisation occurred. The separated precipitate was filtered , washed repeatedly with ethanol and ether, and air-dried. Yield 10.1 g, 91%; m.p. 270-280 $^{\circ}$C.

$\qquad$ Anal: $C_6H_{18}N_3Br_3$: C,19.38; H,4.88; N,11.30%

$\qquad\qquad$ Found: C,19.34; H,4.90; N,11.18%

2.10.2 Preparation of 1,4,7,10-Tetraazacyclododecane Tetrahydrobromide

1,3,5-tris(p-toluenesufonyl)diethyloxyamine, $TsN(CH_2CH_2OTs)_2$

In a 1L three-necked flask fitted with a stirrer and thermometer were placed diethanolamine (21 g, 0.2 mol) and pyridine (2 moles, 162 ml). The flask was surrounded by a water bath to lower the temperature of the mixture to 10 $^{\circ}$C. At this temperature p-toluenesulfonyl chloride (114 g, 0.6 mol) was added in portions over a period at such a rate that the temperature did not exceed 20 $^{\circ}$C at any time. The mixture was stirred for a further 3 hr at a temperature below 20 $^{\circ}$C, after which it was diluted with 300 ml of concentrated HCl in 1L of ice water. The ester which crystallised out was collected through filtration and tranferred to a 600 ml beaker containing 250 ml of methanol. The mixture was warmed on a steam bath until the ester melted, the beaker was removed from the steam bath and placed on a stirrer and stirred while the mixture cooled. The yellow ester product separated in fairly fine solid form, the product was filtered and air-dried. Yield 70 g, 62%; m.p. 93-95 $^{\circ}$C.

Anal: Cald for $C_{25}H_{29}NO_8S_3$: C,52.89; H,5.15; N,2.47%

Found: C,52.88; H,5.18; N,2.49%

^{13}C NMR in $CDCl_3$: δ 21.5, 1C, CH_3; 21.6, 2C, CH_3; 48.4, 2C, CH_2N; 68.3, 2C, CH_2O; 127.2, 127.9 and 129.9, 2C+6C+4C, Ar; 132.4,135.2,144.1 and 145.2, 1C+2C+1C+2C, quat. Ar.

^{1}H NMR in $CDCl_3$: δ 2.37 and 2.41, s, 9H, CH_3; 3.32, t, 4H, CH_2N; 4.07, t, 4H, CH_2O; 7.23, 7.30, 7.55 and 7.70, d+d+d+d, 12H, Ar.

1,4,7,10-tetra(p-toluenesulfonyl)-1,4,7,10-tetraazacyclododecane, [12]aneN₄.4Ts

The same method for the triazacyclononane was used to synthesise the above compound, with starting reagents of disodium salt **2** at 0.05 mole and an equivalent of $TsN(CH_2CH_2OTs)_2$ in DMF solvent to produce a white solid product. Yield 30 g, 76%; m.p. 284-286 °C.

Anal: Cald for $C_{36}H_{44}N_4O_8S_4$: C,54.80; H,5.62; N,7.10%

Found: C,54.72; H,5.61; N,7.09%

^{13}C NMR in $CDCl_3$: δ 21.5, 4C, CH_3; 52.3, 8C, CH_2N; 127.7 and 129.8, 8C+8C, Ar; 133.9 and 143.9, 4C+4C, quat. Ar.

^{1}H NMR in $CDCl_3$: δ 2.42, s, 12H, CH_3; 3.40, s, 16H, CH_2; 7.29, 7.32, 7.64 and 7.68, d+d, 16H, Ar.

1,4,7,10-tetraazacyclododecane tetrahydrobromide, [12]aneN₄.4HBr

As before, the tetratosylate (8 g) were de-tosylated by heating in 30% hydrobromic-acetic acid (500 ml) under reflux for two days. Yield 3.5 g, 71%; m.p. 248-255 °C dec.

^{13}C NMR in D_2O: δ 45.9, 28C, CH_2

^{1}H NMR in D_2O: δ 2.99, 16H, CH_2; 4.60, 3H, HOD of NH

2.10.3 Preparation of 1-Oxa-4,7,10-Triazacyclododecane Trihydrobromide

Diethylene glycol di-(p-tolunesulfonyl) O(CH₂CH₂OTs)₂

Solid p-tolunesulfonyl chloride (152 g, 0.8 mol) was added in portions to a mechanically stirred solution of diethylene glycol (42 g, 0.4 mol) in pyridine (290 ml) at zero temperature. The mixture was stirred for 2 hr and then hydrochloric acid was introduced dropwise so that the temperature was maintained below 10 °C. A white precipitate was produced which was recrystallised from boiling methanol. The white crystalline product was filtered off, washed with methanol and air-dried. Yield 84 g, 50%, m.p. 87-89 °C, lit. 87-89 °C.

^{13}C NMR in CDCl: δ 21.6, 2C, CH_3; 66.6 and 66.97, 2C+2C, CH_2; 127.9 and 129.8, 4C+4C, Ar; 132.7 and 144.9, 2C+2C, quat. Ar.

^{1}H NMR in CDCl₃: δ 2.41, s, 6H, CH_3; 3.57 and 4.05, t+t, 8H, CH_2; 7.30-7.75, m, 8H, Ar.

1-oxa-4,7,10-triazacyclododecane tri(p-toluenesulfonyl), [12]aneN₃OTs₃

Once again the method for triazacyclononane was performed with 0.04 mol of disodium salt **2** and an equivalent of the above O(CH₂CH₂OTs)₂ as starting reagents. The reaction proceeded the same way to give a white solid product. Yield 20.9 g, 82%; m.p. 194-196 °C.

^{13}C NMR in CDCl₃: δ 21.5, 3C, CH_3; 48, 2C, CH_2N; 50.5 and 50.6, 2C+2C, CH_2N; 71.9, 2C, CH_2O; 127.3, 127.5 and 129.8, 4C+2C, Ar; 135.0, 136.6, 143.3 and 143.6, 2C+1C+1C+2C, quart. Ar.

^{1}H NMR in CDCl₃: δ 2.41 and 2.43, 2s, 9H, CH_3; 3.15,q, 8H, CH_2N; 3.49, t, 4H, CH_2N; 3.64, t, 4H, CH_2O; 7.26-7.80, m, 12H, Ar.

1-oxa-4,7,10-triazacyclododecane trihydrobromide, [12]aneN₃O .3HBr

The tritosylate groups were detosylated with 30% hydrobromic-acetic acid and gave a yield of 4.8 g (73%) from 10 g of 1-oxa-4,7,10-triazacyclododecane tri(p-toluenesulfonyl). The melting point of the product was 253-255 °C as shown in the literature[108].

^{13}C NMR in D_2O: δ 43.7, 2C, CH_2N; 45.0, 2C, CH_2N; 47.5, 2C, CH_2N; 66.7, 2C, CH_2O.

^{1}H NMR in D_2O: δ 3.32, m, 12H, CH_2N; 3.74, t, 4H, CH_2O.

2.10.4 Preparation of 1,4,7-Triazacyclononane-N,N',N''-triacetate Iron III, [FeNOTA]
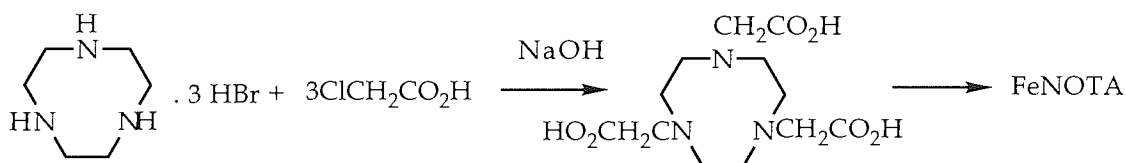
1,4,7-Triazacyclononane-N,N',N''-triacetate, NOTA

Triazacyclononane trihydrobromide (1.65 g, 0.005 mol) was dissolved in water (10 ml) with sodium hydroxide (0.015 mol). To this, a second solution was added containing chloroacetic acid (1.42 g, 0.015 mol) and sodium hydroxide (0.015 mol) in water (10 ml). The mixture was stirred and the temperature was raised to 80 °C. At the same time the pH of the mixture was maintained between 9 and 10 by adding dropwise a further 0.015 mol of NaOH dissolved in 10 ml of water during a period of 12 hr, after which time the reaction was completed.

To the above triacetate ligand mixture was added $FeCl_3$ (0.81 g, 0.005 mol) dissolved in water (10 ml) at 80 °C. The pH of the now yellow mixture was raised to approximately 7 with 0.5M NaOH, and yellow precipitate was

observed. The mixture was filtered off, washed with water and ethanol to give yellow needle-shaped crystals. Yield 0.62 g, 39%.

Anal: Cald for $FeC_{12}H_{18}N_3O_6$: C,40.47; H,5.10; N,11.80%

Found: C,40.52; H,5.06; N,11.79%

2.10.5 Attempted Preparation of 1,4,7-Triazacyclononane-N,N',N''-triphenylacetate
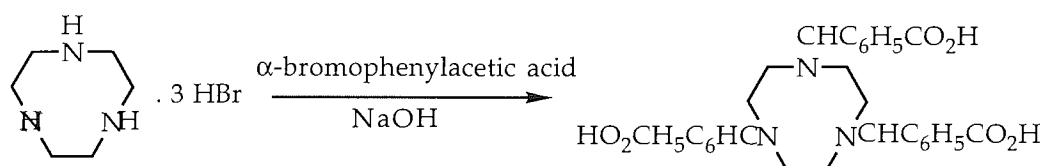
To a solution of triazacyclononane trihydrobromide (1.65 g, 0.005 mol) and NaOH (0.015 mol) in water (15 ml) was added and stirred at 20 °C a second solution containing α-bromophenylacetic acid (3.23 g, 0.015 mol) and NaOH (0.015 mol) in 15 ml of water. The temperature of the reaction was raised to 80 °C and this temperature was maintained for 15 hr, after which time reaction was judged to be complete. After the mixture was cooled, it was acidified to pH 2 where precipitation occurred. The precipitate was filtered off, washed with ice cold water and ethanol, then air-dried. Yield 0.8 g, 33%.

^{13}C NMR in $DMSOD_6$: δ 43.6, 6C, CH_2N; 72.6, 3C, CH-Ar; 126.6, 127.4 and 128.1, 2C+1C+2C, Ar; 140.9, 3C, quat. Ar; 174.6, 3C, carboxylate C.

^1H NMR in $DMSOD_6$: δ 3.02, s, 12H, CH_2N; 4.93, s, 3H, CH; 7.20-7.39, m, 15H, Ar.

The evidence from both NMR spectra indicates the final product is impure, therefore, no conclusion can be made whether the 1,4,7-triazacyclononane-N,N',N''-triphenylacetate product was successfully synthesised. This experiment was not investigated further due to the lack of time available.

2.10.6 Attempted Preparation of 1,4,7-Triazacyclononane-2,3-(4-tert-butyl-benzene)-tritosylate, [9]aneN₃Ts₃-2,3-(4-ᵗBu-benzo)-
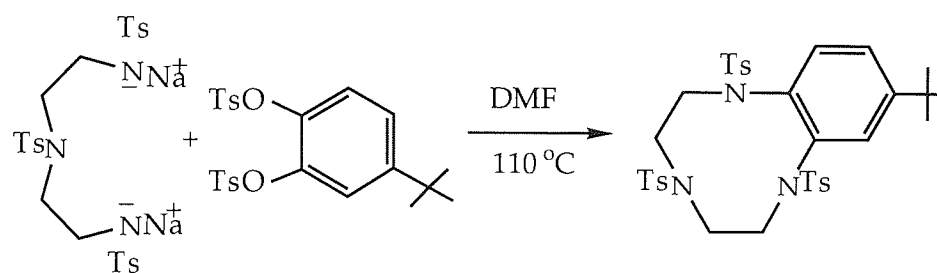
Preparation of 4-tert-butylcatechol-di-p-tosylate
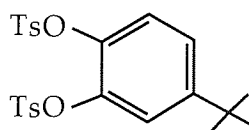
Solid p-toluenesulfonyl chloride (115 g, 0.6 mol) was added in portions to a mechanically stirred solution of 4-tert-butylcatechol (50 g, 0.3 mol) in pyridine (200 ml) at 0 °C. The mixture was stirred for two hours and hydrochloric acid was introduced dropwise (400 ml of 5M) so that the temperature was maintained at below 10 °C. A white product was formed and this was filtered off, washed with methanol and then recrystallised from boiling methanol. Yield 65 g, 46%; m.p. 97-98 °C.

¹³C NMR in CDCl₃: δ 21.7, 2C, CH₃(Ts); 30.9, 3C, CH₃; 34.7, 1C, C; 121.5, 123.6, 124.6, 128.4, 128.5 129.6, 1C+1C+1C+2C+2C+4C, Ar; 132.2, 132.4, 138.7, 140.7, 145.4, 145.5, 151.5, 1C+1C+1C+1C+1C+1C+1C, quart. Ar.

¹H NMR in CDCl₃: δ 1.21, s, 9H, CH₃; 2.41, 2.42, s+s, 6H, CH₃(Ts); 7.11-7.69, m, 11H, Ar.

Attempts to cyclise the above ditosylate of 4-tert-butylcatechol with disodium salt **2** have failed to produce the cyclised product. The products of this reaction were TsN(CH₂CH₂NHTs)₂ and 4-tert-butylcatechol-di-p-tosylate.

2.10.7 Attempted Preparation of [11]aneN$_3$Ts$_3$-3,4-benzo-
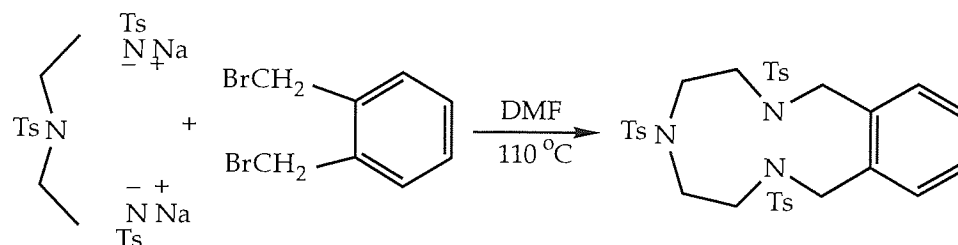
Cyclisation of the above compounds was attempted using the same procedure and the reaction gave a yield of 21%. The reaction was performed mainly to determine why cyclisation in the **2.10.6** reaction did not occur, rather than for any real use for the research target; since the addition of a benzene ring alone does not improve the solubility of metal complex in hydrocarbon solvents to the extent required.

^{13}C NMR in CDCl$_3$: δ 21.3, 21.4, 1C+2C, CH$_3$; 49.5, 2C, CH$_2$; 51.9, 52.7, 2C+2C, CH$_2$; 127.3, 128.8, 129.4, 129.7, 129.9, 131.9, 2C+4C+2C+2C+4C+2C, Ar.

^{1}H NMR in CDCl$_3$: δ 2.36, 2.44, 3H+6H, CH$_3$; 2.9, 8H, CH$_2$-N; 3.36, 4H, CH$_2$-N; 7.08-7.99, 16H, Ar.

2.10.8 Attempted Preparation of [9]aneN$_3$-2,3-hexadecane
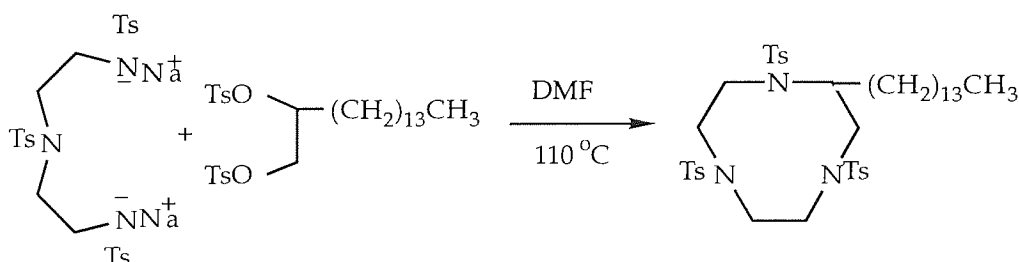
Preparation of 1,2-Hexadecanedioxy-di-p-tosylate

Again solid p-toluenesulfonyl chloride (0.2 mol) was added in portions to a mechanically stirred solution of 1,2-hexadecanediol (0.1 mol) in pyridine (200 ml) at 0 °C. The mixture was stirred for 2 hr before hydrochloric acid (100 ml 5M) was introduced dropwise as previously so that the temperature was

maintained below 10 °C. The precipitate product was filtered off and recrystallised from boiling methanol. Yield 34 g, 60%.

^{13}C NMR in CDCl$_3$: δ 13.8, 1C, CH$_3$R; 21.3, 1C, CH$_3$(Ts); 22.4, 24.9, 1C+1C, CH$_2$; 29.1, 9C, CH$_2$; 31.6, 32.4, 1C+1C, CH$_2$; 49.9, 1C, CH$_3$(Ts); 68.9, 1C, CH; 73.8, 1C, CH$_2$-O; 127.7, 129.6, 129.7, 4C+2C+2C, Ar; 133.1, 144.9, 2C+2C, quart. Ar.
^{1}H NMR in CDCl$_3$: δ 0.83, 3H, CH$_3$R; 1.2, 26H, CH$_2$; 1.55, 2H, CH$_2$; 2.39, 6H, CH$_3$(Ts); 4.53, 1H, CH; 7.24-7.76, 8H, Ar.

Attempts to cyclise 1,2-hexadecanedioxy-di-p-tosylate with the disodium salt (2) were unsuccessful so far. Unfortunately, at that point, the available research time had been used up, so the final outcome of this reaction is still unknown.

2.11 DISCUSSION

Unfortunately, having finally mastered the technique of synthesising macrocyclic polyamines, there was insufficient time left to functionalise these ligands with hydrocarbon substituents. The synthesised macrocyclic polyaza ligands and their polycarboxylate compounds have already been discussed in detail by previous workers, as described in the introduction. Therefore they will not be discussed here.

However, little has been reported on the solubility of these metal complex compounds in polar or non-polar organic solvents. So, the iron complex of the NOTA ligand was synthesised (mainly because it is the easiest reaction to perform) to test for its solubility properties. The FeNOTA complex showed no solubility in organic solvents and only dissolved in boiling water with very low solubilty as mentioned by Wieghardt[92]. Once again, the hydrocarbon

weight of these ligands has to be increased to achieve the solubility required in hydrocarbon environments.

There are two possible routes to increase hydrocarbon weight of these cyclic polyaza ligands:

(i)   functionalisation of the N donor atom

(ii)   functionalisation of the ring itself.

The first route is illustrated by the earlier discussed compounds, i.e. NOTA and DOTA, where the N donor atoms are functionalised by the acetate groups. Since these types of compounds already exist it was decided to initially use this route, to funtionalise the prepared cyclic polyamines. It is kown that FeNOTA complex is insoluble in hydrocarbon. Therefore, a different carboxylate group with more hydrocarbon weight is required and α-bromophenylacetic acid is one such group which is commercially available. Two separate attempts were made before time ran out for this work to increase the hydrocarbon weight of the TACN ligand using this particular carboxylate, but both times resulted in failure. Although failures are mainly due to the method rather than the reaction, i.e not possible.

The second route inolves funtionalisation of the ring and not at the N donor atom. The functionalisation is achieved before the cyclisation step rather than after, in route (i), where the chosen functional group is the actual cyclisation reagents. It is now known from my earlier work that, by adding tertiary butyl groups on to a ligand structure of the metal complex, there will be an increase in the compound's solubility in organic solvents. With this knowledge, attempts were made to synthesise the triazacyclononane tert-butylbenzo substituted macrocyclic polyaza ligand. Before this step, the tert-butyl catechol has to be tosylated before the cyclisation step can take place. So,

the previous procedure involving the tosylation of a diol compound in excess pyridine at 0 °C temperature was used again. Pyridinium chloride separated from the solution when the reaction mixture was added to dilute hydrochloric acid, e.g.

$$ROH + \quad \text{(aromatic ring with SO}_2\text{Cl and CH}_3\text{)} + C_5H_5N \xrightarrow{0\,^\circ C} ROSO_2 \text{—(aromatic ring)—} CH_3 + C_5H_5NH^+Cl^-$$
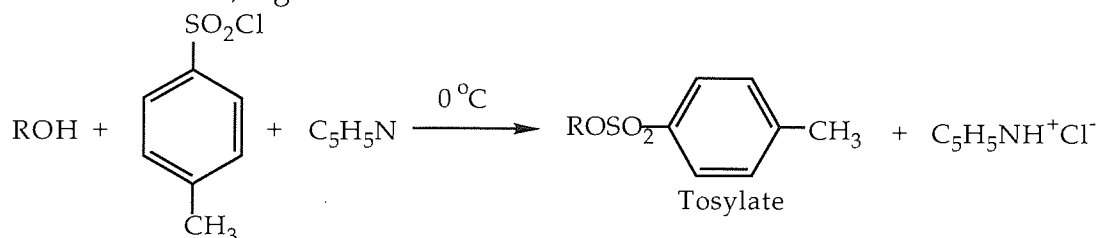
Tosylate

The next step was to cyclise the tosylated tert-butylcatechol and the disodium salt 2 compounds. There were already indications that this reaction may not work but it was nevertheless attempted and the result as expected, was incomplete. In this reaction the aromatic ring with 3 substituents is required to undergo a double nucleophilic substitutions. Generally, aromatic rings will only undergo a reaction towards electrophiles, with the formation of an intermediate carbonium ion. They are normally inert to nucleophiles. There are some substituted benzenes which do react with nucleophiles due to the substituent's ability to activate the ring, e.g. nitrobenzene. The mechanism of this nucleophilic aromatic substitution is similar to that of the electrophilic aromatic substitution except that an anionic rather than a cationic intermediate is involved. The nucleophile is added to the aromatic ring which gives a delocalised anion from which a hybride ion is eliminated:
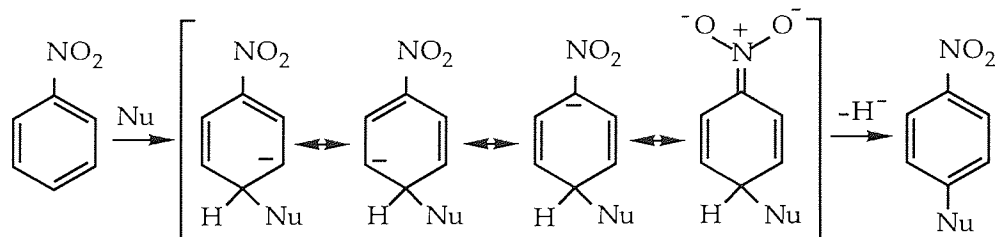
So, the reactivity towards a nucleophile in nitrobenzene when compared with that of the benzene stems from the ability of the nitro-group to stabilise the anionic intermediate by accommodating the negative charged. Further to this, delocalisation can only occur if the nucleophile is added on to the *ortho*

or *para* position; electron-withdrawing substitutuents are activating and *ortho*, *para*- directing, thus conversely electron-releasing groups are deactivating and *meta*- directing. Unfortunately, the tert-butyl group is an electron releasing substituent and therefore deactivating in the cyclisation reaction of the tert-butyl catechol and disodium salt 2, which may explain why the reaction was unsuccessful.

This was proved by the following reaction where the reaction between dibromoxylene and disodium salt 2 was successfully carried through to produce a macrocyclic polyaza compound. This was due to the substitutions occuring at the carbon atoms attaching to the benzene ring and not those of the ring itself, and due to absence of the deactivating group on the benzene ring. One can conclude from this reaction that a double nucleophilic substitution reaction is not possible on aromatic compounds but only on alkyl compounds.

Another group of substituents is needed to produce the desirable hydrocarbon soluble metal complex of these cyclic polyamine ligands. It was decided to use hexadecyl-containing compounds as the substituent group. These compounds would provide an adequate number of carbon atoms required to increase solubility of the metal complex compound. The diol of haxadecanediol was converted to its tosylated compound by the normal method. An attempt was made to cyclise this compound with the disodium salt 2 compound to produce a substituted triazacyclononane compound, but this again resulted in failure. No further reactions were made on this particular cyclisation due to there being no further research time left, and so the reaction is unproven here.

The attempts so far, to functionalise the cyclic polyamine ligands with the chosen large hydrocarbon substituents using the above discussed two routes have all resulted in failures. Although the final desired products of the cyclisation step of the reactions with the hydrocarbon substituents which were selected for the potential ligand were unsuccessful, some cyclised compounds were achieved. The work achieved on the disubstituted xylene reactions have illustrated that cyclisation was not possible at carbon atoms on the benzene ring itself, but only possible at the carbon atoms attaching to the benzene ring. In future, any cyclisation must be targeted on the carbon atoms that are attached to the benzene ring and not the carbon atoms of the benzene ring. Since the majority of the described experiments are incompleted, the final conclusions of these cyclisation reactions are still remain unanswered and will only be answered if further experiments are made.

2.12 CONCLUDING REMARKS

The purpose of this study was to investigate the effect of metal complexes on the combustion of commercial fuels. In respect of this, the first target of the study was successfully achieved. Metal complexes of the Schiff base ligands and the derivative of the acetylacetone were successfully produced, as planned. These complexes are either partly or completely soluble in hydrocarbon fuels and all are stable to oxidation at room temperature. The thermal stability of these complexes will be described in the next chapter.

The metal complexes' solubility in hydrocarbon solvents is a problem which has been encountered with both initial target ligands i.e. acac and saltren. The problem was overcome by attaching large hydrocarbon substituents onto these ligands. These experiments indicated that the tertiary butyl group has more effect than the aromatic group on the solubility of the complexes in hydrocarbon solvents. Complexes of the tertiary butyl substituent ligands are

completely soluble in a hydrocarbon environment, while the complexes of the naphtren, aromatic substituent ligand, show incomplete solubility.

However, not all the results were successful. The attempts to synthesise metal complexes with the macrocyclic ligands resulted in failure. This was due to a large amount of the research time involved in this area of work being consumed by familiarization of the cyclisation methods. Therefore, there was no available time to achieve the synthesis of the metal complexes of these ligands. The work achieved here, however, was not wasted, since the information gained from the reactions of the ligand synthesis are benificial to future reactions. So, this section of the work remains unexplained, mainly due to the time factor, but enough work has been done to lay the foundations for future research work.

Chapter 3

Thermal Analysis of the Metal Complexes

3.1 INTRODUCTION

Thermal methods of analysis may be broadly defined as methods of analysis in which the effect of heat on a sample is studied to provide qualitative or quantitative analytical information. Such studies have a long history[117,118], but it is only in the last 40 years that instrumental improvements have led to methods which are both simple and reliable to operate. This has been accompanied by a steadily widening applicability. Such techniques are now applied across a wide range of areas in which analytical chemistry is used. Current areas of application include environmental measurements, composition analysis, product reliability, stability and chemical reactions. Thermal analysis has been used to determine the physical and chemical properties of polymers, geological materials and coals. An integrated, modern thermal analytical instrument can measure transition temperatures, weight losses and energies of transitions.

Thermogravimetry (TG) or thermogravimetric analysis (TGA) is based on the very simple principle of monitoring the change in weight of a sample as the temperature is varied. By controlling the atmosphere e.g. with oxygen or nitrogen, it may be possible to encourage or suppress oxidation reactions, thus controlling to some extent the nature of the thermal events occurring. When heated over a range of temperatures, ambient to approximately 1000 ^{o}C, many materials undergo weight changes giving characteristic curves. Where the changes can be linked to a particular thermal event, such as oxidation, or loss of water of crystallisation, the size of the step in the curve can be used for quantitative analysis.

Differential thermal analysis (DTA) is a technique which involves heating a test sample and an inert reference sample under identical conditions and recording any temperature difference which develops between them. This

differential temperature is then plotted either against time, or against the temperature at some fixed point within the apparatus. Any physical or chemical change occurring to the test sample which involves the evolution of heat will cause its temperature to temporarily rise above that of the reference sample, thus giving rise to an exothermic peak on the DTA plot. Conversely, a process which is accompanied by the absorption of heat will cause the temperature of the test sample to lag behind that of the reference material, leading to an endothermic peak. Typical behaviour is shown schematically in Figure 3.1.
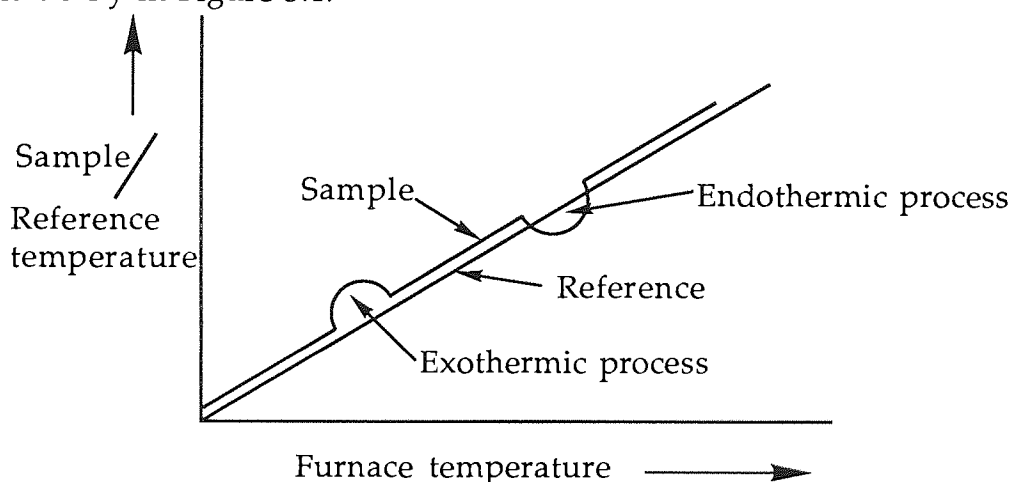
Figure 3.1 Schematic representation of the variation of sample and reference temperature in DTA

In practice temperature differrence (ΔT) vs furnace temperature is plotted giving a thermogram of the type illustrated in Figure 3.2.
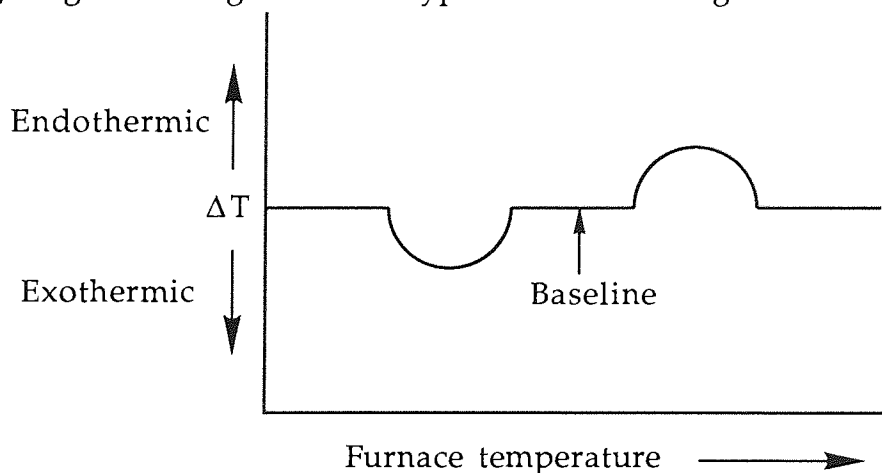
Figure 3.2 ΔT vs T plot to give a schematic DTA trace

The use of microprocessors has both enhanced and simplified the techniques of thermal analysis. The sample is heated at a programmed rate in the controlled environment of the furnace. The changes in selected properties of a sample are monitored by specific transducers, which generate voltage signals. These are then amplified, digitized, and stored on a magnetic disk along with the corresponding direct temperature responses from the sample. The data may also be displayed or plotted in real time.

A major advantage of microcomputer systems in thermal analysis is that the operator seldom, if ever, needs to repeat an analysis because of an improper choice of ordinate scale sensitivity. The software does this rescaling after all the data has been collected. In some systems both axes are automatically rescaled after the last data point has been received. When the amount of time necessary to obtain thermal data is considered, the advantage is obvious.

3.2 APPARATUS AND METHOD

A thermal analytical instrument is an apparatus which enables a sample to be heated at a uniform rate whilst its temperature and one or more of its physical properties are measured and recorded. Such an instrument therefore contains four basics components:

    (i)   Sample holder– measuring system. This is the heart of any apparatus. It comprises the thermocouples, sample containers and, in certain cases, a ceramic or metallic block.

    (ii)   Furnace– heat source having a large uniform temperature zone.

    (iii) Temperature programmer– to supply energy to the furnace in such a manner as to ensure a reproducible rate of change of temperature.

(iv) Recording system-- method of indicating and/ or recording the e.m.f. (suitably amplified) from the differential and temperature measuring thermocouples.

All thermal analyses were performed on a LINSEIS thermobalance system which runs on an SI-RTWD program. The complete system consists of the following components:

- ◆ LINSEIS thermobalance with amplifier
- ◆ SI-RTWD: remote controllable temperature controller
- ◆ LINSEIS L2045 recorder with RS232 interface
  Supplying the channels: channel 1: temperature

  channel 2: TG signal

  channel 3: DTA signal
- ◆ IBM PC XT/AT and IBM Graphic Printer
- ◆ LINSEIS L1640 plotter.

The following diagram shows the connection of the components:
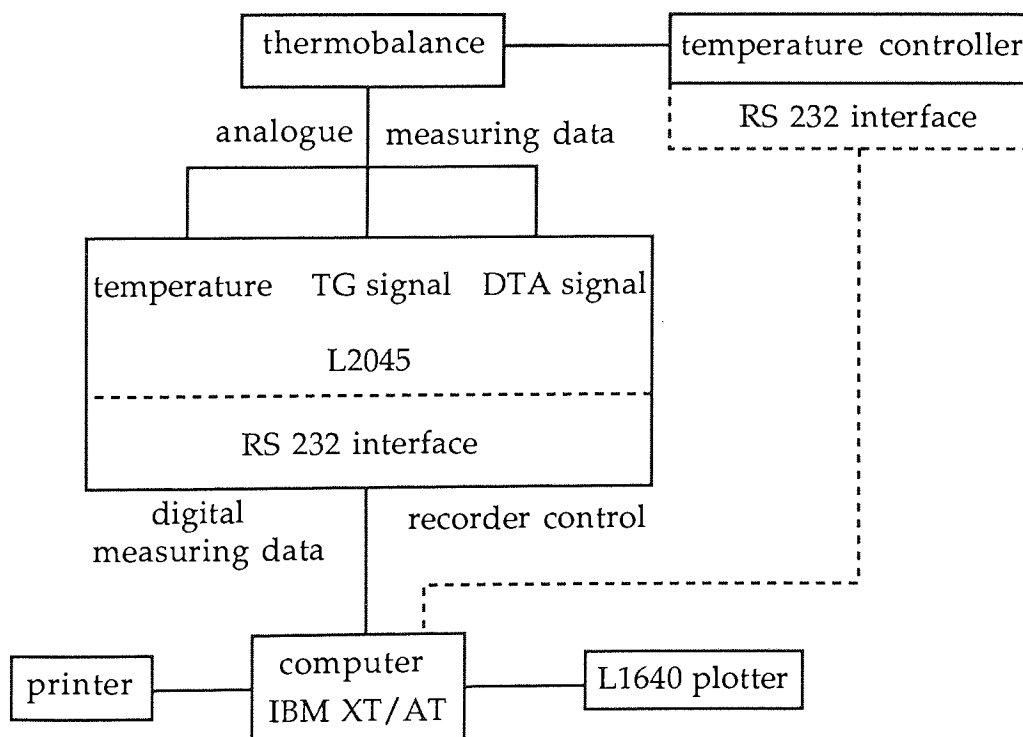
SI-RTWD is a menu-controlled program for the measurement and evaluation of TG/DTA curves. The program offers:

- simple program operation via menus
- error compensation of the measuring system by using a system specific calibration curve at the measurement.
- graphic recording during the measurement
- recording and transmitting the measuring values to the computer by using the L2005, L2006, and L8500 recorders
- easy evalution on the screen by means of function and cursor buttons:
  - onset temperature
  - reaction temperature
  - manifold output possibilities
  - screen graphic
  - printer graphic (hardcopy)
  - coloured plotter graphic

The thermal analyses were performed using an alumina sample holder, in the atmosphere of air, and at a heating rate of 10 K/Min with a maximum furnace temperature of 550 ^{O}C.

3.3 RESULTS AND DISCUSSION

3.3.1 Ce(DPM)$_3$

The thermal analytical curves for Ce(DPM)$_3$ are shown in Figure 3.1. The DTA and TG processes evidently show the decomposition of the above cerium complex with the combustion of the DPM groups. According to the TG, there is a loss of 75% between the temperature range of 170-283 ^{O}C. This is due to the removal of 3 DPM groups during the decomposition process and the theoretical figure for this is 72% without the two oxygen atoms required for the formation of CeO$_2$. The decomposition process of the DPM coincides

with the exothermic effects observed between the temperature range of 170-260 ^{O}C, where a small exothermic effect followed by a big exothermic effect occurred. The remaining mass of 25% corresponds to the CeO_2 (26%), as expected.

3.3.2 Ce-saltren

The thermogravimetric curve for Ce-saltren is complicated (Figure 3.2). The decompositon process of the complex takes place in the temperature range of 232-378 ^{O}C. The TG shows that there is a very small gain in mass of 0.8% at temperature up to 176 ^{O}C and then is followed by a small loss of 2%, probably due to the small trace of impurity in the compound. This is followed by the decomposition stage where a mass loss of up to 72% is observed within the temperature range of 232-378 ^{O}C, compared with the theoretical figure of 76% for the loss of a saltren, without allowance for the oxygen required for the formation of CeO_2. The theoretical figure after account is taken of the two oxygen atoms is 71%. Thus the decomposition corresponds with the series of exothermic effects due to the oxidation processes for the saltren, resulting in CeO_2. The DTA shows that this decomposition stage is a complex process consisting of six exothermic effects, with the first being the largest of several oxidation process. The remaining mass of 28% at temperatures above 378 ^{O}C is due to the CeO_2 (29%).

3.3.3 Fe-saltren

The simultaneous TG and DTA curves for Fe-saltren are given in Figure 3.3. The TG shows that two steps of mass losses occured between 267-420 ^{O}C and 420-515 ^{O}C. The first step is a mass loss of 35% due to the initial combustion processes which corresponds with the exothermic effects and, when calculated, this figure represents the combustion of 9C, 15H and 4N (35%). These atoms are equal in number to those of the tris-2-aminoethylimine

group of the ligand, and therefore, the two exothermic effects are due to the loss of the hydrocarbon and the nitrogen. The second step and final mass loss of 51% must be due to the benzene rings. This figure matches the figure for the remaining 18C, 15H and 2O (51%), with the allowance of an oxygen atom for the formation of FeO (> 515 ^{O}C). The exothermic effect between 400-440 ^{O}C corresponds to this decomposition stage and thereby shows the thermal stability of aromatic over aliphatic compounds. The remaining mass of 13% at the temperature of above 515 ^{O}C is due to the FeO formation (14%).

3.3.4 Ce-naphtren

The thermal analytical curves for Ce-naphtren are shown in Figure 3.4. Again, the similar two stage decomposition from Ce-naphtren to CeO_2 is observed as previously seen for Fe-saltren. The TG shows the initial decomposition stage with a mass loss of 23% in the temperature range of 210-478 ^{O}C, which is due to the combustion of the tris-2-aminoethylimine group i.e. 9C, 15H and 4N (24%). So the aliphatic part of the naphtren ligand has decomposed first. This is followed by the second stage of the decomposition, which involves a mass loss of 51% between the temperature range of 478-550 ^{O}C, and the theoretical figure for the remaining aromatic atoms with respect to the first stage is 53%. However, the TG curve appears to indicate that the decomposition process is still continuing above the maximum temperature that can be obtained with the apparatus. This would explain why the remaining mass at 550 ^{O}C is 26% rather than the expected 23% for CeO_2. The DTA shows a complex process of combustion for the decomposition of this cerium complex.

3.3.5 Fe-naphtren

The thermogravimetric curves for Fe-naphtren are given in Figure 3.5. Again, the TG shows a steady decomposition of the complex, starting at 244

^{O}C and still continuing above the maximum temperature of 550 ^{O}C. According to the DTA there are three exothermic effects in the temperature range of 215-438 ^{O}C which correspond to the combustion processes of the decomposition. Here, the decomposition of the Fe-naphtren to the iron oxide is incomplete in this temperature range, and therefore a further experiment with a higher maximum temperature is required in order for a conclusion to be made.

3.3.6 Ce-^{t}Bu-saltren .2H$_2$O

The TG curve for Ce-^{t}Bu-saltren.2H$_2$O (Figure 3.6) shows the first mass loss of 4% between 200 ^{O}C and 258 ^{O}C. It is due to the complete dehydration of the salt (4%). However, the DTA curve does not show an endothermic effect, as expected for the removal of the water molecule An explanation for this is that the endothermic effect has been overlapped by the large subsequent exothermic effect. The dehydration is immediately followed by the decomposition of the salt between 258 ^{O}C and 297 ^{O}C with a mass loss of 22%. This corresponds to the combustion of the tris-2-aminoethylimine group (21%), also present in this complex. Further decomposition occurs above 297 ^{O}C and continues beyond the maximum temperature. Therefore any further suggestions would be mere speculation without more experiments involving higher achievable temperatures. The final product would be expected to be CeO$_2$, this would have a residual mass figure of 22%. The TG curve indicates a maximum mass loss of 76% allowed for this experimental temperature range. Therefore, we can say that the end of the decomposition process has almost been reached.

3.3.7 Fe-^{t}Bu-saltren

The thermal analytical curves for Fe-^{t}Bu-saltren are shown in Figure 3.7. The TG curve shows that at room temperatures the iron salt apppears to gain a mass of 7.8%. This figure would correspond to three water molecules. This is

followed by a mass loss of 6.4% between 16-34 °C and then a further loss of 1% between 34-237 °C, which corresponds to the loss of 2.5 H_2O and 0.5 H_2O respectively. The DTA curve shows no endothermic effect, but a small exothermic effect is observed for these temperature ranges. This would contra-indicate a dehydration process, and therefore maybe another process has taken place here. However, the shape of the TG curve i.e. a curve initially decreasing, then becoming horizontal, usually indicates the drying of a precipitate. Then over the temperature range of 240-550 °C, there is a decomposition process which corresponds to four exothermic effects. The TG curve suggests that the decomposition process is again continuing beyond the maximum achievable temperature. However, the 83% mass loss indicates that the combustion process has almost reached its end with the formation of FeO (89% mass loss). The TG curve indicates that the decomposition consists of overlapping reactions with no stable intermediates. Again, no conclusion can be made here without further analysis.

3.4 CONCLUDING REMARKS

All the metal complexes appear to show thermal stability at temperatures up to 200 °C, except Ce(DPM)$_3$ which start decomposing at 170 °C. This cerium complex shows the smallest decomposition temperature range, i.e.170-282 °C. Therefore, Ce(DPM)$_3$ is the least stable complex out of all the complexes tested. The reason for this is due to the smaller coordination number of the DPM ligand compared to the higher tripod type ligands. Of the tripod complexes, only the complexes of the saltren ligand decomposed within the limit of the furnace temperatures. This does not indicate that the substituted saltren complexes are thermally more stable since they all start decomposing at approximately 250 °C. However, it does indicate that the decomposition process is slower in these substituted saltren complexes and this is due to the substituted components. So, the goals of synthesing hydrocarbon soluble and thermally stable complexes have been achieved.

Figure 3.3 TG and DTA curves for Ce(DPM)₃
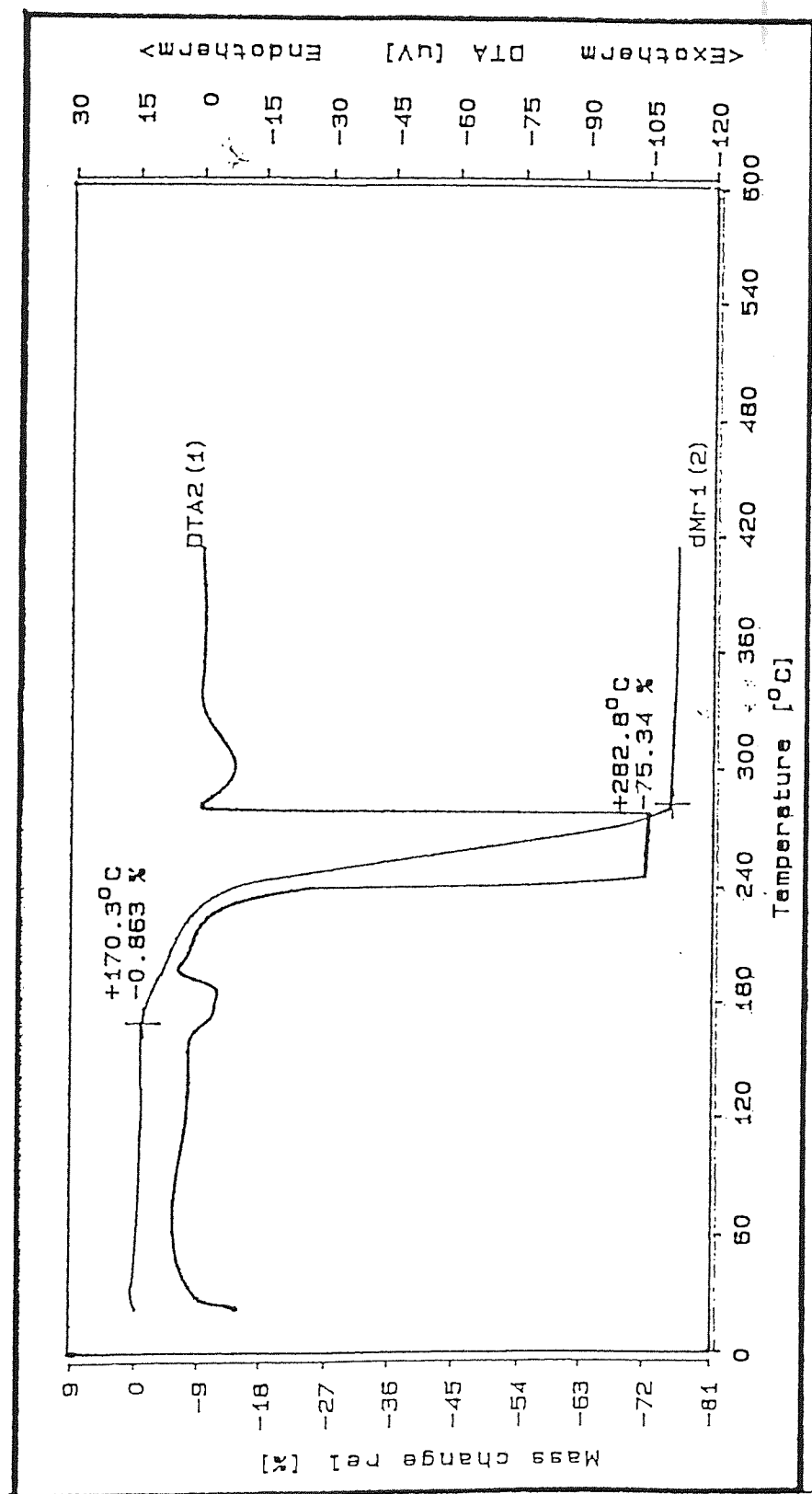
Sample: Ce(DPM)₃   CeC₃₃H₅₇O₆   26.90 mg   Atmosphere: Air   Rate: 10.0 K/Min
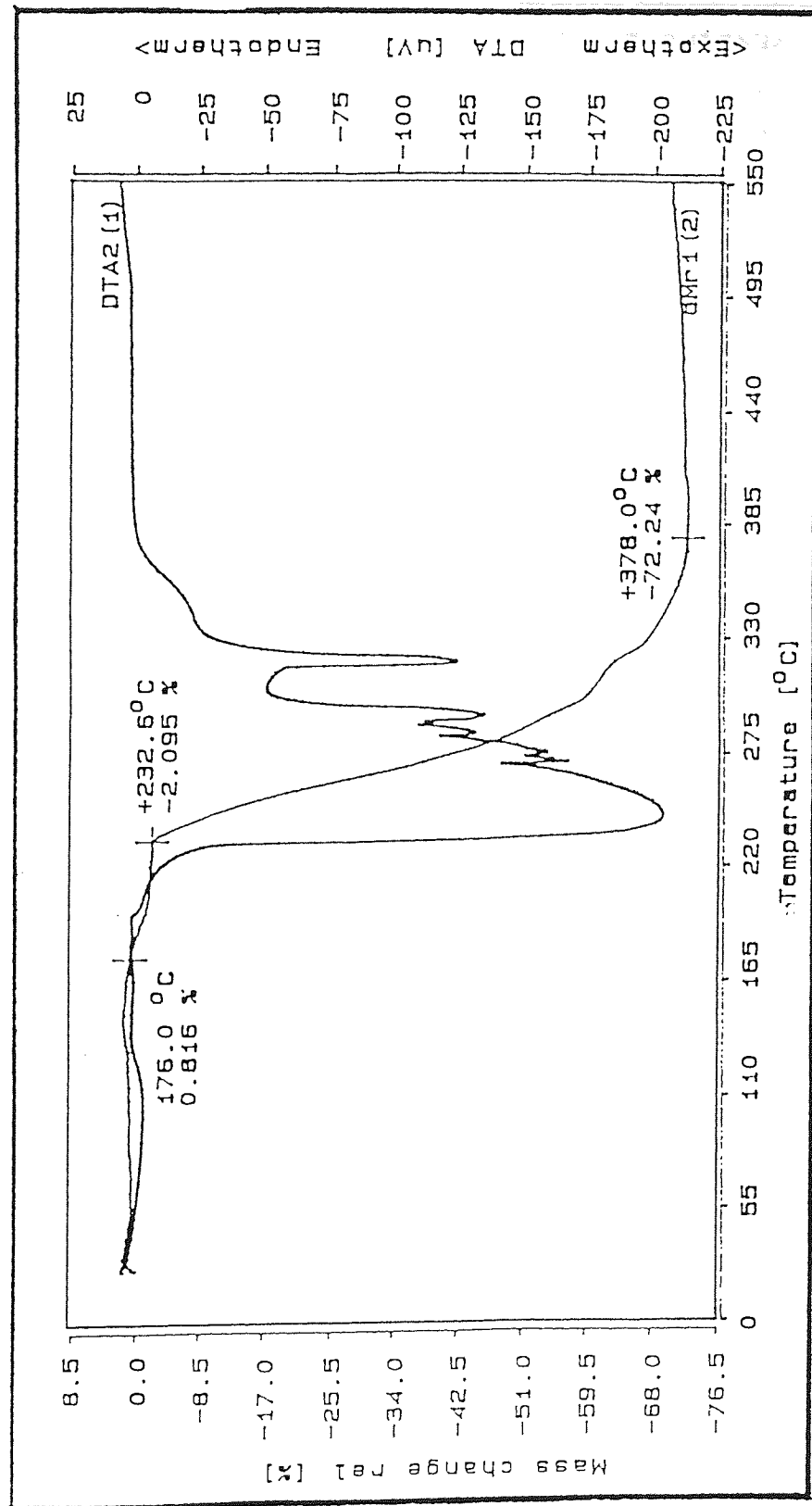
Sample: Ce-saltren   CeC$_{27}$H$_{27}$N$_4$O$_3$ 10.40 mg   Atmosphere: Air   Rate: 10.0 K/Min

Figure 3.4 TG and DTA curves for Ce-saltren
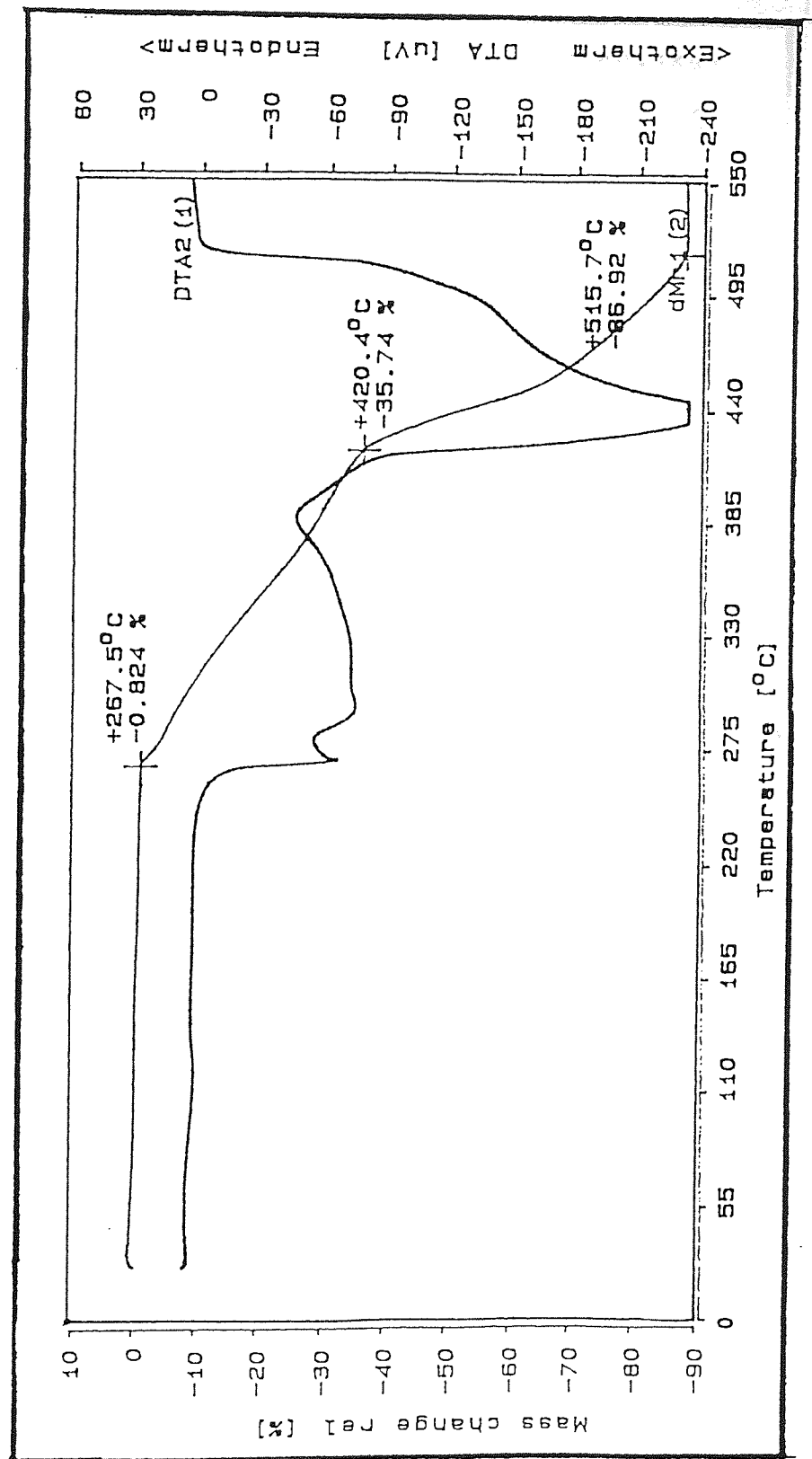
Sample: Fe-saltren   FeC$_{27}$H$_{27}$N$_4$O$_3$ 24.60 mg   Atmosphere: Air   Rate: 10.0 K/Min

Figure 3.5 TG and DTA curves for Fe-saltren

Figure 3.6 TG and DTA curves for Ce-naphtren
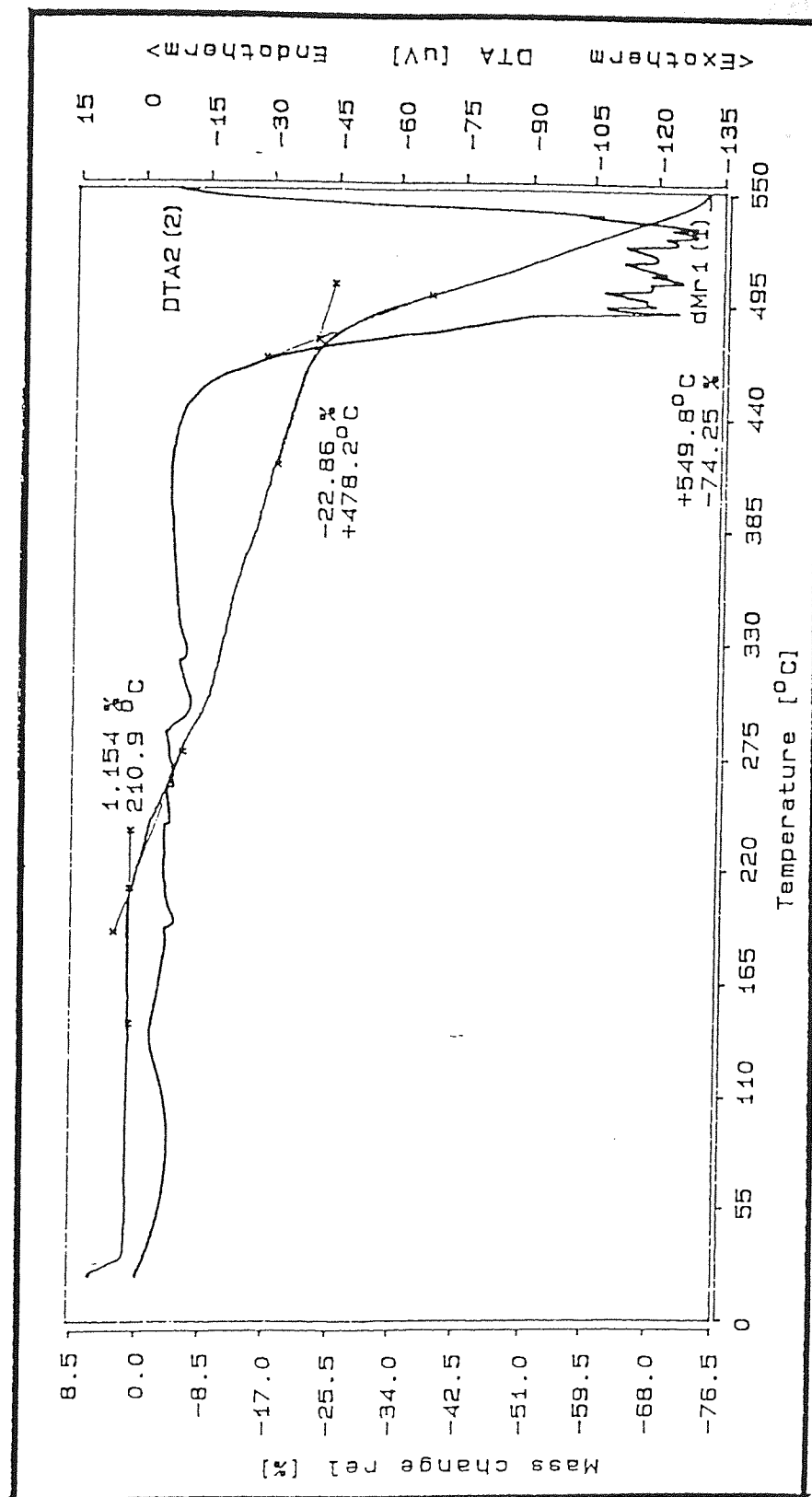
Sample: Ce-naphtren   CeC$_{39}$H$_{33}$N$_4$O$_3$ 10.06 mg   Atmosphere: Air   Rate: 10.0 K/Min

Figure 3.7 TG and DTA curves for Fe-naphtren
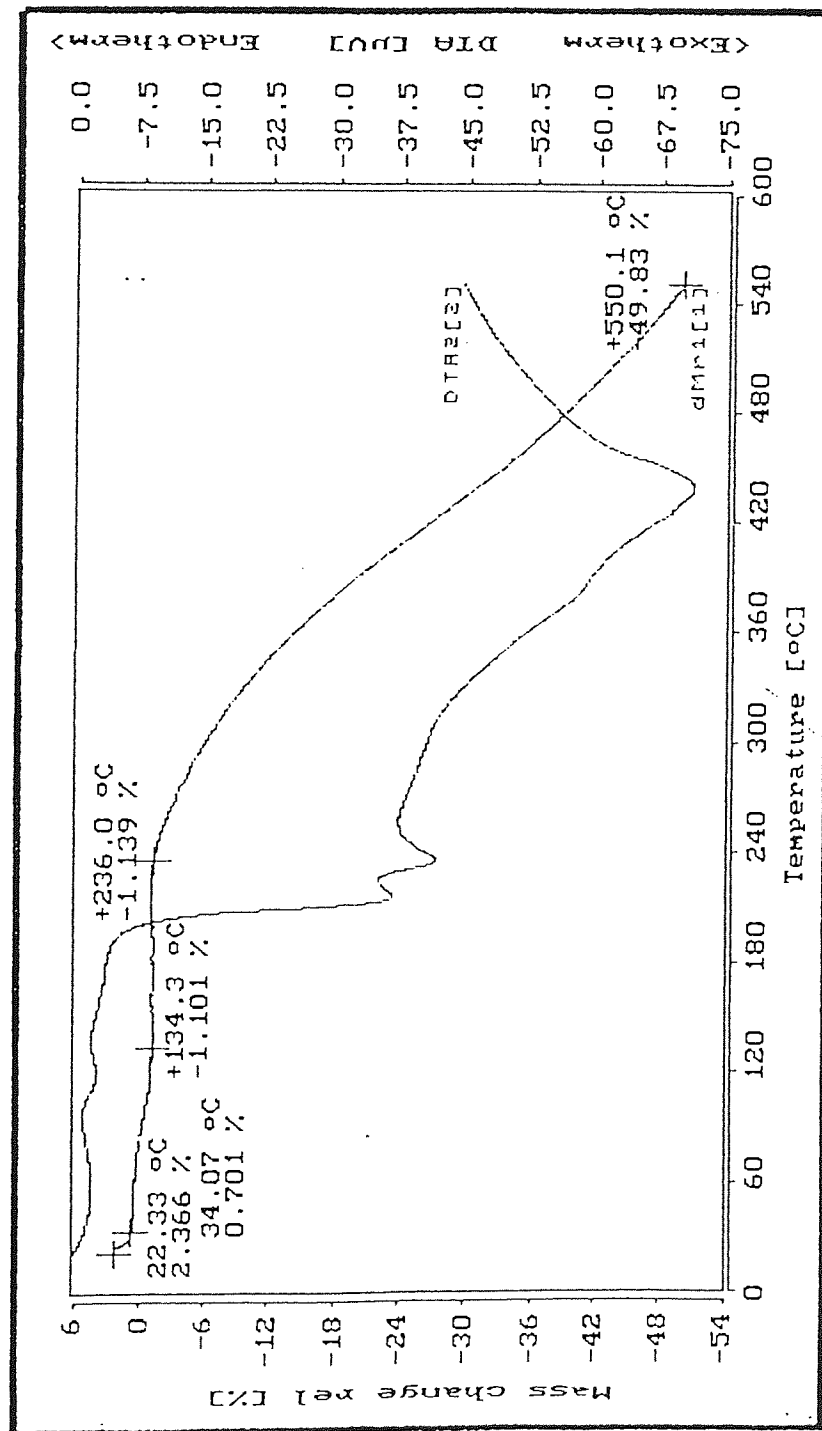
Sample: Fe-naphtren   FeC$_{39}$H$_{33}$N$_4$O$_3$ 23.60 mg   Atmosphere: Air   Rate: 10.0 K/Min
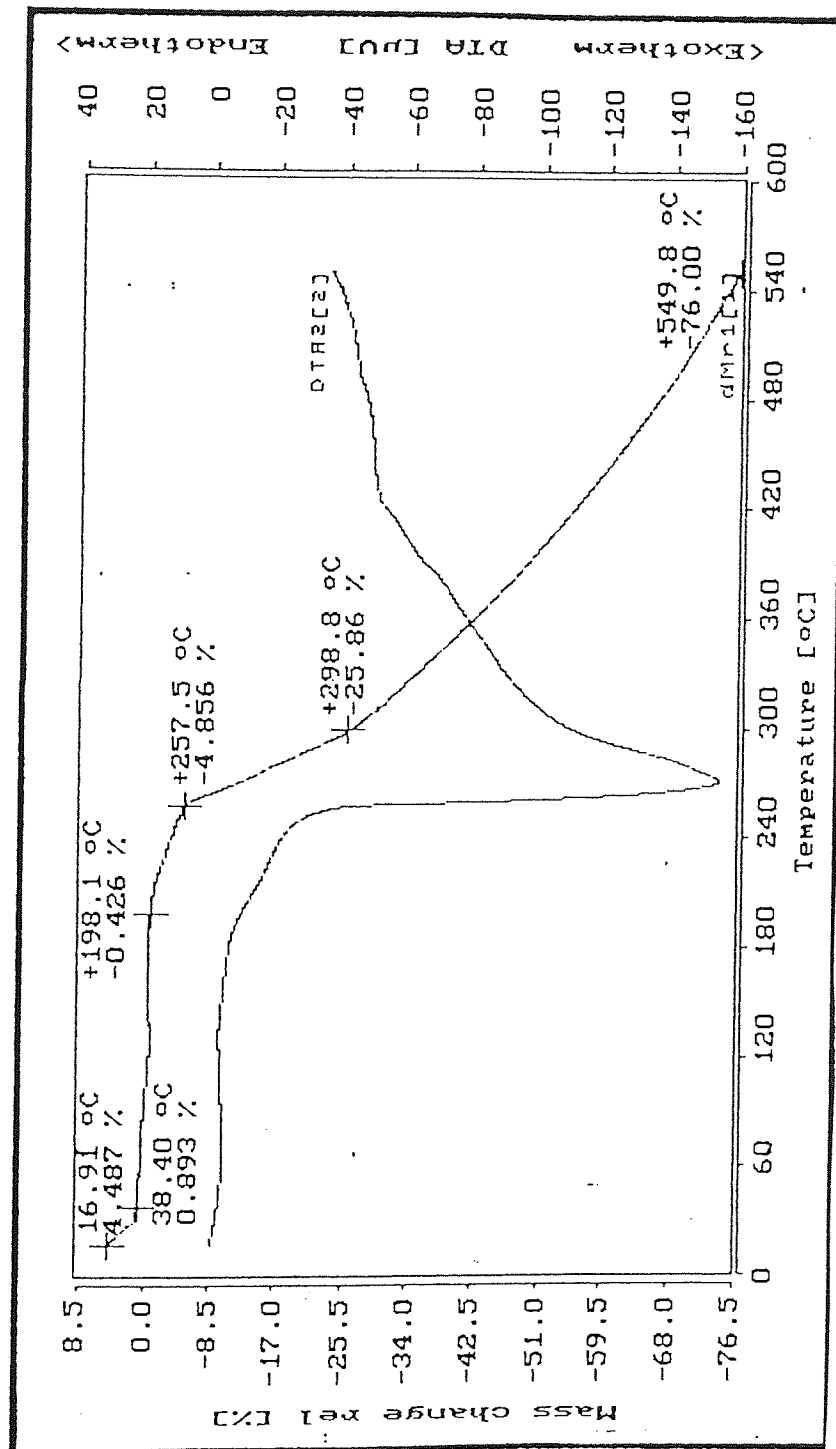
Sample: Ce-^{t}Bu-saltren   CeC$_{39}$H$_{51}$N$_4$O$_3$ 21.25 mg   Atmosphere: Air   Rate: 10.0 K/Min

Figure 3.8 TG and DTA curves for Ce-^{t}Bu-saltren
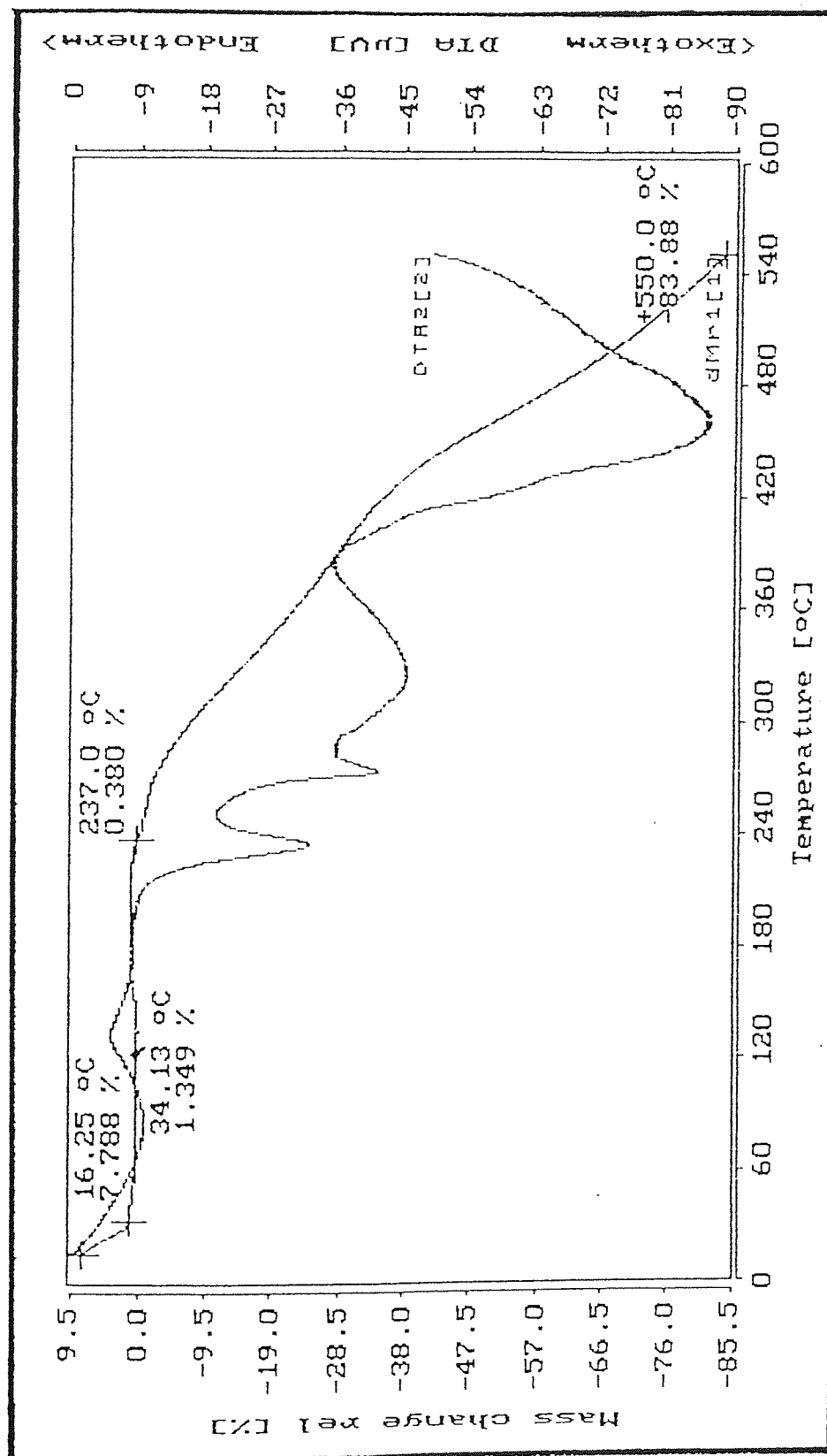
Sample: Fe-^{t}Bu-saltren   FeC$_{39}$H$_{51}$N$_4$O$_3$ 12.90 mg   Atmosphere: Air   Rate: 10.0 K/Min

Figure 3.9 TG and DTA curves for Fe-^{t}Bu-saltren

Chapter 4

Diesel Combustion Bomb.

" The Effect of Metal Complexes on Combustion of Diesel Fuel Studied with the Aid of a Combustion Bomb ".

4.1 INTRODUCTION

The processes that take place inside the combustion chamber of a diesel engine are far from ideal from the viewpoint of the role of the metal additives in assisting combustion. We need to appreciate the designer's ultimate purpose as well as his more practical targets before we can discuss additives fully.

To obtain the maximum thermal efficiency from the burning of hydrocarbon fuel it would ideally be necessary to release the heat energy of the fuel under constant-volume conditions, i.e. a constant volume bomb. Such behaviour would require that the combustion took place instantaneously and homogeneously, with no variation from one engine cycle to the next (nor from one day to the next). Such ideal combustion behaviour of the fuel and air mixture would in turn require that the ignition event be perfectly repeatable, and that the flame process be both infinitely fast and repeatable so that there would be no heat loss to the walls of the combustion chamber and cylinder and no emission of partially burnt or other undesirable combustion products.

In practice, this thermodynamic ideal for the diesel combustion engine is subject to limitations of both chemical kinetics and fluid dynamics of the fuel and air as they are fed through the reciprocating engine. The fuel and air do not react instantaneously and the combustion process is a heterogeneous one.

In view of the great difficulty in conducting experimental work on engines under fully controlled conditions, it was initially decided to investigate the metal complex additives using a 'combustion bomb'. This chapter describes the findings for the various metal complexes that were investigated for their effect on the combustion processes of the diesel fuel under controlled

conditions, with the aid of a diesel combustion bomb which simulates the combustion process in the D.I. diesel engine.

A small team of research workers at Bath University have developed a unique combustion bomb capable of simulating many of the most important characteristics of the high swirl D.I. diesel engine combustion system. The combustion rig is claimed to reproduce the condition of high air pressure (up to 60 bar), high temperature (up to 700°C) and swirling air motion to be found at the start of fuel injection in small to medium sized D.I. diesel engines. A single-shot fuel injection system supplies fuel to the chamber under engine-like conditions. The mechanical details of the rig are described more fully by Packer[119].

The fuel injection and combustion event typically occupies from 1 to 30 milliseconds, and the maximum amount of information from the experiment is required during this period. The injector needle valve opening and combustion chamber pressure are monitored by various transducers. The microcomputer-based data acquisition and control system controls the fuel injection sequence and records the subsequent transducer output at a sampling rate up to 70 kHz.

At the end of the test the transducer outputs captured by the system can be examined on the oscilloscope. If the data is satisfactory it may then be transferred via another micro-computer to the university mainframe computer for complete analysis. This operation is very time consuming at present, as the Bath design dates back several years. Before describing further details of the combustion bomb, a fuller understanding of the diesel combustion processes is needed.

4.1.1 Reason for Bomb Programme

It is essential to determine the mechanism of action of the catalyst in the engine combustion chamber and to ascertain minimum dosage requirements to achieve a given effect. This will contribute significantly towards the development of an optimized and economical product formulation. The bomb programme would provide the required information on the effect metal additives have on the ignition quality of "reference" diesel fuels in the absence of cetane improvers and detergents.

It is considered that these basic requirements can only be achieved by a comprehensive study over a wide range of bomb operating conditions and under controlled conditions on the diesel combustion bomb. The Bath group's diesel combustion bomb was fully instrumented to provide all the necessary output data so that the precise values emerge on overall improvement of the combustion processes and to elucidate the mechanism by which the improvement is brought out (viz, by a heterogeneous deposition mechanism due to catalyst build-up on the combustion chamber surface, or by vapour phase action in the bulk of fuel-air charge). Since fuels are supplied as a single-shot injection (see **4.3.2**) into the combustion chamber and under non-swirl conditions we can safely say that the catalyst effect would predominately be gas phase mechanism. Firm judgements should also be possible as to exactly how the catalyst affects the combustion process (eg. perhaps by reducing "delay periods").

4.2 THE DIESEL COMBUSTION PROCESS

While the chemical reactions that occur during the combustion are undoubtedly very similar both in spark-ignition and in diesel engines, the physical aspects of the two combustion processes are quite different. In the spark-ignition engine under normal operating conditions, the fuel is

essentially in an all-gaseous state and also the fuel, air and residual gases are uniformly mixed at the time of the ignition. The combustion starts by an electric spark at one fixed point and at a crank angle that is subject to accurate control. By contrast, combustion in the diesel engine is achieved by compression ignition, hence the name compression ignition engine. In the diesel engine air, diluted by a small fraction of the residual gas, is compressed and liquid fuel is injected into the cylinder. This is followed by combustion, which starts by auto-ignition nuclei at numerous locations in the combustion chamber.

4.2.1 Pre-ignition Processes

The pre-ignition processes in diesel engines may be divided into physical and chemical processes.

- the physical processes are:
  - spray disintegration and droplet formation,
  - heating of the liquid fuel and evaporation, and
  - diffusion of the vapour into the air to form a combustible mixture.

- The chemical processes are:
  - the decomposition of heavy hydrocarbons into lighter components, and
  - the pre-ignition chemical reactions between the decomposed components and oxygen.

Rapid compression of air within the cylinders generates the heat required to ignite the fuel as it is injected. The ignition occurs when the rate of heat release exceeds the rate of heat transfer. The spatial location at which ignition occurs is not fixed, as it depends on where the correct air/fuel ratio exists

together with the appropriate local temperature. The physical and the chemical delays taking place inside the combustion chamber are attributed to the formation of the necessary local conditions for ignition. Subsequent combustion is then, to some extent, regulated by the rate of fuel injection, as well as by mixing and diffusion processes. The major controlling factor is, however, the need for the fuel to find oxygen.
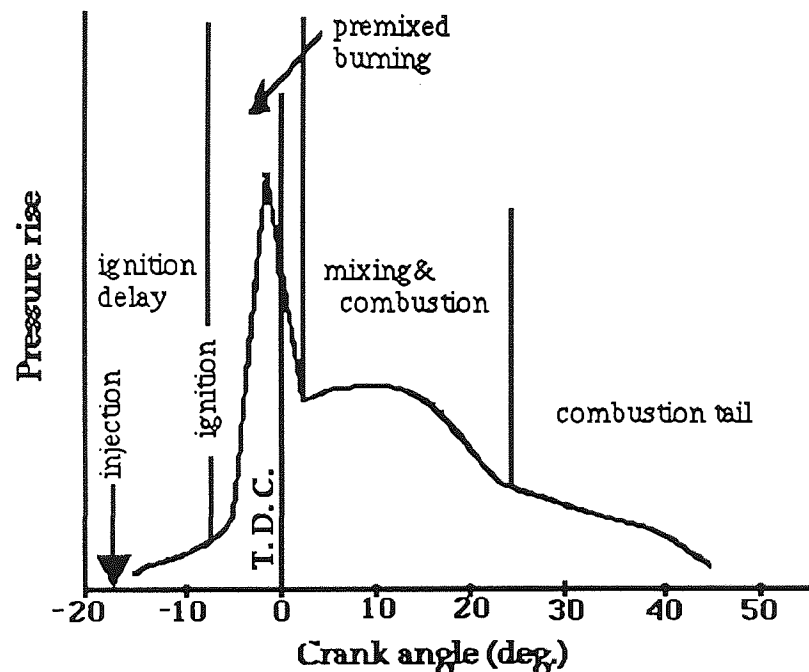
Figure 4.1 Diesel Engine Combustion Cycle

The combustion cycle as illustrated in Figure 4.1 can be considered to consist of several phases[24]. These include the *ignition delay,* an initial phase which follows compression and starts when the fuel is injected into the combustion chamber. It then involves a physical delay followed by a chemical delay, during which time the reactions of combustion proceed only slowly, but gradually increase towards the ignition point. That is caused by the onset of rapid exothermic chemical reactions. It can be recognised from the rapid pressure rise in the chamber. Therefore, the term *ignition delay* refers to the time interval between the start of the fuel injection and the first manifestation of a pressure rise due to combustion alone.

The ignition delay is followed by *pre-mixed burning*, a phase in which the fuel-air mix prepared during the delay phase ignites in uncontrolled combustion. The rate and effect of combustion in this second phase is therefore very dependent upon the length of the ignition delay and the quantity of fuel introduced during the delay period. The duration of this phase in effect depends on the engine running conditions, i.e. high-load and -speed conditions produce little pre-mixed burning, but at other times when there is more pre-mixed fuel a sharp rise in combustion will be detected.

A long ignition delay results in a high first peak for the measured pressure rise, since a greater mass of fuel has been prepared during the longer delay period. A short delay and high values of trapped mass of fuel both result in a small peak. The duration of the ignition delay is therefore one of the most important criteria affecting the diesel engine, having a great effect on the combustion process, mechanical stresses, engine noise and on exhaust emissions.

Diesel engine combustion photography reveals that, during and after the uncontrolled combustion period, flame propagation takes place towards the centre of the spray cone. Diffusive combustion now predominates and the air swirl becomes particularly significant in assisting the rate at which oxygen encounters the fuel droplets. This phase is termed *mixing controlled* or *diffusion controlled*, a phase in which a lower combustion rate prevails (see Fig. 4.1).

The final period of combustion is characterised by a much lower combustion rate which often continues well down into the engine expansion stroke (see Fig. 4.1). This is again a diffusive combustion process and is termed the

combustion tail, in which orange coloured luminous flames are apparent. These are due to the rapid production of carbon particles at this stage.

4.2.2 Catalyst Activity Mechanisms

As discussed above, the diesel engine combustion process is characterised by auto-ignition following on from injection in relatively high compression ratio engines. The fuel injection process is highly important since it controls spray atomization and distribution in the chamber. Evaporation around individual fuel droplets ensues and this is followed by ignition after a delay period. This period comprises both a physical delay and a chemical delay. One approximation to its magnitude was proposed by Wolfer[120] in 1938 in the following equation. Subsequent workers proved this to be true.

$$\text{Ignition Delay (ms)} = 0.44 \exp(4650/T) / P^{1.19}$$

Where T is the absolute temperature at ignition point and P is the pressure measured in atmospheres.

Wolfer's experiments were conducted using a constant volume bomb in which the pressure and temperature prior to ignition could be preset, and its internal geometry or air swirl rate altered. Wolfer measured the ignition delay period, as defined by the increase in chamber pressure, for a wide range of initial conditions, chamber geometrics and inlet air swirl velocities. His results indicated strong dependence on pre-ignition temperature and pressure for all fuels having cetane numbers greater than 50, though no definite conclusion could be reached concerning the effect of the air swirl or injection characteristics.

One could hypothesise (and find out from the following additive tests) that

the presence of a catalyst might reduce the chemical delay in the premixed lean-flame region by accelerating the pre-combustion reactions. This would be predominantly a gas-phase effect and the increased local temperatures would promote faster ignition. The catalyst in this context would act as an ignition improver, thereby enhancing fuel quality.

Recent studies[121-123] related to the effect of ignition improvers on ignition delay in compression ignition engines show that addition of ignition improvers to diesel fuels reduces ignition delay period, and therefore, it enhances combustion. All ignition improvers reported so far are of organic materials, mainly alkyl nitrates and peroxides, as discussed in Chapter 1. Griffiths and co-workers[121] showed that small additions of di-tert-butyl peroxide as an additive to fuels (C_4 alkanes and alkenes) can considerably reduce the ignition delay, but only for the alkane fuels. Hansen and co-workers[122] examined the effect of addition of ethanol, and ethanol and additives, on ignition delay in diesel engine; the results show that ethanol increases the ignition delay and thermal efficiency; however the addition of an ignition improver to these fuels decreased the rates of premixed heat release by reducing the ignition delay. Pritchard and co-workers[123] showed that, under their chosen operating conditions (compression ratio 7.5:1, with a block temperature of $100^{\circ}C$), diesel fuel of cetane number 50 would ignite only very feebly with ignition delays in excess of about 9 ms; but in the presence of various additives, iso-octyl nitrate, di-tert-butyl peroxide, tert-butyl perbenzoate, 1,1-di-(tert-butyl peroxy) cyclohexane, and 1,1-di-(tert-butyl peroxy)-3,3,5-trimethyl cyclohexane, ignition delays of between 3 and 7 ms were observed. Although the thermal decomposition rates of these additives span approximately a factor of 60, the ignition delays do not correlate with these rates.

But, going back to the combustion cycle, at the end of the premix phase when the fuel is burnt at the fuel mixing rate, if the mixing rate is still increasing the heat release diagram shows a characteristic double hump. At this phase a catalyst may also be of benefit in enabling a more complete and faster reaction to occur in the fuel-rich region of the spray cone.

The different phases of the diesel engine combustion process outlined so far will be mainly influenced by a gas-phase mechanism of a catalyst. In this respect, it would be advantageous for the catalyst itself to be in a gas-phase rather than a particulate phase. This is because increased diffusion rates are possible in the gas-phase enabling a much greater volume of fuel/air mixture to be affected by the catalytic activity compared with that which would occur if heterogeneous activity in localised areas around individual catalyst particles took place.

4.3 THE COMBUSTION BOMB RIG

The full description of the main components of the bomb and its associated equipment is given in reference 119. In this section the author describes only the components which are of direct interest to this investigation.

The complete experimental arrangement consists of three major systems. A general view of the complete combustion rig showing all the major features of the system is presented in Figure 4.2, and shows the

- ◆ combustion chamber and drive assembly,
- ◆ single-shot fuel injection system, and
- ◆ data acquisition and control.

4.3.1 Combustion Chamber and Drive Assembly

Figure 4.4 shows a cross-section of the combustion bomb which illustrates the

associated combustion chamber injector with its injector mounting, and the attached thermocouple and pressure transducers. For a full view see Figure 4.3. The injection pump, amplifier and oscilloscope are also shown. All the tests described in this thesis were performed on the bomb under non-swirl condition, as the swirler connected to the combustion chamber was unserviceable throughout the research period.

Air pressure and temperature prior to injection are controlled respectively by using an external storage bottle feeding the chamber through a precision regulating valve, and by using high intensity (3.5kW) heating coils embedded in the walls of the combustion chamber. Coil temperature is continuously monitored during the heating period by embedded thermocouples, while the power output is regulated in accordance with a predetermined temperature-time schedule.

4.3.2 Single-Shot Fuel Injection System

This system is required to supply a known quantity of fuel as a single injection into the combustion chamber and to be easily interfaced with the controlling micro-computer. The single-shot fuel injection system is based on a six-element in-line fuel pump, with only one line being operational and supplying the CAV 'S-type' four hole injector (hole diameter = 0.3 mm), through a 1 metre length of high pressure fuel pipe. The injector is equipped with a fuel line pressure transducer to monitor the injection process.

A 0.19 kW single phase motor drives the fuel pump via a V-belt at a set pump speed. A powerful solenoid acts directly on the fuel pump rack which remains in the closed position when the solenoid is de-energised. The injection sequence is controlled by an external microprocessor, and covers initiation of rack movement and the duration of rack open period.

4.3.3 Data Acquisition and Control System

Fuel injection, mixing and combustion under diesel engine conditions are extremely rapid events occupying a matter of milliseconds. So, a micro-computer (Commodore PET) is used to maximise the amount and quality of the data that can be collected and stored from the single-shot injection. The micro-computer consists of three systems which control and record the events occurring from the point of the injection to the end of the combustion. This is shown schematically in Figure 4.5.

- The data acquisition card, consisting of an MP 6812 analogue to digital converter and a 6522 versatile interface adapter (VIA), is used to capture accurately the data from the two channels. These are the fuel line pressure (channel 1) and the combustion chamber pressure (channel 2). This system can provide a high speed data acquisition frequency of 30 kHz, or 10 kHz per channel. Data acquisition is carried out on a cyclic basis between the channels, and here 999 samples per channel were recorded.

- The oscilloscope output card is used to display the data held in the computer for channels 1 and 2. The oscilloscope display only shows a portion of the total data. However, the system allows the user to scan each channel at will to examine all the results. If the data is satisfactory, it is transferred to tape and transmitted from a second micro-computer to the university mainframe computer for complete analysis. This is a slow, labour intensive process which should be replaced by a more modern interfacing device.

- The solenoid control card is used to control a single-shot of fuel into the combustion chamber. The single-shot is achieved by running a

fuel injector pump with its throttle normally closed but with a high power solenoid attached to the throttle linkage (the fuel rack). To produce a single injection the solenoid is energised for a sufficient duration to open the fuel rack.

Once the experimental conditions, i.e. pressure and temperature, have been established, the user-defined controlling variables are entered into the computer. The system may now be started and this proceeds via the data acquisition card.

4.3.4 Calibration of the Transducers

The fuel line pressure transducer, with maximum capacity of 1000 bar, was calibrated against a dead-weight tester and the output from the bridge amplifier was displayed on the PET, with the PET set in calibration mode. A calibration curve was produced and the calibration value was found to be 3.378 bar/bit (for channel 1).

The combustion chamber pressure transducer was calibrated by fitting it into a block which contains a pressure inlet, a calibrated static pressure transducer, and a rapid release exhaust ball-valve. The transducer block was supplied with nitrogen gas at pressures up to 150 bar which were monitored on the DVM connected to the carrier amplifier. Nitrogen gas was then released suddenly by rapidly opening the ball-valve and the subsequent transducer output was captured on a storage oscilloscope. In addition, the rig data acquisition system was used to record the transient information for further
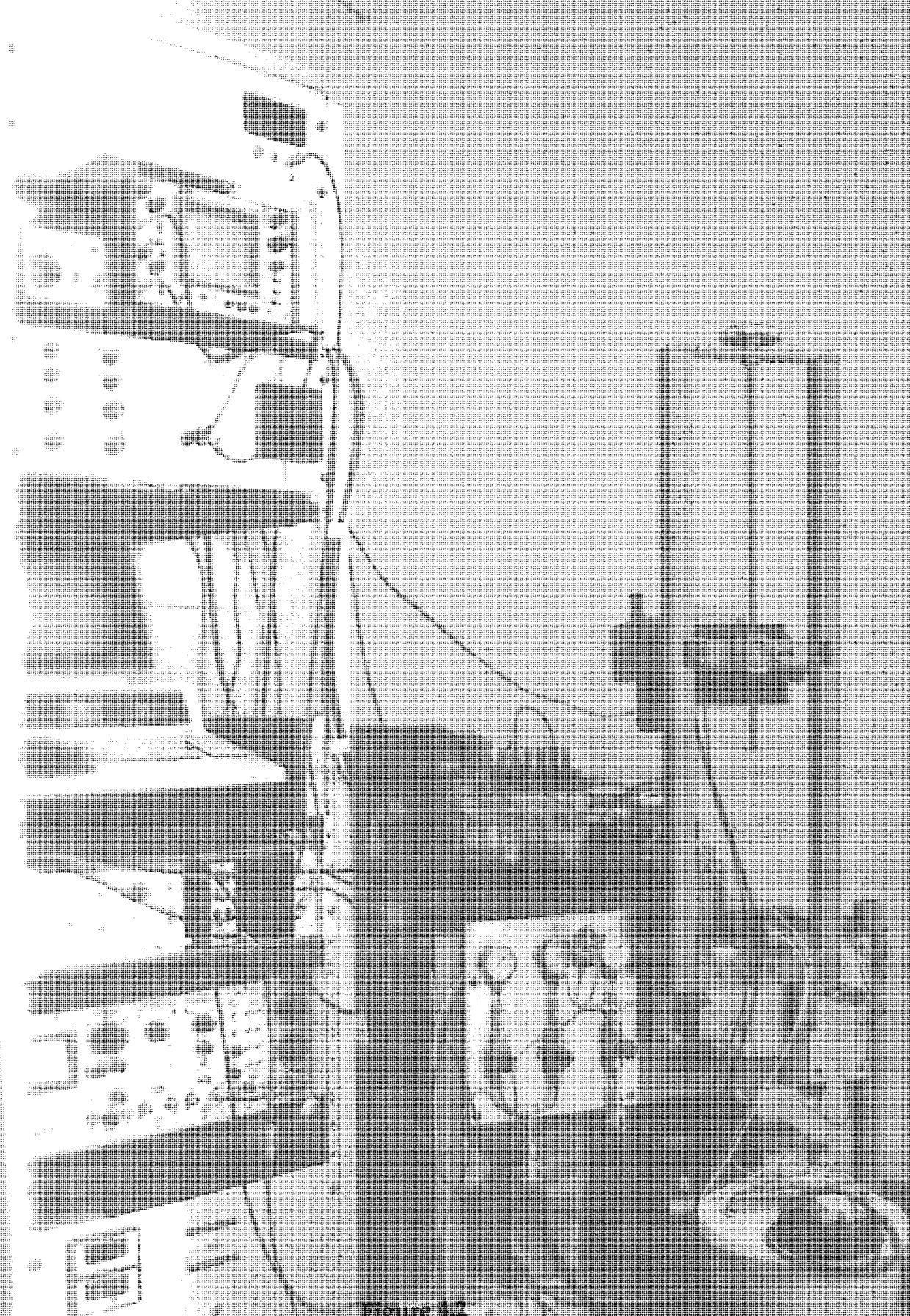
Figure 4.2

An Overall View of the Combustion Rig

with the Control and Data Acquisition Systems
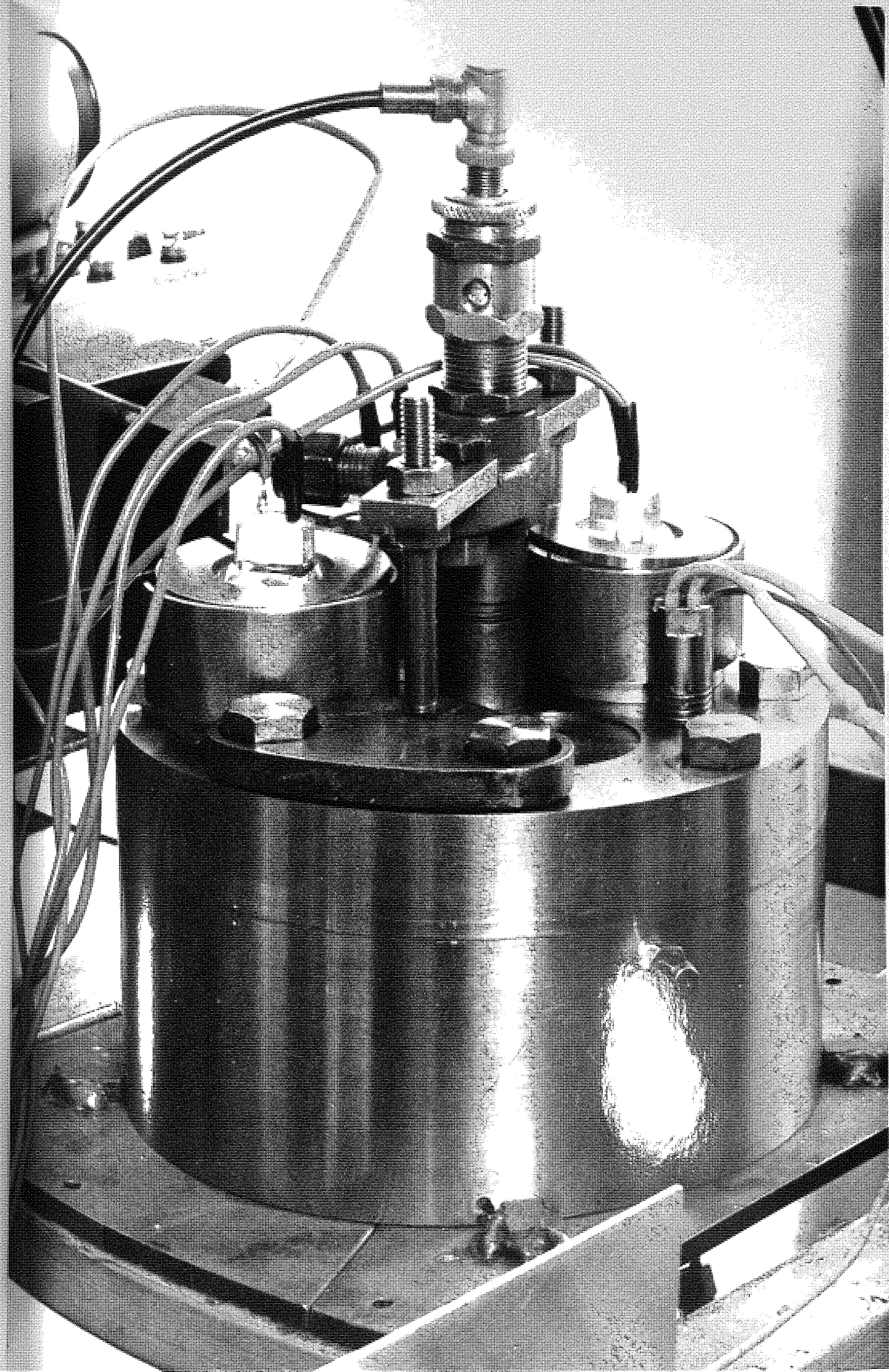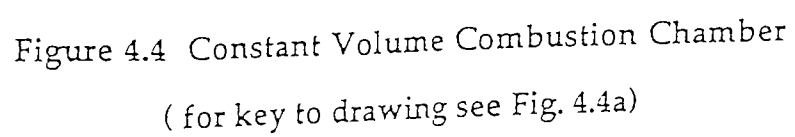
(reproduced with the permission from Bath University)
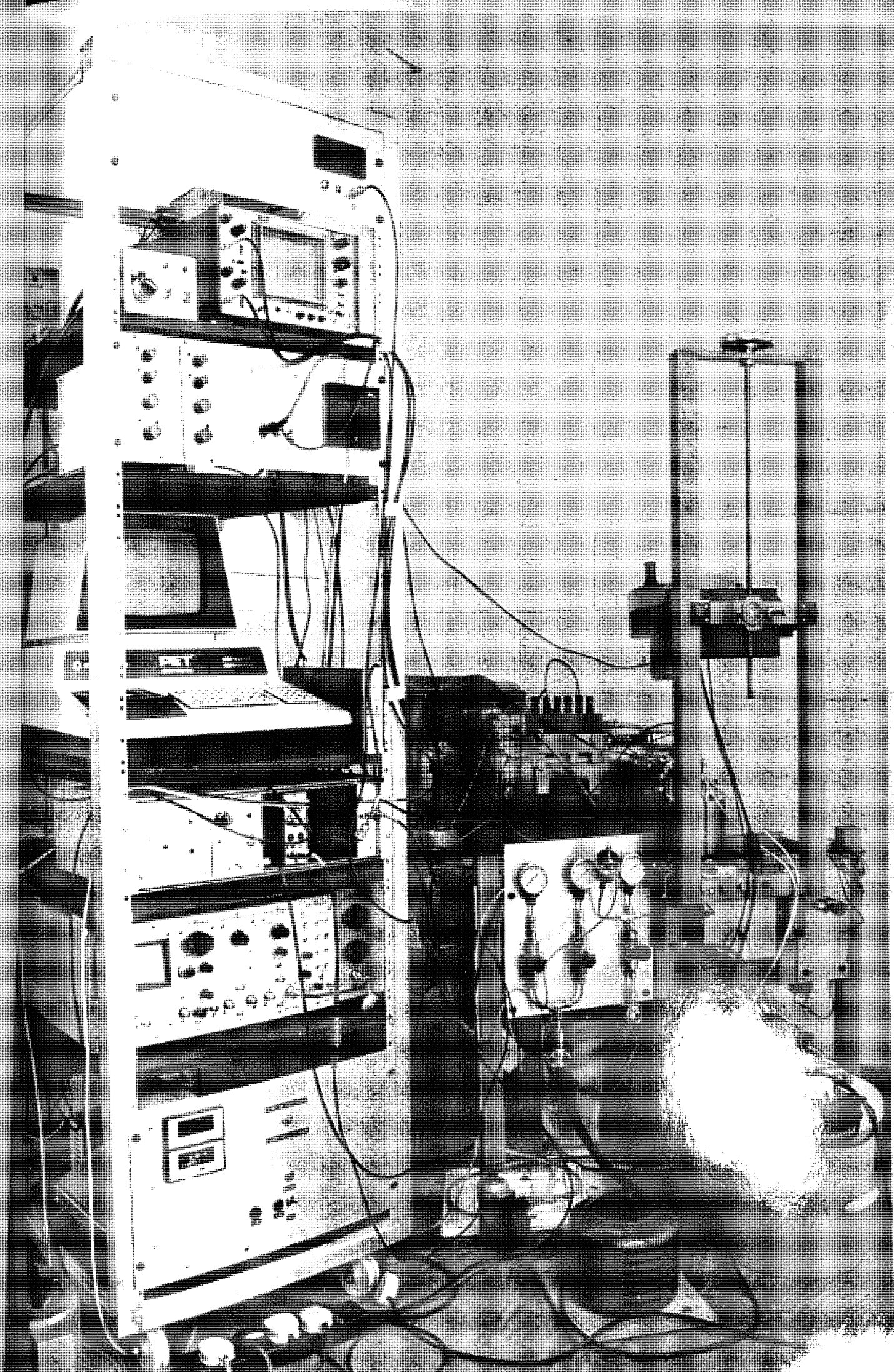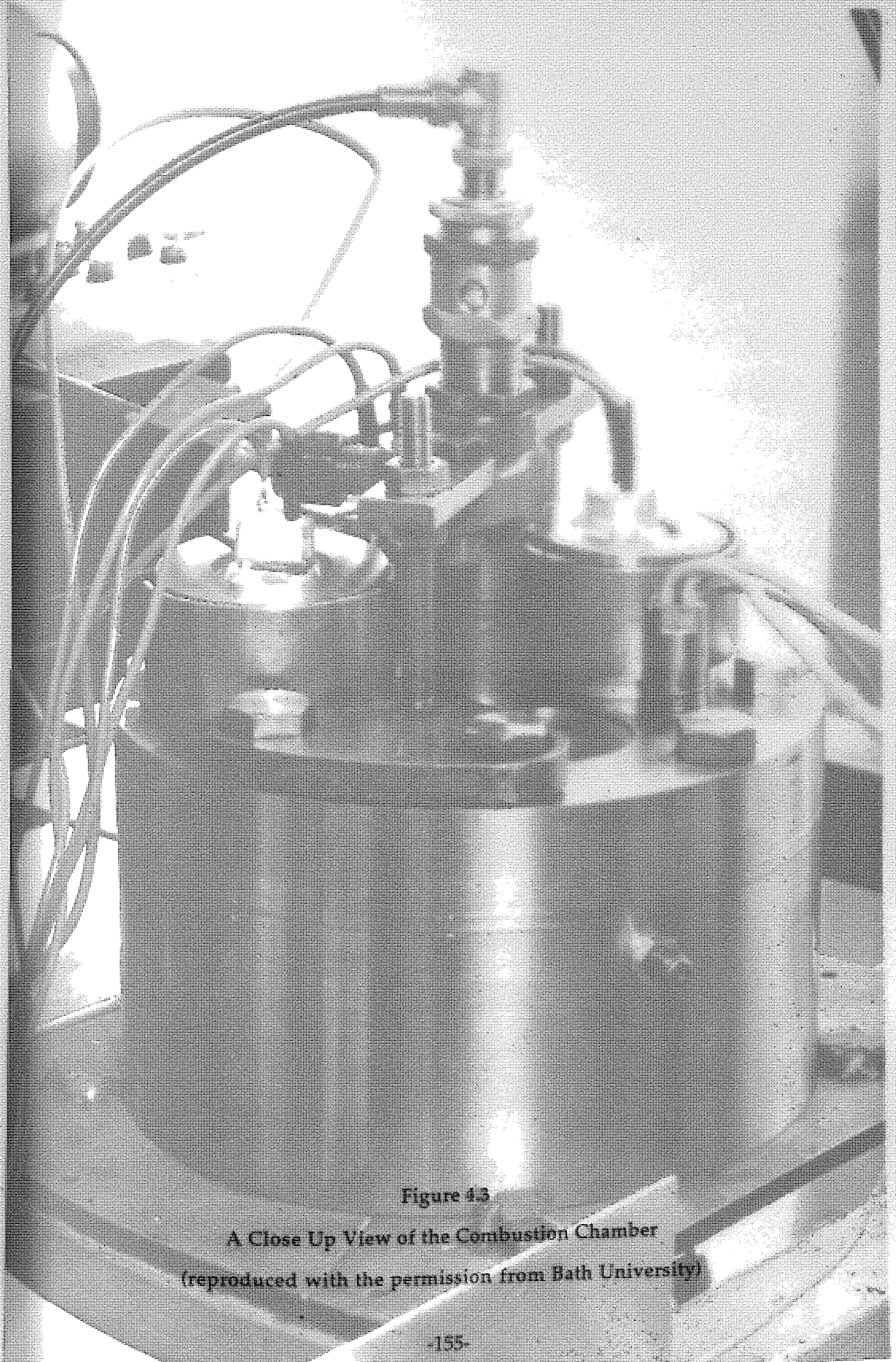
Figure 43

A Close Up View of the Combustion Chamber

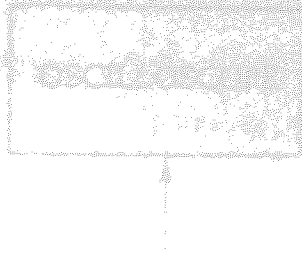(reproduced with the permission from Bath University)

Figure 4.4 Constant Volume Combustion Chamber

(for key to drawing see Fig. 4.4a)

1.   exhaust valve

2.   swirler

3.   injection pump

4.   O-ring

5.   bearing

6.   pulley

7.   bearing

8.   tachometer

9.   bearing

10.   motor

11.   amplifier

12.   cooling water jacket

13.   detector of tachometer

14.   pulley

15.   electric furnace

16.   combustion chamber

17.   thermocouple

18.   pressure transducer

19.   cooling water jacket

20.   fuel injection nozzle

21.   light beam choppering type needle lift detector

22.   pressure gauge

23.   inlet valve

Figure 4.4a Key to Figure 4.4
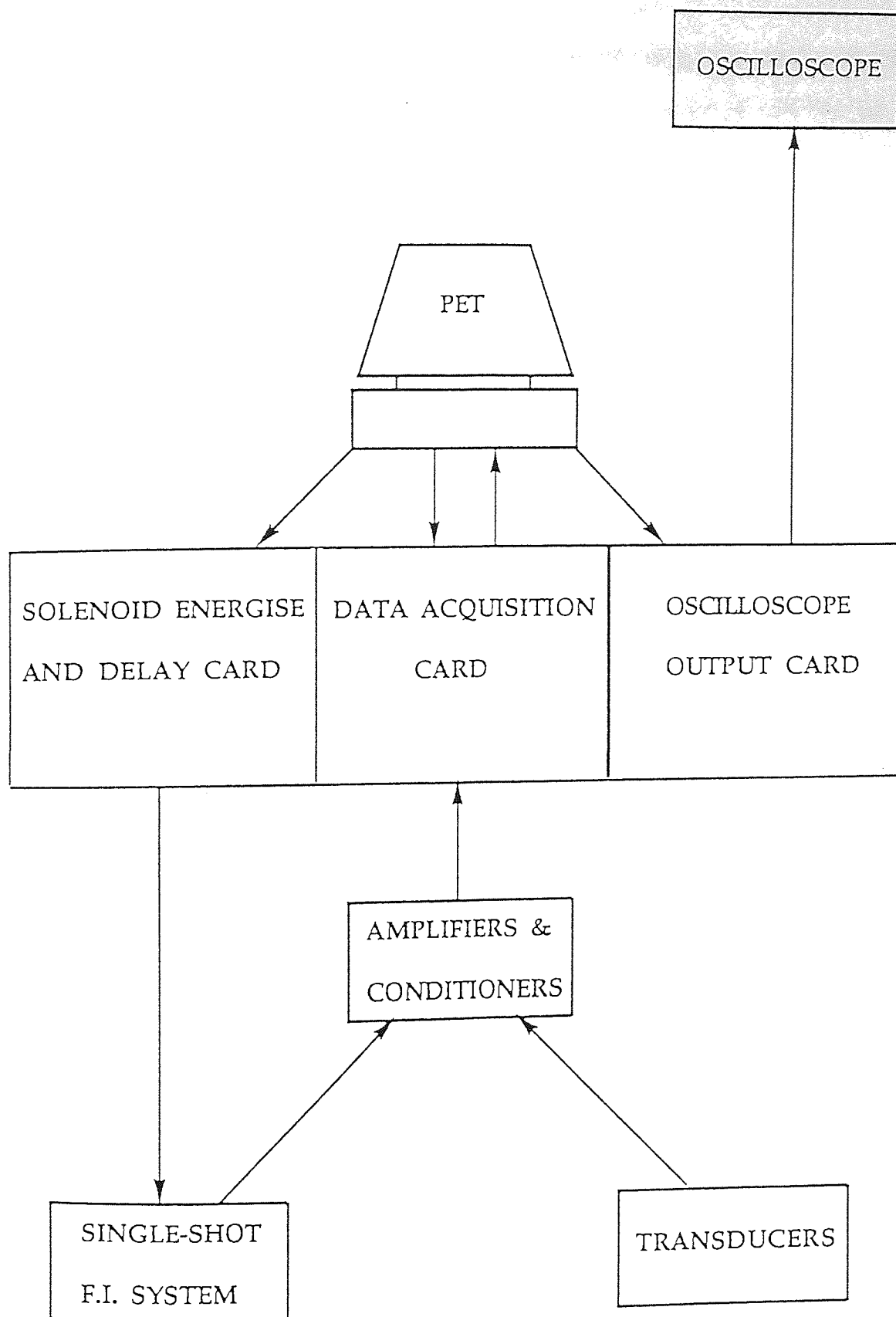
Figure 4.5 Rig Control and Data Acquisition System

analysis. A plot of voltage output against pressure drop was produced which provided the calibration constant and the calibration value is 1.42 bar/bit (for channel 2).

4.4 COMBUSTION BOMB EXPERIMENTAL METHODS

The following experiments were carried out in a series of programmed tests, designed to investigate the effect of metal complexes on the combustion of diesel fuel at various metal additive concentrations, and at the same time to investigate the potential applicability of the rig to this kind of study.

Some of the metal additives used in these tests are not completely soluble in the diesel fuel, and were therefore used in combination with an organic solvent which is miscible in diesel fuel. The solvents employed were oxygenated hydrocarbons such as ethylene glycol dimethyl ether (EGDME) and tetrahydrofuran (THF), and the preferred concentration amounted to 5% of the volume of the fuel. The diesel fuel used in this chapter was not of the normal commercial diesel fuel, but from INTEREUROPE. It contains no additives and has a cetane number of 53 (max.).

The final concentrations of metal additives added to the diesel fuel were in the range of 50 to 200 parts of the compound per one million parts of diesel. In this study, all part per million figures are on a weight to volume basis i.e., mg/litre, and percentages are given by volume, unless otherwise indicated. The investigation of the following metal complexes is described in this chapter.

- dimethylcyclooctadiene platinum(II), [$Pt(CH_3)_2COD$],
- tris(dipivaloyemethanato) cerium(III), [$Ce(DPM)_3$],
- bis(acetylacetonato) platinum(II), [$Pt(acac)_2$], and
- bis(acetylacetonato) palladium(II), [$Pd(acac)_2$].

The additive test experiments were carried out under the following four sets of conditions:

- condition 1- Pressure 50 bar, Temperature 500°C,
- condition 2- Pressure 60 bar, Temperature 500°C,
- condition 3- Pressure 50 bar, Temperature 600°C, and
- condition 4- Pressure 60 bar, Temperature 600°C.

4.5 RESULTS AND DISCUSSION

4.5.1 Diesel Fuel (Reference Fuel 1)

The first step of the programme for this kind of study is to investigate the reference fuels, then the effect of the additives, to provide an indication of the influence of the additives on the combustion process. Since some of the metal additives are not directly soluble in diesel fuel, there were three reference fuels in this investigation i.e., diesel, diesel+THF, and diesel+EGDME. The baseline tests were performed under conditions 1 to 4, and for each condition, five experiments were carried out. This is a small number dictated by practical factors during the research. A larger number would have been preferable. From these results averages (AVG), standard deviations (STG), and individual data were obtained. The first set of tests involved untreated diesel fuel under the above four conditions. The results from these experiments and the statistical evaluation are represented in Table 4.1.

Since the combustion processes of diesel fuel are related to the ignition delay period and the rate of pressure rise, these parameters were calculated for each experiment (see Table 4.1), using the recorded data obtained from the two recorded channels, which represent the fuel line pressure and chamber pressure. Each channel contains the pre-programmed recording of the 999 samples at an interval of 15 microseconds.

Thus the following quantities were obtained:-

◆ ignition delay; the time of injection minus the time at which combustion pressure starts to rise, $t_2 - t_1$,

◆ maximum gradient; the pressure of the first local peak divided by the time of the first local peak, $P_1 / t_3 - t_2$,

◆ average rate; the maximum pressure divided by the time of maximum pressure, $P_2 / t_4 - t_2$, and

◆ magnitude of maximum pressure.

Ignition delay is known to be correlated with initial chamber pressure (P) and temperature (T) as proposed by Wolfer in his equation. As with Wolfer's case, the present experiments were conducted using a constant volume bomb in which the pressure and temperature prior to ignition were preset. The data for the diesel reference fuel (reference 1) shows good positive correlation for ignition delay with temperature from the conditions examined, therefore agreeing with Wolfer's equation. The ignition delay period is at its longest under conditions 1 and 2, i.e. at the low temperature. As the temperature is increased from 500°C to 600°C to condition 3 or 4, so the delay period decreases. The data also shows a weak correlation for ignition delay with pressure (1/P) between conditions 3 and 4, where the initial chamber pressure increases from 50 bar to 60 bar, but shows negative correlation between conditions 1 and 2, which is not consistent with Wolfer's equation. From this equation one would expected reference fuel 1 to have its shortest delay periods under condition 4, which corresponds with the results in Table 4.1. However, one would expected the longest delay periods to be at condition 1, not as found for condition 2. The determined values of the ignition delay are subject to large standard deviations. This is at least in part due to the long 15 microsecond interval set between measurements.

Under normal conditions, one would expected the combustion process to produce a series of pressure rise peaks, with the initial peak having the maximum magnitude followed by smaller pressure rise peaks, and with the final peak having the smallest magnitude. This maximum magnitude for the first pressure rise peak is due to the ignition delay period prior to ignition. The ignition delay is known to be correlated with the initial rate of pressure rise, i.e. the longer the delay the greater the initial gradient. Therefore, the first pressure peak is indeed very important even if it is not the absolute maximum, since the initial pressure rise leading up to it is a pre-mixed fuel burning phase and is directly linked to ignition delay. Subsequent peaks, whether they are greater (which were observed on some tests) or less than this initial peak are the result of a diffusion burning process in which the fuel is combusting at a similar rate to that of injection. The greater the diffusion peak, the greater the combustion efficiency. In these experiments, the diffusion burning process is expected to be lower than normal due to the absence of air swirl, mentioned earlier, thus reducing the mixing between oxygen and fuel. Figure 4.6 is a plot of these two parameters for the diesel reference fuel over a full range of bomb conditions, excluding one very different datum which has a gradient of 0.176 bar/μs. Overall the correlation is weak although some results at the same conditions show good correlation.

If the maximum pressure occurs at the first 'peak' on the pressure diagram (which is usually the case) then this pressure should correlate well with the maximum gradient. Figure 4.7 confirms this by showing a reasonably good positive relationship. However, for these experiments the best positive correlation was observed between the magnitude of the temperature rise and the ignition delay (Fig. 4.8). The temperature rise is proportional to the rate of heat release from the initial combustion reactions, which is proportional to the volume of pre-mixed fuel.

Table 4.1 Test Data of the Untreated Diesel Reference Fuel

Ignition Delay/μs t_2-t_1	Maximum Gradient/bar μs^{-1} P_1/t_3-t_2	Average Gradient/bar μs^{-1} P_2/t_4-t_2	Maximum Pressure/bar P_2	Temperature Rise/$^{\circ}$C
		CONDITION 1		
375	0.173	0.110	38.00	41.00
405	0.181	0.130	43.00	40.00
390	0.181	0.124	41.00	44.00
405	0.143	0.109	36.00	43.00
315	0.176	0.169	38.00	43.00
AVG: 378	0.171	0.128	39.20	42.20
STD: 37	0.016	0.024	2.77	1.64
		CONDITION 2		
435	0.127	0.086	31.00	35.00
435	0.140	0.094	31.00	39.00
420	0.127	0.087	30.00	36.00
435	0.127	0.086	31.00	42.00
420	0.127	0.088	30.00	37.00
AVG: 429	0.130	0.088	30.60	37.80
STD: 8	0.006	0.003	0.55	2.78
		CONDITION 3		
300	0.152	0.092	28.00	30.00
270	0.120	0.090	27.00	30.00
315	0.178	0.098	31.00	31.00
315	0.160	0.103	31.00	28.00
300	0.152	0.095	30.00	34.00
AVG: 300	0.152	0.096	29.40	30.60
STD: 18	0.021	0.005	1.82	2.19
		CONDITION 4		
300	0.190	0.109	31.00	32.00
270	0.133	0.100	30.00	31.00
255	0.124	0.094	31.00	25.00
240	0.180	0.110	33.00	29.00
300	0.178	0.115	31.00	25.00
AVG: 273	0.161	0.106	31.20	28.84
STD: 27	0.030	0.008	1.10	3.29

It is clear from an inspection of these data for the diesel reference fuel, that variability of results may be a problem when comparisons are made between fuels with and without the additives. The standard deviation for each parameter was calculated to help in the comparison of sets of results, as shown in Table 4.1. The deductions for this reference fuel test are that the bomb appears to show reasonable correlation between ignition delay and temperature, but not with pressure as proposed by Wolfer, and it also shows no definite correlation between ignition delay and rate of maximum pressure rise for this fuel.
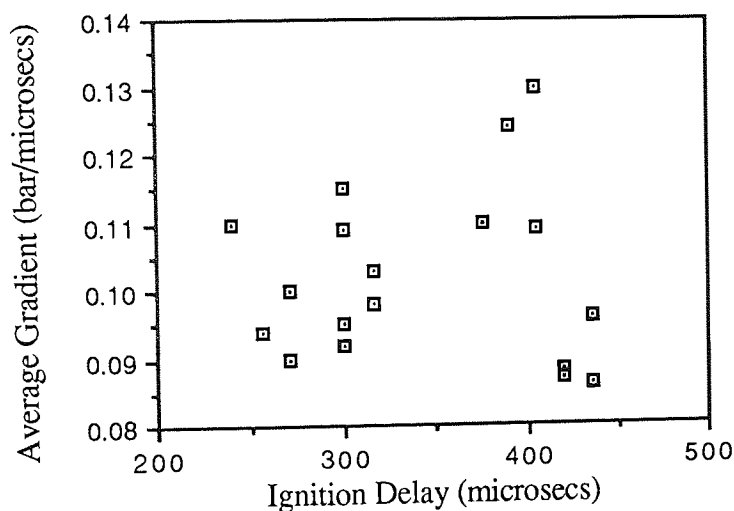

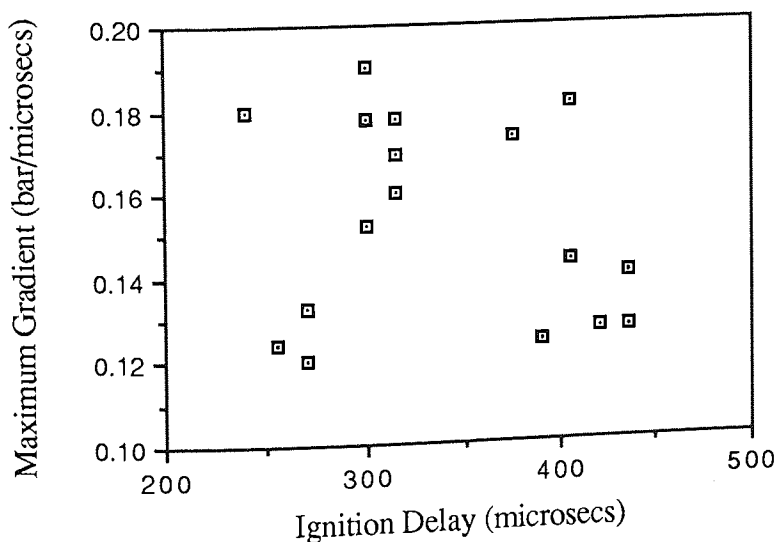**Figure 4.6 Ignition Delay versus Average Gradient of Diesel Reference Fuel**

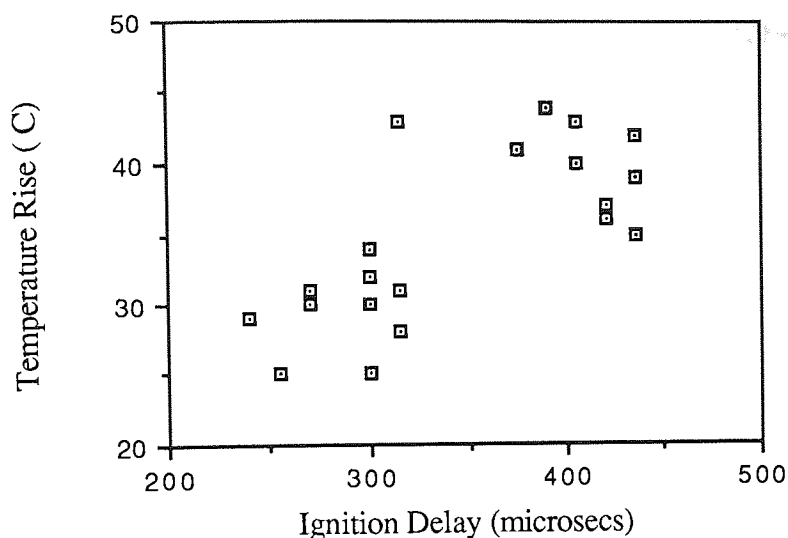**Figure 4.7 Ignition Delay versus Maximum Gradient of Diesel Reference Fuel**

Figure 4.8 Ignition Delay versus Temperature Rise of Diesel Reference Fuel

4.5.2 Pt(CH₃)₂COD at 100 ppm

Again, on inspection of the data for the above additive (Table 4.2) the variability of results can be seen as similar to the previous results and so comparisons between reference and treated fuels will be difficult. Standard deviation alone is not enough here to show any significant difference between these sets of data and those of the untreated fuel, and so to further ease the analysis of the data between these sets of means, it was decided to perform a statistical Student's t-Test (see Appendix- Student's t-Test), for each of data sets, for all the parameters and bomb conditions. The Student's t-Test is used to determine if there is a significant difference between the reference fuel and the treated fuel data sets. Usually significance is defined in terms of a confidence level of 95%. The calculated t-Test results are represented by the asterisk symbol in the following tables, below each pair of compared data sets. An asterisk (*) indicates that the means of the samples are different at this confidence interval.

Table 4.2 shows the same trend of correlations for the delay period with initial chamber temperature and pressure as seen for the diesel reference fuel. The

reference fuel data for the same parameter are shown in bold and brackets in the table. Therefore, the data for the above treated fuel also obey Wolfer's equation for the delay period, thus indicating that increasing the temperature and pressure of the combustion chamber (condition 4) reduces the delay period. The only recognisable differences for the delay period between the reference fuel and this treated fuel are observed at condition 3, which shows a slight increase in delay period, equal to the sum of the standard deviations, and at condition 2 where the Student's t-Test shows a definite reduction of the average delay period compared with reference fuel. Therefore, it agrees well with the suggested mechanisms for metal additive catalyst activity, reducing the delay period. Reduced delay periods are desirable in diesel engines since the rate of heat release, and hence rate of pressure rise, during the uncontrolled combustion period are both reduced. Engine knock is correspondingly decreased.

For the other parameters, significant differences between the reference and platinum-treated fuel are observed at condition 2, where increases in maximum gradient, average gradient and maximum pressure rise are observed. However, these data do not agree with reference 122, which shows correlation between ignition delay and thermal efficiency, where the addition of an ignition improver to the fuels decreased the rates of premixed heat release by reducing ignition delay. But alternatively, this catalyst may be operating under a different mechanism thereby showing increases in these parameters with decreased ignition delay. Other significant differences between the reference and the treated fuels are observed at condition 3 for the ignition delay and the average gradient parameters. However, this time the increased ignition delay correlates with the increased average gradient. As the test results for these two conditions contradict each other the value of the results is not convincing. Therefore, the deduction of catalyst activity becomes mere speculation. At condition 1, the data show real changes for the maximum gradient and the temperature rise parameters, but as with all the other data for this 100 ppm platinum-treated fuel, these data show inconsistency. So in

conclusion, there were no major and general changes between reference fuel 1 and $Pt(CH_3)_2COD$ at 100 ppm treated diesel fuel.

Table 4.2 Test Data of $Pt(CH_3)_2COD$ at 100 ppm

Ignition Delay/μs t_2-t_1	Maximum Gradient/bar μs^{-1} P_1/t_3-t_2	Average Gradient/bar μs^{-1} P_2/t_4-t_2	Maximum Pressure/bar P_2	Temperature Rise/^oC
		CONDITION 1		
381±31	0.140±0.015	0.112±0.010	36.40±2.51	36.80±1.90
(378±37)	(0.171±0.016)	(0.128±0.024)	(39.20±2.77)	(42.20±1.64)
	*			*
		CONDITION 2		
379±31	0.170±0.024	0.166±0.027	36.40±2.51	36.80±1.90
(429±08)	(0.130±0.006)	(0.088±0.003)	(30.60±0.55)	(37.80±2.78)
*	*	*	*	
		CONDITION 3		
330±12	0.149±0.018	0.114±0.008	31.50±1.00	31.50±1.60
(300±18)	(0.152±0.021)	(0.096±0.005)	(29.40±1.82)	(30.60±2.19)
*		*		
		CONDITION 4		
281±08	0.146±0.019	0.098±0.008	30.00±0.00	28.20±1.30
(273±27)	(0.161±0.030)	(0.106±0.008)	(31.20±1.10)	(28.40±3.29)

4.5.3 $Pt(CH_3)_2COD$ at 50 ppm

Comparison of the data for the reference fuel 1 and the diesel fuel with the additive at 50 ppm, show small differences at condition 2 in the two gradients

Table 4.3 Test Data of $Pt(CH_3)_2COD$ at 50 ppm

Ignition Delay/μs t_2-t_1	Maximum Gradient/bar μs^{-1} P_1/t_3-t_2	Average Gradient/bar μs^{-1} P_2/t_4-t_2	Maximum Pressure/bar P_2	Temperature Rise/$^{\circ}C$
		CONDITION 1		
400±35	0.178±0.055	0.121±0.027	40.00±1.73	33.00±0.00
(378±37)	(0.171±0.016)	(0.128±0.024)	(39.20±2.77)	(42.20±1.64)
				*
		CONDITION 2		
416±33	0.146±0.005	0.109±0.015	32.00±1.00	37.00±2.10
(429±08)	(0.130±0.006)	(0.088±0.003)	(30.60±0.55)	(37.80±2.78)
	*	*	*	
		CONDITION 3		
315±30	0.137±0.016	0.119±0.011	33.00±1.00	28.40±2.90
(300±18)	(0.152±0.021)	(0.096±0.005)	(29.40±1.82)	(30.60±2.19)
		*	*	
		CONDITION 4		
300±09	0.173±0.014	0.110±0.015	33.00±1.41	27.60±5.40
(273±27)	(0.161±0.029)	(0.106±0.008)	(31.20±1.10)	(28.84±3.29)
*				

and maximum pressure parameters, but not in the ignition delay and the temperature rise parameters. So these data do not correlate with the ignition delay period for this condition and the same is also observed at condition 4. The reduction of the $Pt(CH_3)_2COD$ metal additive concentration to this level is seen to produce no effect at all upon the combustion process of diesel fuel. The results for the above tests are very disappointing, as I expected this additive to reduce the ignition delay and thermal efficiency, i.e. average gradient, and set a good example of what a positive result would look like for later comparison. Reference 76 claims that this additive improves

combustion efficiency in diesel fuel and it is known that ignition improver reduces ignition delay, and hence, premixed combustion. In my tests the $Pt(CH_3)_2COD$ complex is unsuccessful as an additive, except perhaps at very much higher dose levels than those used here.

4.5.4 Ce(DPM)₃ at 200 ppm

Table 4.4 Test Data of Ce(DPM)₃ at 200 ppm

Ignition Delay/μs t_2-t_1	Maximum Gradient/bar μs^{-1} P_1/t_3-t_2	Average Gradient/bar μs^{-1} P_2/t_4-t_2	Maximum Pressure/bar P_2	Temperature Rise/$^{\circ}C$
		CONDITION 1		
360±21	0.140±0.011	0.097±0.004	32.20±1.10	44.40±3.58
(378±37)	(0.171±0.016)	(0.128±0.024)	(39.20±2.77)	(42.20±1.64)
			*	*
		CONDITION 2		
405±64	0.149±0.016	0.095±0.006	28.13±2.12	49.50±1.64
(429±08)	(0.130±0.006)	(0.088±0.003)	(30.60±0.55)	(37.80±2.78)
	*			*
		CONDITION 3		
330±42	0.145±0.023	0.107±0.009	32.00±2.83	43.20±1.30
(300±18)	(0.152±0.021)	(0.096±0.005)	(29.40±1.82)	(30.60±2.19)
				*
		CONDITION 4		
300±00	0.112±0.003	0.010±0.009	32.00±1.41	29.25±2.63
(273±27)	(0.161±0.030)	(0.106±0.008)	(31.20±1.10)	(28.40±3.29)

The test data for the Ce(DPM)₃ metal additive at 200 ppm are shown in Table 4.4. On inspection of the data, the Student's t-Test results indicate that there are few significant differences between the reference fuel and this treated fuel.

Therefore, one can only deduce that the Ce(DPM)$_3$ metal additive at 200 ppm has little or no effect on the combustion process of diesel fuel at these four preset bomb conditions. So, increasing the temperature and pressure here has no effect on the additive activity.

4.5.5 Ce(DPM)$_3$ at 100 ppm

Surprisingly, Table 4.5 shows that some significant differences between reference and treated fuels are observed for condition 2 (higher pressure, lower temperature) and not for the other three conditions with the cerium additive at 100 ppm. Decreases in the delay period, maximum gradient, average gradient, and magnitude of the maximum pressure are observed when compared with the reference fuel 1. Therefore, the data show a positive correlation between the delay period and the initial rate of pressure rise. This in turn affects the average rate of pressure rise and also the magnitude of the pressure maximum. The shorter ignition delay results in a lower first peak, since the chemical delay has been catalytically reduced in the pre-mixed lean-flame region by accelerating the pre-combustion reactions. This agrees with the results obtained by Hansen (ref 122) for an ignition improver.

Under the conditions of 500°C and 60 bar, this cerium catalyst appears to be acting as an ignition improver in this situation, thereby enhancing fuel quality. As mentioned previously, reduced delay periods are desirable in diesel engines in order to reduce engine knock. Except for the delay period, the results for this cerium complex additive at 100 ppm are almost the opposite of those at 200 ppm under condition 2. However, further tests are needed to confirm that this difference between the two concentrations is real. But, on the basis of these results, it appears that the cerium catalyst operates best under lower concentration. A firm conclusion can not be made without

further tests, which were precluded by time requirements and a lengthy breakdown of the Combustion Bomb rig, but it does seem that this cerium additive at 100 ppm and at 500°C shows some some effects on the combustion processes by reducing the chemical delay period, thereby reducing the initial rate of combustion and so the magnitude of maximum pressure, as hypothesised.

Table 4.5 Test Data of Ce(DPM)$_3$ at 100 ppm

Ignition Delay/μs t_2-t_1	Maximum Gradient/bar μs^{-1} P_1/t_3-t_2	Average Gradient/bar μs^{-1} P_2/t_4-t_2	Maximum Pressure/bar P_2	Temperature Rise/°C
CONDITION 1				
345±15	0.144±0.030	0.139±0.015	38.67±2.08	35.25±0.96
(378±37)	(0.171±0.016)	(0.128±0.024)	(39.20±2.77)	(42.20±1.64)
				*
CONDITION 2				
345±21	0.038±0.007	0.033±0.004	26.50±0.71	35.40±3.21
(429±08)	(0.130±0.006)	(0.088±0.003)	(30.60±0.55)	(37.80±2.78)
*	*	*	*	
CONDITION 3				
285±21	0.164±0.028	0.097±0.004	32.50±2.12	33.50±10.15
(300±18)	(0.152±0.021)	(0.096±0.005)	(29.40±1.82)	(30.60±2.19)
CONDITION 4				
285±21	0.158±0.021	0.105±0.016	32.00±1.41	33.67±7.64
(273±27)	(0.161±0.030)	(0.106±0.008)	(31.20±1.10)	(28.40±3.29)

So far, the results demonstrate that Ce(DPM)$_3$ is most effective as a catalyst under the conditions of low temperature and high pressure. Increasing the temperature from 500°C to 600°C has not increased the catalytic effect. In fact it makes it less pronounced. Since the ignition delay period is already reduced without additive under higher bomb temperature according to Wolfer's equation, this will make the catalyst less effective anyway as there is less active time for the catalyst to function. If this is the case, then may be there is a connection between the catalytic activity and temperature.

The data for the Pt(CH$_3$)$_2$COD tests are most disappointing, since the results on this compound were expected to show good positive correlations. The reports made in the patent literature clearly claim that this compound, when used as a fuel additive, improves the operating efficiency of internal combustion engines in terms of the increased power output per unit of fuel burned. Unfortunately, the data for this complex show no real effect on combustion compared with the reference fuel, and even suggest an opposite effect at condition 2, i.e. ignition delay is slightly shorter but there is a higher initial rate of pressure rise and an increase in maximum pressure rise. Probably the patent claim is being disproved under these experimental conditions. However, it is important to stress that the claims for this platinum additive were performed under entirely different conditions, i.e. at a very low level of dosage (0.1 to 1 ppm) with an oxygenated solvent and also under full-size, loaded engine conditions.

4.5.6 Diesel + EGDME 5% (Reference Fuel 2)

When the above reference fuel data were compared with diesel reference fuel 1 (Table 4.6), no significant differences were observed between the two sets of data, except for the average gradient, maximum pressure rise and tempera-ture rise parameters at condition 2. This indicates that the addition of

ethylene glycol dimethyl ether (EGDME) oxygenated solvent at 5% to the diesel fuel does not have any significant effect on the combustion processes of diesel.

Table 4.6 Test Data of Diesel + EGDME 5% (Reference Fuel 2)

Ignition Delay/μs t_2-t_1	Maximum Gradient/bar μs^{-1} P_1/t_3-t_2	Average Gradient/bar μs^{-1} P_2/t_4-t_2	Maximum Pressure/bar P_2	Temperature Rise/^{o}C
		CONDITION 1		
390±15	0.164±0.014	0.109±0.010	37.50±1.92	35.20±1.50
(378±37)	(0.171±0.016)	(0.128±0.024)	(39.20±2.77)	(42.20±1.64)
				*
		CONDITION 2		
395±38	0.138±0.007	0.036±0.003	28.00±0.00	33.33±2.33
(429±08)	(0.130±0.006)	(0.088±0.003)	(30.60±0.55)	(37.80±2.78)
		*	*	*
		CONDITION 3		
305±23	0.146±0.017	0.138±0.033	30.67±3.51	29.60±1.70
(300±18)	(0.152±0.021)	(0.096±0.005)	(29.40±1.82)	(30.60±2.19)
		*		
		CONDITION 4		
300±00	0.187±0.004	0.115±0.005	33.50±0.58	27.70±2.10
(273±27)	(0.161±0.030)	(0.106±0.008)	(31.20±1.10)	(28.40±3.29)
			*	

When any differences can be observed between these two reference fuels they are usually detected on the oscilloscope in the shape of the curve of pressure rise against time. Reference fuel 2 shows distinctive but close double peaks towards its maximum value; the second peak being the greater (Fig. 4.13). This could be due to the presence of the EGDME, a second solvent. Again all

the data still show a wide variability between tests, which makes them less reliable.
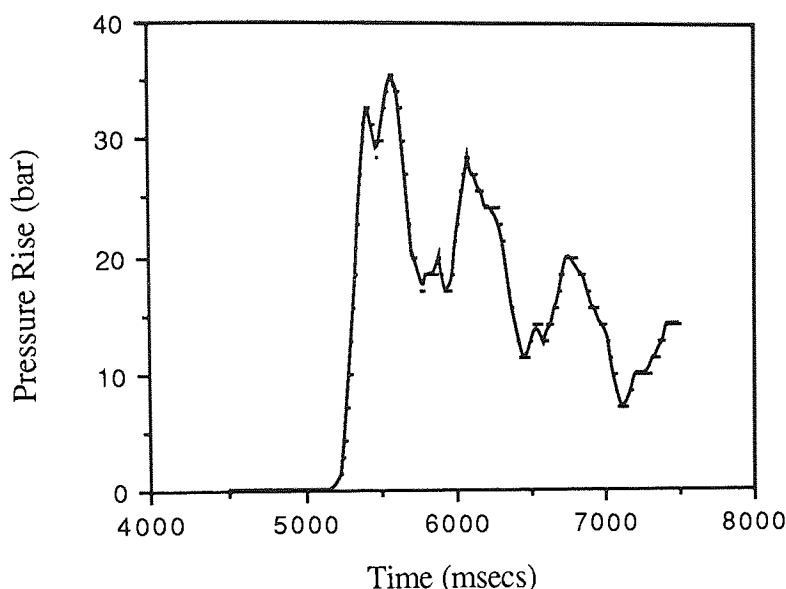
Figure 4.9 An example of the double peaks observed in some Reference
Fuel 2 Tests

Essentially these are useful results for this study, since the two sets of data are almost the same. One does not want the added oxygenate solvent to have any effects upon the combustion processes of the diesel reference fuel. The analysis of the results from the treated fuel is made simpler as any changes observed can be attributed to the additive and not the oxygenated solvent.

4.5.7 Pt(acac)$_2$ at 50 ppm + EGDME

The data in Table 4.7 are the results of the tests with the above additive. The data show a positive ignition delay correlation with temperature as required by Wolfer's equation. The delay also correlates with pressure at conditions 1 and 2, but not at conditions 3 and 4. However, when comparing the data of the above platinum additive with those of the reference fuel 2, there appear to be no statistically significant differences. The conclusion drawn from these data must be that fuel containing Pt(acac)$_2$ at 50 ppm+ EGDME at 5% exhibits

an identical combustion process to that of reference fuel 2 and therefore has shown no catalytic effect at these bomb conditions.

Table 4.7 Test Data of Pt(acac)$_2$ at 50 ppm + EGDME 5%

Ignition Delay/μs t_2-t_1	Maximum Gradient/bar μs^{-1} P_1/t_3-t_2	Average Gradient/bar μs^{-1} P_2/t_4-t_2	Maximum Pressure/bar P_2	Temperature Rise/^{o}C
		CONDITION 1		
395±46	0.113±0.030	0.103±0.036	36.00±2.00	33.30±1.70
(390±15)	(0.164±0.014)	(0.109±0.009)	(37.50±1.91)	(35.20±1.50)
		CONDITION 2		
383±51	0.151±0.008	0.128±0.042	30.50±3.54	44.80±2.90
(395±38)	(0.138±0.031)	(0.036±0.003)	(28.00±0.00)	(33.33±2.33)
		*		*
		CONDITION 3		
290±09	0.151±0.020	0.115±0.020	31.40±0.89	33.50±1.87
(305±23)	(0.146±0.017)	(0.138±0.033)	(30.67±3.51)	(29.60±1.70)
				*
		CONDITION 4		
300±00	0.213±0.029	0.120±0.013	33.00±0.00	34.67±4.93
(300±00)	(0.187±0.001)	(0.115±0.005)	(33.50±0.58)	(27.70±2.10)
	*			*

4.5.8 Pt(acac)$_2$ at 100 ppm + EGDME

Table 4.8 shows there are few statistically significant differences between the reference fuel 2 and this increased concentration platinum treated fuel (100 ppm) under all the bomb conditions applied. The average gradient and the magnitude of maximum pressure parameters at condition 2, and the ignition delay and maximum gradient at condition 4 are different. As seen previous-

ly, these data do not correlate with one another, and thus can be termed as 'freak' data. Again, the Pt(acac)$_2$ additive has shown no effect on the combustion process of diesel fuel even with doubling the additive concentration. This is not too surprising since the previous platinum tests have showed no effect on the ignition delay, perhaps these results may suggest that platinum complexes have no catalytical effect on the combustion process of diesel fuel, but more tests are needed before this suggestion can be made definitely.

Table 4.8 Test Data of Pt(acac)$_2$ + EGDME 5% at 100 ppm

Ignition Delay/μs t_2-t_1	Maximum Gradient/bar μs^{-1} P_1/t_3-t_2	Average Gradient/bar μs^{-1} P_2/t_4-t_2	Maximum Pressure/bar P_2	Temperature Rise/^{o}C
		CONDITION 1		
382±11	0.148±0.040	0.112±0.065	37.00±1.41	37.30±4.30
(390±15)	(0.164±0.014)	(0.109±0.009)	(37.50±1.91)	(35.20±1.50)
				*
		CONDITION 2		
383±11	0.121±0.010	0.105±0.006	36.00±1.63	32.30±2.70
(395±38)	(0.138±0.031)	(0.036±0.003)	(28.00±0.00)	(33.33±2.33)
		*	*	
		CONDITION 3		
297±27	0.177±0.011	0.106±0.004	31.33±1.53	32.00±3.54
(305±23)	(0.146±0.017)	(0.138±0.033)	(30.67±3.51)	(29.60±1.70)
		CONDITION 4		
345±00	0.222±0.031	0.116±0.004	34.00±0.00	28.60±1.80
(300±00)	(0.187±0.001)	(0.115±0.005)	(33.50±0.58)	(27.70±2.10)
*	*			

The conclusion drawn from these two platinum tests is that this platinum complex with EGDME oxygenated solvent has no catalytic effect on combustion of diesel fuel even after doubling the additive concentration and with various bomb conditions. Perhaps this may change if the additive concentration is decreased rather than increased as were performed here.

4.5.9 Pd(acac)₂ at 50ppm + EGDME

Table 4.9 Test Data of Pd(acac)$_2$ at 50 ppm + EGDME 5%

Ignition Delay/μs t_2-t_1	Maximum Gradient/bar μs^{-1} P_1/t_3-t_2	Average Gradient/bar μs^{-1} P_2/t_4-t_2	Maximum Pressure/bar P_2	Temperature Rise/^{o}C
		CONDITION 1		
386±23	0.164±0.004	0.091±0.011	34.00±2.31	37.80±1.30
(390±15)	(0.164±0.014)	(0.109±0.009)	(37.50±1.91)	(35.20±1.50)
				*
		CONDITION 2		
385±11	0.148±0.021	0.103±0.006	35.25±2.06	35.00±2.80
(395±38)	(0.138±0.031)	(0.036±0.003)	(28.00±0.00)	(33.33±2.33)
		*	*	
		CONDITION 3		
300±00	0.167±0.000	0.105±0.007	33.00±0.00	26.30±1.90
(305±23)	(0.146±0.017)	(0.138±0.033)	(30.67±3.51)	(29.60±1.70)
				*
		CONDITION 4		
300±21	0.157±0.010	0.100±0.008	30.50±1.29	31.67±6.11
(300±00)	(0.187±0.001)	(0.115±0.005)	(33.50±0.58)	(27.70±2.10)
	*		*	

The test results for the above palladium complex are shown in Table 4.9. Again, this Pd(acac)$_2$ at 50 ppm also showed few statistically significant differences between treated and reference fuels. The different data at 500°C and 600°C are inconsistent in that they do not correlate with other data. The conclusion must be that this complex also has no effect on the combustion process of diesel fuel.

4.5.10 Pd(acac) $_2$ at 100 ppm + EGDME

Table 4.10 Test Data of Pd(acac)$_2$ at 100 ppm+ EGDME 5%

Ignition Delay/μs t_2-t_1	Maximum Gradient/bar μs^{-1} P_1/t_3-t_2	Average Gradient/bar μs^{-1} P_2/t_4-t_2	Maximum Pressure/bar P_2	Temperature Rise/°C
		CONDITION 1		
368±32	0.161±0.028	0.154±0.034	38.50±1.14	39.50±7.58
(390±15)	(0.164±0.014)	(0.109±0.009)	(37.50±1.91)	(35.20±1.50)
		CONDITION 2		
345±00	0.134±0.001	0.120±0.008	35.00±0.82	42.40±5.32
(395±38)	(0.138±0.031)	(0.036±0.003)	(28.00±0.00)	(33.33±2.33)
		*	*	*
		CONDITION 3		
285±00	0.116±0.023	0.097±0.004	30.00±0.00	28.40±4.39
(305±23)	(0.146±0.017)	(0.138±0.033)	(30.67±3.51)	(29.60±1.70)
		CONDITION 4		
285±00	0.220±0.010	0.108±0.003	31.00±1.41	32.80±7.53
(300±00)	(0.187±0.001)	(0.115±0.005)	(33.50±0.58)	(27.70±2.10)
*	*		*	

Table 4.10 shows the test data of the above treated fuel tests which, again, are inconsistent in their differences from the data for the reference fuel 2. Again, the above two palladium tests show no definite catalytic effects in the reduction of ignition delay and thermal efficiency. These results might be related to the corresponding platinum additive results, as both metal belong to the same group, and therefore, no differences in catalytic effect of the metal ion. So in general we can say that increasing the Pd(acac)$_2$ metal additive concentration to this level produces no effect at all upon the combustion process of diesel fuel and, by extension, this palladium complex is useless as an additive.

4.5.11 Diesel + THF 5% (Reference Fuel 3)

The data presented in Table 4.11 are the results of the reference fuel 3 tests and also the data of the diesel reference fuel 1 tests which again are in bold and brackets. Table 4.11 shows for the first time that the ignition delay data correlates well with the Wolfer's proposed equation, in both temperature and pressure. At condition 1 there appears to be no differences in the behaviour of references fuel 3 and 1. The decrease in the temperature rise does not correlate well with all changes in the other parameters for this condition. However, at condition 2, the decrease in ignition delay, although it did not effect the initial rate of pressure rise, did effect both the overall rate of pressure rise and the maximum pressure rise, although these effects show a negative correlation with respect to the shorter ignition delay data. At condition 3, the ignition delay shows an increase compared to reference fuel 1. All the parameters remain unchanged at condition 4. Overall, the results are slightly different from what I would have expected. I expected the results to show reductions in ignition delay and average gradient under all conditions when compared with undosed diesel fuel. Since THF is an oxygenated organic compound, it would also behave the same as those

already known oxygenated ignition improver. However, this has made my task of comparing data between this reference fuel and doped-fuel easier.

Unlike EGDME, THF has some influence on the combustion processes of diesel fuel with increased bomb temperature. These changes are for the ignition delay period, rate of pressure rise and magnitude of maximum pressure rise. Therefore, this reference fuel test data showed that the task of comparing these data with doped-fuel data will be more difficult than that of the previous reference fuel 2.

Table 4.11 Test Data of Diesel + THF 5% (Reference Fuel 3)

Ignition Delay/μs t_2-t_1	Maximum Gradient/bar μs^{-1} P_1/t_3-t_2	Average Gradient/bar μs^{-1} P_2/t_4-t_2	Maximum Pressure/bar P_2	Temperature Rise/^oC
		CONDITION 1		
416$\pm$14	0.196$\pm$0.028	0.121$\pm$0.007	40.25$\pm$0.50	37.29$\pm$0.95
(378$\pm$37)	(0.171$\pm$0.016)	(0.128$\pm$0.024)	(39.20$\pm$2.77)	(42.20$\pm$1.64)
				*
		CONDITION 2		
385$\pm$38	0.141$\pm$0.014	0.111$\pm$0.006	35.25$\pm$2.06	42.40$\pm$1.67
(429$\pm$08)	(0.130$\pm$0.006)	(0.088$\pm$0.003)	(30.60$\pm$0.00)	(37.80$\pm$2.80)
*		*	*	
		CONDITION 3		
330$\pm$00	0.177$\pm$0.020	0.129$\pm$0.026	30.60$\pm$0.59	33.30$\pm$3.80
(300$\pm$18)	(0.152$\pm$0.021)	(0.096$\pm$0.005)	(29.40$\pm$1.82)	(30.60$\pm$2.20)
*		*		
		CONDITION 4		
308$\pm$32	0.204$\pm$0.073	0.112$\pm$0.018	30.50$\pm$0.58	29.80$\pm$0.96
(273$\pm$27)	(0.161$\pm$0.029)	(0.106$\pm$0.008)	(31.20$\pm$1.10)	(28.84$\pm$3.29)

4.5.12 Pt(acac)₂ at 50 ppm THF

Table 4.12 Test Data of Pt(acac)₂ at 50 ppm + THF 5%

Ignition Delay/μs t_2-t_1	Maximum Gradient/bar μs^{-1} P_1/t_3-t_2	Average Gradient/bar μs^{-1} P_2/t_4-t_2	Maximum Pressure/bar P_2	Temperature Rise/^{o}C
		CONDITION 1		
355±57	0.101±0.025	0.051±0.019	33.33±0.58	40.80±2.20
(416±14)	(0.196±0.028)	(0.121±0.007)	(40.25±0.50)	(37.29±0.95)
	*	*	*	*
		CONDITION 2		
355±31	0.073±0.007	0.027±0.003	25.33±2.08	38.00±2.60
(385±38)	(0.141±0.014)	(0.111±0.006)	(35.25±2.06)	(40.40±1.67)
	*	*	*	
		CONDITION 3		
295±17	0.151±0.015	0.100±0.003	30.00±1.73	28.30±1.50
(330±00)	(0.177±0.020)	(0.1.29±0.026)	(30.60±0.59)	(33.30±3.80)
*				
		CONDITION 4		
305±23	0.195±0.028	0.112±0.007	32.23±1.15	24.40±1.95
(308±32)	(0.204±0.073)	(0.112±0.018)	(30.50±0.58)	(29.80±0.96)
			*	*

Table 4.12 represents the data from the tests of the Pt(acac)₂ additive at 50 ppm with THF as the oxygenated solvent. The data show a good positive correlation between both rates of pressure rise and magnitude of the maximum pressure rise at 500°C. These data might also be expected to correlate with the ignition delay data. Unfortunately, there is too large a standard deviation. The calculated Student's t-Test results show that the ignition delay for these data are significantly not different between reference and treated fuels. The

average rates of pressure rise are much lower at 500°C than are found for the reference fuel. This can be understood by considering the pressure rise peak shown in Figure 4.18.

In these two conditions the location of the maximum pressure rise is late and, since the maximum pressure rise occurred at the second peak rather than at the normal first peak, the average gradient is reduced. This could suggest that the metal additive has an effect on the diffusion burning process, where the fuel is combusting at a similar rate to that of injection. If so, the greater the peak of the diffusion burning process, the greater the combustion efficiency. The data indicate no real changes at 600°C. Again, these data also suggest there may be a connection between catalyst activity and initial bomb temperature as the majority of the catalytic effects observed are at 500°C. The negative point is that the ignition delay periods at this temperature remain unchanged between the reference and treated fuels, but only partly due to the large standard deviation. Therefore more test are needed to strengthen these catalytic observations.
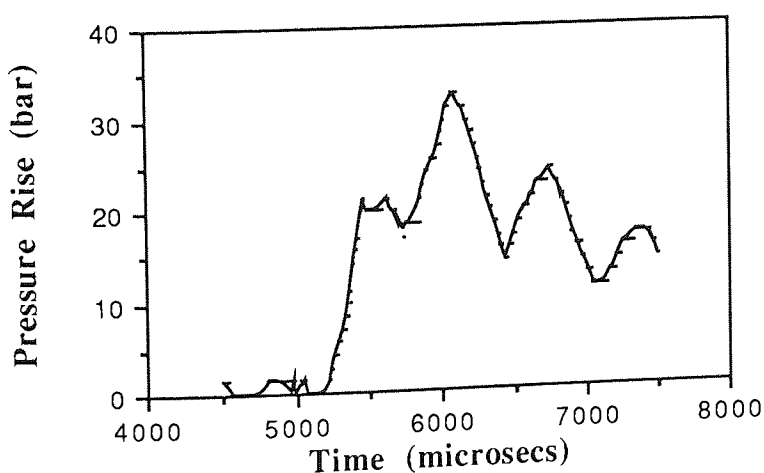
Figure 4.10 Double Peaks of Pressure Rise Observed at Conditions 1 and 2 for Pt(acac)$_2$ + THF at 50 ppm

Since the data for the tests at conditions 1 and 2 showed some consistencies, it may be safe to conclude that, at 50 ppm, Pt(acac)$_2$ with THF as the oxygenated

solvent genuinely has an effect on the combustion process of diesel fuel at 500°C. At this temperature the catalyst appears to reduce the rate of pressure rise and therefore in part behaved as hypothesised, except for the delay period.

4.5.13 Pt(acac)$_2$ at 100 ppm + THF

Table 4.13 Test Data of Pt(acac)$_2$ at 100 ppm + THF 5%

Ignition Delay/μs t_2-t_1	Maximum Gradient/bar μs^{-1} P_1/t_3-t_2	Average Gradient/bar μs^{-1} P_2/t_4-t_2	Maximum Pressure/bar P_2	Temperature Rise/^{o}C
		CONDITION 1		
398±74	0.133±0.047	0.087±0.048	27.50±4.95	43.60±2.40
(416±14)	(0.196±0.028)	(0.121±0.007)	(40.25±0.50)	(37.29±0.95)
			*	*
		CONDITION 2		
340±09	0.109±0.008	0.043±0.015	25.25±3.20	38.00±3.50
(385±38)	(0.141±0.014)	(0.111±0.006)	(35.25±2.06)	(40.40±1.67)
	*	*	*	
		CONDITION 3		
320±35	0.152±0.021	0.131±0.024	36.00±2.00	29.00±5.05
(330±00)	(0.177±0.020)	(0.1.29±0.026)	(30.60±0.59)	(33.30±3.80)
			*	
		CONDITION 4		
310±31	0.183±0.054	0.110±0.007	32.00±1.73	29.00±2.65
(308±32)	(0.204±0.073)	(0.112±0.018)	(30.50±0.58)	(29.80±0.96)

Again, Table 4.13 shows a positive correlation between the initial and the average rate of pressure rise under condition 2 as was seen in Table 4.12 for the same additive but at a lower concentration. The difference is that at this concentration not all the tests show the double peaks observed for 50 ppm. At

600°C the data show no significant differences between doped and reference fuels. Once again, any catalyst effect is associated with 500°C bomb temperature and not 600°C, perhaps then there is a connection between catalytic activity and metal complex decomposition temperature as discussed earlier. The table indicates that increasing the additive concen-tration and bomb temperature has produced no increase in catalyst activity. We can deduce from the above two platinum tests that this complex is useful as an additive when use with THF oxygenated solvent and at bomb condition of 500°C and 60 bar. The results appear to show some characteristics of an ignition improver, but reliability of the data puts a question mark over this observation, plus the different observations from previous platinum tests.

4.5.14 Pd(acac)$_2$ at 100 ppm + THF

Table 4.14 shows the test data for the Pd(acac)$_2$ additive at a 100ppm level. The data show the familar inconsistency, with most unchanged between reference and doped fuels. Therefore, we can conclude that this additive at this concentration has no effect upon combustion of diesel fuel. One can speculate that the results for the 50 ppm will be the same as the above 100 ppm results, the conclusion will then be this palladium complex is useless as an additive. The data for this test are not included here because the data were lost during the data processing step.

Table 4.14 Test Data of Pd(acac)$_2$ at 100 ppm + THF 5%

Ignition Delay/μs t_2-t_1	Maximum Gradient/bar μs^{-1} P_1/t_3-t_2	Average Gradient/bar μs^{-1} P_2/t_4-t_2	Maximum Pressure/bar P_2	Temperature Rise/^{o}C
		CONDITION 1		
360±63	0.118±0.036	0.103±0.015	35.00±1.41	37.30±0.60
(416±14)	(0.196±0.028)	(0.121±0.007)	(40.25±0.50)	(37.29±0.95)
			*	
		CONDITION 2		
405±42	0.145±0.017	0.142±0.012	35.00±1.41	39.80±2.50
(385±38)	(0.141±0.014)	(0.111±0.006)	(35.25±2.06)	(40.40±1.67)
	*	*		
		CONDITION 3		
323±11	0.136±0.010	0.124±0.003	32.50±2.12	34.40±6.03
(330±00)	(0.177±0.020)	(0.1.29±0.026)	(30.60±0.59)	(33.30±3.80)
		CONDITION 4		
292±11	0.189±0.016	0.115±0.001	32.00±1.41	34.60±2.70
(308±32)	(0.204±0.073)	(0.112±0.018)	(30.50±0.58)	(29.80±0.96)
				*

4.6 CONCLUDING REMARKS

A number of conclusions may be drawn from these data:

◆ The purpose of using the bomb was to provide stable and repeatable start-of-test conditions and so maximise the chances of obtaining repeatable data. However, this was not overly successful, due to the time required to do each test and to the effort required to process the

data. These limitations reduced the number of repeat tests to a low value. Despite this, the test conditions were considerably more controllable than in an ordinary engine, which is a positive gain.

◆ The method of data analysis seems reasonable given the restrictions on the form in which the data is obtained. The expected correlations are just about visible.

◆ Test-to-test repeatability is a concern, but probably nothing can be done about this except to obtain vastly more data.

◆ Of the oxygenated solvents used for the purpose of enhancing the solubility of metal complexes in diesel fuel, only THF has an effect upon the combustion of the diesel fuel. Therefore, EGDME would be a better solvent for these kind of additive tests, as its lack of influence on combustion, makes data analysis more straight forward.

◆ $Pt(CH_3)_2COD$ does not show any consistent effects on combustion, as were expected on the basis of the patent claims made for it. This is most disappointing, since the purpose of performing these experiments was to obtain reference data for a metal complex which has a definite effect as an additive.

◆ $Ce(DPM)_3$ shows some signs of affecting the combustion of diesel fuel, but only at $500^{\circ}C$. The maximum effect of this cerium complex on combustion is observed at a 100 ppm concentration and at a pressure of 60 bar. In these situations the cerium catalyst acts as an ignition improver, therefore enhancing fuel quality. The tests proved that

there was no advantage in increasing the additive concentration level from 100 to 200 ppm.

- ◆ $Pt(acac)_2$ shows some effects on combustion at a concentration of 50 ppm when it is introduced using THF as the oxygenated solvent. At this concentration the metal complex had an effect on the diffusion burning process. This is indicated by the double peaks observed for these data where the second peak is the maximum pressure rise peak. Again, more tests are needed before firm conclusion can be made of this observation.

- ◆ $Pd(acac)_2$ complex has no effect on combustion using either oxygenated solvent at a dosage level of 100 ppm. However, firm conclusion can not be drawn at this point because of the absence of the 50 ppm test results and as this is only one set of data.

Chapter 5

The Effect of Metal Complexes on Combustion in Diesel Engines

5.1 INTRODUCTION

In this chapter the results from the following metal additive test programmes on the combustion of diesel fuel are presented. In the experiments described in this chapter the additives were tested on engines of various sizes, from an engine test bed to a vehicle, to give some indication of any potential in commercial uses, whether for improving fuel efficiency, reducing exhaust emissions, or maybe even both.

Firstly, the history of engine development is very briefly discussed and then the general details of the engine design and operation. To some extent this has already been outlined for diesel engines in Chapter 4. The reason for the following test programmes has also been partly discussed in Chapter 4, for the mechanism of the catalyst on combustion of diesel fuel. However, here we extend the reason for investigating the effect of the catalyst on the combustion of diesel fuel to the reduction of the noxious gaseous emissions from combustion of additive treated diesel fuel. The metal additives used in this chapter are the metal complexes synthesised in Chapter 2.

The terms "torque output" and "load absorbed by the dynamometer" is are often used in this chapter. The dynamometer is perhaps the most important item in the test cell, as it is used to measure the engine torque (T). Torque is a measure of an engine's ability to do work and is defined by the following equation.

$$T = Fr$$

where

F = force on the dynamometer scale, lbf and

r = length of dynamometer arm, ft.

5.2 DIESEL ENGINES

In 1892, Rudolph Diesel took out a patent[124] for an engine with a very high compression ratio. After compression the temperature of the air charge would be sufficient to vaporise and ignite liquid fuel sprayed into the charge. The limitations of materials and fabrication prevented the immediate realisation of this idea and the first successful engine built in 1897 employed air blast injection. Fuel was metered at low pressure and pumped to the atomiser under high pressure using the direct injection method which Diesel originally intended.

The present day's increasing interest in the study of diesel engine combustion, emissions and economy is caused by growing concern about the depletion of energy resources and damage to the environment attributable to the large increase in the number of automobiles. The diesel engine, being the most economically known power plant, has gained popularity in many applications, including heavy and medium duty vehicles. More recently it has been considered in many parts of the world as a replacement for the regular spark-ignition (SI), also known as the gasoline engine, in some passenger car applications.

Cylinder operating pressures are much higher than in gasoline engines, requiring heavier components to withstand increased stresses and consequently limiting engine speed, although the thermal efficiency is considerably higher.

The high thermal efficiency of the diesel engine results mainly from the relatively high compression ratio required to start the autoignition process without spark-ignition. The advantage of not having spark-ignition is that a throttle valve to control the power output (which is needed in gasoline

-190-

engines) is not necessary. It is known that in order to obtain good fuel economy from an internal combustion engine it is desirable to operate unthrottled. This is one of the reasons why the diesel engine gives better economy than the gasoline engine, although the diesel engine suffers from other problems such as high noise and high smoke at full load. In comparison, the gasoline engine suffers from relatively high fuel consumption, requires a high octane fuel, and the untreated exhaust contains high concentrations of pollutants, mainly carbon monoxide, unburnt or partially burnt hydrocarbon, and nitrogen oxides.

In this section studies of the improvements to be made in fuel economy and exhaust emissions when diesel engines are operated on fuels dosed with metal complexes are reported. These two factors are due directly to the diesel fuel combustion process, an account of which now follows.

5.2.1 Diesel Engine Operation

In diesel engines, air alone is inducted into the cylinder. The fuel is injected directly into the engine cylinder just before the start of the combustion process. The engine load is controlled by varying the amount of fuel injected into the cylinder for each cycle; the air flow at a given engine speed is essentially unchanged.

The operations of a typical four-stroke naturally aspirated diesel engine are the intake stroke, the compression stroke, the expansion stroke, and the exhaust stroke. The compression ratio of diesels is much higher than typical gasoline engine values, and is in the range 12 to 24:1, depending on the type of diesel engine and whether the engine is naturally aspirated or turbocharged. Air at close-to-atmospheric pressure is inducted during the *intake stroke* and then compressed to a pressure of about 40 bar with the

temperature reaching above 500°C during the *compression stroke*. At an angle of about 20° before top dead centre (TDC), fuel injection into the engine cylinder commences. The liquid fuel jet atomises into drops and entrains air. The liquid fuel evaporates; fuel vapour then mixes with air to within combustible proportions. The air temperature and pressure are above the fuel's ignition point. Therefore, after a short *delay period*, spontaneous ignition (autoignition) of parts of the mono-uniform fuel air mixture initiates the combustion process, and cylinder pressure rises above the initial (non-firing) cylinder pressure. The flame spreads rapidly through that portion of the injected fuel which has already mixed with sufficient air to burn. As the expansion process proceeds, mixing between air, fuel, and burning gases continues, accompanied by further combustion (*expansion stroke*). At full load, the mass of fuel injection is about 5% of the mass of air in the cylinder. Increasing levels of black smoke in the exhaust show that there is a limit to the amount of fuel that can be burned efficiently. At the end of the expansion stroke the exhaust valve starts to open, and the irreversible expansion of the exhaust gases is termed 'blow-down'. The exhaust valve remains open, and as the piston travels up the cylinder the remaining gases are expelled. At the end of the *exhaust stroke*, when the exhaust valve closes some exhaust gas residuals will be left. These will dilute the next charge, as the cycle starts again. In the following investigations all the engines used are of four-stroke cycle, however the diesel engines can also be operated in two-stroke cycle.

In the two-stroke diesel engine cycle, compression, fuel injection, combustion, and expansion processes are similar to the equivalent four-stroke cycle processes. The two-stroke cycle differs in that it eliminates the separate intake and exhaust strokes. In the two-stroke diesel engine cycle the processes of charging and discharging the cylinder occur while the piston is approaching

bottom dead centre (BDC) before the end of the expansion stroke and after the beginning of the compression stroke. The pressure head required for the flow of the fresh charge into the cylinder is produced in the crankcase.

This engines requires two piston strokes or only one revolution for each cycle. In the two-stroke cycle engine, the exhaust ports are opened near the end of the expansion stroke, permitting the blow-down of the exhaust gases, and reducing the pressure in the cylinder. The charge of air flows in and is compressed in the crankcase compartment to just above the atmosphere pressure. Intake ports are uncovered by the piston soon after the opening of the exhaust, and the compressed charge flows into the cylinder. Part of the fresh charge flows out of the exhaust ports at the end of the scavenging period. In gasoline engines, but not in diesel engines, this results in the loss of fresh fuel in the exhaust and in high unburned hydrocarbons levels being emitted with the exhaust gases.

The main advantage of the two-stroke cycle engine, if compared with the four-stroke cycle engine, is that it has twice as many expansion strokes per cylinder per revolution. But, because of the poor scavenging and volumetric efficiencies of these engines the power output per unit piston displacement volume is only about 30% more than the four-stroke cycle engine.

The main disadvantages of this engine are the poor scavenging efficiency and difficulty of lubrication. In some crankcase scavenged engines, lubricating oil is added to the fuel for piston-liner lubrication, which results in additional unburned hydrocarbons in the exhaust. In carburetted engines, poor fuel economy is an additional disadvantage of the two-stroke cycle engine.

5.2.2 Types of Diesel Combustion Systems

Diesel engines are divided into two basic categories according to their combustion chamber design:

- **Direct-Injection** (DI) engines, which have a single open combustion chamber into which fuel is injected directly, and

- **Indirect-Injection** (IDI) engines, where the chamber is divided into two regions and the fuel is injected into the "pre-chamber" (situated above the piston crown) which is connected to the main chamber via a nozzle, or one or more orifices.

IDI engine designs are generally only used in the small high speed passenger car. With each category there are several different chamber geometrical, air-flow, and fuel-injection arrangements.

5.3 SINGLE CYLINDER DIESEL ENGINE TEST PROGRAMME

5.3.1 Experimental Set-up

A series of dynamometer tests were conducted in which a Tangye VCP-1 diesel engine was connected to and loaded by a Heenan-Froude hydraulic dynamometer. The engine had the following specifications:

Engine Type	Tangye Single Cylinder
Cycle of Operation	Four-Stroke Diesel Cycle
Cylinder Head	Direct-Injection
Bore x Stroke	114.2 x 146 mm
Displacement	1.4955 litre
Compression Ratio	18:1

Fuel is supplied to the engine from a flask with a two litre capacity. At the outlet a stop valve is fitted (see Fig. 5.1) and the fuel flows by gravity to an engine driven fuel circulating pump which discharged through a filter to the

fuel pump supplying the injector. A 100 ml capacity glass burette graduated in millilitres is connected into the main fuel line on the suction side of the fuel circulating pump; this, together with a stop valve fitted upstream of the burette, is used for fuel consumption measurements.
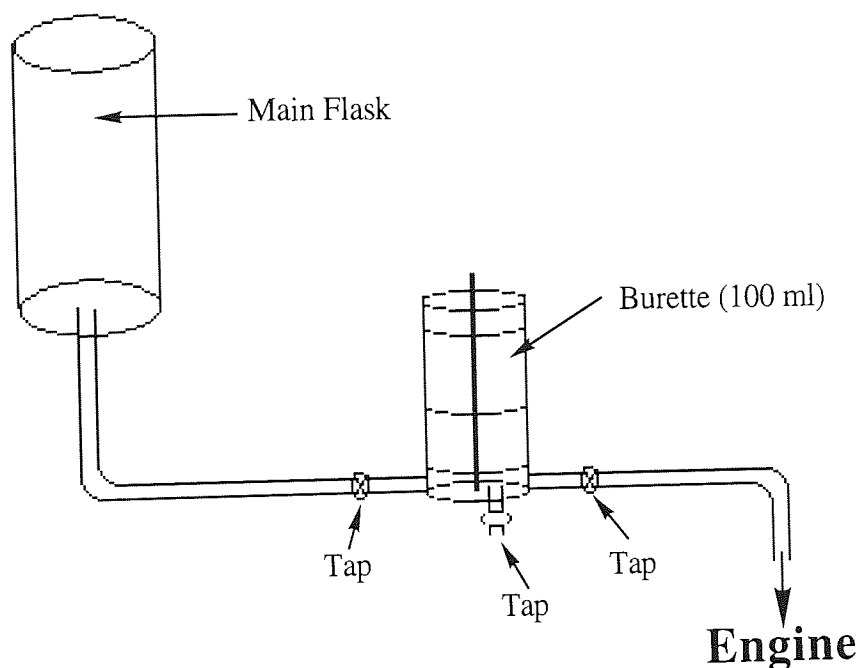
Figure 5.1 Fuel System of the Tangye Diesel Engine (unscaled)

Exhaust Gas System

Figure 5.2 shows the layout of the exhaust system. The section of the exhaust pipe closest to the cylinder head was fitted with an exhaust sampling probe as illustrated in Figure 5.2. The exhaust pipe is extended to vent outside the building, where the exhaust gases are released to the atmosphere. The exhaust pipe is lagged with asbestos tape to prevent condensation. An exhaust gas sampling probe was made for the following tests which consisted of a perforated stainless steel tube (1/4 in diameter) and this was inserted into the exhaust pipe as shown in Fig. 5.2. The holes on the sampling probe were drilled at regular intervals (1/2 in) and at right angles to the next pair of holes, with a diameter of 1/16 of an inch.

Exhaust gas sampling probe

Analyser (CO$_2$)

Exhaust pipe

Stop valve

Analyser (HC & CO)

Outlet to atmosphere

sampling probe

exhaust gas
flow

exhaust pipe

stop valve

to analysers

to atmosphere
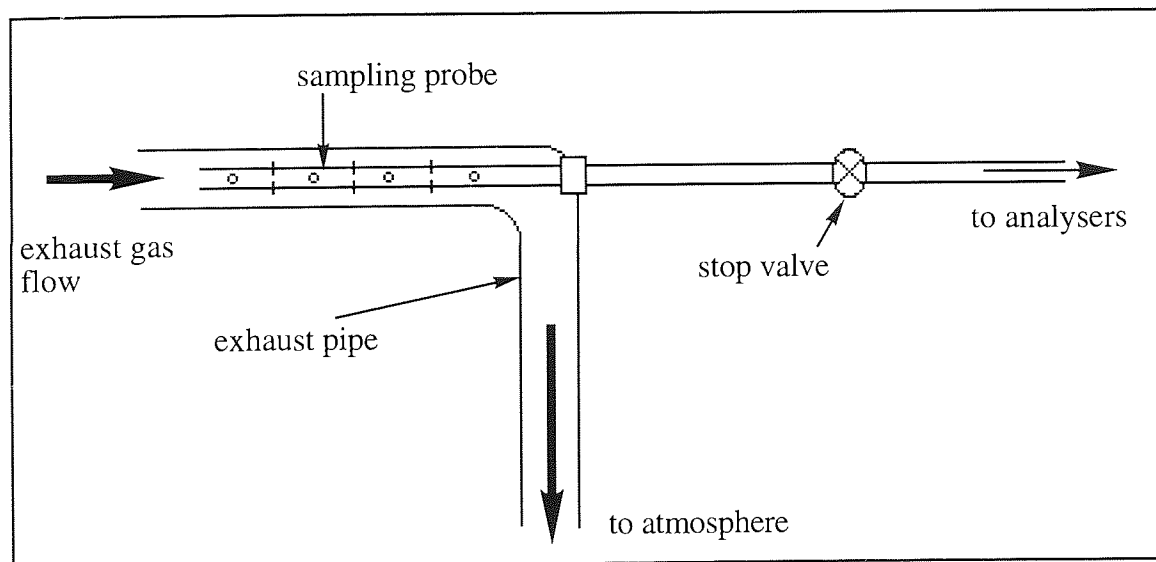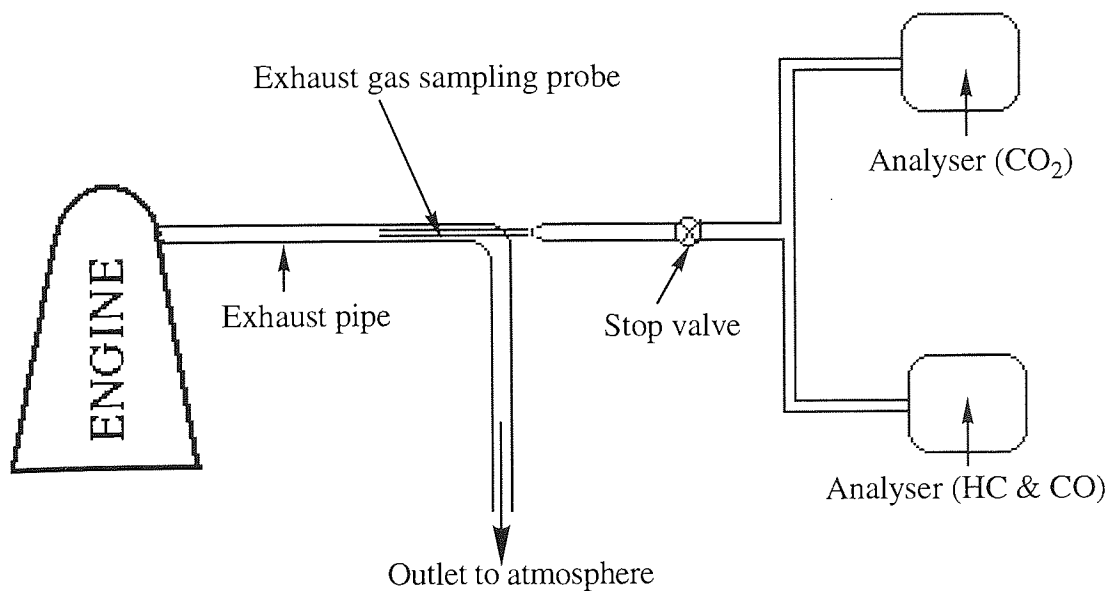
Close up view of the sampling probe

Figure 5.2 Exhaust Gas Analysis System of the Tangye Diesel Engine

The percentage by volume of carbon dioxide in the exhaust gases was measured by a HORIBA MEXA- 211GE analyser with a measuring range of 0-20 volume %. The percentage by volume of carbon monoxide and the ppm of hydrocarbon were measured using a HORIBA MEXA- 324GE analyser with a measuring range of 0-10 vol. % and 0-1000 ppm, respectively.

5.3.2 Experimental Procedure

Tests were conducted to determine the effect on the concentrations of CO, HC and the fuel consumption at various engine loads of adding various additives in different dosages to the diesel fuel. Previous work in this field by Sprague and co-workers[21,22,76] with Pt-group metal coordination compounds showed that dosed fuel containing these complexes can improve fuel efficiency and reduce exhaust emissions.

The fuels used in this test programme were of two categories, baseline and treated fuels. The baseline fuels were of two types, diesel and diesel treated with 5% of THF oxygenated solvent as also described in the previous chapter. Esso commercial diesel fuel was used in this investigation to test for the catalytic potential of metal additives.

In the following tests, additives were either mixed with the fuel directly or with the aid of an oxygenated solvent i.e. THF. The metal complexes used in this investigation were those synthesised in previous experiments, discussed in Chapter 2. The treated fuels were obtained by adding to the diesel fuel a number of additives at dosages in the range of 5-100 ppm. The metal complexes $Ce(DPM)_3$, $La(DPM)_3$, Fe-naphtren, Ce-naphtren, Fe-^{t}Bu-saltren, and Ce-^{t}Bu-saltren, were used.

At the beginning of each test, the engine was run on the tested fuel for a warming-up period of 60 minutes, at a constant engine speed of 1200 rpm with no-load added, to attain steady running conditions. All the tests performed were run at this speed. During each of these runs, the time the engine took to consume a measured 100 ml quantity of fuel was recorded. It was decided to perform ten runs at each of three engine operating condition, with loads of 0 lbf, 15 lbf, and 30 lbf (the maximum available load). Also

recorded were the exhaust gas analyses. The data listed in the following tables are the averages. Also listed are the results of the Student's t-Test, for each data set. As with the previous chapter, an asterisk indicates that the means of the baseline and the treated fuels are different at a 95% confidence interval. The results for these metal additives tests are summarised in the following tables, but the data for carbon dioxide are not listed here, but are included in the appendix with the full results of these investigations.

5.4 RESULTS AND DISCUSSION

5.4.1 Diesel Fuel (Baseline 1)

As before, the baseline data (diesel) were obtained first to provide a standard against which the effect that metal additives upon combustion can be judged. They are listed in Table 5.1.

Table 5.1 Test Data of the Untreated Diesel Fuel (Baseline 1)

Load (lbf)	Time for 100 ml consumption (s)	Carbon Monoxide (%)	Hydrocarbons (ppm)
0	401	0.15	35
15	260	0.14	40
30	172	0.21	55

5.4.2 Ce(DPM)₃ at 25, 50 and 100 ppm

Table 5.2 shows the averaged test data for the named cerium additive and for baseline 1. The consumption times for 100 ml of diesel fuel containing 25 ppm of the cerium additive are all longer than the baseline fuel at all three engine operating conditions. The difference gradually decreases as the load increases. The data show that the catalyst is more efficient at low load i.e. low

Table 5.2 Test Data of Ce(DPM)$_3$ at 25, 50 and 100 ppm

Load (lbf)	Time for 100 ml consumption (s)		Carbon Monoxide (%)		Hydrocarbons (ppm)	
	baseline 1	with additive	baseline 1	with additive	baseline 1	with additive
25 ppm						
0	401	411 *	0.15	0.15	35	45 *
15	260	267 *	0.14	0.11 *	40	20 *
30	172	175 *	0.21	0.09 *	55	35 *
50 ppm						
0	401	411 *	0.15	0.16	35	40 *
15	260	267 *	0.14	0.12 *	40	30 *
30	172	172	0.21	0.09 *	55	30 *
100 ppm						
0	401	391 *	0.15	0.18 *	35	45 *
15	260	257 *	0.14	0.16 *	40	40
30	172	168 *	0.21	0.13 *	55	55

cylinder temperatures. As the F/A ratio is smaller at low loads the cylinder temperature is also lower since excess air reduces thermal efficiency. The catalyst activity is less pronounced as the load increases; i.e. higher cylinder temperature, since the F/A ratio is higher at high loads. This may suggest that there is a connection between temperature and catalyst activity, as seen in Chapter 4. Unlike the data observed in Chapter 4, these data are consistent.

Therefore at this level of dosage the above cerium complex has a small effect on the diesel combustion process, with a range of fuel efficiency gains of 2 to 3%, compared to the baseline under all three engine operating conditions. Here the catalyst acts as an ignition improver, thus enhancing the fuel ignition quality, and thereby improving the combustion efficiency.

The data of Table 5.2 also show that the cerium treated fuel has an effect on the concentration of the unburned hydrocarbons compared to the baseline fuel. A reduction of the HC level occurs under engine operating conditions with loads added, but under no-load engine operating conditions the treated fuel appears to have a negative effect with increased HC emissions, even though there is a reduction of 36% in the emission at 30 lbf (full-load), and a greater one of 50% at 15 lbf (half-load)

HC emissions are the result of the incomplete combustion of the hydrocarbons in diesel fuel, and the inability to complete the combustion inevitably must affect the combustion efficiency. Except for the data, at no-load engine condition, this is borne out in the results. That exception does put a question mark either against the reliability of the data or over the hypothesis that maximising combustion efficiency will minimise the HC emissions. Alternatively, HC reduction is achieved through another mechanism i.e. by the metal oxide in the bulk of the fuel-air charge or those deposited on the combustion chamber's surfaces. Thus at no-load condition, the excess air reduces the thermal efficiency and so reduces the catalytic effect of the metal oxide. The concentration of the catalyst is also smaller at this load since the F/A ratio is smaller. This would also explain the increases of HC reduction efficiency with increasing load on the engine.

The data of Table 5.2 show no significant changes between the treated and baseline fuels for the carbon monoxide concentration in the exhaust at no-

load on the engine. However, there are significant reductions as the load increases. Concentration of CO is reduced by 57% at 30 lbf load and by 21% at 15 lbf load. At no-load the concentration of CO shows no changes compared to the baseline. This is to be expected, as complete combustion is difficult to attain at the lower temperatures existing in the combustion chamber under this condition. The CO data correlate well with the fuel consumption times, indicating that the reduction of CO concentration is related to the combustion efficiency.

The data in Table 5.2 agree with the results obtained by Sprague and co-workers[21,22,76] when complexes of Pt-group metal were tested under a similar conditions. These workers describe a method for catalysing fuel for internal combustion engines which comprises of mixing the fuel with an additive containing several Pt-group metal compounds in an amount equivalent to a supply of 0.01-1.0 ppm of metal. Suitable Pt-group metal compounds include (a) Pd acetylene complexes, (b) Rh or Ir allyl complexes, e.g., $Rh(C_3H_5)_3$ and $Ir(C_3H_5)_5$, (c) Pt(IV) compounds having the general formula R_1PtR_2; where R_1=aryl, alkyl, or their mixtures, and R_2= hydroxyl, acetylacetonate, cyclopentadiene or pentamethyl cyclopentadiene, (d) a compound of the general formula L_1MR_3, where L_1 is a butadiene or cyclohexadiene derivative, M=Rh or Ir, and R_3= cyclopentadiene or pentamethyl cyclopentadiene. These Pt-group metal results showed an improvement in fuel efficiency and a reduction in exhaust emissions with dosed fuels compared with undosed fuel.

So from these data (Table 5.2), the deduction must be that this cerium complex at 25 ppm has had some effect on the diesel combustion processes by improving the fuel efficiency at all three engine conditions. The additive also reduced the HC and CO emissions at engine operating conditions with loads

added. This is most encouraging since the majority of the engine running times in a vehicle are operated under some loads, due to the rolling resistance from the friction of the tyres and the aerodynamic drag of the vehicle.

At 50 ppm (Table 5.3), the data exhibit almost the same catalytic effects at this dosage as were found at a 25 ppm dosage. The exception being for the fuel consumption time at full-load engine condition where the data remain the same for the treated and baseline fuels. At lower loads the treated fuel showed a very small improvement in fuel efficiency compared to the baseline fuel. At 50 ppm dosage, the catalyst appears to produce maximum reductions at full-load for both the CO and HC concentrations with 43% and 45%, respectively, compared to the baseline 1. This is useful as higher concentrations of the exhaust emissions occur at engine conditions near to full-load. The overall deduction from this test is that increasing the additive dosage level from 25 ppm to 50 ppm causes little improvement in the catalyst activity.

Data had also been collected under conditions in which the concentration of the additive was 100 ppm. The results are also shown in Table 5.2. In general the catalytic effect has deteriorated at this dosage level The fuel consumption times are shorter for the treated fuel compared to the baseline, thus indicating poorer combustion efficiency. At this concentration the cerium additive has reduced the fuel quality which probably increases the ignition delay period. Long ignition delay means shorter available burning time. Consequently, there is poorer combustion efficiency, therefore giving rise to CO and HC concentrations in the exhaust. There is only one positive catalytic effect, at full-load for the CO concentration. This must indicate that the CO reduction is achieved merely by the presence of the cerium oxide rather than by better combustion efficiency. This arise from the metal deposition on the

combustion chamber surfaces or in the exhaust train, or possibly even from both causes. This would agree with a recent report[18] which states that reduction of diesel particulate matter and hydrocarbons were caused by the catalytic oxidation of an Fe_2O_3 coating that developed inside the engine's combustion chamber.

From these three dosage tests it can be concluded that the catalyst shows different behaviour at different $Ce(DPM)_3$ concentrations and loads. The data show that the effect of the catalyst is more pronounced at lower level of dosages and low loads, and increasing the dosage from 25 ppm to 100 ppm has reduced the rate of improvement of the combustion efficiency. The fuel consumption times are longest at 25 ppm and 50 ppm dosages compared to the baseline. In these cases the catalyst acts as an ignition improver by reducing the chemical delay. Also, the catalyst activity for the combustion efficiency appears to be connected to temperature or load with maximum efficiency at low temperature, in agreement with the data discussed in Chapter 4. The tests also show a close relationship between the combustion efficiency and the concentrations of CO and HC emissions, as hypothesised. Hence maximum reduction of CO and HC concentrations, and maximum combustion efficiency were observed at low dosages. In these tests the catalyst must operate under a gas phase mechanism, since varying the additive concentration produced an immediate effect upon the combustion of diesel fuel.

5.4.3 La(DPM)₃ at 25, 50 and 100 ppm

The test data for $La(DPM)_3$ additive at a dosage level of 25 ppm are listed in Table 5.3. Under engine running conditions of no-load the data show no

Table 5.3 Test Data of La(DPM)$_3$ at 25, 50 and 100 ppm

Load (lbf)	Time for 100 ml consumption (s) with		Carbon Monoxide (%) with		Hydrocarbons (ppm) with	
	baseline 1	additive	baseline 1	additive	baseline 1	additive
25 ppm						
0	401	402	0.15	0.18 *	35	35
15	260 *	265	0.14	0.13	40	25 *
30	172 *	170	0.21	0.14 *	55	45 *
50 ppm						
0	401 *	420	0.15	0.14	35	45 *
15	260 *	269	0.14	0.10 *	40	20 *
30	172	172	0.21	0.10 *	55	35 *
100 ppm						
0	401 *	408	0.15	0.18 *	35	45 *
15	260 *	270	0.14	0.13	40	30 *
30	172 *	174	0.21	0.12 *	55	35 *

statistical significant differences between the lanthanum treated fuel and the baseline fuel for the fuel consumption time and HC parameters, with the exception of the CO parameter, where a negative result occurred. The data for the half-load condition show positive catalytic effects for the fuel consumption time and HC parameters, but no changes in the CO parameter between treated and baseline fuels. A very small increase of 2% for the fuel

consumption time and a reduction of 38% for the HC concentration are obtained with this treated fuel. However, at full-load engine condition the catalytic effect on the fuel efficiency is less pronounced, but more pronounced for the CO parameter and not so much for the HC. These results are different from what I had expected in showing a small increase in fuel efficiency. As lanthanum only has one oxidation state, the suggested mechanism would rule out any effect on its part. Thus, this additive must achieve its effects via a different mechanism.

One explanation behind these improvements of the combustion efficiency is that the lanthanum additive might affect the diffusion burning process rather than the pre-mixed burning phase, since lanthanum only has one oxidation state and therefore would not undergo the hypothetical mechanism discussed in Chapter 1 for a metal catalyst with more than one oxidation state, e.g. cerium, which gives a reduction of the ignition delay period. At the diffusion burning phase the lanthanum catalyst might influence the combustion of the remaining fuel-air charge, since the temperature in the cylinder has increased sharply after the uncontrolled burning process. Here, the catalyst might lower the ignition temperatures of the fuel and therefore improve the fuel ignition quality which would promote faster combustion.

Any catalytic effectiveness due to this lanthanum additive at 25 ppm depends on the engine operating condition. The data clearly show that for better fuel efficiency the catalyst must be operated in part-load conditions and for the reduction of the noxious exhaust emissions the catalyst is most effective between half-load and full-load.

At a 50 ppm level of dosage the above lanthanum treated fuel (Table 5.3) shows better fuel efficiency than the 25 ppm dosage. There is an improved

fuel efficiency at no-load and half-load conditions, 5% and 3% improvements respectively. At full-load, there is no improvement. The results for the exhaust emissions are similar to those obtained for the cerium tests, with reductions in CO and HC concentrations observed at half- and full-load engine conditions, and no changes at no-load condition. The CO and HC concentrations in the exhaust emissions are halved at full-load and half-load.

Under no- and full-load conditions the exhaust emission data do not relate well with the fuel consumption time data, the relationship between improved fuel efficiency and reduced exhaust emissions is not strong. As, the La catalyst must be operating under a different mechanism from that of Ce, to reduce the CO and HC concentrations, the most likely mechanism involves the metal formed in the initial uncontrolled combustion reactions. This would explain the higher reduction rate of the CO and HC concentrations and the lower combustion efficiency at high loads, where high temperatures will optimum catalyst acitivity. It is known that lanthanum oxide can catalyse the oxidation of CO to CO_2 at high temperature.

Again, the results for the lanthanum treated fuel at the highest dosage, 100 ppm, (Table 5.3) show similar catalytic effects to those observed at 50 ppm dosage. The fuel consumption times for the treated fuel show small increases compared to the baseline fuel at all load conditions, and maximum reduction of the CO and HC concentrations occurred at full-load. The levels of reduction observed are slightly lower than those of the 50 ppm treated fuel. However, it is still much better than the cerium additive at this dosage where the cerium treated fuel shows a negative effect or no improvement at all. As at the lower dosages, the CO and HC concentrations found here at no-load show no catalytic effect compared to the baseline fuel. Again, probably due to

the low temperature in the combustion chamber at this engine operating condition.

Thus far, both cerium and lanthanum complexes of the DPM ligand show substantial effects on the combustion processes of diesel fuel, and the direction of these effects also depends upon the metal additive concentration. The cerium additive has a marked effect at low additive concentrations, while the lanthanum additive has its greatest effect at higher additive concentrations. The two metal additives must be operating under different mechanisms for their involvement in the combustion efficiency. Since lanthanum only exhibits compounds with a +3 oxidation state, we can presume that its catalyst activity is found during the diffusion burning process, either from the presence of the lanthanum oxide formed in the combustion chamber or the lanthanum additive in the fuel mixture. Increasing the lanthanum additive dosage produces further improvements in fuel efficiency. If time had permitted it would have been interesting to study a mixed La/Ce additive.

5.4.4 Diesel + THF at 5% (Baseline 2)

Table 5.8 containing the data for the baseline 2 fuel test, where diesel fuel is diluted with 5% of THF oxygenated solvent. This solvent was chosen simply due to its availability at the time of these investigations. It's use is dictated by the inability of certain metal additives to dissolve completely in diesel fuel on their own.

The THF solvent appears to cause definite improvements in fuel efficiency under all three engine conditions, with maximum improvement at half-load. For exhaust emissions, THF shows no effect at no-load, but some reduction for the concentrations of CO and HC at half- and full-loads. In part, these

results confirm those described in Chapter 4, but they also agree with those cited in references discussed in Chapter 1 in which oxygenated organic compounds are said to be ignition improvers.

Table 5.4 Test Data of Diesel + THF (5%)

Load (lbf)	Time for 100 ml consumption (s) baseline 1 baseline 2		Carbon Monoxide (%) baseline 1 baseline 2		Hydrocarbons (ppm) baseline 1 baseline 2	
0	401 *	410	0.15	0.14	35	40
15	260 *	274	0.14 *	0.10	40 *	20
30	172 *	175	0.21 *	0.10	55 *	40

Therefore, the THF solvent has influenced the combustion process of diesel fuel and also affected the emission concentrations of CO and HC, thus making the task of data analysis increasingly more difficult between baseline and treated fuels. These improvements could possibly overlap any effects that the metal additive may have exerted in the following tests. They are almost identical to those qouted in Table 5.3.

5.4.5 Ce-naphtren at 5, 25 and 50 ppm

The test data for Ce-naphtren plus THF (5%) treated with 5, 25 and 50 ppm dosages are shown in Table 5.5. Once again, we can see the general pattern observed previously. The additive has a positive effect on the fuel consumption times at all loads. CO emissions are slightly raised at zero load but drop with increasing load, as also do the HC emissions, at 5 ppm level of dosage. At the higher additive loadings (Table 5.5) its effects are unremittingly bad.

Table 5.5 Test Data of Ce-naphtren at 5, 25 and 50 ppm

Load (lbf)	Time for 100 ml consumption (s) with		Carbon Monoxide (%) with		Hydrocarbons (ppm) with	
	baseline 2	additive	baseline 2	additive	baseline 2	additive
5 ppm						
0	410	416 *	0.14	0.16 *	40	45
15	274	275	0.10	0.09	20	25
30	175	179 *	0.10	0.08 *	40	30 *
25 ppm						
0	410	388 *	0.14	0.18 *	40	40
15	274	262 *	0.10	0.12 *	20	20
30	175	167 *	0.10	0.13 *	40	45
50 ppm						
0	410	375 *	0.14	0.22 *	40	65 *
15	274	254 *	0.10	0.18 *	20	40 *
30	175	168 *	0.10	0.23 *	40	65 *

The Ce-naphtren additive tests illustrate the great difference which the behaviour of dosages have on the catalyst activity of this additive. At a low dosage of 5 ppm the treated fuel shows some catalytic effect , by improving the fuel efficiency and also reducing the concentrations of CO and HC emissions, but only at high loads. However, at higher dosages (up to 50 ppm) the fuel

data shows no beneficial effects at all. Poorer fuel efficiency and higher exhaust emissions are seen than for baseline 2 alone. This could be because catalytic activity is connected to the decomposition properties of the metal complex. In this case, the Ce-naphtren complex starts decomposing at a much higher temperature than is found for, say $Ce(DPM)_3$, see Chapter 3. Therefore, at high dosages, this metal additive could hinder the diesel combustion process, as the majority of the additive in the fuel-air charge will still be in its original form and may reduce the ignition quality of the fuel.

5.4.6 Fe-naphtren at 5, 12.5 and 25 ppm

The test data for the Fe-naphtren treated fuel at a 5 ppm dosage are shown in Table 5.6. Unlike the Ce-naphtren additive at this concentration, this iron additive shows no beneficial catalytic effect at any engine operating conditions used. The data also show either no changes or negative results at higher additive loadings. This material should not be used as an additive for improving the diesel fuel combustion and reducing exhaust emissions as it exhibits no desirable features.

5.4.7 Ce-^{t}Bu-saltren at 5 and 25 ppm

Table 5.7 shows the test data for the Ce-^{t}Bu-saltren treated fuel with a dosage level of 5 ppm. The treated fuel data show no catalytic effect when compared with baseline 2, which was unexpected as this complex contains all the features thought to be necessary for a good pro-oxidant additive. This test in fact showed that the metal additive has hindered the combustion process rather than improving it at this dosage. At 25 ppm its behaviour was worse.

Table 5.6 Test Data of Fe-naphtren at 5, 12.5 and 25 ppm

Load (lbf)	Time for 100 ml consumption (s) with		Carbon Monoxide (%) with		Hydrocarbons (ppm) with	
	baseline 2	additive	baseline 2	additive	baseline 2	additive
5 ppm						
0	410	396 *	0.14	0.17 *	40	45
15	274	261 *	0.10	0.12 *	20	35 *
30	175	174	0.10	0.12 *	40	55 *
12.5 ppm						
0	410	361 *	0.14	0.23 *	40	55 *
15	274	247 *	0.10	0.20 *	20	40 *
30	175	167 *	0.10	0.12 *	40	45
25 ppm						
0	410	400 *	0.14	0.17 *	40	55 *
15	274	270 *	0.10	0.12 *	20	35 *
30	175	177 *	0.10	0.08 *	40	35

Table 5.7 Test Data of Ce-^{t}Bu-saltren at 5 and 25 ppm

Load (lbf)	Time for 100 ml consumption (s) with		Carbon Monoxide (%) with		Hydrocarbons (ppm) with	
	baseline 2	additive	baseline 2	additive	baseline 2	additive
5 ppm						
0	410	403 *	0.14	0.16 *	40	50 *
15	274	272 *	0.10	0.11	20	30 *
30	175	176	0.10	0.11	40	45
25 ppm						
0	410	386 *	0.14	0.21 *	40	45
15	274	253 *	0.10	0.15 *	20	35 *
30	175	172 *	0.10	0.10	40	45

5.4.8 Fe-^{t}Bu-saltren at 5 and 25 ppm

The iron complex of the same ligand (^{t}Bu-saltren) was also tested. The results are shown in Table 5.8, for the 5 and 25 ppm dosages. At full-load the metal additive appears to show a useful effect on the fuel consumption time and the concentration of CO emissions, for the lower dosage. The effect of the additive is to improve the fuel efficiency and lower the CO emissions at this load. However, there are no signs of any effect at the other engine loads, the same as the baseline, except for the fuel consumption times where negative results were obtained. Table 5.8 also shows the data for this iron additive test at 25 ppm, which cast some doubt on the positive results observed at 5 ppm

for the full-load condition. Perhaps they were freak data. This test shows that increasing the additive dosage has produced no catalytic activity. Again, there is probably a connection between catalytic activity and rate of additive decomposition, since Fe-^{t}Bu-saltren also has a long decomposition temperature range which starts at 237°C and continues beyond 550°C.

The cerium and iron metal complexes with ^{t}Bu-saltren ligand show no beneficial catalytic activity upon combustion. With increasing additive concentration, from 5 ppm to 25 ppm, reduced the combustion efficiency and increased the exhaust emissions are found. These materials are useless.

Table 5.8 Test Data of Fe-^{t}Bu-saltren at 5 and 25 ppm

Load (lbf)	Time for 100 ml consumption (s) with		Carbon Monoxide (%) with		Hydrocarbons (ppm) with	
	baseline 2	additive	baseline 2	additive	baseline 2	additive
5 ppm						
0	410	393 *	0.14	0.16 *	40	40
15	274	272 *	0.10	0.11	20	15 *
30	175	180 *	0.10	0.08 *	40	35
25 ppm						
0	410	390 *	0.14	0.23 *	40	40
15	274	258 *	0.10	0.13 *	20	40 *
30	175	171 *	0.10	0.09	40	40

5.5 CONCLUSIONS

From this single cylinder diesel test programme, it can be concluded that substantial changes can be brought about by the use of metal complexes as additives. The direction of the changes is influenced by the concentration, engine load condition, and the additive itself. The mechanism for the catalyst appears to be a gas-phase mechanism. Changing the additive level of dosages produces an immediate change in catalytic activity. Thus the catalytic activity must be in the gas-phase because the additive concentrations used for these tests are too small to have an immediate effect on surface deposition. Not all the metal complexes tested are successful as additives.

Both $Ce(DPM)_3$ and $La(DPM)_3$ show some potential, although the direction which brought about the catalytic effects are different with these additives. $Ce(DPM)_3$ is more effective at lower dosage levels, while $La(DPM)_3$ is more pronounced at high dosages. The $La(DPM)_3$ additive may be of benefit in the diffusion burning phase, where the catalyst enables more and a faster reaction to occur in the fuel-rich region of the spray cone. The cerium additive probably acts by reducing the ignition delay and thereby acting as an ignition improver, thus enhancing fuel ignition quality.

Except for Ce-naphtren at 5 ppm dosage, all the other tests for the iron and cerium complexes of the Schiff base ligands gave detrimental results. They are useless as an additive. At 5 ppm Ce-naphtren appears to improve combustion efficiency and to reduce the CO and HC concentrations in the exhaust emissions when compared with the base fuel, but only at this low dosage. A finding consistent with the results obtained for the $Ce(DPM)_3$ tests. The tests indicate that a relationship exists between catalytic activity and the rate of additive decomposition. The additives with the faster rate of decomposition, e.g. $Ce(DPM)_3$, appear to produce the more pronounced catalyst activity in these tests. It is now worth investigating the $Ce(DPM)_3$ additive effect on a vehicle engine.

5.6 FORD DIESEL P100 PICK-UP TRUCK TEST PROGRAMME

5.6.1 Test Procedure

A Ford diesel P100 pick-up truck with approximately 67,000 recorded mileage was used as a test vehicle to provide data on a diesel engine. This investigation was performed at Engineering Research & Application (ERA) Ltd, Dunstable.

Baseline testing for gaseous emissions was conducted according to the ECE 15/04 drive cycle, which represents a cold start with a 4 Km drive through city traffic and was simulated on a chassis dynamometer. The dynamometer absorption was adjusted to simulate the resistances encountered under actual road conditions and an inertial mass was used to simulate the vehicle weight. The test consists of four identical cycles, a cycle being a fixed programme of idles, accelerations, cruises and decelerations. During the test the vehicle exhaust was sampled for analysis. However, the following tests were done with the engine hot to improve repeatability, after a mileage accumulation of 700 miles which is equivalent to about two fuel tanks. Two sets of gaseous emissions data were recorded.

Following baseline testing, the vehicle fuel was treated with Ce(DPM)$_3$ additive at a dosage of 50 ppm and then the baseline test procedure was repeated, and the gaseous emssions were recorded. The treated fuel was prepared by mixing the additive very throughly with a commercial diesel fuel before adding that mix to the fuel tank. As before, this cerium additive was dissolved directly in diesel fuel without using any oxygenated solvents. The base fuel was drained from the fuel system before the treated fuel was added to the vehicle. The vehicle was allowed to accumulate 680 miles of on-the-road driving with the additive before it was retested. Treatment was

maintained during that period through the use of pre-packaged additive introduced into the vehicle's fuel tank at each fuel fill-up to maintain the test additive concentration. The exhaust emissions analysers used for this set up are those of the emissions bench consisting of;

Signal	3000	-	HC Analyser
Signal	4000	-	NOx Analyser
Cussons	NDIR	-	CO Analyser
Cussons	NDIR	-	CO_2 Analyser

The data for this investigation are summarised in Table 5.9. Each number average of the two sets of measurements and the full results are listed in the appendix.

5.6.2 Results and Discussion

Table 5.9 ECE 15/04 Emissions Test Data of Ce(DPM)$_3$ at 50 ppm

	Baseline	Treated	% Increase	% Decrease
CO_2 (%)	0.480	0.485	1.04	
HC (ppm)	8.3	6.4		22.4
CO (ppm)	29.1	24.8		14.6
NOx (ppm)	14.8	13.4		9.3
MPG (U.S.)	20.5	20.3		1.1

Using a single cylinder diesel engine on a test bed some catalytic success was achieved with the Ce(DPM)$_3$ additive upon the combustion of diesel fuel. Naturally, the next step was to investigate this additive on a vehicle, so the data for the vehicle test (Table 5.9) were obtained. The cerium additive tests were performed to provide data for the fuel efficiency and gaseous emissions under a standard drive cycle, i.e. ECE 15/04. This would give us a more

realistic picture of how the additive may affect the diesel combustion process in everyday driving, thereby demonstrating some additive potential for commercial uses.

The treated fuel data show a reduction for the HC and CO emissions compared to base fuel, as anticipated. Therefore, the additive has had an effect, particularly on the HC emission. But, the reduction for the NOx emission is unexpected. The fuel efficiency for the treated fuel shows only a small decrease compared to the baseline fuel. Unlike the Tangye single cylinder tests, these data cover a range of load conditions and are average values. Overall they show little pro-oxidant activity, as was such shown in the Tangye test programme.

The small reduction for the NOx emissions is most unexpected considering that the treated fuel data showed poorer combustion efficiency. Catalytic activity that reduces the delay period will correspondingly reduce NOx production which occurs almost exclusively by the kinetic, Zeldovich mechanism in the pre-mixed lean fuel zone in the periphery of the fuel spray where fuel/air ratios are conducive to NO formation and " residence times" are longest. Alternatively NOx reduction may be linked to the reductions of the HC and CO. As a reduction of the HC and CO concentrations would have taken some of the available oxygen in the combustion chamber for their oxidation reactions, this in turn would produce a lower rate of oxidation between N_2 and O_2, which agrees with the increased CO_2. However, firm conclusions should not be drawn at this stage for the effect upon NOx concentration without further tests. The reduction might still be a freak result or not of statistical significance.

Since the data show no relation between fuel efficiency and exhaust emissions, the additive must be operating under a different mechanism to

that discussed earlier for the reduction of the exhaust emissions. Metal deposition on the combustion surfaces could be the prime cause for this improvement in emissions, but there are still too many unresolved possibilities. For example, the high air swirl often present "may sweep up" some of the catalyst from the surface into the bulk of the charge where it can then participate in the gas-phase reactions with the evaporating fuel. This could only be observed if we were to open up the combustion chamber and examine the metal surface deposition. More tests are needed.

5.7 CONCLUSIONS

This investigation proved that under a ECE 15/04 drive cycle the $Ce(DPM)_3$ additive has had an effect, but only to reduce the exhaust emissions and not the fuel efficiency at a 50 ppm dosage level. The test data suggests that under all these on-the-road engine operating conditions the additive has no catalytic effect upon combustion efficiency. From this test programme it can be concluded that there is no connection between catalytic activity for the exhaust emissions and combustion efficiency.

5.8 CONCLUDING REMARKS

A number of overall conclusions may be drawn from the results of all these diesel engine test programmes:

◆ A metal additive's catalytic activity depends upon the additive itself. Of the metal complexes tested, only $Ce(DPM)_3$ and $La(DPM)_3$ complexes are successful as an additive. Complexes with the same metal ion but with a different ligand showed significant differences in catalytic activity.

◆ The test results indicate that there is a connection between catalytic activity and additive decomposition temperature/ and or additive rate of decomposition, i.e. $Ce(DPM)_3$ has produced a more pronounced catalytic effect than the other additives, due to its having a faster rate

of decomposition and a lower decomposition temperature than the others.

◆ The behaviour of the additive is influenced both by the concentration of the additive and the engine load. For improving fuel efficiency, catalytic activity is more pronounced at low dosages and loads, and deteriorates with increasing concentrations and loads. Catalytic activity for the reduction of the exhaust emissions is more pronounced with increasing loads, and also at low dosages.

◆ Overall, there appears to be no correlation between maximising combustion efficiency and minimising noxious exhaust emissions with the treated fuel. The metal additive was only effective in reducing the noxious gaseous emissions.

◆ The catalyst operates via a gas-phase mechanism in the combustion chamber, where it improves the combustion efficiency at certain engine conditions and also reduces the noxious gaseous emissions.

Chapter 6

An Investigation of the Effect of a Cerium Complex on Combustion of Gasoline Fuel and of Lanthanide Metal Oxides on Exhaust Gas Treatment

6.1 INTRODUCTION

The work done so far has focused mainly on engine emissions. Further reductions in emissions can be obtained by removing pollutants from the exhaust gases in the engine exhaust system. Devices developed to achieve this result include catalytic converters (oxidising catalysts for HC and CO, reducing catalysts for NOx, and three-way catalysts for all three pollutants), thermal reactors (for HC and CO), and traps or filters for particulates.

The temperature of the exhaust gas in a spark-ignition (SI) engine can vary from 300 to 400°C during idle to about 900°C at high-power operation. The most common range is 400 to 600°C. SI engines usually operate at a fuel/air ratio near to the stoichiometric mixture i.e. 14.7:1. The exhaust gas may therefore contain modest amounts of oxygen (when lean) or more substantial amounts of CO (when rich). In contrast, diesel engines, where load is controlled by the amount of fuel injected, always operate lean. The exhaust gas therefore contains substantial oxygen and is at a lower temperature (200 to 500°C). Removal of gaseous pollutants from the exhaust gases after they leave the engine cylinder can either be thermal or catalytic. In order to oxidise CO, temperatures in excess of 700°C are required.

Catalysed oxidation of CO and HC in the exhaust can be achieved at temperatures as low as 250°C. Thus effective removal of these pollutants occurs over a much wider range of exhaust temperatures than can be achieved with thermal oxidation. The only satisfactory method known for the removal of nitric oxide (NO) from exhaust gas involves catalytic processes. Removal of NO by catalytic oxidation to NO_2 requires a temperature below 400°C (from equilibrium considerations) and the subsequent removal of the NO_2 produced. Catalytic reaction of the NO with added ammonia (NH_3) is not practical because of the transient variations in NO produced in the engine.

Reduction of NO by CO, HC, or H_2 in the exhaust to produce N_2 is the preferred catalytic process. It is only feasible in the SI engine exhausts for temperature reasons. The use of catalysts in SI engines for CO, HC, and NO removal has become widespread.

In Chapter 1 the use of catalytic converters involving the use of platinum group metals, which are already in great demand by the motor industry, was described. Therefore, the intention here was to seek another catalytic system which, simultaneously, could make use of a metal additive for improvements in the combustion chamber and of the resultant metal oxide in the exhaust system for after-treatment of the exhaust gases. All investigations described in this chapter were performed for convenience on SI engines, but with a view to use in a diesel engine. The results of these investigations are summarised below.

This section starts with a brief introduction to the history of SI engine development. The fundamental operating principles for the SI engines are almost the same as for the compression ignition engines, apart from the ignition of the fuel/air charge. Also included in this section are introductions to the development of the catalytic converter and to electron microprobe analysis, i.e. the scanning electron microscope (SEM). This instrument was used for the microanalysis of the metal deposited on the exhaust system surfaces. The additive and catalyst testing programmes in this chapter were all performed at E.R.A. Ltd and the results are presented in the following sections.

6.1.1 Spark-Ignition Engines

In 1862, Nikolaus A. Otto tested a four cylinder engine operating on a four stroke cycle[125]. The gas/air mixture was drawn into the cylinder on one

stroke, compressed on the next, and exploded, driving the piston back down the cylinder on the "working stroke". The gases were exhausted on the fourth stroke to complete the cycle. The mechanical parts were unable to withstand the severe stresses resulting from the compressive cycle and in 1867 Otto began to build non-compressive atmospheric engines in which the mixture was exploded to drive the piston up the vertical cylinder. The piston carried a rack driving on a spur gear which was coupled to a flywheel through a free wheel operating on the up-stroke. As the gases cooled, the piston was pushed into the cylinder by atmospheric pressure and power was transmitted to the flywheel.

Otto finally perfected a four-stroke engine for which he also developed magneto ignition in 1876. It was essentially a stationary engine requiring large volumes of gaseous fuel. This limitation led to investigations into methods of utilising liquid fuels, and vaporising them so that an explosive mixture could be drawn into the engine. Much of the intervening period has been concerned with the development and refinement of such liquid fuelled engines.

The past three decades have seen new factors for change become important which have significantly affected engine design and operation. These factors are, first, the need to control the automotive contribution to urban air pollution and, second, the need to achieve significant improvements in automotive fuel consumption.

It is now known that the spark-ignition engines in today's automobiles and trucks are a major source of urban air pollution. As a consequence, SI engine emission control technology has developed rapidly and a substantial amount of basic research on engine combustion and pollutant formation has been

carried out. Therefore, it would be careless at this stage of the research not to investigate the catalytic effect of the Ce(DPM)$_3$ additive upon the combustion of gasoline fuel. In SI engines, the fuel and air are usually mixed together in the intake system prior to entry to the engine cylinder, using a carburettor, and ignition is initiated by a spark. From this, one would not expect the cerium catalyst to show any improvements on the combustion efficiency, since the previous mechanisms put forward are based on the catalyst's improving the fuel ignition quality by reducing the ignition delay period, i.e. it would be effective only in the diesel combustion process. However, it is worth investigating the possibility that the catalyst has an effect upon the exhaust emissions.

6.1.2 Catalytic Converters

The evolution of the automotive catalyst formulations from simple oxidation systems to the current three-way catalyst arose from a number of studies[126-132]. In 1959, Chandler and Van Derveer[110] were the first to report on the development of a catalytic converter for the oxidation of the exhaust hydrocarbons. The paper reports on the efficiency of a vanadium pentoxide catalyst in a catalytic converter system. Overall operating efficiencies of 60 to 73% can be expected in the removal of exhaust hydrocarbons. The vanadium pentoxide catalyst shows resistance to being poisoned by the decomposition products of tetraethyl lead (TEL). However, other attempts at catalytic purification of exhaust gases have been thwarted by the use of TEL in the fuel, since this compound can rapidly poison catalysts by coating them with deposited lead. Eventually, this compound was widely claimed to be a harmful pollutant, with the result that calls were made for it to be phased out of use by 1975. This involved either redesigning engines to cope with lower octane fuels or improving petroleum refining to develop high octane lead-free fuel. The latter has been achieved. The way was therefore cleared for

catalytic reactors to form a viable part of the emission control concept[8]. That can be argued to be the main justification for the use of lead-free petrol. The aim in using catalyst systems is to remove CO and HC by oxidation to carbon dioxide and water, and to remove NOx by either reduction to N_2 or by decomposition to N_2 and O_2. Unfortunately, simple decomposition catalysts are too ineffective to be used in car exhaust reactors, the weight of catalyst required being prohibitive. However, the reduction of NOx by the CO or HC present in the exhaust is a much faster reaction allowing a viable reactor design to be reached.

The oxidation and reduction mechanisms involved have important implications for the type of emission control system to be used. Up to 1975 the required NOx emissions could be achieved by exhaust gas recirculation (EGR), and, therefore, for 1975 the preferred system consisted of oxidation catalysts for the control of CO and HC emissions and EGR engine modification for the control of NOx. Secondary air is supplied to the exhaust for catalytic oxidation using a small air pump.

The U.S.A. 1976 emission requirements demanded much lower NOx levels which could not be met using EGR, as the higher recirculation rate required imposes a severe power loss. Therefore, a second catalyst bed was used for the control of NOx and this operated in a net reducing atmosphere. Air from a pump was fed into the gas stream after the reduction catalyst. This fed an oxidation catalyst for the control of the CO and HC emissions.

Research performed at Johnson Matthey has shown that the platinum group metals are the most active materials available for controlling the type of pollutants produced by the automobile[8]. Catalysts are typically supported upon ceramic monoliths or alumina pellets. The former are washed coated

with an alumina layer prior to impregnation with a noble metal catalyst. The noble metal most commonly used in exhaust catalysts is platinum, but this is usually promoted by a second noble metal, generally palladium or rhodium. Platinum/rhodium is the most frequently used combination in the present oxidation catalysts, although pure platinum and platinum/palladium are also used.

Three-Way Catalysts

Engine designers have continued to improve the engine efficiency and the control of the catalyst feed gas. Improved fuel control yielded a system using a catalyst which operated best near the stoichiometric point. Thus the Three-Way Catalyst (TWC) could be developed and many recent vehicles use this type of system. The name three-way comes from the fact that all components, CO, HC, and NOx are treated in the same catalyst at the same time, according to the following generalised reactions:

$$2CO + 2NO \longrightarrow 2CO_2 + N_2$$

$$HC + NO \longrightarrow CO_2 + H_2O + N_2$$
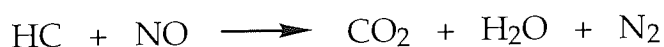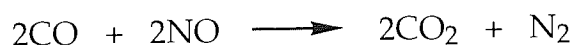
In the development of these catalysts it was identified that ruthenium and rhodium were the most capable of adsorbing and promoting the removal of NOx under carefully controlled conditions, such that the emissions reaching the catalysts were close to reaction stoichiometry. Both of these metals showed high activity and selectivity, when combined with platinum, in converting NOx to harmless nitrogen. Unfortunately, ruthenium possesses a volatile oxide, ruthenium tetraoxide, which is formed on the catalyst during the lean excursions that occur even with the best fuel management systems. Thus while ruthenium/platinum catalyst systems gave high initial activity, this performance deteriorated on ageing due to the loss of ruthenium. Hence

all TWC are now based on the Rh/Pt system which do not suffer the same volatility problem.

The stoichiometry of the emissions reaching the catalyst can be controlled by a closed loop feedback system incorporating an oxygen or Lambda-sensor[133]. The λ sensor is an oxygen concentration cell with an oxygen ion in a solid electrolyte which provides a sharp voltage step at the stoichiometric air/fuel ratio, and which serves as a control signal. The signal is used to regulate the fuel management system and thus provides a stoichiometric gas composition to the catalyst.

6.1.3 Catalyst Activity Mechanisms

The current theory of catalysts centres around the "active site". The active site may be viewed as the point on the catalyst material crystallite where the electronic forces are optimum for the catalytic reaction to take place. The catalytic process is illustrated by the following example: CO and O_2 are chemisorbed on the catalyst and can react readily because of their proximity and orientation. The process of adsorption also results in a weakening of the bond of the CO molecule because some of the energy is shared with the surface. Thus, it can be broken or addition bonds to the C be made more easily. The reaction between CO and oxygen is thus easier and more rapid. The basic requirement of such a catalyst is that it chemisorbs the molecules in the desired temperature range and in such a fashion, including geometry, that the reaction occurs readily. Then, the products having achieved a lower energy state, must desorb at the same temperature, thus freeing the active site for additional reactions.

A constituent which adsorbs strongly on an active site without later desorbing may limit the reaction, thus "poisoning" the catalyst. Scavengers in leaded

gasoline can do this. The lead in the leaded gasoline also poisons the catalyst, but it does so by masking the whole surface indiscriminately.

Highly polar molecules are more strongly adsorbed and less polar molecules are readily desorbed on metal and metal oxide automotive catalysts. One might think that CO is not easily handled catalytically because CO is not very polar and CO_2 is even less polar. Unfortunately, CO is more polar than oxygen and therefore under rich conditions the CO tends to cover the active parts of the catalyst, preventing the oxygen from being adsorbed and thus slowing the reaction. This is sometimes referred to as CO "poisoning".

Hydrocarbons are harder to handle catalytically. Methane, for example, is essentially non-polar and is thus the hardest hydrocarbon to oxidise catalytically. Acetylene, on the other hand, is also present in the automotive exhaust. It is quite polar and may, in some circumstances, be strongly absorbed and cover the active site of the catalyst, interfering with the reaction.

6.1.4 Electron Microprobe Analysis

Electron microprobe analysis is used to measure the energy or wavelength of emitted X-rays to provide elemental analysis of a specimen. This measuring equipment is normally attached to a scanning electron microscope[134] (SEM). The principles of electron microprobe analysis are that when an electron (10-30 keV) strikes an atom of a specimen a vacancy in an electron shell is created[135]. For analysis, such interactions are of significance if an inner orbital electron has been removed. An outer orbital electron will enter the vacancy and the energy difference between the outer and inner orbital states results in the emission of an X-ray. The important features of this process are the following:

1. The vacancy is created in an inner orbital, which is essentially unaffected by chemical bonding, or by the state of the atom.

2. The ionisation energy of the electron that fills this vacancy is of much lower energy and so the emitted X-ray energy is virtually that of the inner orbital.

3. The energy of the inner orbital will be characteristic of the atomic number of the atom so that either wavelength or energy analysis of the X-rays will identify the atom concerned.

The accuracy of the method will obviously be less with elements of a low atomic number, as the difference in energy between outer and inner orbitals is smaller, resulting in X-rays of lower energy which are difficult to measure. The analysis becomes more quantitative as the atomic number of the specimen increases[136]. Usually the electron microscope attachments are limited to elements above sodium.

The emitted X-rays can be analysed by the energy dispersive analyser, which consists of a lithium-impregnated silicon detector, and the whole energy spectrum is recorded simultaneously and presented via a multichannel analyser. For qualitative analysis the spectrum is recorded in a few seconds and the specimen can be identified easily. For quantitative analysis, however, some instrumental corrections must be made. As both the efficiency of the characteristic X-ray production and the ability to detect them deteriorates as the atomic number decreases, extra care is thus required with low atomic number specimens.

All analyses reported in this chapter were performed on an SEM instrument (Cambridge Instruments Stereo Scan 90), which is fully adapted for micro-analytical purposes. The SEM is connected to a Link System, loaded with a

pre-set program prior to measurement, and a Mitsubishi Video Copy Processor which can be used to take photo prints. Here, the SEM was used to detect cerium oxide in the samples collected from the exhaust system. Quantitative analysis of cerium was not possible due to the presence of carbon atoms in the samples. These C atoms make it impossible to determine 100%, since the energies of the carbon atom are not detected. Therefore, the 100% recorded is that of the detected elements only. However, this method is quick and also gives a good approximate percentage of the cerium oxide in the sample, excluding C.

The relationship between the mass concentration of an element and the intensity of its characteristic X-ray emission, excited by an electron probe, is now fairly well understood. The composition of an unknown sample can therefore be derived accurately from measurements of the intensity from each element present, each measurement being expressed as a ratio with the intensity from a known standard excited under the same conditions. In deriving this "measured intensity ratio" k_A, it is assumed that the peak measurements on specimen and standard, I_{spec} and I_{std}, are already corrected for instrument deadtime and background, and normalised to the unit mass concentration of element A in the standard. Thus:-

$$k_A = I_{spec} / I_{std} \cdot C_A \, std$$

where $C_A \, std$ is the mass concentration of element A in the standard. The primary input for the program is therefore a set of k values, one for each element in the unknown, or if one remains unmeasured, its concentration can be determined by difference from 100%.

6.2 THE INVESTIGATION OF γ-ALUMINA PELLETS COATED WITH MISCH METAL AND LANTHANIDE METAL OXIDES AS POTENTIAL CATALYST CONVERTERS

6.2.1 Introduction

Having studied the effect that the metal complexes have upon the combustion processes, it was reasonable to investigate the effect that some of these additives' metal oxides might have in reducing the partial oxidation products of the combustion processes to more desirable final products before their exit from the exhaust system. As mentioned earlier, previous investigations involving the use of platinum group metals in internal combustion engines have led to the development of the catalytic converter for emissions reduction. However, because of the high cost and low availability of these metals, it would be an advantage if another system were to be developed, which could operate at a comparable efficiency, but at a lower cost.

In the past, work has been carried out with these noble metals in conjunction with another metal. The literature reports[137-139] have shown that cerium oxide is added at a loading of 2-30 wt % to the alumina pellets or washcoat of three-way catalysts for several reasons: Ce can store oxygen, and oxygen picked up by the Ce on the surfaces of the catalytic converter during lean excursions is available to oxidise CO during rich excursions. Ce stabilises noble metal dispersion against thermal damage and favourably alters the catalytic ability.

Again, my research interest lies purely in the lanthanide group metals. Therefore, the following investigations were performed to examine the effect that these lanthanide metal oxides have on conversions of HC and CO to CO_2 and H_2O, and also the possibility of reducing the NOx concentration, although we recognise that this last conversion is unlikely to occur.

In this research, a system called the "exhaust box" was used to investigate these conversions, in which metal-doped γ-alumina pellets are situated along the exhaust pipe near the engine to increase the temperature and surface area for suitable catalyst conditions, in a container or "box". The exhaust gases emitted from the engine can then be converted to more desirable products before leaving the exhaust system.

The chemistry of lanthanide doped aluminas has already been investigated by Kato[140]. Kato showed that the addition of lanthanide oxides retard the transformation of γ–Al_2O_3 to α–Al_2O_3, and the associated sintering which occurs. This sintering has been a problem with γ–Al_2O_3 based catalytic converters, since it slows down activity at high temperatures, which are associated with exhaust emissions.

The γ-alumina pellets were coated with Misch metal and lanthanide oxides prior to the following investigations. Misch metal was chosen for the first experiment as it is the unseparated mixture of the lanthanide metals. This experi-ment would provide information on the catalytic activity of a number of lanthanide metals. Also investigated were alumina pellets doped with cerium oxide, and lanthanum oxide, in order to provide further information on the catalytic activity of individual metals in terms of their reducing exhaust emissions.

6.2.2 Experimental

6.2.2.1 Preparation of the Catalytic Converters

Misch metal is a mixture of rare earth metals, 94-99%, with a typical major composition of:

Ce = 50-60%, La = 25-30%, Nd = 15-30%, and Pr = 4-6%.

In the U.K. Misch metal is only available commercially as an alloy of nickel, MNi_5, M=Misch metal, one of the Hystor alloys.

A method was devised for the best way of screening the alloy. The same method was also used to prepare the different lanthanide metal oxides, as reagents for a catalytic converter.

1. The alloy was dissolved in the minimum quantity of concentrated nitric needed to form a nitrate solution of the nickel and the lanthanides.

2. The solution was diluted and soaked onto a high surface area γ-alumina pellet support.

3. After absorption, the soaked pellets were roasted to a temperature (400°C) at which all nitrates on the pellets would be converted to the respective oxides.

4. Finally, the oxide catalyst was put into an exhaust box with maximum surface area support for partial oxidations of exhaust gases.

It is known that platinum exhaust control catalysts rely on a small ratio of Pt/support, and therefore the pellets were made so that the catalyst/support ratio would be about 2% wt/wt. The exhaust box used in these tests has a capacity of 1 litre, thus two litres of the doped pellets were produced for multiple testing, but unfortunately, only one set of tests was performed due to the busy schedule of work at E.R.A.

Two litres of γ-alumina pellets weighed 1007g and therefore 20.14 g of Misch metal-nickel alloy was required for a 2% coating. This alloy was dissolved in a minimum of concentrated nitric acid to leave a green solution of the nickel and Misch metal nitrates. After all the alloy was completely dissolved, the mixture was diluted to the correct volume required to completely cover the total surface area of the pellet, to prevent any wastage of catalyst.

Previous test showed that in 24 hours, 200 ml of γ-alumina pellets absorbed 100 ml of water. Therefore, 1 litre of solution was required for 2 litres of pellets.

The nitrate solution and γ-alumina pellets were mixed evenly in a 5 litre beaker by stirring with a thick glass rod to increase surface area absorption. A glass rod was used in order to prevent contamination by other metals. The beaker was covered and left for 24 hours to let the pellets absorb all the nitrate solution. After 24 hours, all pellets showed a green colour which indicated the presence of nickel nitrates. They were then roasted in a furnace at 400°C, to convert the nitrates to oxides, and for 6 hours to ensure complete conversion. The text reference shows that all lanthanide and nickel nitrates were converted to their respective oxides below this temperature. The pellets turned to a black colour during roasting. The same method was repeated for the lanthanum and cerium oxide-coated pellets with the starting reagent already existing in its nitrate form, i.e. $La(NO_3)_3$ and $Ce(NO_3)_3$. Finally, the oxide-coated pellets were tested for emission control using an exhaust box.

6.2.2.2 Apparatus and Engine Testing Procedure

Due to its availability, a spark-ignition engine was used to test for exhaust emissions, rather than a diesel engine. Since the main emission gases are known to be the same in both engines, i.e. HC, CO and NOx, this does not matter. A single cylinder Hydra research engine connected to a McClure dynamometer was used to carry out the investigations, and the engine had the following specifications:

Engine Type	Hydra Single Cylinder
Bore x Stroke	80.26 x 88.9 mm
Displacement	0.45 litre
Air-Fuel/Ratio	Various from 13 to 18:1

The engine was run at 3087 rpm with a load of 19.4 Nm over a range of air/fuel ratios from 13 to 18. An 'exhaust box' was designed to fit into the standard exhaust system of the test bed (Fig. 6.1). This exhaust box, with a volume of approximately 1 litre, was used to hold the prepared pellets. It was fitted close to the engine to increase the catalyst working temperature. The exhaust box was fitted with apparatus to monitor the temperature of the exhaust gases pre- and post-catalyst chamber and, at the same time, the levels of HC, CO and NOx were monitored. This gives an indication of the catalytic efficiency in removing the undesirable products. The exhaust box was connected to the emissions bench, via a three-way tap, which consisted of;

Ratfisch RS55	-	HC analyser
Cussons NDIR	-	CO_2 Analyser
Cussons NDIR	-	CO Analyser
Thermoelectron	-	Chemiluminescent - NOx Analyser
Model 10		
Paramagnetic	-	O_2 Analyser

This engine testing procedure was carried out on untreated γ-alumina pellets and also nickel/Misch metal oxide, cerium oxide, and lanthanum oxide of γ-alumina pellets. The results are summarised in the following sub-sections and the full results are listed in the appendix.
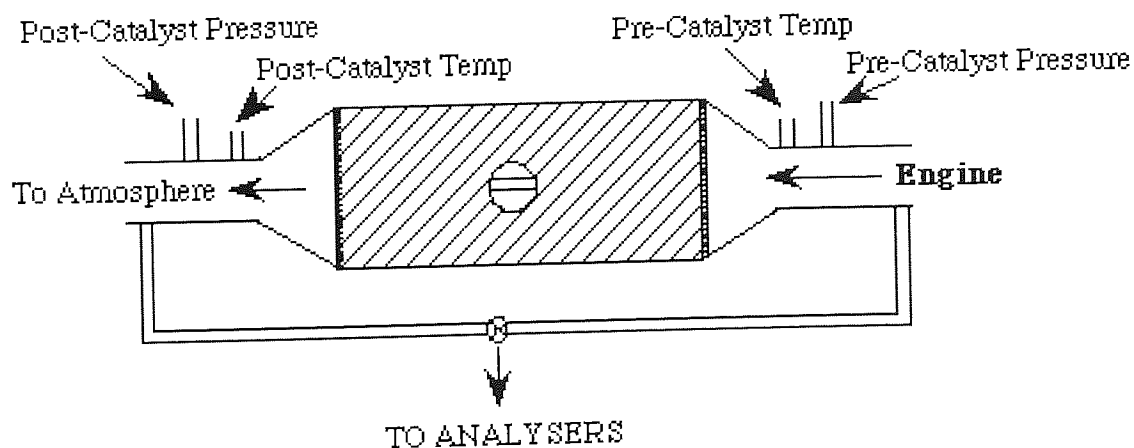
Figure 6.1 Diagram of the 'exhaust box' used in these investigations

6.2.3 Results and Discussion

The doped γ-alumina pellets were tested for exhaust emission control as described above. The results obtained for each individual test were displayed on separate graphs. Graphs of catalyst efficiency (%) were plotted against air/fuel ratios and are shown in the following figures. Exhaust emissions are monitored as pre- and post-catalyst box. The percentage difference of pre- and post-catalytic process is compared with the percentage prior to entry into the box to give a measure of catalytic efficiency. The exhaust temperatures were also monitored as pre- and post- exhaust box and these data are also plotted against air/fuel ratios on a separate graph. This is important because it shows the working temperature of the catalyst, and indicates when a reaction may be occuring. However, before testing any of the doped γ-alumina pellets, a baseline run was first carried out on the untreated γ-alumina pellets.

6.2.3.1 Untreated Pellets (Baseline)

Figure 6.2a shows that the untreated pellets have some potential in removing undesirable exhaust products. It seems untreated pellets worked best under a lean air/fuel ratio with a maximum of 41% efficiency for HC and only 2% for CO. The figure shows that, as the HC efficiency curve increases, the opposite effect is happening to the CO curve. This indicates some relationship between HC and CO, i.e. the HC is being converted at least in part to CO rather than solely carbon dioxide. There is no change for NOx throughout the air/fuel ratio. Figure 6.2b shows that the temperature curves of the exhaust, pre- and post-catalyst box, have the same trend, and also exhibit smaller temperature changes at a low and high air/fuel ratio. A smaller temperature difference at a leaner air/fuel ratio corresponds to maximum catalytic efficiency, because partial oxidation of HC would give off heat, thereby, keeping the temperature drop to a minimum. So, any reference to baseline must take into account this HC reduction by the untreated pellets.

6.2.3.2 Nickel-Misch Metal Oxides-Treated Pellets

The efficiency for HC removal in the above catalyst has a maximum of 42% (Fig. 6.3a), indicating no real changes by comparison to the untreated pellets. The only real difference is that nickel-Misch metal-treated pellets reach maximum efficiency at a lower air/fuel ratio than did untreated pellets, in which case they are less suitable in this research application than are untreated pellets. At about the stoichiometric air/fuel ratio, the treated pellets have a 28% efficiency for CO, 42% for HC and the NOx remain the same, but as the air/fuel ratio increases, the efficiency of CO drops sharply, as does the HC, but more slowly than CO. There is no advantage in using Misch metal in a catalytic converter.

6.2.3.3 Lanthanum Oxide-Treated Pellets

The results for the lanthanum oxide coated pellets (Fig. 6.4a), show a smaller increase in efficiency than did the previous results. The curve of HC of this figure rises as it moves towards a leaner air/fuel ratio reaching a maximum of 34% and then drops off. Comparison of this curve with the baseline curve shows that lanthanum oxide does nothing to enhance catalytic reaction, since the baseline has a higher percentage of HC conversion efficiency than lanthanum oxide treated pellets, at all air/fuel ratios. That is, this curve indicates a reduction in efficiency for the conversion of HC. The NOx and CO are unaltered in comparison with the untreated pellets. Therefore, lanthanum oxide is not a suitable catalyst for the control of exhaust emissions.

6.2.3.4 Cerium Oxide-Treated Pellets

Figure 6.5a shows the results for the cerium oxide-treated pellets test. The HC efficiency curve of cerium oxide treated pellets rises sharply as the air/fuel ratio increases, reaching a maximum efficiency of 70% at a 15.7 air/fuel ratio before tailing off slowly. By comparing this curve with the baseline curve, the figure shows an actual increase of 30% of HC conversion for cerium oxide.

Again, the temperature drop (Fig. 6.5b) at the point of the maximum efficiency of the catalyst is at its smallest. This is caused by the heat release during the conversion reactions of HC to CO_2. The other principle difference between the untreated- and cerium oxide treated- figures is the behaviour of the CO curve. The efficiency indicated by this curve also increases as the air/fuel ratio is increased before tailing off, following the same pattern as HC, and reaching a maximum efficiency of 28%, the highest value found for CO conversion. The importance of this pattern is that it shows that most of the HC oxidation product is CO_2 and not CO. This is behaviour of the type needed for a good catalytic converter. Again, the NOx curve remains unaffected by cerium oxide. This inactivity was found to be the same for all pellets examined, including baseline pellets, indicating that the prepared catalysts only support an oxidation reaction. Which is why precious metals are used commercially in the three-way converters.

The conclusions drawn from these results are that cerium oxide shows the highest catalytic activity, probably due to it's having two available oxidation states. Cerium oxide therefore has the potential to be a catalyst for the control of exhaust emissions, and so must be examined in further detail before firm conclusion can be made of the above observations. Figure 6.5 shows that the curves are tailing off towards the end, so it would be of interest to investigate the effect of operating the engine under an even leaner air/fuel ratio, since the maximum air/fuel ratio for this test was only 16.5.

Having reached the conclusion that cerium does have potential use both as an additive for fuel and as a catalyst converter, the next stage of the research was structured so that both of the above catalytic activities can be investigated simultaneously to provide maximum catalyst activity. This is described below.

Figure 6.2a Catalyst Efficiency versus Air/Fuel Ratio of the Untreated Pellets

Figure 6.2b Catalyst Temperature versus Air/Fuel Ratio of the Untreated

Pellets

Figure 6.3a Catalyst Efficiency versus Air/Fuel Ratio of the Nickel-Misch Metal Oxides Treated Pellets

Figure 6.3b Catalyst Temperature versus Air/Fuel Ratio of the Nickel-Misch Metal Oxides Treated Pellets

Figure 6.4a Catalyst Efficiency versus Air/Fuel Ratio of the Lanthanum Oxide Treated Pellets

Figure 6.4b Catalyst Temperature versus Air/Fuel Ratio of the Lanthanum Oxide Treated Pellets
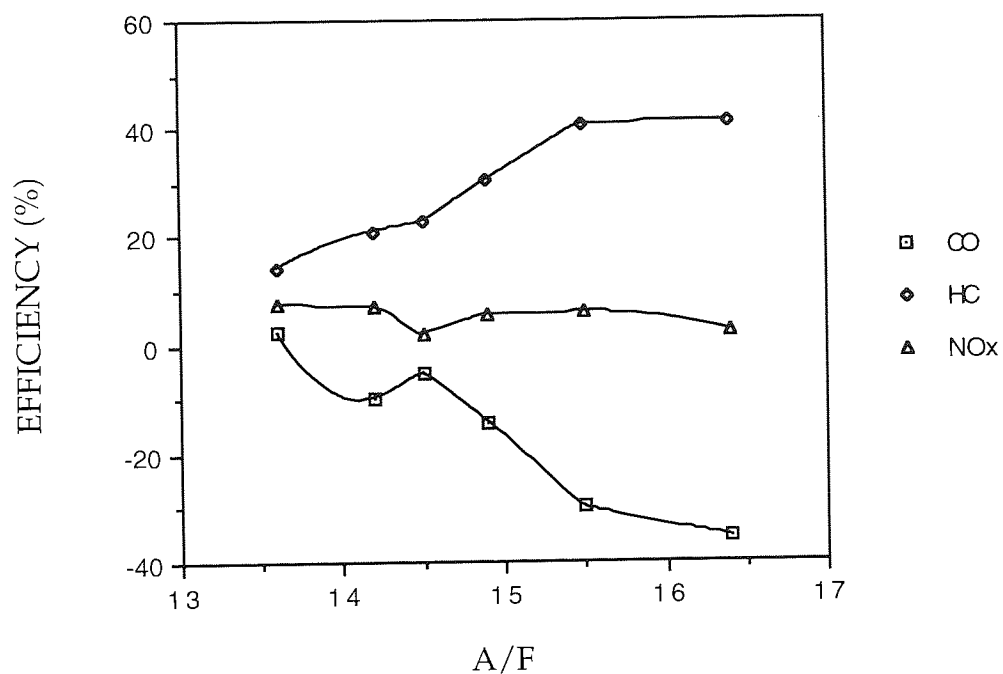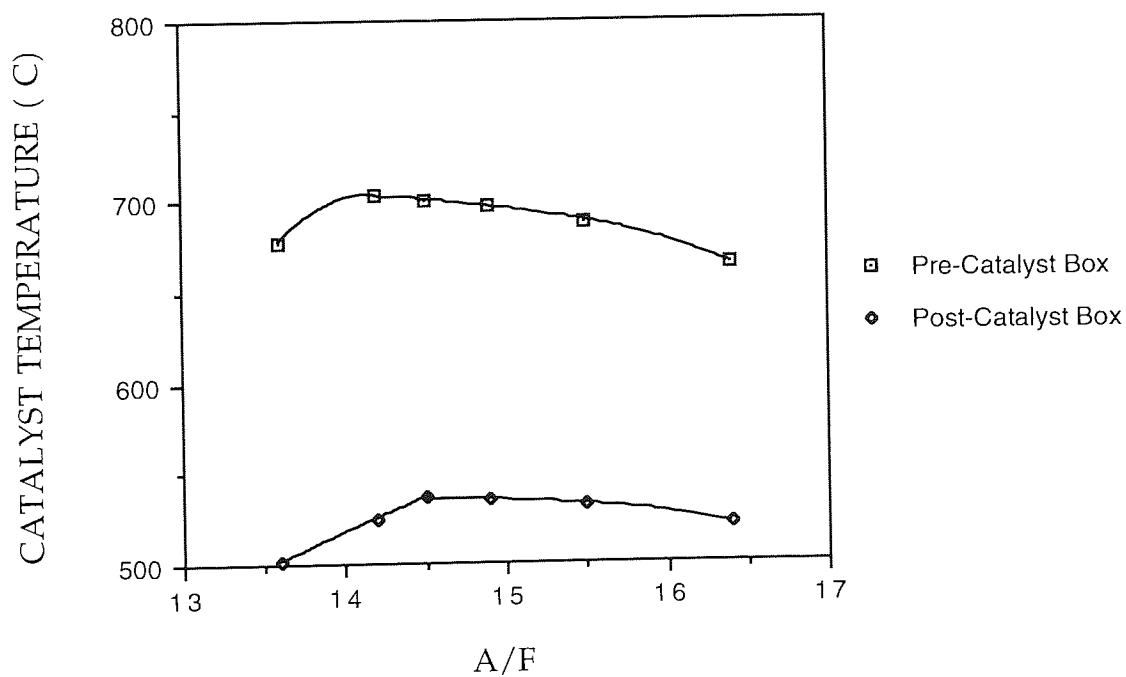
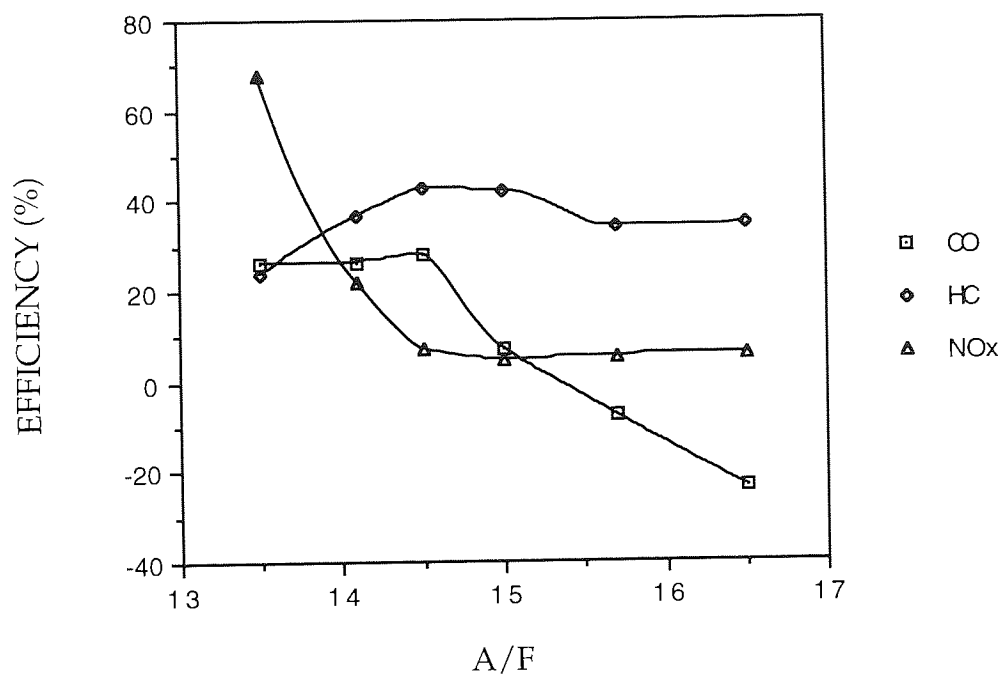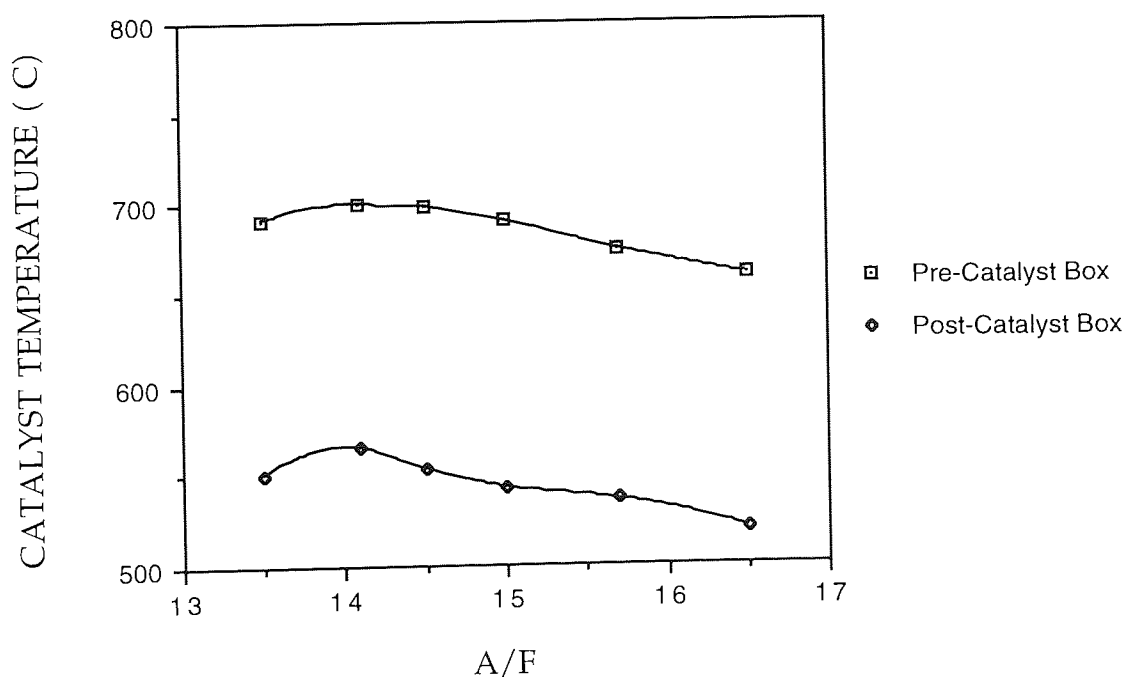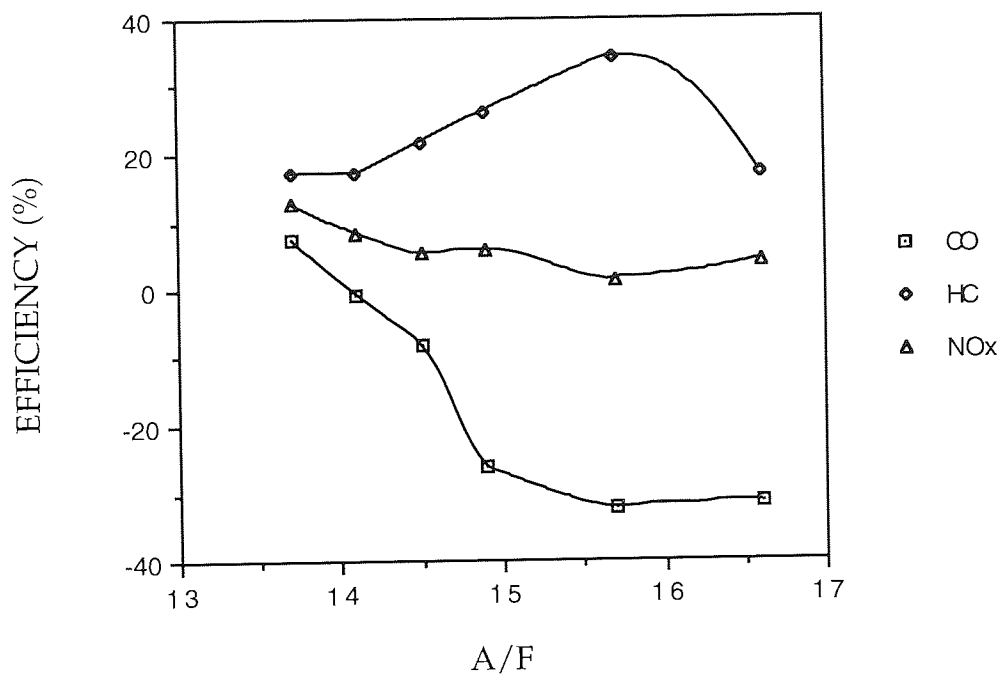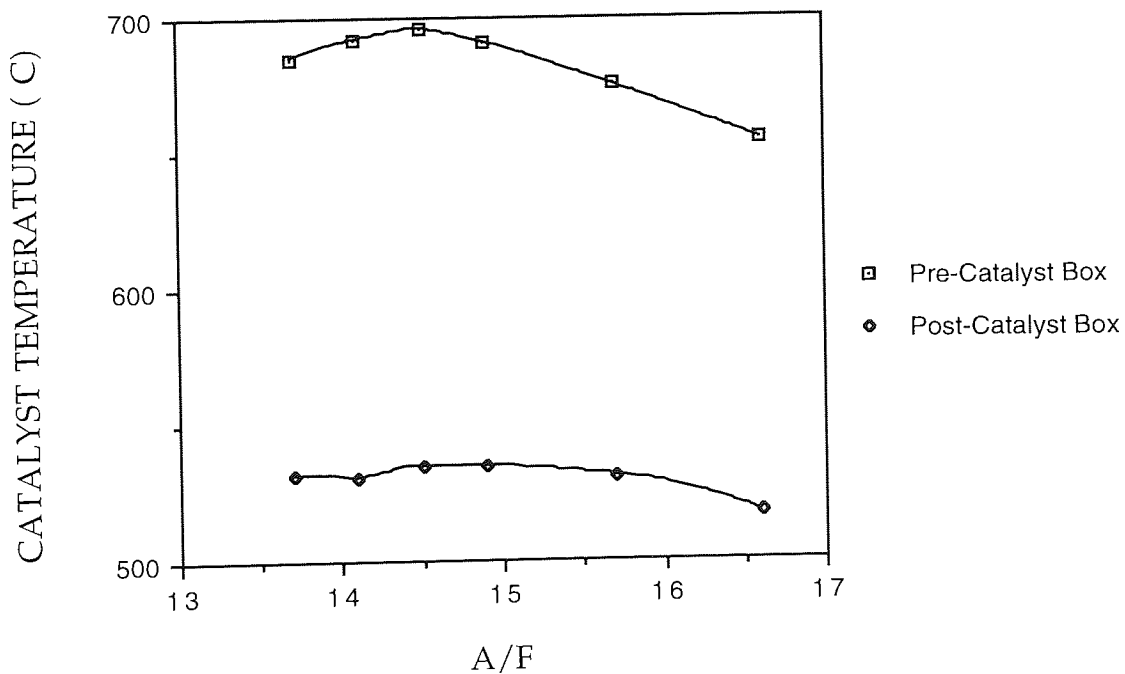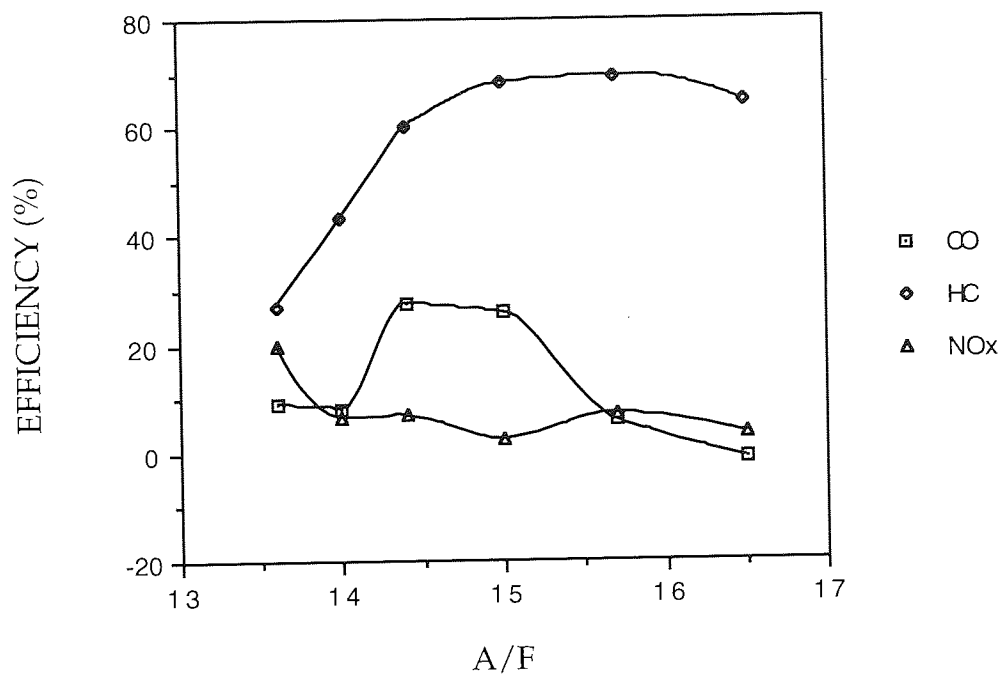Figure 6.5a Catalyst Efficiency versus Air/Fuel Ratio of the Cerium Oxide
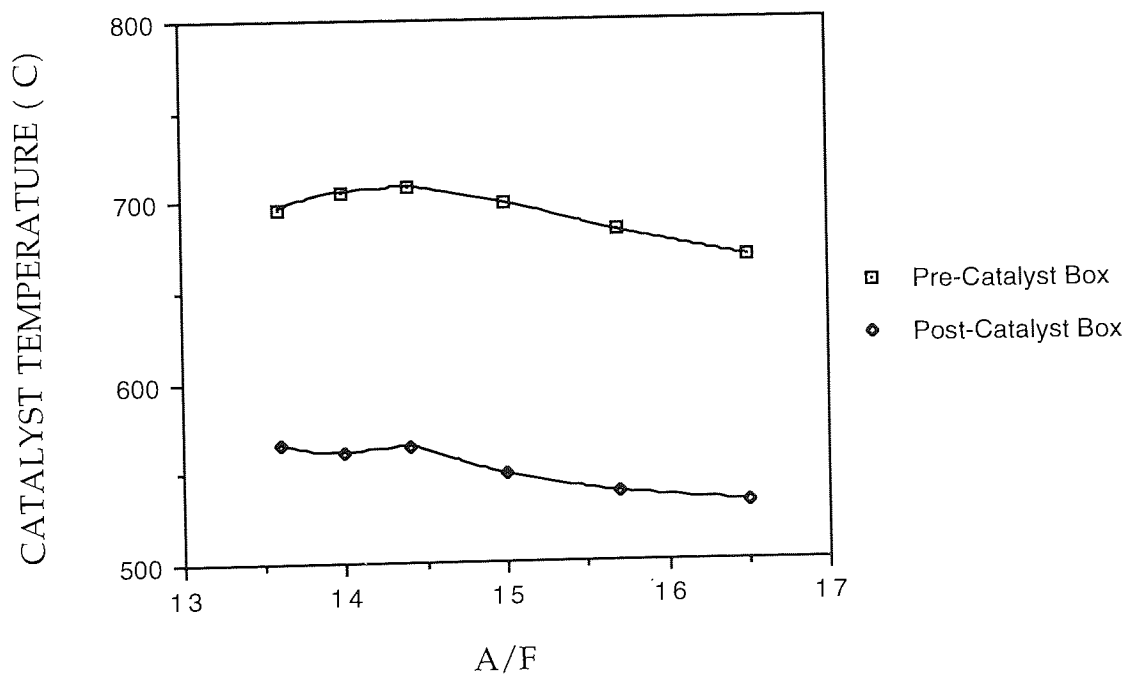
Treated Pellets

Figure 6.5b Catalyst Temperature versus Air/Fuel Ratio of the Cerium Oxide

Treated Pellets

6.3 AN INVESTIGATION OF THE EFFECT OF A CERIUM ADDITIVE UPON THE COMBUSTION OF GASOLINE FUEL AND CERIUM OXIDE TRAPPED FOR CATALYTIC CONVERTER USES

6.3.1 Introduction

Only cerium showed catalytic activity in both the combustion chamber and the exhaust box. Here investigations are described in which, cerium was tested for any catalysed reduction of the exhaust emissions from a vehicle. By making use of the cerium both inside the combustion chamber and in the exhaust system, a maximum reduction in exhaust emissions might be achieved. If this were to work, the system would be free of any additive poisoning problem, suffered by earlier investigations on metal oxide catalytic converter systems, and at the same time would be cheaper. The investigations now focus on reducing the noxious exhaust emissions, since previous tests had shown no significant improvement in fuel efficiency with cerium treated fuel.

For this investigation, the active cerium oxide must be distributed over a large surface area so that the mass-transfer characteristics between the gas phase and the active catalytic surface are sufficient to allow close to 100% conversion with high catalytic activity. One such system employs a ceramic honeycomb structure or monolith, and it is this system which was used here to trap and support the cerium oxide from the exhaust gases from the combustion chamber. The monoliths were held in a metal case in the exhaust stream to filter or impregnate the cerium oxide into a highly porous alumina washcoat that is applied to the passage walls. The trapped cerium oxide might then be used as a catalytic converter, to reduce the remaining harmful exhaust emissions before they are emitted into the atmosphere. Two attempts were made to test this hypothesis using a Rover M16i and a Renault F2N engines.

Fuels dosed with metal complexes have been tested in the recent years for their effect in lowering the ignition temperatures of exhaust particulates collected in the particulate traps of the diesel exhaust systems[16,141,142]. Recently, Sprague[16] and his colleagues described a method for generating a diesel engine particulate trap with a fuel containing an additive of the Pt-group metal coordination compound; Hill and co-workers[141] found that small amounts of Ti and Zr complexes dissolved in diesel fuel affects the ignition temperatures of exhaust particulates collected in the particulate trap, the metal additives do this by lowering the ignition temperatures of the exhaust particulates; Dorer and co-workers[142] show that Mn and Cu complexes also affect the afterburning of particulates emitted with exhaust gases. However, in this research the concentrations of CO and HC were examined rather than the particulate.

An SEM instrument was used to detect the presence of cerium in the samples collected from the catalytic metal casing and various parts of the exhaust system. The presence of cerium in these samples would mean that any reductions in exhaust emissions could have been caused by cerium oxide.

6.3.2 Renault F2N Test Programme

6.3.2.1 Experimental

Once again, the Ce(DPM)$_3$ complex was chosen as the additive for the gasoline fuel test, due to its high solubility in commercial fuels, without the use of an oxygenated solvent. This complex is the only one that showed any additive potential in the diesel engine tests. In this programme the additive was tested using a Renault F2N spark-ignition engine in a test cell at E.R.A. Ltd. The engine was connected to and loaded by a Froude F18 hydraulic dynamometer and had the following specifications:

Engine Type	Rover M16i; 4 cylinders
Bore and Stroke	81 x 83.5 mm
Displacement	1721 cm^3
Compression Ratio	9.2:1

The engine operated at a speed of approximately 3000 rpm with a load of approximately 50 Nm to simulate road conditions of high speed cruising (e.g. 70 mph on the motorway). In this programme, baseline testing for gaseous emissions was conducted using unleaded gasoline fuel (BS 7070), and as before the fuel was then treated with various dosages of the Ce(DPM)$_3$ additive for the additive testing. Gaseous emissions were measured at an interval of 30 minutes for pre- and post-catalyst emissions. A catalytic converter system was fitted into the exhaust close to the engine, to increase catalytic efficiency by increasing the temperature of the working condition of the catalyst. The catalyst case contained two ceramic monoliths coated with an alumina layer, which were used to filter or impregnate the cerium catalyst as the exhaust gases flowed through them. The monoliths were protected from damage by an insulation layer before being sealed in a metal case. As with the Hydra test (Fig. 6.1), the catalytic converter system was fitted with a temperature control apparatus and it was also connected to a portable analyser (MEXA 201GE) for CO and HC measurements.

6.3.2.2 Results and Discussion

The exhaust emission results for the untreated fuel are shown in Table 6.1. The first set of measurements are slightly different from the rest as the engine has not been stabilised. As expected, the emission data show no significant difference for the CO and HC concentrations between the pre- and post-catalyst box , as the fuel used here was untreated.

Table 6.1 Exhaust Emissions Data of the Untreated Fuel (Baseline 1)

CO (%)		HC (ppm)		Temperature (°C)	
PRE-CAT	POST-CAT	PRE-CAT	POST-CAT	PRE-CAT	POST-CAT
5.8	5.5	380	450	520	513
4.6	4.6	300	300	556	538
4.6	4.6	300	295	561	538
4.6	4.6	315	310	561	537
4.5	4.4	300	290	562	538
4.5	4.4	300	295	564	539
4.5	4.4	315	295	563	539
4.5	4.4	310	295	564	539
4.6	4.6	300	290	561	538

Table 6.2 Exhaust Emissions Data of Ce(DPM)$_3$ at 100 ppm & 200 ppm Tests

CO (%)		HC (ppm)		Temperature (°C)	
PRE-CAT	POST-CAT	PRE-CAT	POST-CAT	PRE-CAT	POST-CAT
At 100 ppm					
5.5	5.5	550	550	521	507
5.5	5.5	550	550	524	511
5.5	5.4	550	550	525	512
4.7	4.6	400	380	550	540
4.3	4.3	250	240	551	538
4.3	4.3	255	240	552	538
4.3	4.3	250	240	552	538
4.3	4.3	250	240	553	538
At 200 ppm					
4.3	4.3	250	245	553	540
4.3	4.3	250	250	554	540

4.3	4.3	255	250	553	540
4.2	4.3	255	250	554	540
4.2	4.3	255	250	553	540
4.2	4.3	255	250	553	541
4.3	4.2	260	260	552	539
4.3	4.2	260	260	552	538

Ce(DPM)$_3$ at 100 ppm and 200 ppm

Table 6.2 shows the data for the tests where the fuel was treated with 100 ppm and 200 ppm of cerium additive respectively. It was decided that two additive tests should be performed before any baseline measurement was repeated. If cerium is deposited on the monolith in these tests, then subsequent baseline tests should show how much the catalyst affected the post-catalyst data when compared with pre-catalyst data. At 100 ppm, the engine stopped after three sets of reading as it ran out of fuel, hence the slightly different subsequent set of data. Therefore, the first three sets of data should be disregarded in this discussion. The engine was restarted and left to run for an hour with this treated fuel to obtain stability before further measurements were made. From this point, the cerium treated fuel appears to show a very small reduction in the CO and HC concentrations compared to those for the untreated fuel. The exhaust emission temperatures are also slightly lower than for the baseline. The data for the 100 ppm treated fuel suggest that the cerium additive has had a slight catalytic effect upon the combustion process. However, in the further tests at 200 ppm, the data for the treated fuel suggest that the additive has no significant catalytic effect on the combustion process.

The treated fuel data pre- and post-catalyst emissions show too small a difference at both dosages to be described as a catalytic effect. The reason for

these results could be that not enough cerium oxide was deposited on the monoliths' surfaces through these two tests, or that the monoliths used were unable to filter the cerium oxide in these conditions. The initial cause can be rectified through ageing, but the later cause would be harder to rectify, involving modifying the monolith structure to increase filtration. So, more additive tests were performed to increase catalyst deposition, as no catalytic effect had been observed for the above tests.

Table 6.3 Exhaust Emissions Data of Baseline 2 Test

CO (%)		HC (ppm)		Temperature ($^{\circ}$C)	
PRE-CAT	POST-CAT	PRE-CAT	POST-CAT	PRE-CAT	POST-CAT
5.4	5.3	320	310	532	513
5.4	5.3	315	290	533	513
5.2	5.0	320	290	534	515
5.2	5.0	315	295	532	512
5.1	5.0	270	260	532	511
5.1	5.0	410	400	530	511
5.2	5.1	425	410	529	510
5.2	5.1	420	395	531	510
5.2	5.1	420	395	531	510

Table 6.4 Exhaust Emissions Data of Ce(DPM)$_3$ at 50 ppm Test

CO (%)		HC (ppm)		Temperature ($^{\circ}$C)	
PRE-CAT	POST-CAT	PRE-CAT	POST-CAT	PRE-CAT	POST-CAT
4.8	4.8	410	390	533	512
5.0	5.0	400	390	533	513
5.1	5.0	400	390	532	513

HC analyser will not zero; engine warmed up before continued test					
4.6	4.4	250	250	522	505
4.4	4.2	230	180	521	504
4.4	4.3	230	180	526	511
4.6	4.3	250	180	526	510
4.7	4.4	250	180	525	509
4.6	4.3	250	180	526	510

Table 6.5 Exhaust Emissions Data of Baseline 3 Test

CO (%)		HC (ppm)		Temperature (^{o}C)	
PRE-CAT	POST-CAT	PRE-CAT	POST-CAT	PRE-CAT	POST-CAT
4.2	2.6	420	360	527	505
4.3	2.6	390	320	525	509
4.4	2.8	360	300	533	514
4.3	2.5	370	310	525	506
4.3	2.5	370	320	525	506
4.2	2.5	370	320	526	506
4.3	2.5	370	320	526	507
4.4	2.6	375	320	525	504

Baseline testing was repeated after the above additive tests to give some indication as to the reliability of the additive results, and the results are listed in Table 6.3. However, the pre-catalyst emission data for the baseline 2 (Table 6.3) test are not the same as those obtained for baseline 1 (Table 6.1). The data in Table 6.3 show a large deviation between interval measurements, which therefore make the data inconsistent and unreliable. Inconsistencies in the data could be due to analyser error. This was noticed in the subsequent

additive test (Table 6.4) where the hydrocarbon analyser would not return to zero. This raises some doubt over the results obtained for the previous tests. Additive testing was temporarily halted to allow the analyser to be repaired before the resumption of additive and catalytic converter testing.

Ce(DPM)$_3$ at 50 ppm

The investigation was resumed after the analyser had been repaired. At 50 ppm (Table 6.4), the data show no significant additive effect on the CO concentration compared to the data for the baselines 1 and 3 (Table 6.1 and Table 6.5 respectively), taken before and after the 50 ppm additive test. This is also the case for the data for the pre- and post-catalyst, which indicates that there is no catalytic effect on CO reduction in either the combustion chamber or the catalyst converter box. Reductions apparently occur for the pre-catalyst HC emission compared to the two baselines, but because of the variation of the baseline data there must be doubt over the validity of the results. The catalytic converter results for the HC emission show reductions ranging from a minimum of 22% to a maximum of 28%. If this is truly the case then the cerium catalyst has now become active, probably it has been deposited on the surfaces of the monoliths. This could also explain the observed reduction in the pre-catalyst HC emission, as it is most likely that some of the cerium catalyst has also been deposited on the surfaces of the exhaust system in front of the catalyst box. Therefore, the HC emissions were already being affected prior to entering the catalyst box. These reductions correspond to the smaller temperature drops observed between the pre- and post-catalyst emissions compared to the baselines. That is, oxidation reactions are taking place in which heat is released.

The baseline 3 results (Table 6.5) are now beginning to show some catalytic converter effect on both CO and HC concentrations. Table 6.5 shows that the

majority of the catalytic effect is for CO reduction rather than for HC. A maximum 40% reduction in CO concentration was observed, whereas the HC reduction only reached a maximum of 14%.

Once again, problems with the analyser were encountered in the subsequent tests and the programme was abandoned after them as the analyser was not repairable. As a result of this, all the data obtained in this Renault engine test programme are slightly suspect. These tests results are listed below.

The catalytic converter system was removed from the exhaust system after the emission tests to allow the presence of any cerium deposits to be determined. Photographs of this converter system can be seen in Figures 6.6 and 6.7.

Samples were taken from various part of the exhaust system including the catalytic converter. Cerium analyses were performed on a SEM instrument which was fully adapted for elemental analysis. The sample analyses indicate that traces of cerium metal had been deposited along the exhaust system and in the catalytic converter system. The full results of the analyses are listed in the appendix. Also, the analytical data show that other metals such as iron and aluminium were present in samples collected at the manifold outlet and down-pipe inlet, and that the cerium concentration decreases as one moves away from the engine, through the catalytic converter, to the tail pipe. If this test programme were to be repeated with another analyser, then any reductions in exhaust emissions could be attributed to the deposited cerium catalyst.

Table 6.6 Exhaust Emissions Data of Ce(DPM)$_3$ at 100 ppm Test

CO (%)		HC (ppm)		Temperature ($^{\circ}$C)	
PRE-CAT	POST-CAT	PRE-CAT	POST-CAT	PRE-CAT	POST-CAT
6.8	4.4	390	330	525	507
6.6	4.3	390	330	525	507
6.7	4.4	400	340	527	511
6.7	4.3	400	340	527	511
6.8	4.4	420	330	528	511
6.8	4.4	420	330	527	511
6.8	4.3	420	340	528	510
6.8	4.2	420	340	527	513

Table 6.7 Exhaust Emissions Data of baseline 4 Test

CO (%)		HC (ppm)		Temperature ($^{\circ}$C)	
PRE-CAT	POST-CAT	PRE-CAT	POST-CAT	PRE-CAT	POST-CAT
6.3	4.0	450	370	524	507
6.4	3.8	450	380	525	505
6.4	3.8	450	370	525	507
6.4	3.8	450	370	525	508
6.4	3.8	450	370	525	508
6.4	3.8	450	370	524	507
6.4	3.8	450	370	524	507
6.4	3.9	450	380	525	508

Table 6.8 Exhaust Emissions Data of Ce(DPM)$_3$ at 50 ppm

| CO (%) | | HC (ppm) | | Temperature ($^{\circ}$C) | |
PRE-CAT	POST-CAT	PRE-CAT	POST-CAT	PRE-CAT	POST-CAT
7.0	4.6	370	340	524	505
7.0	4.5	370	340	523	505
7.0	4.5	370	330	524	505
7.2	3.9	380	310	521	503
7.1	3.8	370	320	523	505
7.2	3.8	370	320	522	504
7.1	3.7	370	320	521	503
7.1	3.6	370	330	521	504

6.3.2.3 Conclusion

No unequivocal conclusion can be drawn from this Renault F2N programme testing for catalytic activity due to the faults which occurred with the analyser. As the test programme was not completed, the results are not totally reliable. However, legitimate conclusions can be drawn from the occurence of metal deposition, as cerium oxide was deposited on the monolith surfaces and also along the exhaust system. Since this test was abandoned, further tests are needed. As an aside, it may be noted that these experiments consumed considerable quantities of additive and proved to be very expensive, at least in university research terms.

Figure 6.6 Photograph of the catalytic converter system after the Ce(DPM)$_3$ additive tests (front view)
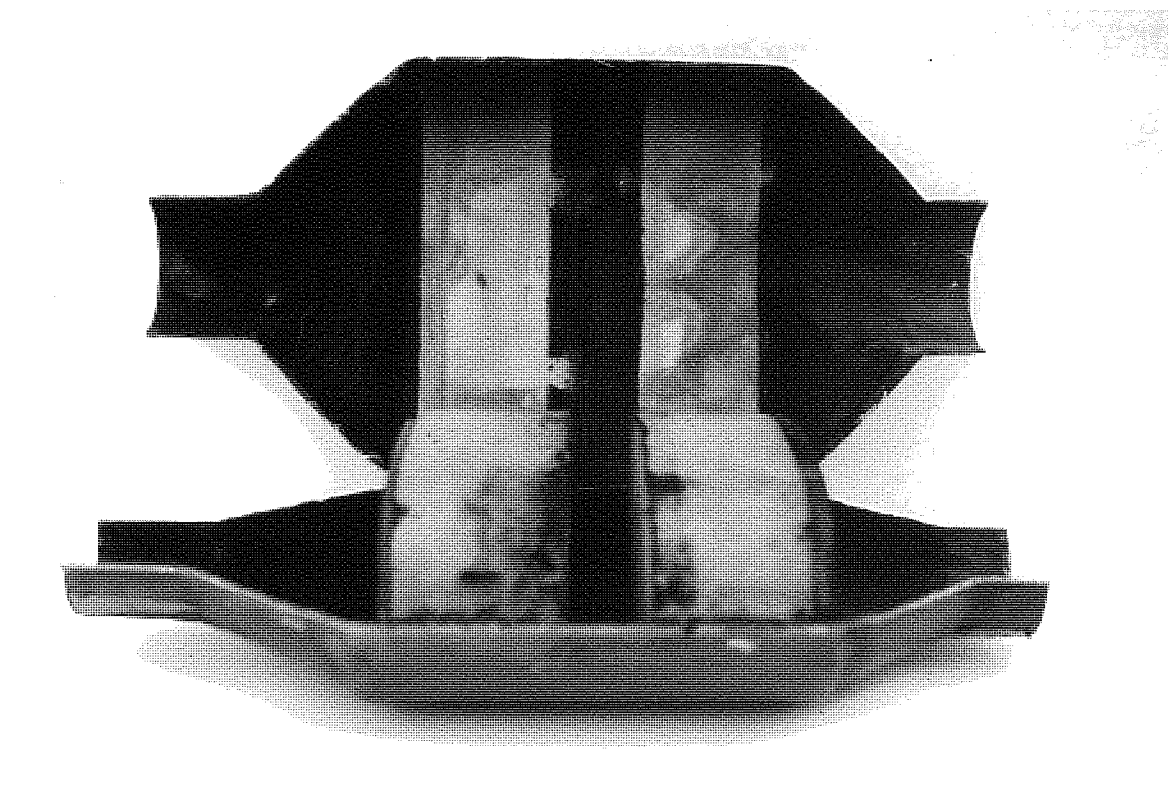

Figure 6.7 Photograph of the catalytic converter system after the Ce(DPM)$_3$ additive tests (side view)

6.3.3 Rover M16i Test Programme

The Renault F2N test programme could not be repeated through lack of access time to the engine, while there was no substitute analyser available. All the analysers were already in use by E.R.A. for customer tests. Therefore, the author had to wait for the next available time which my sponsor could provide to repeat the previous additive and catalytic converter testing. Eventually, a Rover engine became available to perform this test. The engine operating condition of this additive test was nevertheless limited for commercial reasons.

6.3.3.1 Experimental

Additive testing was performed with a Rover M16i spark-ignition, in which the engine was connected to and loaded by a Borchi and Saveri eddy current dynamometer. The engine had the following specifications:

Engine Type	Rover M16i; 4 cylinders
Bore and Stroke	84.45 x 89 mm
Displacement	1.994 litre
Compression Ratio	10:1
Air-Fuel/Ratio	14.7:1

To comply with a customer durability test, which was running in parallel with my experiments, the following engine conditions were used. The cerium additive test was operated at a part load condition, i.e. 90 Nm, at a stoichiometric fuel/air ratio, and the engine speed was kept at 5250 rpm. Because only one test could be done, it was decided to treat the BS 7070 fuel with a dosage of 100 ppm to guarantee some cerium deposition. The previous test procedure for the measurement of the exhaust emissions was repeated here, where the gaseous samples were measured at a 30 minute interval. The catalytic converter system was connected to an emissions bench consisting of;

Cussons 3000 - HC Analyser

Cussons 4000 - NOx Analyser

Cussons NDIR - CO_2 Analyser

Cussons NDIR - CO Analyser

Cussons Paramagnetic - O_2 Analyser

Sample Oven and Temperature Controllers

6.3.3.2 Results and Discussion

The results for the Rover M16i test are summarised in the following tables. Exhaust emission data for the untreated fuel are listed in Table 6.9 and the data show no significant difference between pre- and post-catalyst pollutant levels. This indicates that the alumina washcoat has had no catalytic effect upon the exhaust emissions at this engine operating condition, which can only benefit the data analysis of the cerium additive's effect.

Test data for the cerium treated fuel are listed in Table 6.10. The treated fuel data show no significant catalytic effect upon combustion for CO monoxide emission, as the CO emission data for the pre-catalyst are the same for both the untreated and treated fuels. For the treated fuel the average data for the pre-catalyst emissions show an increase in HC emission when compared with the untreated fuel. This indicates that the cerium additive has had no catalytic effect upon the combustion of gasoline fuel and further supports the CO emission results. The table also shows that the pre-catalyst HC emission concentration increases with time in the treated fuel. Therefore, the results suggest that the cerium additive has hindered the combustion process rather than improving it at this engine condition. This would agree with the earlier hypothesis that this kind of metal complex additives will only affect the diesel combustion process by reducing the ignition delay period. For improve combustion in spark ignition engines an additive must be able to lengthen the delay period.

Once again, the CO and HC emissions data show no significant differences between pre- and post-catalyst for the treated fuel, which can only mean that the cerium oxide either has no catalytic potential in this application or that there was insufficient catalyst deposition. The catalytic converter system was removed from the exhaust system and opened up for analysis. From visual observation, the catalytic converter metal casing appears to be fairly clean with hardly any deposits, such as soot, which were clearly evident in the Renault test. Microanalyses performed on the SEM shows that cerium is present in the catalytic converter system along with other metals. The print-out of these microanalyses can be seen in the appendix.

Table 6.9 Exhaust Emissions Data of Untreated BS 7070 Fuel

	PRE-CAT EMISSIONS			POST-CAT EMISSIONS		
Test Hours	CO (%)	CO_2 (%)	HC (ppm)	CO (%)	CO_2 (%)	HC (ppm)
0.5	0.9	14.5	620	0.8	14.5	620
1	0.9	14.5	610	0.8	14.6	610
1.5	0.7	14.5	610	0.7	14.6	610
2	0.75	14.5	610	0.75	14.5	600
2.5	0.75	14.6	580	0.75	14.6	590
3	0.8	14.5	620	0.85	14.5	640
3.5	0.85	14.4	610	0.75	14.5	620
4	0.85	14.5	600	0.8	14.5	590
AVG	0.81	14.5	610	0.78	14.5	610

Table 6.10 Exhaust Emissions Data of Ce(DPM)$_3$ Treated Fuel at 100 ppm

	PRE-CAT EMISSIONS			POST-CAT EMISSIONS		
Test Hours	CO (%)	CO_2 (%)	HC (ppm)	CO (%)	CO_2 (%)	HC (ppm)
0.5	0.8	14.4	580	0.8	14.4	580
1	0.8	14.5	580	0.8	14.5	580
1.5	0.8	14.4	590	0.8	14.4	600
2	0.8	14.4	580	0.8	14.6	580
2.5	0.8	14.5	580	0.8	14.6	580
3	0.8	14.5	590	0.8	14.6	590
3.5	0.8	14.6	590	0.8	14.6	600

4	0.8	14.6	590	0.8	14.6	590
4.5	0.8	14.6	590	0.8	14.7	590
5	0.8	14.5	590	0.8	14.6	590
5.5	0.8	14.5	590	0.8	14.6	590
6	0.8	14.2	690	0.9	14.3	650
6.5	0.8	14.3	670	0.75	14.4	650
7						
7.5	0.85	14.4	670	0.75	14.4	650
8	0.8	14.3	670	0.75	14.4	650
8.5	0.85	14.4	670	0.75	14.4	650
9	0.8	14.3	670	0.75	14.4	650
9.5	0.8	14.3	670	0.75	14.4	650
10						
10.5	0.78	14.4	670	0.75	14.4	680
11	0.8	14.5	690	0.85	14.5	690
11.5	0.8	14.4	685	0.8	14.4	680
12	0.8	14.5	700	0.75	14.5	690
12.5	0.8	14.5	690	0.8	14.4	690
13	0.8	14.5	720	0.8	14.5	720
13.5	0.75	14.5	690	0.75	14.5	690
14	0.8	14.5	700	0.8	14.5	690
14.5	0.78	14.5	720	0.74	14.5	725
15	0.8	14.5	700	0.85	14.5	695
15.5	0.75	14.6	720	0.74	15.6	730
16	0.75	14.4	710	0.74	14.5	720
16.5	0.74	14.5	740	0.74	14.6	750
17	0.75	14.5	730	0.75	14.5	740
17.5	0.7	14.2	850	0.7	14.4	830
18	0.7	14.2	820	0.75	14.2	830
18.5	0.75	14.3	900	0.7	14.3	890
19	0.75	14.4	870	0.7	14.4	830
19.5	0.75	14.2	860	0.75	14.3	830
20	0.8	14.3	890	0.8	14.3	900
20.5	0.75	14.4	850	0.75	14.4	850
21	0.8	14.4	810	0.8	14.4	810
21.5	0.85	14.4	810	0.75	14.4	810
22						
22.5	0.85	14.4	840	0.85	14.4	820
23	0.85	14.4	830	0.85	14.4	840
23.5						
24						
24.5	0.85	14.4	840	0.85	14.4	840
25	0.85	14.4	860	0.85	14.4	860
AVG	0.79	14.4	710	0.78	14.5	710

6.3.3.3 Conclusions

The conclusions drawn from this Rover test programme, based solely on this one set of data, are that the $Ce(DPM)_3$ additive had no effect upon the combustion of gasoline fuel, as hypothesised, and the cerium oxide deposited on the catalytic converter system showed no catalytic activity under these engine conditions over the period of the single test. Microanalysis shows that cerium oxide was deposited in the catalytic converter system, but the quantity remained uncertain.

These results are very disappointing since the previous individual test had shown catalytic potential for cerium in catalytic converter, but the catalytic activity for the additive in gasoline fuel is behaving as expected with no effect on combustion. Perhaps conclusions should not be drawn so soon for this type of investigation, after just one set of results. Further testing was not possible for the author as the company was unable to provide time for it. Therefore, the original question raised in this investigation remains unanswered.

6.4 CONCLUDING REMARKS

A number of conclusions may be drawn from these tests:

◆ The data suggest that $Ce(DPM)_3$ additive shows no catalytic activity upon the combustion of gasoline fuel in a spark ignition engine, which shows the hypothesis is correct for saying that these metal additives will only work in compression ignition engines.

◆ The catalytic converter tests performed with the use of an exhaust box where the γ-alumina pellets were coated with metal oxide prior to being fitted into the exhaust system show that cerium oxide has the highest catalytic conversion efficiency for both HC and CO emissions.

Catalytic activity was affected by the air/fuel ratio, i.e. cerium catalyst demonstrates maximum reduction between 14:1 to 17:1.

-260-

◆ However, the catalytic deposition test shows no catalytic activity with cerium oxide. This might suggest that not enough cerium oxide was deposited on both monolith surfaces to be fully effective for the conversion of the exhaust emissions.

Chapter 7

Conclusions and Suggestions for Future Work

7.1 SUMMARY OF THE THESIS

The aim of the work described in this thesis has been to synthesise metal complexes with multi-dentate ligands and study their effect upon the combustion of fuels, especially diesel fuel. Also included in this thesis are accounts of investigations of the lanthanide metal oxides and their potential use as catalytic converters. Following the catalytic converter tests, fuel dosed with a cerium additive was tested for catalytic activity, both as an additive and also as a catalytic converter, using a spark-ignition engine. In these experiments a ceramic monolith was used to maximise the area for the deposition of cerium oxide, the cerium-containing product of combustion.

Metal complexes with multi-dentate ligands, such as the derivatives of acetylacetone and the Schiff base ligands, were successfully synthesised for testing. An initial problem encountered with some of the metal complexes was their inability to dissolve directly in the commercial fuels. The problem was solved by attaching extra hydrocarbon substituents to the ligands. The results show that the metal complexes with aliphatic substituents were more soluble in a hydrocarbon environment than the metal complexes with aromatic substituents. Aliphatic substituents have a greater influence over the ability of the metal complex to dissolve in non-polar solvents than do aromatic substituents. Therefore, any future syntheses of hydrocarbon-soluble metal complexes should contain a high number of aliphatic groups, such as the tertiary butyl group.

All attempts to synthesise hydrocarbon-soluble cerium complexes with polyamine macrocyclic ligands resulted in failure. As most of the research time assigned for the synthesis of the macrocyclic ligand complexes was spent in familiarization with the cyclisation methods, not enough time remained to be used profitably on the metal complex synthesis.

Thermal analyses were conducted on those metal complexes used as additives, to study their thermal stability. This is an important property since one would not want the metal complex to decompose in the fuel system prior to its entering the combustion chamber. Also in diesel engines, the fuel is pre-heated immediately before combustion. All analyses showed that the metal complexes used here are thermally stable up to 170°C. Metal complexes with a substituted ligand show a slower decomposition rate, certainly as solids, than do those with the non-substituted ligand. However, all metal complexes start decomposing at approximately the same temperature. This clearly suggests that the rate of the decomposition is related to the number and type of substituent groups.

Initially, the metal additives were studied for their catalytic effect upon the combustion of diesel fuel with the aid of a diesel combustion bomb. The use of the combustion bomb was decided upon to reduce the cost, and to provide stable and repeatable start-of-test conditions, and so maximise the chances of obtaining reproducible data. This was found to be valid for the cost and for the start-of-test conditions, but the results did not show good reproducibility. This can be attributed to the relatively small number of experiments performed for each test condition. It is difficult to obtain reliable data from a set of only five experiments performed for each condition. But that low number is dictated by the time-consuming data-processing step, and the limited access time to the bomb. Despite that, deductions can be made from the data of these tests. The data show that in general the additives have little catalytic effect, although there may be some minor differences between doped and reference fuels. These differences that do occur are mainly found at the bomb temperature of 500°C, but not at 600°C This may indicate a connection between catalyst activity and temperature. The data also indicate that the metal additives are more effective as catalysts at low dosage levels.

The investigations show some potential for cerium and platinum complex additives, and also that the diesel combustion bomb with better data collection could be useful in this kind of investigation. This is encouraging as the focus of this project centred on cerium metal additives. Finally, the bomb investigations have shown that the catalyst mechanism is a gas phase action in the bulk of the fuel-air charge, where the catalyst reduces the ignition delay period, and acts as an ignition improver.

Next, additive tests were conducted on a single cylinder diesel engine in a laboratory test bed at Aston to give some indication of the effect that metal additives have upon combustion efficiency and exhaust emissions. A number of conclusions may be drawn from the results of this test programme and they are the following:

1. The catalytic activity of the metal additive varies from one additive to another Of all the additives tested, only $Ce(DPM)_3$ and $La(DPM)_3$ showed any effect, which suggests that the ligand of the complex is important to the catalytic activity. Other complexes containing the same metal, cerium, were inactive.

2. This led to the suggestion that the catalytic activity is connected to the additive's rate of decomposition. The results show that the $Ce(DPM)_3$ additive had the fastest rate of decomposition of the complexes studied, and showed a more pronounced catalytic effect than the other additives. Perhaps the size or mass of the ligand is the key property.

3. The concentration of the additive and the engine load were also found to influence catalytic activity in this test programme. The activity for the improvement of fuel efficiency is more pronounced at low dosages and loads,

and then deteriorates with increasing dosages and loads. Catalytic activity for the reduction of exhaust emissions is more pronounced with increasing loads, and also at low dosages. With hindsight, some of the negative results may be due to over-dosing.

4. In general, the additive results appear to show no correlation between the maximisation of combustion efficiency and the minimisation of noxious exhaust emissions, as might have been expected; but only show catalytic activity for the reduction of the emissions. When catalytic activity occured it did so via a gas-phase mechanism, because increasing the level of additive dosages produces an immediate change in catalytic effect. This would not be observed for a heterogeneous deposition mechanism, for which a catalyst build-up on the combustion chamber surface would be necessary.

Finally, the most promising catalyst, $Ce(DPM)_3$, was tested on a vehicle engine to give a full indication of its catalyst potential. A diesel pick-up truck was used for this investigation, in which the exhaust emissions were fully tested with a standard ECE 15/04 drive cycle. The results show improvements for HC and CO emission concentrations, with a maxi-mum reduction of 22% for HC emissions compared to the untreated fuel. Again the results showed no improvement in fuel efficiency, a finding consistent with the data obtained in the previous tests.

Of the catalytic converter tests, cerium again gave the highest catalytic activity amongst the lanthanide metals. Cerium oxide coated alumina pellets show a catalytic conversion efficiency reaching a maximum of 70% at 15.7 A/F ratio for HC emission and 25% for CO emission. From this result, cerium certainly has some potential as a catalyst for the reduction of HC and CO emissions.

The Ce(DPM)$_3$ additive was also used to investigate the possibility that a metal complex might have an effect upon the combustion of gasoline fuel and the results show, as expected, no effect upon the combustion process. At the same time, two ceramic monoliths were fitted into a catalytic converter system and placed in the exhaust system, with the intention of trapping the cerium oxide, formed from the additive, by surface deposition for the purpose of catalytic converter testing. With the aid of a SEM, adapted for microanalytical purposes, traces of the presence of cerium oxide were found in samples taken from the catalytic converter system. Although the test data showed these traces of cerium oxide in the catalytic converter, there was no significant catalytic effect. However, it must be said that this deduction is based solely on one short investigation, which may not have run for enough time.

7.2 CONCLUSIONS

Overall, the results do not coincide with our early hypothesis that metal complexes with multi-dentate ligands might act as potential pro-oxidant additives. We expected metal complexes with a higher denticity to show more pronounced catalytic effects, but instead the opposite occured. The difference in activity between the additives with the same core metal ion is attributed to differences in their ligands and thermal stability. The different coordinations of a metal ion to various organic ligands show the significance of the organic portion of the additive in improving combustion processes of diesel fuel. This might suggest that the metal ion plays no part in the catalyst mechanism, in contrast to my suggestion in Chapter 1, that catalytic effects would probably occur through the ability of a metal ion to transfer an electron between its two oxidation states. It is most likely that any activity exhibited by these metal additives occurs through decomposition from the complexes. This supports the Ce(DPM)$_3$ results for showing the highest catalytic effect as

it has the lowest decomposition temperatures, while the least catalytic effect is found with additives having the highest decomposition temperatures. Therefore, the effectiveness of these additives can be interpreted in terms of the number of radicals produced during decomposition. Perhaps this explains why in the large numbers of paper published in recent years on ignition improvers, most additives are organic rather than coordination compounds. Also, any observed reduction in exhaust emissions was expected to be related to combustion efficiency, i.e. increasing combustion efficiency would lead to a drop in exhaust emissions. However, the research shows that the only plausible catalyst mechanism for combustion efficiency found here is in the gas phase, while the reduction of exhaust emissions is effected by the metal oxide either in the gaseous phase or as a deposit on the engine's combustion chamber. There were small signs that this was operating in the diesel combustion bomb tests, but there are large standard deviations in the results. More data are needed.

A major problem suffered by this investigator was that most of the experimental work on additive testing was performed outside Aston, and access time for these experiments was severly restricted by commercial considerations. This is to be expected as the company needs customers to be profitable, and since it is only a small company it was not always able to accommodate research immediately.

7.3 SUGGESTIONS FOR FUTURE WORK

All the engine testing for additive potential described in this thesis has been limited to a small number of tests. Extensive and expensive engine testing is needed before any catalytic effects can be firmly demonstrated Therefore, future work should focus first upon more extensive testing of the compounds described here.

Also, it would be worth investigating the simultaneous effects that the Ce(DPM)$_3$ additive plus the cerium oxide catalytic converter might have on the reduction of exhaust emissions in a diesel engine, since the cerium catalytic converter test performed on the spark-ignition engine showed a considerable reduction in HC and CO emissions. The fact that this cerium additive already showed a catalytic effect upon the exhaust emissions prior to entering the catalytic converter system can only be a bonus.

Any further synthesis should be focused on the synthesis of a low decomposition temperatures complex.

Finally, if any additive is successful, a thorough safety and hazard analysis must be completed before it could be accepted for commercial use. Testing should start with the additive itself and then the exhaust emissions.

References

[1]   Haagen-Smit, A. J., Chemistry and physiology of Los Angeles smog, *Industrial & Engineering Chemistry*, **44**, 1342-1346, (1952).

[2]   Haagen-Smit, A. J., & Fox, M. M., Ozone formation in photochemical oxidation of organic substances, *Industrial & Engineering Chemistry*, **48**, 1484-1487, (1956).

[3]   Haagen-Smit, A. J., & Fox, M. M., Automobile exhaust and ozone formation, Vehicle Emissions, Society of Automotive Engineers, Inc., New York, pp. 1-6, (1964).

[4]   "Pollution blamed for thick fog in Madrid",*The Times*, 9th January, pp. 4, (1981).

[5]   "Angry Athens is under a cloud",*The Times*, 22nd April, pp. 1, (1981).

[6]   Rogers, L. H., Report on photochemical smog,*J. Chem. Educ.*, **35**, 310-313, (1938).

[7]   Harrison, B., Cooper, B. J. & Wilkins, A. J. J., Control of nitrogen oxide emissions from automobile engines, *Plat. Metals Rev.*, **25**, (1), 14-21, (1981).

[8]   Acres, G. J. K. & Cooper, B. J., Automobile emission control systems-Platinum catalysts for exhaust purification, *Plat. Metals Rev.*, **16**, (3), 74-86, (1972).

[9]   Diwell, A. F., & Harrison, B., Car exhaust catalysts for Europe- The development of lead tolerant platinum catalyst systems for emission control, *Plat. Metals Rev.*, **25**, (4), 142-151, (1981).

[10]   Sexton, M.D., Smith, A.K., & Martella, D.J, Fuel oil compositions, International Patent WO 9308244, (1993).

[11]   Gonzalez, F., Catalytic clean combustion promoter compositions for liquid fuels used in internal combustion engines, U.S. Patent 920825, (1992).

[12]   Hart, R.J., Ibrahim, T., & Jackson, G., Polymeric additives, International Patent WO 9215623, (1992).

[13] Tachibana, T., Hirata, K., Nishida, H., & Osada, H., Effect of ozone on combustion of compression ignition engines, *Combustion Flame*, **85**, (3-4), 515-519, (1991).

[14] Khinkova, M.K., Synthesis and action of ecological additives for diesel fuel, *Oxid. Commun.*, **14**, (1-2), 43-47, (1991).

[15] Buxton, J.P., Fuel compositions containing peresters, U.K. Patent 900808, (1990).

[16] Peter-Hoblyn, J.D., Valentine, J.M., Epperly, W.R., Sprague, B.N., & Kelso, D.T., Method for reducing particulate emissions from a diesel engine with organometallic platinum-group metal coordination composition, International Patent WO 9312207, (1993).

[17] Peter-Hoblyn, J.D., Valentine, J.M., Epperly, W.R., Sprague, B.N., & Kelso, D.T., Method for reducing pollution emissions from a diesel engine with organometallic platinum-group metal coordination composition, International Patent WO 9312206, (1993).

[18] Zeller, H.W., & Westphal, T.E., Effectiveness of iron-based fuel additives for soot control, Bur. Mines Rep. Invest., RI 9438, 32 pp., (1192).

[19] Wallace, G.M., Diesel fuels and fuel oils containing manganese carbonyl compound combustion improvers, overbased alkaline earth detergents, and ashless dispersants, Eur. Patent EP 476196 A1 920325, (1992).

[20] Wallace, G.M., Diesel fuel and fuel oil compositions containing combustion improvers, overbased detergents, and metal deactivators, Eur. Patent EP476197 A1 920325, (1992).

[21] Epperly, W.R., & Sprague, B.N., Method for catalyzing fuel for powering internal combustion engines, International Patent WO 9101361, (1991).

[22] Epperly, W.R., Sprague, B.N., Kelso, D.T., & Bowers, W.E., Method for reducing emissions from or increasing the utilizable energy of fuel for powering internal combustion engines, International Patent WO 9007561, (1990).

[23] Acres, G. J .K., Platinum catalysts for diesel engine exhaust purification, *Plat. Metals Rev.*, **14**, (3), 78-85, (1970).

[24] Heywood, J. B., Internal Combustion Engine Fundamentals, McGraw-Hill, New York, (1988).

[25] Zeldovich, Y. B., The oxidation of nitrogen in combustion explosions, *Acta Physicochimica U.R.S.S.*, **21**, (4),577-628, (1946).

[26] Newhall, H. K., & Shahed, S. M., Kinetics of nitric oxide formation in high-pressure flames, Proc. 13th Int. Symp. Combustion, The Combustion Institute, 381-390, (1971).

[27] Starkman, E. S., Steward, H. E. & Zvonow, V. A., Investigation into the formation and modification of exhaust emission precursors, SAE Paper 690020, (1969).

[28] Bennett, P. A., Jackson, M. W., Murphy, C. K. & Randall, R. A., Reduction of air pollution by control of emissions from automotive crankcases, Vehicle Emissions, Society of Automotive Engineers, Inc., New York, pp. 224-253, (1964).

[29] Nebel, G. J., Automotive exhaust gas treatment- An Industry Report, Vehicle Emissions, Society of Automotive Engineers, Inc., New York, pp. 269-273, (1964).

[30] Dietrich, H. H., Automotive exhaust hydrocarbon reduction during deceleration by induction system devices, Vehicle Emissions, Society of Automotive Engineers, Inc., New York, pp. 254-268, (1964).

[31] Hagen, D. F. & Holiday, G. W., The effect of engine operating and design variables on exhaust emissions, Vehicle Emissions, Society of Automotive Engineers, Inc., New York, pp. 206-223, (1964).

[32] Wentworth, J. T. & Daniel, W. A., Flame photographs of light load combustion point the way to reduction of hydrocarbons in exhaust gas, Vehicle Emissions, Society of Automotive Engineers, Inc., New York, pp. 121-136, (1964).

[33] Shinn, J. N. & Olson, D. R., Some factors affecting unburned hydrocarbons in combustion products, Vehicle Emissions, Society of Automotive Engineers, Inc., New York, pp. 137-145, (1964).

[34] Jackson, M. W., The influence of air-fuel ratio, spark timing and combustion chamber deposits on exhaust hydrocarbon emission, Vehicle Emissions, Society of Automotive Engineers, Inc., New York, pp. 175-191, (1964).

[35] Daniel, W. A. & Wentworth, J. T., Exhaust gas hydrocarbons- Genesis and Exodus, Vehicle Emissions, Society of Automotive Engineers, Inc., New York, pp. 192-205, (1964).

[36] Brownson, D. A. & Stebar, R. F., Factor influencing the effectiveness of air injection in reducing exhaust emissions, Vehicle Emissions- Part II, Society of Automotive Engineers, Inc., New York, pp. 103-120, (1967).

[37] Cantwell, E. N. & Pahnke, A. J., Design factors affecting the performance of exhaust manifold reactors, Vehicle Emissions- Part II, Society of Automotive Engineers, Inc., New York, pp. 121-145, (1967).

[38] Calpan, J. D., Smog Chemistry points the way to rational vehicle emission control, Vehicle Emissions- Part II, Society of Automotive Engineers, Inc., New York, pp. 20-31, (1967).

[39] Chandler, J. M., Struck, J. H. & Voorheis, W. J., The Ford approach to exhaust emission control, SAE Paper 660163, (1966).

[40] Beckman, E. W., Fagley, W. S., & J. O. Sarto, Exhaust emission control by Chryler- The cleaner air package, Vehicle Emissions- Part II, Society of Automotive Engineers, Inc., New York, pp. 178-191, (1967).

[41] Kopa, R. D., Control of automotive exhaust emission by modifications of the carburetion system, SAE Paper 660114, (1966).

[42] Tuttle, J. H. & Toepel, R. R., Increased burning rates offer improved fuel economy- NOx emissions trade-off in spark-ignition engines, SAE Paper 790388, (1979).

[43] Henein, N. A. & Bolt, J. A., The effect of some fuel and engine factors on diesel smoke, SAE Paper 690557, (1969).

[44] Marshall, W. F. & Hurn, R. W., Factor influencing diesel emissions, SAE Paper 680528, (1968).

[45] Barnes, G. J., Relation of lean combustion limits in diesel engines to exhaust odour intensity, SAE Paper 680445, (1968).

[46] Zelenka, P., Kriegler, W., Herzog, P. L. & Cartellieri, W. P., Way toward the clean heavy-duty diesel, SAE Paper 900602, (1990).

[47] Cooper, B. J. & Thoss, J. E., Role of NO in diesel particulate emission control, SAE Paper 890404, (1989).

[48] Hundleby, G. E., Low emission approaches for heavy-duty gas-powered urban vehicles, SAE Paper 892134, (1989).

[49] Gill, A. P., Design choices for 1990's low emission diesel engines, SAE Paper 880350, (1988).

[50] Yoshida, K., Makino, S, Sumiya, S, Muramatsu, G. & Helferich, R., Simultaneous reduction of NOx and particulate emissions from diesel engine exhaust, SAE Paper 892046, (1989).

[51] Chandler, J. M., Smith, A. M. & Struck, J. H., Development of the concept of non-flame exhaust gas reactors, Vehicle Emissions, Society of Automotive Engineers, Inc., New York, pp. 299-313, (1964).

[52] Searles, R. A., Car exhaust pollution control- lean burn engines and the continuing requirement for platinum-containing autocatalysts, *Plat. Metals Rev.*, **32**, (3), 123-129, (1988).

[53] Truex, T. J., Searles, R. A. & Sun, D. C., Catalyst for nitrogen oxides control under lean burn conditions- the opportunity for new technology to complement platinum group metal autocatalysts, *Plat. Metals Rev.*, **36**, (1), 2-11, (1992).

[54] Gumbleton, J. J., Bolston, R. A. & Lang, H. W., Optimizing engine parameters with exhaust gas recirculation, SAE Paper 740104, (1974).

[55] Fussell, D. R., Richard, G. P., & Wade, D., "Manifold reaction with exhaust recirculation for control of automotive emissions", Paper C130, Air Pollution In Transport Engines, Inst. Mech. Engnrs., London, (1971).

[56] Henault, C., "The influence of valve overlap on oxides of nitrogen exhaust emission", Paper C148, Air Pollution In Transport Engines, Inst. Mech. Engnrs., London, (1971).

[57] Walder, C. J., Reduction of emissions from diesel engines, SAE Paper 730214, (1973).

[58] Enga, B.E., Catalytic filters control diesel engine exhaust- Particulate emissions substantially reduced using platinum group metal catalysts, *Plat. Metals Rev.*, **26**, (2), 50-57, (1982).

[59] Sercombe, E. J., Exhaust purifers for compression ignition engines-Catalytic control of diesel exhaust gases, *Plat. Metals Rev.*, **19**, (1), 2-11, (1975).

[60] Wall, J. C., Shimpi, S. A. & Yu, M. L., Fuel sulphur reduction for control of diesel engine particulate emissions, SAE Paper 872189, (1987).

[61] Oser, P & Thoms, U., Particulate control systems for diesel engines using catalytically coated and uncoated traps with consideration of regeneration techniques, SAE Paper 830087, (1983).

[62] Enga, B. E., Buchmann, M. F., & Lichtenstein, I. E., Catalytic control of diesel particulate, SAE Paper 820184, (1982).

[63] Wade, W. R., White, J. E. & Florek, J. J., Diesel particulate trap regeneration techniques, SAE Paper 810118, (1981).

[64] Andrews, G. E., Iheozor-Ejiotor, I. E, & Pang, S. W., Diesel particulate SOF emission reduction using an exhaust catalyst, SAE Paper 870251, (1987).

[65] Ball, D. J., & Stack, R. G., Catalyst consideration for diesel converters, SAE Paper 902110, (1990).

[66] Cooper, B. J. & Roth, S. A., Flow-through catalysts for diesel engine emissions control, *Plat. Metals Rev.*, **35**, (4), 178-187, (1991).

[67] Brubacher, M. L., Reduction of diesel smoke in California, SAE Paper 660548, (1966).

[68] Golothan, D. W., Diesel engine exhaust smoke: The influence of fuel properties and the effects of using barium-conataining fuel additive, SAE Paper 670092, (1967).

[69] Miller, C. O., Diesel smoke suppression by fuel additive treatment, SAE Paper 670093, (1967).

[70] Hare, C. T., Springer, K. J. & Bradow, R. L., Fuel and additive effects on diesel particulate- development and demonstration of methodology, SAE Paper 760130, (1976).

[71] Truex, J. J., Pierson, W. R., McKee, D. E, Shelef, M & Baker, R. E, Effects of Barium fuel additive and fuel sulfur level on diesel particulate emissions, *Environment Science & Technology*, **14**, (9), 1121-1124, (1980).

[72] Glover, I. J., The fuel additive approached towards the alleviation of the nuisance of diesel smoke, *J. Inst. Petrol.*, **52**, (509), 137-160, (1966).

[73] Owen, K., Gasoline and Diesel Fuel Additives, Critical Reports on Applied Chemistry, Vol. 25, John Wiley & Sons, Chichester, (1989).

[74] Lyons, W. E. & McKone, L. J., Method of operating an internal combustion engine, U.S. Patent 2086775, (1937).

[75] Lyons, W. E. & McKone, L. J., Method of operating an internal combustion engine, U.S. Patent 2151432. (1939).

[76] Bower, W. E., Fuel additives and fuel containing soluble platinum group metal compounds and use in internal combustion engines, International Patent WO86/03492, (1986).

[77] Parshall, G. W., Homogeneous catalysis- The application and chemistry of catalysis by soluble transition metal complexes, Wiley-Interscience, London, (1986).

[78] Emanuel, N. M., Maizus, Z. K. & Skibida, I. P., The catalytic activity of transition metal compounds in the liquid-phase oxidation of hydrocarbons, *Angew. Chem. Int. Ed.*, **8**, 97-107, (1969).

[79] Hori, B., Kobayashi, H. & Takezawa, N, Oxidation of carbon monoxide with nitrous oxide over CeO_2, *React. Kinet. Catal. Lett.*, **33**, (2), 311-316, (1987).

[80] Bunzli, J. C. & Wessner, D., Complexes of the lighter lanthanoid nitrates with 15-crown-5 and 18-crown-6 ethers: Synthesis and Characterisation, *Hel. Chem. Acta*, **61**, 1454-1461, (1978).

[81] Adam, F. A., El-Haty, M. T. & Abdula, N. A, Coordination of Y(III), Ce(III), La(III) and Zr(IV) with some salicylidenearomatic Schiff bases, *J. Chinese Chem. Soc.*, **31**, 49-54, (1984).

[82] Radecka-Paryzek, W., The template synthesis and characterisation of hexaaza 18-membered macrocyclic complexes of Cerium(III), Praseodymium(III) and Neodymium(III) nitrates, *Inorg. Chim. Acta*, **109**, L21-L23, (1985).

[83] Morgan, G. T. & Drew, H. D. K, Researches on residual affinity and coordination. Part II. Acetylacetones of selenium and tellurium, *J. Chem. Soc.*, **17**, 1456-1465, (1920).

[84] Marchi, L. E., Metal derivatives of 1,3-diketones, *Inorganic Syntheses*, **2**, 10-17, (1946).

[85] Fernelius, W. C. & Bryant, B. E., Preparation of metal derivatives of 1,3-diketones, *Inorganic Syntheses*, **5**, 105-113, (1957).

[86] Uitert, L. V. & Fernelius, W. C., Studies on coordination compounds. VIII. Some factors concerning the effect of the terminal groups on the chelating abilities of β-diketones, *J. Chem. Soc.*, **75**, 3862-3864, (1953).

[87] Pinnavaia, T & Fay, R. C., Tetrakis(2,4-pentanedionato)cerium(IV) and tetrakis(1,1,1-trifluoro-2,4-pentanedionato)cerium(IV),*Inorganic syntheses*, **12**, 77-80, (1770).

[88] Adams, J. T. & Hauser, C. R., The acylation of methyl ketones with aliphatic esters by means of sodium amide- Synthesis of β-diketones of the type $RCOCH_2COR$, *J. Amer. Chem. Soc.*, **66**, 1220-1222,(1944).

[89] Hammond, D. C., Nonhebel, D. C. & Wu, C. S., Chelates of β-diketones. V. Preparation and properties of chelates containing sterically hindered ligands, *Inorg. Chem.*, **2**, 73-76, (1963).

[90] Kistner, C. R., Hutchinson, J. H., Doyle, J. R. & Storlie, J. R., Metal-Olefin Compounds. IV. The preparation and properties of some aryl and akyl platinum(II)-Olefin compounds, *Inorg. Chem.*, **2**, (6), 1255-1261, (1963).

[91] Clark, H. C. & Manzer, L. E., Reactions of (π-1,5-cyclooctadiene) organoplatinum(II) compounds and the synthesis of perfluoroalkyl-platinum complexes, *J. Organomet. Chem.*, **59**, 411-423, (1973).

[92] Liu, S. & Gelmini, L, Rettig, S. J., Thompson, R. C. & Orvig, C., Synthesis and characterisation of lanthanide [Ln(L)]$_2$ complexes of N_4O_3 amine phenol ligands with phenolate oxygen bridges: Evidences for very weak magnetic exchange between lanthanide ions, *J. Amer. Chem. Soc.*, **114**, 6081-6887, (1992).

[93[Norman, R. O. C., Principles of Organic Synthesis, Methuen & Co. Ltd., London, (1968).

[94] Penderson, C. J., Cyclic polyethers and their complexes with metal salts, *J. Amer. Chem. Soc.*, **89**, 7017-7036, (1967).

[95] Izatt, R. M., Bradshaw, J. S., Nielson, S. A., Lamb, J. D. & Christensen, J. J., Thermodynamic and kinetic data for cation-macrocycle interaction, *Chem. Rev.*, **85**, 271-339, (1985).

[96] Lindoy, L. F., The Chemistry of Macrocyclic Ligand Complexes, Cambridge University Press, Cambridge, (1989).

[97] Izatt, R. M. & Christensen, J. J., Synthesis of Macrocycles- The design of Selective Complexing Agents, Wiley-Interscience, New York, (1987).

[98] Curtis, N. F. & Reader, G. W., Some cyclic tetra-amines and their metal-ion complexes. Part VIII. Cobalt(III) complexes of 3,3-dimethyl-1,5,8,11-tetra-azacyclotridecane, *J Chem. Soc. Dalton Trans.*, 1453-1460, (1972).

[99] Chang, C. A. & Rowland, M. E., Metal complex formation with 1,10-diaza-4,7,13,16-tetraoxacyclooctadecane-N,N"-diacetic acid. An approach to potential lanthanide ion selective reagents, *Inorg. Chem.*, **22**, 3866-3869, (1983).

[100] Stetter, H. & Frank, W., Complex formation with tetraazacycloalkane-N,N',N",N'''-tetraacetic acids as a function of ring size, *Angew. Chem. Int. Ed. Engl.*, **15**, (11), 686-686, (1976).

[101] Takahashi, M. & Takamoto, S., The preparation of trivalent metal chelates with some N_3O_3-type ligands, *Bull. Chem. Soc. Jap.*, **50**, (12), 3413-3414, (1977).

[102] Haflinger, H. & Raden, T. A., Metal complexes of macrocyclic ligands. XII. A complexone-like tetraazamacrocycle, *Hel. Chim. Acta*, **62**, 683-688, (1979).

[103] Desreux, J. F., Nuclear magnetic resonance spectroscopy of lanthanide complexes with a tetraacetic tetraaza macrocycle. Unusual conformation properties, *Inorg. Chem.*, **19**, 1319-1324, (1980).

[104] Delgado, R. & Frausto Da Silva, J. J. R., Metal complexes of cyclic tetra-azatetra-acetic acids, *Talanta*, **29**, 815-822, (1982).

[105] Wieghart, K., Bossek, U., Chaudhuri, P., Herrmann, W., Menke, B. & Weiss, J., 1,4,7-triazacyclononane-N,N',N"-triacetate (TCTA), a hexadentate ligand for divalent and trivalent metal ions. Crystal structures of [Cr(III)(TCTA)], [Fe(III)(TCTA)] and Na[Cu(II)(TCTA)] .2NaBr.8H$_2$O, *Inorg. Chem.*, **21**, 4308-4313, (1982).

[106] Loncin, M. F., Desreux, J. F. & Merciny, E., Coordination of lanthanides by two polyamino polycarboxylic macrocycles: Formation of highly stable lanthanide complexes, *Inorg. Chem.*, **25**, 2646-2648, (1986).

[107] Cacheris, W. P., Nickle, S. K. & Sherry, A. D., Thermodynamic study of lanthanide complexes of 1,4,7-triazacyclononane-N.N',N''-triacetic acid and 1,4,7,10-tetraazacyclododecane-N,N',N'',N'''-tetraacetic acid, *Inorg. Chem.*, **26**, 958-960, (1987).

[108] Amorim, M. T. S., Delgado, R., Frausto Da Silva, J. J. R., Candida, M., Vaz, T. A. & vilhena, M. F., Metal complexes of 1-oxa-4,7,10-triazacyclododecane-N,N',N''-triacetic acid, *Talanta*, **35**, (9), 741-745, (1988).

[109] Helps, I. M., Parker, D., Morphy, J. R. & Chapman, J., General routes for synthesis of mono, di and tri-N-substituted derivatives of cyclam, *Tetrahedron*, **45**, (1), 219-226, (1989).

[110] Cortes, S, Brucher, E., Geraldes, C. F. & Sherry, A. D., Potentiometry and NMR studies of 1,5,9-triazacyclododecane-N,N',N''-triacetic acid and its metal ion complexes, *Inorg. Chem.*, **29**, 5-9, (1990).

[111] Spirlet, M. R., Rebizant, J., Loncin, M. F. & Desreux, J. F., Structural characterisation of a Terbium(III) complex with 1,4,8,11-tetraaza-cyclotetradecane-1,4,8,11-tetraacetic acid. Lanthanide ions and the conformation of the 14-membered macrocycles, *Inorg. Chem.*, **23**, 4278-4283, (1984).

[112] Greenwood, N. N. & Earnshaw, A., Chemistry of the Elements, Pergammon, New York, pp. 1434, (1984).

[113] Richman, J. E. & Atkin, T. J., Nirogen analogs of crown ethers, *J. Amer. Chem. Soc.*, **96**, 2268-2270, (1974).

[114] Koyama, H. & Yoshino, T., Synthese of some medium sized cyclic triamines and their Cobalt(III) complexes, *Bull. Chem. Soc. Jap.*, **45**, 481-484, (1972).

[115] Searle, G. H. & Gene, R. J., Improved Richman-Atkin syntheses of cyclic polyamines particularly 1,4,7-triazacyclononane and 1,4,7-triazacyclododecane, with the aid of cation-exchange in purification and isolation, *Aust. J. Chem.*, **37**, 959-970, (1984).

[116] Atkin, T. J., Richman, J. E. & Oettle, W. F., Macrocyclic polyamines: 1,4,7,10,13,16-hexaazacyclooctadecane, *Organic Syntheses*, **58**, 86-97, (1978).

[117] [Smothers, W. J. & Chang, Y., Handbook of Differential Thermal Analysis, Chemical Publishing Company, New York, (1966).

[118] Mackenzie, R. C., Differential Thermal Analysis, Vol. 1, Acadamic Press Inc. Ltd., London, (1970).

[119] Packer, J. P., Diesel Type Combustion Studies in High Swirl Chambers, PhD Thesis, University of Bath, (1983).

[120] Wolfer, H. H., Ignition Lag in the Diesel Engines, VDI-Forschungsheft, No. 392, (Sept. 1938).

[121] Griffiths, J.F., Pappin, A.J., Al-Rubaie, M.A.R., & Sheppard, C.G.W., Fundamental studies related to combustion in diesel engines, Proc. Inst. Mech. Eng., IMechE Conf., 1991-1991 (Inter. Comust. Engine Res. Univ., Polytech. Coll.) 151-158, (1991).

[122] Hansen, A.C., Taylor, A.B., Lyne, P.W.L., & Meiring, P., Heat release in the compression-ignition combustion of ethanol, Trans. ASAE, **32**, (5), 1507-1511, (1989).

[123] Clothier, P.Q.E, Moise, A, & Pritchard, H.O., Effect of free- radical release on diesel ignition delay under simulated cold-starting conditions, *Combustion Flame*, **81**, 242-250, (1990).

[124] Diesel, E., Goldbeck, G. & Schildberger, F., From Engines to Autos, Henry Regnery Co., Chicago, (1960).

[125] Judge, A. W., Modern Petrol Engines, 3rd Ed., Chapman & Hall Ltd, London, (1965).

[126] Van Derveer, R. T., & Chandler, J. M., The development of a catalytic converter for the oxidation of exhaust hydrocarbons, SAE Paper 295P, (1959).

[127] Gandhi, H. S., Piken, A. G., Shelef, M. & Delosh, R. G., Laboratory Evaluation of Three-way catalysts, SAE Paper 760201, (1976).

[128] Hegedus, L. L. & Gumbleton, J. J., Catalysts, computer, and cars: a growing symbiosis, CHEMTECH, October, 630-642, (1980).

[129] Cooper, B. J., Durability of Platinum-containing automotive exhaust control catalysts- improvements in resistance to thermal degradation, Plat. Metals Rev., 27, (4), 146-155, (1983).

[130] Church, M. L., Cooper, B. J. & Willson, P. J., Catalyst formations 1960 to present, SAE Paper 890815, (1989).

[131] Ihara, K., Murakami, H. & Ohkubo, K., Improvement of Three-way catalyst performance by optimizing Ceria impregnation, SAE Paper 902168, (1990).

[132] Taylor, K.C., Catalysts in cars, CHEMTECH, September, 551-555, (1990).

[133] Ducker, H., Friese, K-H. & Haecker, W-D., Ceramic aspects of the Bosch Lambda-Sensor, SAE Paper 750223, (1975).

[134] Oatley, C. W., The Scanning Electron Microscope- Part 1 The Instrument, Cambridge University Press, Cambridge, (1972).

[135] Thornton, P. R., Scanning Electron Microscopy, Chapman & Hall Ltd., London, (1968).

[136] Salter, W. J. M., A Manual of Quantitative Electron Probe Microanalysis, Structural Publications Ltd., London, (1970).

[137] Summer, J. C. & Ausen, S. A., Interaction of cerium oxide with noble metals, J. Catalysis, 58, 131-143, (1979).

[138] Yao, Y. , The oxidation of CO and hydrocarbons over noble metal catalysts, *J. Catalysis*, **87**, 152-162, (1984).

[139] Oh, S. H. & Eickel, C. C., The effects of cerium addition on oxidation kietics over alumina-supported catalysts, *J. Catalysis*, **112**, 543-555, (1988).

[140] Shibata-Yanagisawa, M., Kato, M., Seto, H., Ishizawa, N., Mizutani, N. & Kato, M., *J. Amer. Ceram. Soc.*, **70**, (7), 503-509, (1987).

[141] Hill, G.R., Di Biase, S.A, & Detar, M.B., Titanium and Zirconium complexes, and fuel composition, International Patent, WO 8802392, (1988).

[143] Dorer, C.J., & Tupa, R.C., Manganese and copper containing compositions, International Patent WO 8501513, (1985).

APPENDICES

APPENDIX 1

STATISTICAL ANALYSIS OF DATA

A1.1 Standard Deviation

$$s = \sqrt{\frac{\sum (x-\bar{x})^2}{n-1}}$$

s = standard deviation, x = measurement,
$\bar{x}$ = arithmatic mean, and n = number of measurements.

In this equation the denominator is (n-1) rather than n when the number of measurement is small.

A1.2 Confidence Level

When a small number of observations is made, the value of the standard deviation (s), does not by itself give a measure of how close the sample mean ($\bar{x}$) might be to the true mean. It is, however, possible to calculate a confidence level to estimate the range within which the true mean may be found. The limits of this confidence level, known as the confidence limits, are given by the expression:

Confidence limits of μ, for n replicate measurements,

$$\mu = \bar{x} + \frac{ts}{\sqrt{n}}$$

where *t* is a parameter that depends upon the number of degrees of freedom and the confidence level required.

A1.3 Student's t-test

This is a test used to compare the mean from a sample with some standard value and to express some level of confidence in the significance of the comparison. It is also used to test the difference between the means of two sets of data $\bar{x}_1$ and $\bar{x}_2$.

The value of t is obtained from the equation:

$$t = \frac{(\bar{x}-\mu)\sqrt{n}}{s}$$

where μ is the true value.

It is then related to a set of t-tables in which the probability of the t-value falling within certain limits is expressed as percentage relative to the number of degrees of freedom.

APPENDIX 2

ECE 15.04 EMISSION TESTING

A1.4 ECE 15.04 Type I Test

This is a specified drive cycle that represents a cold start with a 4 Km drive through city traffic and is simulated on a chassis dynamometer. The dynamometer absorption is adjusted to simulate the resistances encountered under actual road conditions and an inertial mass simulates the vehicle weight.

The Type I Test consists of 4 identical cycles, a cycle being a fixed programme of idles, acceleration, cruises and deceleration (see illustration). During the test the vehicle exhaust is collected for analysis.

The exhaust gas collected is diluted using purified ambient air and the diluted sample extracted by a blower via a venturi nozzle (critical flow venturi).

A portion of this diluted exhaust gas, having the same instantaneous composition is collected in a large sample bag.

At the same time, a partial flow of ambient air (background air) is collected in a second sample bag.

At the conclusion of the test, the concentration of the emitted gases in the first sample bag is exactly the same the mean concentration of the extracted exhaust/air mixture.

With the known delivery rate of the venturi system and density values, it is possible to calculate the masses of the substances emitted during the test.

The contents of the two sample bags are passed through the analyser bank to measure CO, CO_2, HC and NOx. This is done no longer than 30 minutes after the end of the test.

The content of CO and HC + NOx is then calculated to produce a figure of grammes per test and compared to the class test limit the pass/fail/retest result is dependent on the percentage ratio between limit and test totals, see below:

If the first test is equal to or less than 70% of the legislative exahaust pollutant limit, then the vehicle is passed on a one test basis.

If the first test is up to 85% of the limit, i.e. greater than 70%, then a second test is called for.

Providing the first and second test combined results are no more than 170% of limit, then a pass is issued.

If the combined results of test 1 and 2 are greater than 170% of limit, then a third test is required.

Providing all three tests are within the limit, or indeed the overall average is 1.1 of the limit, then the vehicle has passed.

Test setup

for ECE, Japan, Sweden, Switzerland, Australia, Mexico
1 Brake, 2 Flywheel, 3 Exhaust, 4 Air filter, 5 Dilution air, 6 Cooler, 7 Sample Venturi tube,
8 Gas temperature, 9 Pressure, 10 Venturi tube, 11 Fan, 12 Sample bag,
14 To outlet.
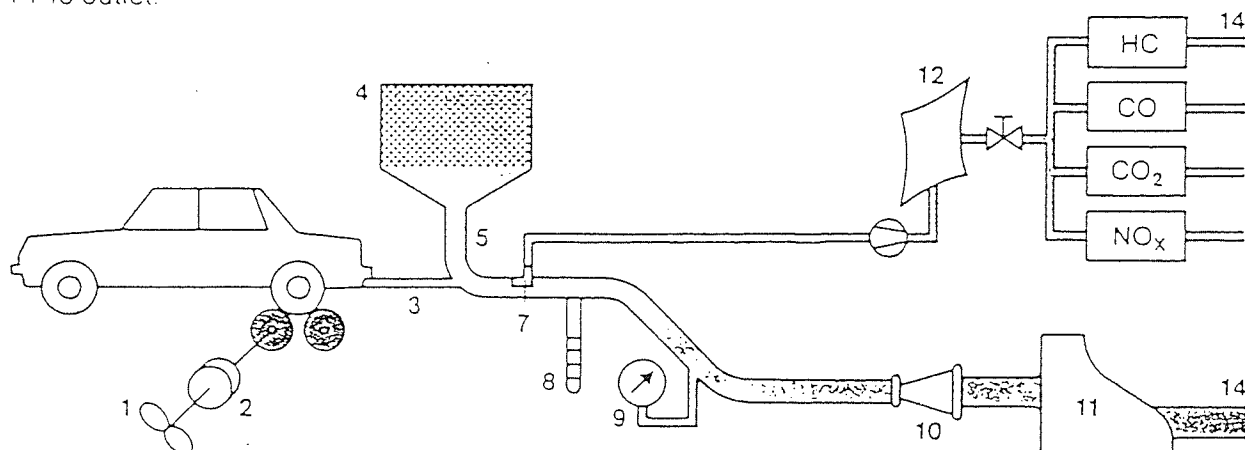
ECE/EEC driving cycle (ECE Test Type I).

Cycle length:	1.013 km	avg. speed:	18.7 km/h
Test distance:	4.052 km		(27.01 km/h*)
No. of cycles/test:	4	max. speed:	50 km/h
Cycle duration:	195 s	*without idle phases (idle percentage: 31%).	
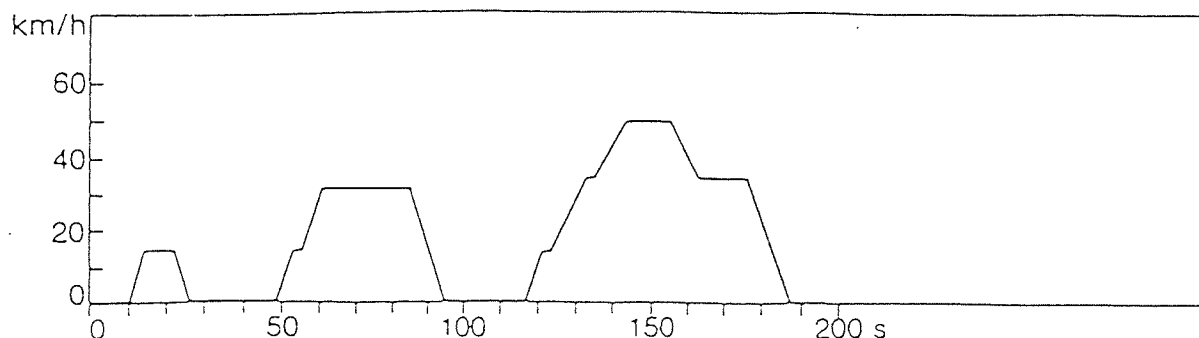
APPENDIX 3

DIESEL FUEL ADDITIVES TEST RESULTS

TANGYE VCP-1 TEST RESULTS

A1.5 Diesel (Baseline 1)

LOAD: 0lb

Fuel Flow (ml/s)	400	402	400	400	401	400	402	400	400	401	400
CO (%)	0.15	0.15	0.14	0.14	0.14	0.15	0.14	0.16	0.17	0.16	0.16
HC (ppm)	40	40	30	30	40	30	30	30	40	30	40
CO_2 (%)	2.22	2.23	2.25	2.25	2.25	2.25	2.24	2.23	2.21	2.21	2.20

LOAD: 15lb

Fuel Flow (ml/s)	261	259	260	260	260	260	260	260	260	260
CO (%)	0.14	0.14	0.13	0.13	0.14	0.14	0.16	0.13	0.14	0.13
HC (ppm)	40	40	40	40	40	40	40	40	40	40
CO_2 (%)	4.25	4.28	4.30	4.29	4.20	4.21	4.23	4.28	4.28	4.27

LOAD: 30lb

Fuel Flow (ml/s)	172	172	172	172	172	172	172	172	172	172
CO (%)	0.20	0.20	0.21	0.22	0.21	0.21	0.22	0.21	0.21	0.22
HC(ppm)	50	60	50	60	50	60	50	60	50	60
CO_2 (%)	7.04	7.04	7.07	7.00	7.07	7.03	7.02	7.02	7.03	7.03

A1.6 Ce(DPM)$_3$ at 25 ppm

LOAD: 0 lb

Fuel Flow (ml/s)	411	411	411	411	411	411	411	411	411	411
CO (%)	0.15	0.15	0.15	0.15	0.15	0.15	0.15	0.15	0.15	0.15
IIC (ppm)	40	50	40	50	40	50	40	50	40	50
CO$_2$ (%)	2.05	2.04	2.04	2.09	2.11	2.11	2.12	2.11	2.13	2.13

LOAD: 15 lb

Fuel Flow (ml/s)	267	267	267	267	267	267	267	267	267	267
CO (%)	0.11	0.11	0.11	0.11	0.11	0.11	0.11	0.11	0.11	0.11
IIC (ppm)	10	20	30	20	20	20	20	20	20	20
CO$_2$ (%)	3.95	3.92	3.95	3.96	3.95	3.95	3.97	4.02	4.01	4.00

LOAD: 30 lb

Fuel Flow (ml/s)	175	175	175	175	175	175	175	175	175	175
CO (%)	0.09	0.09	0.09	0.09	0.09	0.09	0.09	0.09	0.09	0.09
HC(ppm)	30	40	30	40	40	40	30	40	40	30
CO$_2$ (%)	6.80	6.80	6.78	6.78	6.80	6.80	6.72	6.74	6.74	6.74

A1.7 Ce(DPM)$_3$ at 50 ppm

LOAD: 0 lb

Fuel Flow (ml/s)	411	411	411	411	411	411	411	411	411	411
CO (%)	0.16	0.16	0.16	0.16	0.16	0.16	0.16	0.16	0.16	0.16
HC (ppm)	40	40	30	40	50	40	40	40	50	40
CO$_2$ (%)	2.01	2.23	2.25	2.26	2.27	2.24	2.23	2.21	2.21	2.20

LOAD: 15 lb

Fuel Flow (ml/s)	268	267	267	267	267	266	266	267	267	266
CO (%)	0.13	0.12	0.13	0.13	0.12	0.13	0.12	0.12	0.12	0.12
HC (ppm)	30	20	30	30	30	20	30	30	30	30
CO$_2$ (%)	3.89	3.92	3.90	3.88	3.88	3.86	3.84	3.87	3.92	3.88

LOAD: 30 lb

Fuel Flow (ml/s)	173	173	173	172	172	172	172	172	172	172
CO (%)	0.10	0.09	0.10	0.09	0.09	0.09	0.09	0.09	0.10	0.09
HC(ppm)	30	30	40	30	40	30	30	40	30	30
CO$_2$ (%)	6.94	6.86	6.89	6.84	6.88	6.88	6.81	6.86	6.83	6.84

A1.8 Ce(DPM)$_3$ at 100 ppm

LOAD: 0lb

Fuel Flow (ml/s)	392	392	392	391	391	391	391	391	391	391
CO (%)	0.16	0.16	0.18	0.18	0.18	0.18	0.18	0.18	0.18	0.18
HC (ppm)	50	40	50	40	40	50	50	40	50	40
CO$_2$ (%)	2.23	2.23	2.23	2.24	2.25	2.30	2.26	2.26	2.23	2.23

LOAD: 15lb

Fuel Flow (ml/s)	255	256	257	257	257	257	257	257	257	257
CO (%)	0.16	0.16	0.15	0.16	0.16	0.16	0.16	0.15	0.16	0.16
HC (ppm)	30	40	30	30	40	40	50	50	50	40
CO$_2$ (%)	4.15	4.13	4.13	4.22	4.18	4.20	4.16	4.19	4.15	4.15

LOAD: 30lb

Fuel Flow (ml/s)	167	167	168	168	168	168	168	168	168	168
CO (%)	0.15	0.15	0.13	0.13	0.13	0.11	0.11	0.13	0.13	0.13
HC(ppm)	50	60	50	60	50	60	50	60	50	60
CO$_2$ (%)	6.92	6.90	6.88	7.02	7.03	7.03	7.02	7.05	7.04	6.98

A1.9 La(DPM)$_3$ at 25 ppm

LOAD: 0 lb

Fuel Flow (ml/s)	404	403	402	402	402	402	402	402	402	402
CO (%)	0.17	0.17	0.17	0.18	0.19	0.19	0.18	0.18	0.19	0.18
HC (ppm)	30	40	30	40	30	40	40	40	30	40
CO$_2$ (%)	1.97	1.96	1.98	1.99	2.03	2.01	2.08	2.07	2.09	2.08

LOAD: 15 lb

Fuel Flow (ml/s)	266	265	266	266	264	265	265	265	265	265
CO (%)	0.13	0.13	0.13	0.13	0.13	0.14	0.13	0.13	0.13	0.13
HC (ppm)	20	30	20	30	20	30	20	30	20	20
CO$_2$ (%)	3.93	3.97	3.95	3.96	4.00	3.99	3.96	3.97	3.97	3.99

LOAD: 30 lb

Fuel Flow (ml/s)	168	169	170	170	170	170	170	170	170	170
CO (%)	0.15	0.15	0.15	0.13	0.13	0.12	0.13	0.13	0.15	0.13
HC(ppm)	40	50	40	50	40	50	40	50	40	50
CO$_2$ (%)	7.28	7.26	7.23	7.23	7.14	7.14	7.11	7.08	7.10	7.10

A1.10 La(DPM)$_3$ at 50 ppm

LOAD: 0 lb

Fuel Flow (ml/s)	426	424	423	420	420	420	420	420	420	420
CO (%)	0.15	0.15	0.15	0.14	0.14	0.14	0.14	0.14	0.14	0.14
HC (ppm)	40	40	50	40	50	40	40	50	50	40
CO$_2$ (%)	1.95	1.95	1.94	1.92	1.95	1.96	1.97	1.96	1.99	1.96

LOAD: 15 lb

Fuel Flow (ml/s)	269	269	269	270	269	270	270	269	269	269
CO (%)	0.10	0.10	0.10	0.10	0.10	0.10	0.10	0.10	0.10	0.10
HC (ppm)	30	20	30	20	30	20	20	20	20	20
CO$_2$ (%)	3.92	3.89	4.13	3.93	3.93	3.88	3.87	3.89	3.91	3.90

LOAD: 30 lb

Fuel Flow (ml/s)	171	171	171	172	172	172	172	172	172	172
CO (%)	0.09	0.10	0.10	0.10	0.10	0.11	0.10	0.10	0.10	0.10
HC (ppm)	30	40	40	40	30	40	30	40	30	30
CO$_2$ (%)	6.92	6.90	6.88	7.02	7.03	7.03	7.02	7.05	7.04	6.98

A1.11 La(DPM)$_3$ at 100 ppm

LOAD: 0 lb

Fuel Flow (ml/s)	409	408	408	408	408	408	408	408	408	408
CO (%)	0.19	0.19	0.18	0.18	0.18	0.18	0.18	0.18	0.18	0.18
HC (ppm)	40	60	50	50	50	40	50	40	40	40
CO$_2$ (%)	1.99	2.00	2.03	2.04	2.10	2.10	2.10	2.11	2.17	2.15

LOAD: 15 lb

Fuel Flow (ml/s)	272	272	270	270	270	270	270	270	269	269
CO (%)	0.13	0.12	0.12	0.12	0.13	0.13	0.13	0.13	0.13	0.13
HC (ppm)	30	20	40	30	20	30	30	30	40	30
CO$_2$ (%)	3.85	3.80	3.84	3.87	3.83	3.86	3.90	3.94	3.99	4.02

LOAD: 30 lb

Fuel Flow (ml/s)	173	173	174	174	174	174	174	174	174	174
CO (%)	0.12	0.12	0.12	0.13	0.13	0.12	0.11	0.12	0.11	0.12
HC (ppm)	40	30	40	30	40	30	30	30	40	40
CO$_2$ (%)	6.91	6.90	6.86	6.86	6.87	6.83	6.81	6.84	6.74	6.83

A1.12 Diesel + THF at 5% (Baseline 2)

LOAD: 0 lb

Fuel Flow (ml/s)	410	410	410	410	410	410	410	410	410	410	410
CO (%)	0.14	0.14	0.14	0.14	0.14	0.14	0.14	0.14	0.14	0.14	0.14
HC (ppm)	40	40	40	40	40	40	40	40	40	40	40
CO_2 (%)	2.00	2.00	2.02	2.02	2.00	2.02	2.00	2.03	2.00	2.04	2.04

LOAD: 15 lb

Fuel Flow (ml/s)	273	274	274	274	274	274	274	274	274	274
CO (%)	0.10	0.10	0.10	0.10	0.10	0.10	0.10	0.10	0.10	0.10
HC (ppm)	20	20	20	20	20	20	20	20	20	20
CO_2 (%)	3.83	3.82	3.82	3.83	3.80	3.82	3.84	3.85	3.84	3.84

LOAD: 30 lb

Fuel Flow (ml/s)	173	174	175	175	175	175	175	175	175	175
CO (%)	0.11	0.10	0.10	0.10	0.10	0.09	0.10	0.10	0.10	0.10
HC(ppm)	40	40	40	40	40	40	40	40	40	40
CO_2 (%)	6.92	6.98	6.92	3.84	6.80	6.88	6.81	6.83	6.88	6.83

A1.13 Ce-naphtren at 5 ppm

LOAD: 0 lb

Fuel Flow (ml/s)	415	416	416	416	416	416	416	416	416	416	416
CO (%)	0.17	0.17	0.16	0.16	0.16	0.16	0.16	0.16	0.16	0.16	0.16
HC (ppm)	40	50	40	50	40	50	40	40	50	50	50
CO_2 (%)	1.98	1.97	1.99	2.01	2.00	2.02	2.02	2.03	2.03	2.03	2.03

LOAD: 15 lb

Fuel Flow (ml/s)	277	274	275	275	275	275	275	275	275	275	275
CO (%)	0.10	0.10	0.10	0.09	0.09	0.09	0.09	0.09	0.09	0.09	0.09
HC (ppm)	20	30	20	30	20	30	20	30	30	20	30
CO_2 (%)	3.84	3.85	3.85	3.89	3.93	3.92	3.94	3.92	3.92	3.90	3.90

LOAD: 30 lb

Fuel Flow (ml/s)	179	178	179	179	178	179	179	179	179	179	179
CO (%)	0.08	0.08	0.08	0.09	0.09	0.08	0.08	0.08	0.08	0.08	0.08
HC(ppm)	30	30	30	30	30	30	30	30	30	30	30
CO_2 (%)	6.89	6.93	6.72	3.78	6.76	6.73	6.70	6.72	6.72	6.73	6.72

A1.14 Ce-naphtren at 25 ppm

LOAD: 0 lb

Fuel Flow (ml/s)	394	390	388	388	388	388	388	388	388	388
CO (%)	0.18	0.18	0.18	0.18	0.18	0.18	0.18	0.18	0.18	0.18
HC (ppm)	40	30	40	30	40	40	40	50	40	50
CO$_2$ (%)	2.15	2.17	2.15	2.18	2.13	2.16	2.17	2.19	2.23	2.23

LOAD: 15 lb

Fuel Flow (ml/s)	263	264	262	262	262	262	262	262	262	262
CO (%)	0.12	0.12	0.11	0.12	0.12	0.11	0.12	0.12	0.12	0.12
HC (ppm)	20	20	20	20	30	20	20	20	20	20
CO$_2$ (%)	4.10	4.15	4.12	4.14	4.22	4.15	4.11	4.15	4.16	4.12

LOAD: 30 lb

Fuel Flow (ml/s)	166	166	167	167	167	167	167	167	167	167
CO (%)	0.14	0.13	0.14	0.14	0.13	0.13	0.13	0.13	0.13	0.13
HC(ppm)	50	60	50	50	40	30	50	40	40	40
CO$_2$ (%)	7.25	7.34	7.29	7.29	7.24	7.20	7.21	7.22	7.08	7.08

A1.15 Ce-naphtren 50 ppm

LOAD: 0 lb

Fuel Flow (ml/s)	376	375	374	375	375	375	375	375	375	375
CO (%)	0.22	0.21	0.20	0.22	0.22	0.22	0.22	0.23	0.22	0.22
HC (ppm)	60	70	60	70	60	70	60	70	60	70
CO_2 (%)	2.19	2.15	2.21	2.23	2.23	2.26	2.27	2.29	2.25	2.23

LOAD: 15 lb

Fuel Flow (ml/s)	255	254	254	253	254	254	254	254	254	254
CO (%)	0.18	0.19	0.18	0.19	0.18	0.18	0.18	0.19	0.18	0.18
HC (ppm)	30	40	30	40	40	40	40	50	40	40
CO_2 (%)	4.28	4.24	4.26	4.29	4.36	4.35	4.37	4.30	4.28	4.29

LOAD: 30 lb

Fuel Flow (ml/s)	168	168	168	168	168	168	168	168	168	168
CO (%)	0.22	0.25	0.23	0.21	0.23	0.23	0.24	0.23	0.23	0.23
HC(ppm)	70	60	70	60	60	70	60	60	70	70
CO_2 (%)	7.12	7.14	7.12	7.12	7.06	7.13	7.06	7.10	7.00	7.02

A1.16 Fe-naphtren 5 ppm

LOAD: 0 lb

Fuel Flow (ml/s)	395	396	397	396	396	396	396	396	396	396
CO (%)	0.18	0.18	0.18	0.17	0.17	0.17	0.17	0.17	0.17	0.17
HC (ppm)	40	50	40	50	40	50	40	50	40	50
CO$_2$ (%)	2.29	2.30	2.31	2.30	2.27	2.25	2.26	2.25	2.24	2.24

LOAD: 15 lb

Fuel Flow (ml/s)	259	260	261	261	261	261	261	261	261	261
CO (%)	0.13	0.13	0.12	0.12	0.13	0.12	0.12	0.12	0.12	0.12
HC (ppm)	30	40	30	40	30	40	30	40	30	40
CO$_2$ (%)	4.35	4.38	4.33	4.35	4.31	4.35	4.37	4.35	4.35	4.35

LOAD: 30 lb

Fuel Flow (ml/s)	172	172	174	174	174	174	174	174	174	174
CO (%)	0.11	0.13	0.12	0.12	0.12	0.12	0.11	0.12	0.12	0.13
HC(ppm)	60	50	50	60	60	60	50	60	50	60
CO$_2$ (%)	7.09	7.10	7.10	7.10	7.05	7.10	6.90	6.90	6.88	6.88

A1.17 Fe-naphtren 12.5 ppm

LOAD: 0 lb

Fuel Flow (ml/s)	364	362	361	361	361	361	361	361	361	361	361
CO (%)	0.22	0.22	0.23	0.23	0.22	0.23	0.23	0.23	0.23	0.23	0.23
HC (ppm)	50	60	50	60	50	50	60	50	60	50	60
CO_2 (%)	2.29	2.27	2.27	2.26	2.28	2.31	2.27	2.30	2.28	2.28	2.29

LOAD: 15 lb

Fuel Flow (ml/s)	241	245	247	247	247	247	247	247	247	247	247
CO (%)	0.20	0.20	0.21	0.21	0.19	0.19	0.20	0.20	0.20	0.20	0.20
HC (ppm)	40	30	40	40	40	40	40	40	40	40	40
CO_2 (%)	4.26	4.24	4.20	4.33	4.35	4.33	4.36	4.36	4.33	4.35	4.33

LOAD: 30 lb

Fuel Flow (ml/s)	167	167	167	166	167	167	167	167	167	167	167
CO (%)	0.12	0.12	0.10	0.12	0.11	0.12	0.12	0.13	0.12	0.12	0.12
HC (ppm)	40	50	40	50	40	50	50	40	50	40	50
CO_2 (%)	7.14	7.22	7.22	7.23	7.26	7.22	7.10	7.16	7.22	7.20	7.20

A1.18 Fe-naphtren 25 ppm

LOAD: 0 lb

Fuel Flow (ml/s)	402	400	400	400	400	400	400	400	400	400
CO (%)	0.18	0.16	0.17	0.17	0.18	0.17	0.17	0.17	0.17	0.17
HC (ppm)	60	50	60	50	50	60	50	60	50	60
CO_2 (%)	1.99	1.98	1.99	1.99	2.02	2.00	2.04	2.04	2.06	2.08

LOAD: 15 lb

Fuel Flow (ml/s)	273	272	270	270	270	270	270	270	270	270
CO (%)	0.11	0.12	0.13	0.12	0.12	0.12	0.12	0.12	0.12	0.12
HC (ppm)	30	40	30	40	30	40	30	40	30	40
CO_2 (%)	3.90	3.92	3.95	3.92	3.92	3.92	3.90	3.92	3.92	3.92

LOAD: 30 lb

Fuel Flow (ml/s)	174	177	177	177	177	177	177	177	177	177
CO (%)	0.09	0.08	0.08	0.08	0.08	0.09	0.08	0.08	0.08	0.08
HC(ppm)	30	30	40	40	40	30	30	30	30	40
CO_2 (%)	6.73	6.65	6.65	6.77	6.73	6.62	6.72	6.68	6.71	6.74

A1.19 Ce-^{t}Bu-saltren at 5 ppm

LOAD: 0lb

Fuel Flow (ml/s)	403	403	401	403	403	403	403	403	403	403
CO (%)	0.16	0.16	0.16	0.16	0.16	0.16	0.16	0.16	0.16	0.16
HC (ppm)	40	50	40	50	50	50	50	50	50	50
CO$_2$ (%)	2.04	2.04	2.07	2.06	2.12	2.12	2.13	2.15	2.16	2.16

LOAD: 15lb

Fuel Flow (ml/s)	268	271	272	272	272	272	272	272	272	272
CO (%)	0.11	0.11	0.11	0.10	0.11	0.11	0.11	0.11	0.11	0.11
HC (ppm)	40	30	30	30	30	30	30	30	30	30
CO$_2$ (%)	3.84	3.90	3.95	3.98	3.92	3.98	3.94	3.98	3.96	3.96

LOAD: 30lb

Fuel Flow (ml/s)	175	176	177	176	176	176	176	176	176	176
CO (%)	0.11	0.11	0.11	0.12	0.10	0.12	0.10	0.11	0.11	0.11
HC(ppm)	40	50	40	50	40	50	50	40	40	50
CO$_2$ (%)	6.80	6.77	6.77	6.88	6.75	6.73	6.70	6.71	6.72	6.72

A1.20 Ce-tBu-saltren at 25 ppm

LOAD: 0 lb

Fuel Flow (ml/s)	386	383	386	386	386	386	386	386	386	386
CO (%)	0.22	0.21	0.21	0.21	0.21	0.21	0.21	0.21	0.21	0.21
HC (ppm)	40	50	40	50	50	50	40	40	50	40
CO_2 (%)	2.34	2.35	2.32	2.31	2.31	2.30	2.33	2.33	2.31	2.31

LOAD: 15 lb

Fuel Flow (ml/s)	251	252	253	253	253	253	253	253	253	253
CO (%)	0.16	0.16	0.15	0.15	0.15	0.15	0.15	0.15	0.15	0.16
HC (ppm)	40	40	30	40	30	40	30	40	30	40
CO_2 (%)	4.35	4.37	4.36	4.36	4.31	4.35	4.38	4.38	4.37	4.37

LOAD: 30 lb

Fuel Flow (ml/s)	170	171	172	172	172	172	172	172	172	172
CO (%)	0.11	0.10	0.10	0.11	0.10	0.10	0.10	0.10	0.11	0.10
HC (ppm)	40	50	40	50	40	50	50	40	50	40
CO_2 (%)	7.17	7.12	7.14	7.16	7.14	7.11	7.08	7.08	7.10	7.01

LOAD: 0 lb

Fuel Flow (ml/s)	390	393	393	393	393	393	393	393	393	393	393
CO (%)	0.16	0.16	0.17	0.17	0.16	0.16	0.16	0.15	0.16	0.16	0.16
HC (ppm)	40	40	40	40	30	40	40	40	40	40	40
CO_2 (%)	2.25	2.21	2.21	2.27	2.29	2.27	2.27	2.27	2.22	2.22	2.24

LOAD: 15 lb

Fuel Flow (ml/s)	274	273	272	272	272	272	272	272	272	272	272
CO (%)	0.10	0.10	0.11	0.11	0.11	0.11	0.11	0.11	0.11	0.11	0.11
HC (ppm)	10	20	10	20	10	20	10	20	20	10	20
CO_2 (%)	3.87	3.89	3.81	3.82	3.85	3.87	3.87	3.87	3.90	3.88	3.87

LOAD: 30 lb

Fuel Flow (ml/s)	178	179	180	180	180	180	180	180	180	180	180
CO (%)	0.08	0.08	0.08	0.08	0.08	0.08	0.08	0.07	0.08	0.08	0.08
HC (ppm)	30	40	30	40	30	40	30	40	40	40	30
CO_2 (%)	6.45	6.41	6.42	6.42	6.42	6.42	6.42	6.44	6.42	6.42	6.42

A1.22 Fe-tBu-saltren at 25 ppm

LOAD: 0 lb

Fuel Flow (ml/s)	386	389	390	390	390	390	390	390	390	390	390
CO (%)	0.23	0.23	0.23	0.22	0.23	0.23	0.23	0.23	0.23	0.23	0.23
HC (ppm)	40	50	40	40	40	40	40	40	40	40	40
CO_2 (%)	2.27	2.27	2.29	2.28	2.28	2.28	2.27	2.27	2.27	2.28	2.27

LOAD: 15 lb

Fuel Flow (ml/s)	256	257	258	258	258	258	258	258	258	258	258
CO (%)	0.14	0.14	0.14	0.13	0.13	0.12	0.12	0.13	0.13	0.12	0.12
HC (ppm)	40	40	40	40	40	40	40	40	40	40	40
CO_2 (%)	4.23	4.22	4.24	4.25	4.22	4.23	4.27	4.25	4.25	4.15	4.18

LOAD: 30 lb

Fuel Flow (ml/s)	168	169	170	171	171	171	171	171	171	171	171
CO (%)	0.10	0.10	0.09	0.09	0.09	0.10	0.09	0.09	0.09	0.09	0.09
HC(ppm)	40	40	40	60	40	40	40	40	40	40	40
CO_2 (%)	7.95	7.82	7.84	7.80	7.63	7.70	7.74	7.71	7.78	7.78	7.75

FORD DIESEL P100 PICK-UP TRUCK TEST PROGRAMME RESULTS

A1.23 ECE 15/04 Emission Test Data of Untreated Diesel (Baseline)

	TEST 1	TEST 2
CO_2 (%)	0.40	0.48
HC (ppm)	8.869	7.692
CO (ppm)	30.075	28.075
NOx (ppm)	14.46	15.06
Fuel Consumption : 20.503 MPG (U.S.)		

A1.24 ECE 15/04 Emission Test Data of Ce(DPM)$_3$ at 50 ppm

	TEST 1	TEST 2
CO_2 (%)	0.49	0.48
HC (ppm)	6.135	6.724
CO (ppm)	24.575	25.075
NOx (ppm)	13.24	13.54
Fuel Consumption : 20.287 MPG (U.S.)		

APPENDIX 4

CATALYTIC CONVERTER TEST RESULTS

A1.25 Emission Data of the Untreated Pellets (Baseline) Test

PRE-CATALYST BOX					POST-CATALYST BOX							
CO (%)	CO₂ (%)	HC ppm	NOx (ppm)	Temp (°C)	CO (%)	CO₂ (%)	HC ppm	NOx (ppm)	Temp (°C)	ΔT (°C)	A/F
					UNTREATED PELLETS (BASELINE)							
2.3	13.7	640	5400	678	2.25	13.6	550	5000	501	177	13.6
0.91	14.5	575	4400	703	1.0	14.4	455	4100	525	178	14.2
0.55	14.55	530	5100	701	0.58	14.5	410	5000	536	165	14.5
0.21	14.50	495	5800	697	0.24	14.5	345	5500	535	162	14.9
0.10	14.0	420	6100	689	0.13	14.0	250	5750	532	157	15.5
0.085	13.2	375	6150	665	0.12	13.1	220	6000	521	144	16.4

A1.26 Emission Data of the Nickel-Misch Metal Oxides Coated Pellets Test

NICKEL-MISCH METAL OXIDES TREATED PELLETS

PRE-CATALYST BOX					POST-CATALYST BOX					
CO (%)	CO_2 (%)	HC ppm	NOx (ppm)	Temp (°C)	CO (%)	CO_2 (%)	HC ppm	NOx (ppm)	Temp (°C)	A/F
2.30	13.7	640	1550	691	1.70	14.0	490	5000	551	13.6
0.99	14.5	550	2550	700	0.73	14.8	350	2000	566	14.1
0.50	14.6	460	2800	699	0.36	14.7	265	2600	554	14.5
0.14	14.5	390	6250	691	0.128	14.4	225	3100	543	15
0.08	13.9	325	3600	675	0.085	13.6	215	3400	536	15.7
0.07	13.2	320	3400	660	0.089	13.0	210	3200	520	16.5

A1.27 Emission Data of the Lanthanum Oxide Coated Pellets Test

LANTHANUM OXIDE TREATED PELLETS

PRE-CATALYST BOX					POST-CATALYST BOX					
CO (%)	CO_2 (%)	HC ppm	NOx (ppm)	Temp (°C)	CO (%)	CO_2 (%)	HC ppm	NOx (ppm)	Temp (°C)	A/F
2.05	13.7	580	2000	685	1.90	14.0	480	1750	532	13.6
1.10	14.0	530	2400	692	1.11	14.40	440	2200	531	14.1
0.50	14.45	460	2900	696	0.54	14.60	360	2750	535	14.5
0.19	14.60	380	3400	691	0.24	14.50	280	3200	535	14.9
0.09	14.55	335	3500	675	0.11	13.85	220	3450	531	15.7
0.08	13.90	310	3650	655	0.11	13.0	250	3500	517	16.6

A1.28 Emission Data of the Cerium Oxide Coated Pellets Test

CERIUM OXIDE TREATED PELLETS

PRE-CATALYST BOX					POST-CATALYST BOX					
CO (%)	CO_2 (%)	HC ppm	NOx (ppm)	Temp (°C)	CO (%)	CO_2 (%)	HC ppm	NOx (ppm)	Temp (°C)	A/F
2.20	13.75	700	2500	696	2.00	14.00	510	2000	566	13.6
1.10	14.40	650	3000	705	1.01	14.60	370	2800	561	14.0
0.58	14.6	575	3650	708	0.42	14.90	230	3400	564	14.4
0.155	14.45	455	4150	699	0.115	14.55	145	4050	549	15.0
0.086	13.90	410	5000	683	0.081	13.95	125	4650	538	15.7
0.084	13.20	395	4550	668	0.085	13.20	140	4400	532	16.5

APPENDIX 5

ROVER M16i TEST MICROANALYTICAL RESULTS

A1.29 Microanalytical Data of the Pre-Catalyst Box Sample

GAIN	=	20	EV/CHAN
SPECTRUM LENGTH	=	1024	CHANS
PRESET LIVE TIME	=	150	SECS
ACTUAL LIVE TIME	=	150	SECS

WINDOW LABEL	WINDOW CENTRE	FIRST CHANNEL	LAST CHANNEL	% AGE TOTAL
Na	1040	1000	1080	0.44
Mg	1260	1180	1340	0.08
Al	1500	1380	1620	10.49
Si	1740	1660	1840	3.18
P	2000	1880	2140	14.98
S/Mo	2320	2200	2440	4.21
Ca	3680	3540	3840	18.36
Ce	4820	4680	4980	30.96
Mn	5900	5780	6020	0.16
Fe	6360	6100	6640	4.01
Ni	7460	7360	7580	1.55
Cu	8040	7780	8320	4.57
Zn	8640	8460	8820	7.00

A1.30 Microanalytical Data of the Post-Catalyst Box Sample

GAIN	=	20	EV/CHAN
SPECTRUM LENGTH	=	1024	CHANS
PRESET LIVE TIME	=	150	SECS
ACTUAL LIVE TIME	=	150	SECS

WINDOW LABEL	WINDOW CENTRE	FIRST CHANNEL	LAST CHANNEL	TOTAL (%)
Al	1500	1380	1620	8.58
Si	1740	1660	1840	3.40
P	2000	1880	2140	5.07
S/Mo	2320	2200	2440	2.84
K	3320	3240	3420	0.78
Ca	3680	3540	3840	9.26
Ce	4820	4680	4980	46.10
Fe	6360	6100	6640	15.60
Ni	7460	7360	7580	1.70
Zn	8640	8460	8820	6.67

RENAULT F2N TEST MICROANALYTICAL RESULTS

A1.31 Microanalytical Data of Samples Collected at Various Positions of the Exhaust System

Position of Samples In the Exhaust System	Na (%)	Mg (%)	Al (%)	Si (%)	P (%)	S (%)	Cl (%)	K (%)	Ca (%)	Ti (%)	Ce (%)	Cr (%)	Mn (%)	Fe (%)	Ni (%)	Cu (%)	Zn (%)
Manifold Outlet	0.22	0.05	0.74	0.16	0.00	1.14	0.00	0.16	2.84	0.00	4.72	0.00	0.07	85.96	0.00	0.00	3.94
Downpipe Inlet	0.00	0.00	3.05	0.00	0.00	8.72	0.00	0.00	8.33	0.00	11.82	0.00	0.00	59.70	1.18	1.57	5.63
Downpipe Exit	0.00	0.00	3.34	2.65	0.00	10.01	0.00	1.96	9.57	3.58	42.74	0.00	0.00	9.37	1.32	13.00	2.45
Inlet to Catalyst Box	0.00	0.40	5.02	0.51	7.23	7.19	0.00	0.00	4.94	0.91	42.49	3.04	0.00	13.48	0.00	1.62	13.48
Pre-Catalyst Box	0.00	0.34	10.31	0.00	4.30	19.59	3.51	0.00	0.00	0.00	42.13	0.00	0.00	0.00	10.53	1.36	7.93
Middle-Catalyst Box	0.00	0.00	12.90	3.43	0.00	6.87	0.84	0.00	2.32	0.00	50.96	0.00	0.77	13.34	0.00	1.92	6.65
Post-Catalyst Box	1.93	0.21	8.89	4.26	0.00	4.55	0.00	0.00	0.00	0.00	59.59	0.00	0.00	11.03	0.56	8.99	0.00